## Université de Lille

Doctoral School **EDBSL**

University Department **Unit 1011, Lille University, Pasteur Institute of Lille
Nuclear receptors, cardiovascular diseases and diabetes**

Thesis defended by **Artemii Nikitin**

Defended on **18th December, 2019**

In order to become Doctor from Université de Lille

Academic Field **Biology**

Speciality **Immunology**

Thesis Title

# Role of nuclear receptor RORα in regulatory T cells

**Thesis supervised by** David DOMBROWICZ

**Committee members**

| | | | |
|---|---|---|---|
| *Referees* | Agnès LEHUEN | Institut Cochin | |
| | Nicolas VENTECLEF | Centre de Recherche de Cordeliers | |
| *Examiner* | Bart STAELS | Institut Pasteur de Lille, Unversité de Lille, Inserm | Committee President |
| *Supervisor* | David DOMBROWICZ | Institut Pasteur de Lille, Unversité de Lille, Inserm | |

This thesis has been prepared at the following research units.

**Unit 1011, Lille University, Pasteur Institute of Lille**
**Nuclear receptors, cardiovascular diseases and diabetes**

1, Rue du Professeur Calmette
Lille, France

Web Site   http://u1011.pasteur-lille.fr/accueil/

**Inserm**
Institut national de la santé et de la recherche médicale

**Abstract**

Transcription factors of the nuclear receptor superfamily have a vast influence on development and function of regulatory T cell ($T_{REG}$) cells. $T_{REG}$ cells are suppressive immune cells of adaptive immune system. Their main functions are control of inflammatory response mounted by other immune cells and maintenance of local tissue homeostasis. As $T_{REG}$ act at various sites of the body and both in homeostatic and inflammatory state, they need to adequately respond to local tissue-specific cues as well as adapt to aggressive immune environments while preserving their long-lasting tolerogenic properties. This is achieved by weaving complex transcriptional networks, converging at transcription factors with various coordination functions, the main being forkhead box P3 (FOXP3). During last few years, many studies focused on $T_{REG}$ cells found in non-lymphoid tissue (NLT). These populations of $T_{REG}$ are examined in the contexts of homeostasis and many inflammatory diseases, and tissue- or function-specific transcription factor (TF) were assigned to some of them as regulators of development, activation, proliferation, stability, migration and suppressive functions. Retinoic acid receptor-related orphan receptor alpha (ROR$\alpha$) is a nuclear receptor, which controls cerebellum development, liver and whole-body metabolism and differentiation of T-helper ($T_H$)17, type 2 innate lymphoid cells (ILC2) and type 3 innate lymphoid cells (ILC3). ROR$\alpha$ is highly expressed in NLT $T_{REG}$, including populations in visceral adipose tissue (VAT), intestine and skin, and gets more and more mentions in the articles dedicated to $T_{REG}$ in NLT. These ROR$\alpha$-expressing populations of $T_{REG}$ were all shown to be involved in various pathologies. However, ROR$\alpha$ role in $T_{REG}$ was directly addressed only once in a recent study. It's active involvement in various processes, high expression in NLT $T_{REG}$ and lack of knowledge make ROR$\alpha$ an attractive target for investigation, to deepen current view of homeostasis control by $T_{REG}$ and thus better understand mechanisms of development of associated diseases. To attain these objectives, a mouse strain with $T_{REG}$-specific ROR$\alpha$ deficiency was generated. Our central hypothesis is that ROR$\alpha$ controls development or function of $T_{REG}$ cells in homeostasis of NLT and potentially in inflammatory diseases. For studying a role of ROR$\alpha$ in NLT $T_{REG}$ during control of tissue homeostasis, in particular, VAT $T_{REG}$, we have charachterized phenotype of untreated ROR$\alpha^{Foxp3/Foxp3}$ mice and challenged mice with a model of diet-induced obesity (DIO). In both cases we have found an important role of $T_{REG}$-expressed ROR$\alpha$. To further investigate a role of ROR$\alpha$ in $T_{REG}$ during pathologies and it's contribution to various types of immune response we have tested an involvement of ROR$\alpha$ in $T_{REG}$ in the model of allergic pathology, namely house dust mite (HDM)-induced allergic airway inflammation (AAI) model.

To elucidate molecular mechanisms of ROR$\alpha$ action in $T_{REG}$ cells, we have performed gene expression profiling of $T_{REG}$ cells from examined tissues and conditions *in vivo*, as well as *in vitro*. We also have studied a role of ROR$\alpha$ in epigenetic landscape of $T_{REG}$ cells *in vitro* by probing histone acetylation marks genome wide. As a result of this study, we have gained a broader understanding of $T_{REG}$ control by nuclear receptors and TF in general in homeostatic conditions and during inflammation. Nuclear receptors proved to be useful targets for therapeutic agents thanks to their versatile functions inside the cell and to ligand-dependency. Given the crucial importance of $T_{REG}$ cells in organismal homeostasis and their involvement in numerous pathologies, targeting particular cues inside these cells may be a powerful tool in new treatment strategies. Results of our study might serve as a basis for development of novel pharmaceutical agents targeting ROR$\alpha$.

**Resumé**

Les facteurs de transcription de la superfamille des récepteurs nucléaires jouent de multiples rôles dans le développement et la fonction des lymphocytes T régulateurs ($T_{REG}$). Les $T_{REG}$ sont des cellules régulatrices/suppressives qui contrôlent les réponses d'autres types cellulaires et l'homéostasie locale des tissus. Comme les $T_{REG}$ sont actives au sein de divers organes, tant à l'homéostasie qu'en conditions inflammatoires, ils doivent répondre à la fois aux contexte local au sein du tissu et à un environnement immunologiquement agressif tout en préservant leurs propriétés tolérogéniques au cours du temps. Ces caractéristiques apparemment antinomiques sont contrôlées par un réseau transcriptionnel complexe au sein duquel le facteur de transcription FOXP3 joue un rôle prédominant. Au cours des dernières années, de nombreuses études se sont intéressées aux $T_{REG}$ présent dans les tissus non lymphoïdes (NLT). Ces populations ont été étudiées aussi bien à l'homéostasie qu'en conditions inflammatoires dans diverses pathologies. Des facteurs de transcriptions spécifiques d'un tissus ou d'une fonction déterminées ont été mis en évidence et leur rôle régulateur dans le développement, l'activation, la migration et l'immunosuppression a été caractérisé. ROR$\alpha$ est un récepteur nucléaire qui contrôle le développement cérebellaire et hépatique, le métabolisme systémique, la différenciation des lymphocytes auxiliaires $T_H17$, des cellules lymphoïdes innées (ILC) de type 2 et 3. ROR$\alpha$ est fortement exprimé dans les $T_{REG}$ des NLT, y compris dans le tissu adipeux viscéral (VAT), l'intestin et la peau....Ces populations de $T_{REG}$ exprimant ROR$\alpha$ ont été associées à diverses pathologies. Cependant seule une étude récente a été consacrée à leur rôle précis. L'implication de ROR$\alpha$ dans de nombreuses fonction, sa forte expression au sein des $T_{REG}$ des NLT nous a poussé a étudier le rôle de ces $T_{REG}$ exprimant ROR$\alpha$ dans diverses pathologies. Dans ce butit, nous avons généré des souris spécifiquement déficientes pour ROR$\alpha$ au sein des $T_{REG}$ (ROR$\alpha^{\text{Foxp3/Foxp3}}$). Nous avons émis l'hypothèse que ROR$\alpha$ contrôle le développement ou la fonction des $T_{REG}$ en conditions homéostatiques et dans des pathologies inflammatoires des NLT. Aussi nous avons caractérisé le phénotype des animaux ROR$\alpha^{\text{Foxp3/Foxp3}}$ et en particulier les $T_{REG}$ du VAT à l'homéostasie, où la réponse de type 2 est protectrice et dans un modèle d'obésité (et d'insulino-résistance) induit par l'obésité (DIO) dans laquelle nous avons mis en évidence un rôle protecteur important des $T_{REG}$ exprimant ROR$\alpha$ dans ces deux conditions expérimentales. Nous également étudié la contribution de ces cellules dans un modèle d'inflammation allergique (AAI) induite par un acarien (HDM) caractérisé par une forte réponse de type 2 et montré une aggravation de la pathologie. Pour étudier le mécanisme moléculaire de l'action de ROR$\alpha$ au sein des $T_{REG}$, nous avons procédé à une analyse transcriptomique des cellules isolées dans diverses conditions expérimentales *in vivo* et *in vitro* et avons étudié le rôle de ROR$\alpha$ dans les modifications épigénétiques au sein des $T_{REG}$ en caractérisation l'acétylation des histones dans le génome entier. Cette étude nous a permis de mieux appréhender comment les $T_{REG}$ étaient régulées par un facteur nucléaire à l'homéostasie et en conditions inflammatoires. Les récepteurs nucléaires représentent des cibles thérapeutiques intéressantes compte tenu de leur action pléiotropique et de leurs ligands de petite taille. Compte tenu de l'importance des $T_{REG}$ dans l'homéostasie tissulaire et dans de nombreuses pathologies, cibler de tels facteurs au sein de populations cellulaires spécifiques représente une stratégie prometteuse dans le case de ROR$\alpha$ et des $T_{REG}$.

x

# Acknowledgements

# Acronyms

**IFN**-γ  interferon-γ. 2, 3, 6, 8, 9, 17, 44

**IL**-10  interleukin-10. 7–9, 16–18, 43

**IL**-12  interleukin-12. 2, 3, 8, 17

**IL**-13  interleukin-13. 2, 9, 17, 18, 24, 28, 33

**IL**-15  interleukin-15. 4, 5

**IL**-17  interleukin-17. 2, 3, 6, 17, 18, 50

**IL**-1β  interleukin-1 beta. 17

**IL**-21  interleukin-21. 3, 13

**IL**-22  interleukin-22. 2, 18

**IL**-23  interleukin-23. 18

**IL**-2  interleukin-2. 2, 4, 5, 7, 8, 14, 15, 43, 44, 49

**IL**-33  interleukin-33. 13, 14, 16, 24

**IL**-35  interleukin-35. 7, 8

**IL**-4  interleukin-4. 2, 3, 9, 16–18, 24, 28, 33, 44, 49, 50

**IL**-5  interleukin-5. 2, 9, 24, 33

**IL**-6  interleukin-6. 3, 5, 7, 17, 24

**IL**-7  interleukin-7. 4, 5

**IL**-9  interleukin-9. 2

**PPAR**α  peroxisome proliferator associated receptor alpha. 22

**PPAR**δ  peroxisome proliferator associated receptor delta. 22

**PPAR**γ  peroxisome proliferator associated receptor gamma. 12, 13, 22, 50

**PPAR**  peroxisome proliferator associated receptor. 22

**TGF**-β  tumor growth factor beta. 5, 7–9, 14, 16, 18

*sg/sg* *staggerer*. 23, 24, 27, 49

**AAI** allergic airway inflammation. 16, 23, 31–33, 35, 43, 48–50

**AF-1** ligand-independent activation function 1. 21

**AF-2** ligand-dependent activation domain 2. 21

**AhR** aryl-hydrocarbon receptor. 7

**AIRE** autoimmune regulator protein. 4

**AP-1** activator protein 1. 5

**APC** antigen presenting cell. 2, 3, 6, 13

**ATAC-seq** Assay for Transposase-Accessible Chromatin using sequencing. xc, 12

**BAL** bronchoalveolar lavage. 24

**BCR** B cell receptor. 1, 2, 24

**BMI** body mass index. 16

**cAMP** cyclic adenosine monophosphate. 7

**CAR** constitutive androstane receptor. 22

**CD** chow diet. xc, 13, 17, 36, 39

**ChIP-seq** chromatin immunoprecipitation-sequencing. xc, 49, 51

**CLA** cutaneous lymphocyte antigen. 11, 15

**CNS** conserved non-coding sequence. 5, 7, 8, 14, 16

**COX-2** cyclooxygenase 2. 18

**CRTC2** CREB regulated transcription coactivator 2. 18

**CT** circadian time. 23

**cTEC** cortical thymic epithelial cell. 1

**CTLA-4** cytotoxic T-lymphocyte-associated protein 4. 4, 6

**DBD** DNA binding domain. 21

**DC** dendritic cell. 6–9, 13, 15, 16, 18

**DIO** diet-induced obesity. xc, 17, 25, 36, 39, 47, 48

**DREAM** dimerization partner, RB-like, E2F and multi-vulval class B. 33

**DSS** dextran sulfate sodium. xc, 18, 50

**DTR** dyphteria toxin receptor. 14

**EAE** experimental allergic encephalomyelitis. xc, 7, 9

**EBI3** Epstein-Barr virus induced gene 3. 8

**EdU** 5-ethynyl-2'-deoxyuridine. 33

**EGFR** epidermal growth factor receptor. 14, 15

**EOS** eosinophil. 16, 17, 24

**eWAT** epididymal white adipose tissue. 36, 39, 48

**FA** fatty acids. 17, 22

**FGF19** fibroblast growth factor 19. 22

**FOXO1** forkhead box O1. 5

**FOXO3** forkhead box O3. 5

**FOXP3** forkhead box P3. xc, 4–9, 16, 23, 27, 28, 33, 43, 87

**FXR** farnesoid X receptor. 22

**GALT** gut-associated lymphoid tissue. 14

**GCN2** general control nonrepressed 2. 6

**HDAC** histone deacetylase. 5, 8

**HDL** high density lipoproteins. 16, 22

**HDM** house dust mite. 16, 31–33, 35, 43, 48, 49

**HFD** high fat diet. 17, 18, 36–40, 42, 48

**HSC** hematopoietic stem cell. 3

**IBD** inflammatory bowel disease. 18

**ICAM**-**1** intercellular adhesion molecule 1. 6

**IDO** indoleamine 2,3-dioxygenase. 6, 18

**IgE** immunoglobulin E. 48, 57

**IL**-**1Ra** interleukin-1 receptor antagonist. 17

**ILC** innate lymphoid cells. 1

**ILC2** type 2 innate lymphoid cells. xc, 24, 48

**ILC3** type 3 innate lymphoid cells. xc, 24

**IPEX** immunodysregulation polyendocrinopathy enteropathy X-linked. 4

**IPGTT** intraperitoneal glucose tolerance test. 39, 48

**IR** insulin receptor. 16, 17

**IR** insulin resistance. 16, 17, 39

**IRS-1** insulin receptor substrate-1. 16, 17

**iT$_{REG}$** induced regulatory T cell. 8

**iWAT** inguinal white adipose tissue. 36, 39, 48

**LAG3** lymphocyte activation gene 3. 7, 9

**LAP** latency-associated peptide. 9

**LBD** ligand binding domain. 21–23

**LFA-1** lymphocyte function-associated antigen 1. 6

**LPS** lipopolysaccharide. 17, 24

**LXR** liver X receptor. 22

**MAIT** mucosa-associated invariant T cell. 1

**MALT** mucosa-associated lymphoid tissue. 5, 14

**MeDIP-seq** methylated DNA immunoprecipitation and sequencing. xc

**MF** macrophage. 13, 14, 17

**MHC** major histocompatibility complex. 1–3, 6, 7, 13, 17

**mLN** mediastinal lymph node. 29, 33, 35, 36, 39, 43

**mTEC** medullary thymic epithelial cell. 2, 4

**mTORC1** mammalian target of rapamycin complex 1. 18

**mtROS** mitochondrial reactive oxygen species. 48

**NΦ** neutrophil. 17

**NASH** nonalcoholic steatohepatitis. 21, 24, 47

**NFκB** nuclear factor kappa-B. 2, 24, 50

**NK** natural killer cell. 1

**NKT** natural killer T cell. 1, 17

**NLT** non-lymphoid tissue. xc, 11–14, 47, 49, 50, 87

**NO** nitric oxide. 17

**NRP1** neuropilin-1. 7, 8

**OCR** open chromatin region. 12, 13

**OVA** ovalbumin. 16, 23

**PGE2** prostaglandin E2. 18

**PKC**-θ protein kinase C theta. 17

**PSGL**-**1** P-selectin glycoprotein ligand-1n. 15

**pT**$_{REG}$ peripherally generated regulatory T cell. 8

**Ptch** Patched. 23

**PXR** pregnane X receptor. 22

**qPCR** quantitative polymerase chain reaction. 27

**RA** retinoic acid. 8

**RAG** recombination activating gene. 1

**RAR** retinoic acid receptor. 8, 22

**ROR**α retinoic acid receptor-related orphan receptor alpha. xi, xc, 5, 15, 21–25, 27–29, 31, 33, 35–37, 39, 41, 43, 45, 47–51, 87, 88

**ROR**β retinoic acid receptor-related orphan receptor beta. 22

**ROR**γ retinoic acid receptor-related orphan receptor gamma. 22, 23

**ROR**γ**t** retinoic acid receptor-related orphan receptor gamma t. 3, 5, 8, 14, 18, 24, 47, 50

**RORE** ROR response element. 22, 23

**RXR** retinoic X receptor. 8, 22

**SCFA** short chain fatty acids. 8

**SCID** severe combined immunodeficiency. 4

**scRNA**-**seq** single-cell RNA sequencing. 12

**Shh** Sonic hedgehog. 23

**SLE** systemic lupus erythematosus. 9

**SLO** secondary lymphoid organs. 11–14

**SMAD** Sma/mothers against decapentaplegic homolog. 8

**SMAD2** Sma/mothers against decapentaplegic homolog 2. 8

**SMAD3** Sma/mothers against decapentaplegic homolog 3. 5, 7, 8

**SMAD4** Sma/mothers against decapentaplegic homolog 4. 8

**STAT** signal transducer and activator of transcription. 3, 5, 13

**T$_{CM}$** central memory T cell. 11

**T$_{CONV}$** conventional T cell. 4, 6, 7, 13, 23, 57

**T$_{EM}$** effector memory T cell. 11

**T$_{FH}$** T folicular helper. 3, 9

**T$_{H}$** T-helper. xc, 2, 3, 6–9, 12, 16–19, 24, 33, 39, 41, 43–45, 48–50, 88

**T$_{REG}$** regulatory T cell. xi, xc, 1–10, 12–19, 23–25, 27–37, 39, 41–51, 54–57, 87, 88

**T$_{RM}$** resident memory T cell. 11–13

**TCR** T-cell receptor. 1–6, 9, 13, 14, 17, 49

**TET** ten-eleven-translocation. 8

**TF** transcription factor. xc, 3–5, 7, 13, 21, 50, 51, 87

**TG** triglycerides. 47

**TLR** toll-like receptor. 7

**TNBS** trinitrobenzene sulfonic acid. 18, 50

**TNFα** tumor necrosis factor alpha. 16–18, 24, 39

**TNFR** tumor necrosis factor receptor. 7

**TRA** tissue-restricted antigen. 2, 4

**tRNA** transfer ribonucleic acid. 6

**TSDR** T$_{REG}$ cell-specific demethylated region. 5

**VAT** visceral adipose tissue. xc, 12–14, 16–18, 25, 36, 48, 50

# Summary

# List of Figures

# Chapter 1

# Immune regulation by T$_{\text{REG}}$

## 1.1 Diversity of adaptive immune system

### 1.1.1 T cells and B cells

Immune system is broadly divided into 2 interconnected branches: the innate and adaptive arms with the former encompassing cell types and mechanisms acting in immediate response to an exogenous stimulus and the latter requiring "adapation" to to the stimulus, usually upon interactions with the innate system. Indeed, cell types from adaptive immune system are characterized by the expression of highly variable receptors allowing to "adapt" to the stimulus to endow the cell types expressing them with an optimized response. The two main types of cells of adaptive immune system are T and B lymphocytes respectively expressing the T-cell receptor (TCR) and the B cell receptor (BCR).T cells exert either effector of cellular immunity and/or act regulators of the immune response and B cells producing membrane (BCR) or soluble immunoglobulins are involved in humoral immunity and regulation. Conventional TCR and BCR mostly recognize specific peptides but can also recognize other types of structure such as oligosaccharides, glycopeptides, glycolipids [1, 2, 3].The precise delineation of innate vs adaptive immunity is difficult to establish for some non conventional lymphoid subsets expressing low variability receptors such as natural killer T cell (NKT) mucosa-associated invariant T cell (MAIT), and γδT cell cells usually recognizing higly specific antigen structures [4, 5, 6, 7]. Furthermore, some immune cells of lymphoid origin do not express variable receptors and thus are rather associated to innate immunity: namely innate lymphoid cells (ILC) and natural killer cell (NK) [8, 9].

T cells are matured in the thymus [3]. Common lymphoid progenitors, which migrate to the thymus from the bone marrow, proliferate and start to express genes required for generation of TCR. TCR is a protein of immunoglobulin superfamily encoded by α, β, γ, δ gene loci, each containing V (variable), J (junction) and C (constant) segments. β and δ loci also contain D (diversity) segments. T cell progenitors undergo series of rearrangements in V, J segments of TCR genes, facilitated by recombination activating gene (RAG)1 and RAG2 proteins forming V(D)J recombinase enzymatic complex [10]. Vast array of TCR gene variants formed by rearrangement dictates potential amino acid sequence diversity and antigen specificity of TCR of an individual T cells [11]. At this stage T cells express CD3, CD4 and CD8 co-stimulatory molecules on their surface and are called "double-positive" and are found in the cortex of the thymus. Progenitor cells are then selected to become single-positive T cells – either CD4$^+$or CD8$^+$ [12]. During this process, which is called "positive selection", cortical thymic epithelial cell (cTEC) present complexes of peptide-major histocompatibility complex (MHC)-I

or -II molecules to T cells, eliminating those which do not bind to either of the two. Depending on the affinity of the remaining T cells, they receive a signal which triggers CD4$^{+}$ phenotype for cells with MHC-II affinity or CD8$^{+}$ for MHC-I. Then, after CCR7-dependent migration to the medulla of the thymus, CD4$^{+}$and CD8$^{+}$ single-positive T cells are subjected to negative selection. Medullary thymic epithelial cell (mTEC) present them self-peptides, which are found in peripheral tissues, also called tissue-restricted antigen (TRA). Cells with high affinity of their TCR to these antigens are deleted Figure 1.1. This process is also called "central tolerance" in contrast to "peripheral tolerance", where T$_{REG}$ cells play their role, and will be discussed later.

First stages of B cells development take place in the bone marrow [13]. Pro-B cells, derived from common lymphoid progenitor as T cells, undergo rearrangements of their heavy-chain μ BCR genes to become pre-B cells. The process of rearrangement is similar to that described for T cells. Pre-B cells express recombined IgM class heavy chain part of the B cell receptor and a surrogate light chain. Light chain immunoglobulin κ or λ genes are rearranged at this stage and pre-B cell becomes immature B cell to go through negative selection and BCR editing stages at which self-reactive B cells are eliminated. Eventually, the cell becomes mature B cell. At this terminal developmental stage mRNA products of heavy and light chain immunoglogulin genes are linked to the mRNA of either IgM or IgD constant segments via alternative splicing [14]. This results in surface expression of antigen-specific IgM and IgD by naive B cells. Mature naive B cell leaves the bone marrow to stay in a secondary lymphoid organ and activate on encounter of a specific antigen.

After naive T cells leave the thymus, they travel to secondary lymphoid organs and are inactive until presented to an antigen with sufficient affinity by a professional antigen presenting cell (APC) [15]. Together with MHC-antigen complex, which binds to TCR, CD80 and CD86 molecules on the surface of APC are necessary for activation of a T cell. These molecules interact with CD28 costimulatory protein, which induces PI3K-Akt signaling pathway in T cells, and in turn leads to expression of activation and survival genes and stabilization or nuclear translocation of proteins required for further action and differentiation of the cell [16]. One of the main players of activation machinery are NFAT family members, whose nuclear localization is preserved by Akt. NFAT controls many genes, critical for T cell function including interleukin-2 (IL-2) – one of their main regulators of expansion and survival. At the same time, translocation of nuclear factor kappa-B (NFκB) to the nucleus, caused by Akt, promotes expression of survival genes like Bcl-6.

Following activation, T cells undergo processes of extensive mitotic division (or clonal expansion) and terminal differentiation, which also means specialization to respond appropriately to the type of activating agent, in part by gaining distinct spatial preference and behavior patterns. The trigger for these events is cytokine environment surrounding a T cell clone during activation. This type of cell fate is well illustrated by diversity of CD4$^{+}$ cell subsets referred to as T$_{H}$ cells [17].

Originally, the classification of T$_{H}$ cells was binary. T$_{H}$1 and T$_{H}$2 cells participate in distinct types of immune responses [18]. T$_{H}$1 phenotype of a T cell was induced by interleukin-12 (IL-12) and characterized by interferon-γ (IFN-γ) secretion. These cells are important in deploying a cytotoxic CD8 T cells response against intracellular pathogens like viruses or some kinds of bacteria. In contrast, T$_{H}$2 cells, induced by interleukin-4 (IL-4) and secreting IL-4, interleukin-5 (IL-5) and interleukin-13 (IL-13) were shown to play a role in coping with extracellular pathogens like helminths. As the studies evolved, T$_{H}$17 cells were described as crucial for anti-fungal immunity. One more special trait of T$_{H}$17 is that they contribute to the regulation of commensal microorganisms the population size and composition in the intestine [19]. T$_{H}$17 signature cytokines are interleukin-17 (IL-17) and

interleukin-22 (IL-22). $T_H9$ and $T_H22$ cells secrete IL-9 and IL-22 respectively and are both important for intestinal homeostasis and colitis-like inflammation [20] [17]. T folicular helper ($T_{FH}$) cells are concentrated in germinal centers of secondary lymphoid organs and function as B cells activators by producing IL-21 and antibody class switchers by IL-4 secretion. Thus greatly influencing mounting of humoral immune response. These are induced by IL-21 and IL-6.

The common scheme of naive T cells specialization upon TCR and cytokine receptor stimulation includes immediate engagement of proteins from the signal transducer and activator of transcription (STAT) family. In turn, these proteins channel the signal further by activating the master TF. Development and function of the various T cell lineages relies on the expression of specific TFs, which orchestrate most of the transcription network. For instance, IL-12, through STAT4, activates TF T-bet, which induces IFN-γ expression [21]. Exposure of T cells to IL-4 leads to STAT6-mediated engagement of GATA-3 – an epigenetic modifier of $T_H2$ cytokines genes [22]. Similarly, IL-6-STAT3-RORγt-IL-17 pathway works in $T_H17$ cells and $T_{FH}$ cells start to express characteristic surface molecules like PD-1 upon activation of Bcl-6 [23] [24].

## 1.2 Introduction to immune regulation

The benefits of adaptive immune system are high specificity and enormous diversity of it's reactions targeted against pathogens. However, probably the most critical mechanism which makes the whole system efficient is it's ability to hinder attacking of self also called self-tolerance. Processes of self-tolerance are usually classified as central and peripheral. Central tolerance includes negative selection by elimination in the thymus of T cells bearing TCR with high affinity for self-proteins. Peripheral tolerance (outside the thymus) is achieved by several mechanisms. First, prolonged TCR engagement, which happens in case of self-peptide recognition in peripheral tissues induces anergy in T cells. Second, two signals provided py APC are required to turn naive T cells into reactive cells: a cognate peptide-MHC complex which interacts with TCR and CD80 and CD86 molecules binding CD28 (T cells costimulatory surface molecule). This dependancy on APC largely reduces unsolicited T cell activation. Yet another mechanism is at play to fully control adaptive immune response. It is dependent on a specialized population of $CD4^+T$ cells with ability to suppress activation of other immune cells. These cells are called regulatory T cell ($T_{REGS}$). In addition to providing self-tolerance $T_{REGS}$ are involved in resolution of the inflammatory response once elimination of the pathogen is achieved, as well as in prevention of excessively strong immune reactions.

### 1.2.1 History of $T_{REG}$ discovery

$T_{REG}$ cells were discovered using thymectomy of 3-day old mice. These studies demonstrated that after removal of the thymus mice suffer from wasting disease and sterility in females [25, 26]. That was explained later by a finding, that thymus is actually necessary to establish and maintain self-tolerance in neonatal mice. Wasting and sterility were an indication of autoimmune processes, which first manifested in the intestine and ovaries. Adoptive transfer of splenocytes or thymocytes from adult mice into thymectomic neonatal mice reduced autoimmune reactions. Furthermore, thymic epithelium transplant experiments displayed the presence of a lymphocyte population responsible for graft versus host tolerance. Thymic epithelium from quail embryo was transplanted into chicken subjected to thymectomy at early age, before thymus was colonized by hematopoietic stem cell (HSC). That led to generation of functional T cells tolerant to grafts from the donor quail in the recipient chickens [27]. In similar transplantation studies tolerance. As a result, it was concluded that a population of

thymus-derived lymphocytes generated during first three days after birth was capable of providing immune tolerance [28].

Further research aimed to define and describe this population more specifically. Initially, it was understood that suppression was an attribute of CD4$^+$ T cells which are antigen-experienced, but not of naive T cells , which are, in contrast highly pathogenic. Suppression of colitis was observed when CD45RB$^-$CD4$^+$ T cells were adoptively transferred into athymic rats or mice with severe combined immunodeficiency (SCID) together with CD45RB$^{high}$CD4$^+$T cells. The population was soon identified more precisely as CD4$^+$CD25$^+$ T lymphocytes [29]. They alone could ameliorate wasting disease in mice and were named "regulatory T cells". Conversely, non-suppressive CD4$^+$ T cells are now referred to as "conventional T cells". CD25 is the α-chain of IL-2 receptor. It's high expression on $T_{REG}$ surface allows response to IL-2, a critical survival and proliferation factor. Although CD25 was the first true surface marker of $T_{REG}$ cells to be identified, it was also not exclusively expressed by only $T_{REG}$. Later, FOXP3 was described as a distinctive marker of $T_{REG}$ cells, which will be discussed below [30, 31].

## 1.3    Signature characteristics of $T_{REG}$

### 1.3.1    Selection of $T_{REG}$ in the thymus

Although most of the highly self-reactive T cells are eliminated during negative selection in the thymus, some of them survive and develop into a specific population of thymus-derived $T_{REG}$ or t$T_{REG}$ [32]. Several studies utilizing expression of $T_{REG}$-derived TCR in conventional T cell ($T_{CONVS}$) suggest that $T_{REG}$ differentiate mainly from cells bearing TCR with TRA-affinities and -avidities higher than those of normal T cells, but lower than self-reactive T cells clones found in pathology. Autoimmune regulator protein (AIRE) expression in mTEC is particularly important for appropriate intrathymic presentation of peripheral tissue antigens to $T_{REG}$ precursors [33]. Further development along $T_{REG}$ fate requires that a self-reactive cell expresses FOXP3. The strength of TCR stimulation positively correlates with expression level of downstream nuclear receptors from NR4A family [34]. Together with some other transcriptional and epigenetic regulators such as c-Rel, these proteins either induce early stage stable FOXP3 expression and contribute to the regulation of *Foxp3* gene, or trigger negative selection of a cell. As observed in early works, CD25 (IL-2R α-chain) is highly expressed on the surface of $T_{REG}$. $T_{REG}$ induce CD25 as early as at the stage of thymic precursors in contrast to $T_{CONV}$ cells, which upregulate CD25 only upon TCR engagement during activation [35]. It is likely that$T_{REG}$ display higher expression of CD25, together with other TCR-dependent activation molecules like cytotoxic T-lymphocyte-associated protein 4 (CTLA-4) compared to $T_{CONV}$ due to generally higher TCR-signalling activity in $T_{REG}$ as a result of thethymic selection of high-affinity clones. CD25 and it's ligand IL-2 were shown to be dispensable for $T_{REG}$ commitment in the thymus, but critical for maintaining steady FOXP3 expression level and thus providing t$T_{REG}$ stability during their further development and differentiation [36]. In line, *Il2ra* deficiency in mice led to a 50% decrease in t$T_{REG}$ [37]. Some other common γ-chain cytokines IL-7 and IL-15 participate in $T_{REG}$ generation, but are less critical than IL-2 . Although many factors contributing to TCR signaling and FOXP3 regulation at early stages of $T_{REG}$ development were described, one of the central questions about self-tolerance remains largely unanswered: "How do self-reactive $T_{REG}$ precursors escape negative selection?" [38] Figure 1.1.

### 1.3.2    FOXP3 is the main transcription factor of $T_{REG}$

To date, FOXP3 is the most specific marker to distinguish $T_{REG}$ cells from other CD4$^+$T cells. The first clue that connected $T_{REG}$ with FOXP3 came from studies which associated a mutation in human
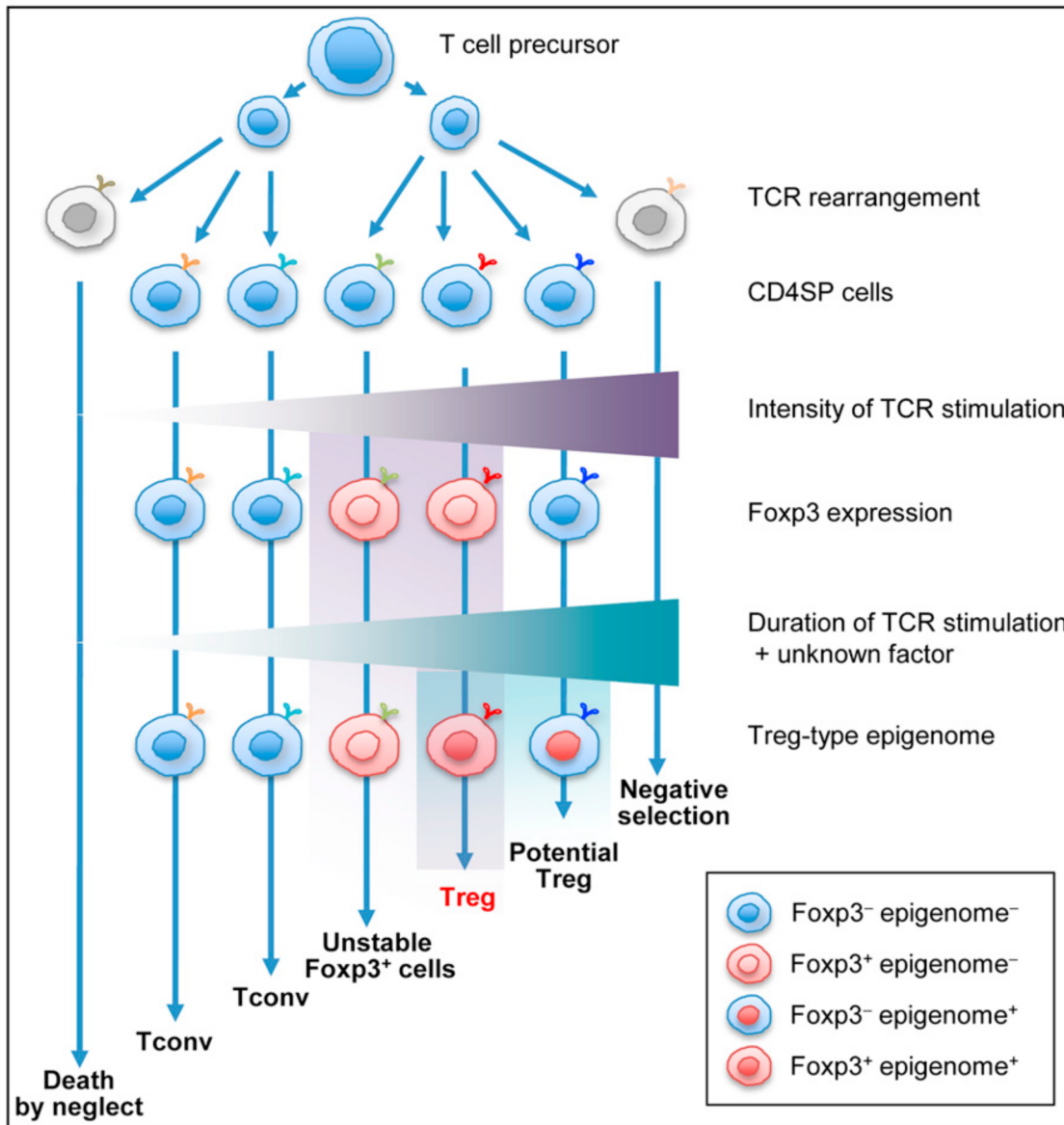
Figure 1.1 – A model for T_REG development in the thymus [39].

FOXP3 gene with immunodysregulation polyendocrinopathy enteropathy X-linked (IPEX) syndrome as well as those associating *Foxp3* mutation with scurfy phenotype in mice [40, 31]. IPEX humans and scurfy mice are both characterized by numerous manifestations of systemic autoimmunity as a result of uncontrolled expansion of CD4$^+$T cells. FOXP3 might be called a master TF of T$_{REG}$ cells. Its pivotal significance is illustrated by the fact that retroviral *Foxp3*-transduction in naive T cells triggers suppressive T$_{REG}$-program. *Foxp3* expression is largely restricted to T$_{REG}$ cells, and plays its major role in these cells as mice with whole-body *Foxp3* deficiency display a phenotype identical to those with T cell-specific deletion [41]. Description of *Foxp3* locus organization is important for understanding of how T$_{REG}$ development and differentiation is guided by FOXP3. *Foxp3* locus contains the following regulatory regions: a *Foxp3* promoter, four enhancer conserved non-coding sequence (CNS) (0, 1, 2, 3). Each of these regulatory regions, especially enhancers, were assigned responsibilities for particular aspects of T$_{REG}$ development, differentiation or stability by several dedicated studies [42, 43, 44]. Engagement of the proximal promoter and a super enhancer CNS0 provide the initial "switch" allowing cell survival and opening of chromatin of other regulatory regions. Publications from Alexander Rudensky laboratory have demonstrated consequences of deletion of each *Foxp3* CNS [44]. CNS3 deletion largely reduced thymic generation of T$_{REG}$ despite mice remaining healthy. On the other hand, CNS1 and CNS2 were dispensable T$_{REG}$ development in the thymus, but contributed at later stages. CNS2 demethylation is now considered a marker of committed T$_{REG}$ lineage and is required for stabilization of FOXP3 expression during T$_{REG}$ proliferation. It is also referred to as T$_{REG}$ cell-specific demethylated region (TSDR). CNS1 deletion led to reduced numbers of T$_{REG}$ in mucosa-associated lymphoid tissue (MALT) of the intestine. In agreement with results of these loss of function studies, transcription factors which bind to described regulatory regions act at respective T$_{REG}$ development stages. As already mentioned, NR4A proteins translate TCR stimulation strength into the decision on T$_{REG}$ commitment or clonal deletion by binding or not to *Foxp3* promoter. Roughly at the same developmental stage, binding of SATB1 to CNS0 turns *Foxp3* regulatory regions into poised state thereby permitting other factors to access their binding sites [42]. c-Rel binds at CNS3 and CNS2 sequences and acts in multiple ways to organize chromatin, thus forming c-Rel containing enhanceosome at *Foxp3* promoter to demethylate CNS2 and facilitate *Foxp3* induction by TCR activation. Forkhead box O1 (FOXO1) and FOXO3 proteins bind to the promoter, CNS1 and CNS3 and control transcription of *Foxp3* and other T$_{REG}$-specific genes. c-Rel deficiency as well as T cell-specific double deficiency in *Foxo1* and *Foxo3* significantly reduce tT$_{REG}$ population size. Several factors act through CNS2, so important for T$_{REG}$ commitment. NFAT binds to CNS2 transmitting TCR activation signal and STAT5 responds to IL-2 (and IL-7, IL-15) receptor ligation. Conversely, STAT3 activated by IL-6 and bound to *Foxp3* CNS2 has an inhibitory effect on *Foxp3* transcription. CNS2 senses many other cues through several other factors. Other factors bind to CNS1 and allow T$_{REG}$ generation in periphery. Namely, Sma/mothers against decapentaplegic homolog 3 (SMAD3) provides *Foxp3* induction in response to tumor growth factor beta (TGF-β) binding to its receptor. Activator protein 1 (AP-1), known as a broad regulator, capable of responding to both TGF-β and IL-2 also activates *Foxp3* transcription through CNS1 [45].

FOXP3 is a DNA-binding protein from forkhead box family acting as a transcriptional regulator. It's amino acid sequence comprises 4 domains: repressor, zinc-finger, leucine-zipper and DNA-binding forkhead (or winged helix). It was shown to form homodimers and interact (and form transcriptional complexes) with numerous proteins including TF (FOXO1, FOXO3, NFAT, RUNX-1, RORα, retinoic acid receptor-related orphan receptor gamma t (RORγt)) and chromatin modifiers such as several histone deacetylase (HDAC) [46, 47, 48, 49, 50]. Interactions generally result in repression of proinflammatory programs.

### 1.3.3   **Foxp3-dependent and -independent transcriptional and epigenetic characteristics of T$_{REG}$**

Experiments with induced *Foxp3* deficiency demonstrated that FOXP3 was dispensable for generation of T$_{REG}$ precursors, but was required for suppressor function of mature T$_{REG}$ cells. While many characteristics of T$_{REG}$ such as CD25 and CTLA-4 expression are established prior to *Foxp3* induction. However, when expressed, FOXP3 further promotes and maintains this characteristic phenotype. On the other hand, FOXP3 acts as a genetic suppressor to block triggering of other possible T$_{H}$-differentiation fates in T$_{REG}$ (for example T$_{H}$17) [51]. FOXP3 functions both directly as a transcription factor and as an epigenetic modifier. Only about 15% of FOXP3-dependent genes are direct targets of the protein, the rest is thought to be controlled indirectly through other transcription factors as well as epigenetically. FOXP3 not only induces T$_{REG}$ gene expression program, but is also required to keep it stable throughout the lifetime of the cell, as shown by conditional deletion of *Foxp3* in developed T$_{REG}$ cells. On the other hand, the most recent understanding of T$_{REG}$ cell defines FOXP3 as central, but neither sufficient, nor absolutely required to define T$_{REG}$-cell signature [52]. Factors like EOS, IRF4, GATA-1... are equally important in this process. T cells which lose FOXP3 expression experimentally or under natural conditions were termed "exT$_{REG}$" and are capable of producing inflammatory cytokines such as IFN-γ or IL-17 thus becoming pathogenic cells [53, 54]. FOXP3 may be an activator or a repressor of genes transcription, and specific histone modifications (H3K9/14ac, H3K4me3 or H3K27me3, H3K9me3) are associated with FOXP3-mediated gene control . Interestingly, sets of genes controlled by FOXP3 differ between thymus-generated tT$_{REG}$ (a bigger set) and pT$_{REG}$ peripherally generated from naive T cells , (See section 1.5) (a smaller subsetset). However, some genes which define T$_{REG}$ surface phenotype and signaling traits are regulated in both T$_{REG}$ subsets (*Ctla4*, *Il2ra*, *Nrp1*, *Icos*, *Map3k8*, *Pde3b*).

## 1.4   **Functions of T$_{REG}$ cells and mechanisms of suppression**

The most extensively studied function of T$_{REG}$ is direct or assisted suppression of effector T cells activation and proliferation. As for other CD4$^{+}$T cells, effector function requires TCR activation by a specific antigen-MHC-II complex and costimulatory molecules on the surface of APC [55]. Although numerous mechanisms of T$_{REG}$-mediated suppression were proposed, their respective importance remains elusive, as well as specific triggers of a particular type of suppression. T$_{REG}$ may exert their inhibitory effect on T cells or affect APC, often dendritic cell (DC), in turn again altering T cells activation. Actions of T$_{REG}$ on other immune cells are often classified as contact-dependent and contact-independent [56]. As T$_{REG}$ fail to suppress responder cells *in vitro* when they are separated by a semi-permeable membrane, contact-dependent suppression is described better and is sometimes considered a core mechanism for T$_{REG}$-mediated immunosuppression [57]. At least *in vitro*, contact-dependent suppression is described as a two-step process [55, 58]. The first step involves aggregation of T$_{REG}$ around immature DC, dependent on lymphocyte function-associated antigen 1 (LFA-1)-intercellular adhesion molecule 1 (ICAM-1) interaction and requiring MHC-II expression by DC. The second step relies on additional engagement of CTLA-4. CTLA-4, expressed on T$_{REG}$ cell surface is capable of binding to costimulatory molecules CD80 and CD86 on APC or T cells. In response to this interaction, responder cells may downregulate CD80 and CD86 and thus become less potent in activating T$_{CONV}$ [59]. It was demonstrated that a CTLA-4-expressing cell can capture CD80 and CD86 molecules from the surface of APC and degrade it during the process called trans(-endo)cytosis [60]. Mechanical competition for CD80/CD86 of APC between CD28 of T$_{CONV}$ and CTLA-4 of T$_{REG}$ also plays a suppressive role. Moreover, some DC secrete indoleamine 2,3-dioxygenase (IDO), an enzyme which catabolizes tryptophan into kynurenine and several other compounds in response to CTLA-4 binding [61]. It was shown that both tryptophan starvation of T cells and direct action

of metabolites on them has immunosuppressive effects. Tryptophan starvation is sensed by general control nonrepressed 2 (GCN2), which blocks protein synthesis by binding transfer ribonucleic acid (tRNA) molecules upon activation. GCN2 pathway contributes to both inhibition of T$_{CONV}$ activation and to T$_{REG}$ generation. Kynurenine, the product of IDO reaction, may affect T cellsdirectly. A ligand-dependent TF aryl-hydrocarbon receptor (AhR) was demonstrated to favor CD4$^+$T cells polarization into T$_{REG}$ cells in response to kynurenine, especially in T$_H$17/T$_{REG}$ plasticity context and generate pT$_{REG}$ cells from naive T cells. There are several other known molecules involved in DC-dependent suppression.

CD40 is a costimulatory molecule expressed on DC surface. Blocking of CD40 leads to absence of DC suppression by T$_{REG}$ [62]. However, suppression itself doesn't result in down-regulation of CD40 on DC.

A20 is an ubiquitin-editing enzyme. It down-regulates toll-like receptor (TLR) and tumor necrosis factor receptor (TNFR) signaling and is called "an antigen presentation attenuator" [63]. Silencing of it's transcription results in hyperactivation of T cells by DC and prevents DC suppression by T$_{REG}$ cells.

Neuropilin-1 (NRP1), a surface molecule on T$_{REG}$ cells and its gene expression is controlled by FOXP3. It promotes long MHC-II dependent interactions of T$_{REG}$ cells with immature DC in the absence of inflammatory stimuli, thereby allowing "default" tolerance. T$_{REG}$ can be activated by a much lower amount of antigen, than T$_{CONV}$, a process likely aided by NRP1 [64].

Lymphocyte activation gene 3 (LAG3) – an inhibitory immune checkpoint molecule expressed on T$_{REG}$ which binds to MHC-II on DC. It's blocking results in decreased supressive activity of T$_{REG}$ [65].

MHC-II expressing T$_{REG}$ were found in humans. They represent a mature population involved in contact-dependent suppression. It was also proposed that this population might provide homeostatic maintenance of other T$_{REG}$ by presenting them self-antigens. It was also found that DC are skewed towards interleukin-10 (IL-10)-secreting tolerogenic phenotype after interaction with T$_{REG}$, compared to interleukin-6 (IL-6) production in response to interaction with T$_{CONV}$ [66].

One more described mechanism involves direct killing of DC by T$_{REG}$ with the help of perforin secretion (similar to their direct targets – T cells) [67]. Another molecule expressed by T$_{REG}$ cells is a β-galactoside binding protein galectin-1. This protein secreted by T$_{REG}$ may induce cell cycle arrest and apoptosis in DC during contact-dependent suppression. When interacting directly with target T cells, T$_{REG}$ either utilize perforin- or granzyme-mediated killing. Alternatively, they can deliver high concentrations of cyclic adenosine monophosphate (cAMP) into effector T cells, which leads to a decrease in IL-2 production by the latter. Moreover, adenosine may be generated pericellulary by CD39 and CD73 nucleases, expressed by T$_{REG}$, also delivering negative signal to T cells. However, these mechanisms, mainly targeting T cells may also contribute to DC suppression.

Another mechanism of T$_{REG}$ suppression is secretion of immunosuppressive cytokines. The three well-described cytokines produced by T$_{REG}$ cells are IL-10, TGF-β and interleukin-35 (IL-35). Mice whole body or T cell-restricted TGF-β1 deficiency develop T cell-mediated autoimmune disease soon after birth. Significant amounts of TGF-β are produced by T$_{REG}$ in both soluble and membrane bound forms. The role of T$_{REG}$-secreted TGF-β stays controversial. Especially it is so *in vitro*, as earlier studies used blocking of TGF-β and found contrasting results: some research groups found partial abrogation of suppression upon TGF-β blocking, while others claimed this cytokine was dispensable for T$_{REG}$ function *in vitro* [68]. *In vivo*however, it seems to be clear that T$_{REG}$-expressed TGF-β is needed for control of T$_H$17 response in the intestine during colitis. Most groups agree that the main function of TGF-β is rather to promote activity and stability of T$_{REG}$ cells through their surface receptor and generate T$_{REG}$ cells in periphery. The latter is in agreement with the fact that TGF-β signaling-controlled protein SMAD3 activates FOXP3 via binding to CNS1 indispensable for pT$_{REG}$. Turning naive T cellsinto T$_{REG}$ may likely be triggered by both soluble TGF-β secreted by multiple cell types in periphery and by surface membrane-bound form of TGF-β on T$_{REG}$ (in a so-called "infectious

tolerance" process) [69, 56].

IL-10 is probably the least controversial among $T_{REG}$ cytokines. It was shown to be important for immunosuppression by $T_{REG}$ *in vitro*, in T cell transfer colitis and experimental allergic encephalomyelitis (EAE) models. Mice with $T_{REG}$-specific inactivation of *Il10* display spontaneous inflammation at environmental interfaces. Several other studies which used models of IL-10 or IL-10R deletion all revealed a key role of this cytokine in the intestine. What is more, during skin inflammation $T_{REG}$ needed to sense IL-10 to restrain IFN-γ production by T cells. [69, 56, 70]

IL-35 is a protein from IL-12 family (a pairing between Epstein-Barr virus induced gene 3 (EBI3) and p35 of IL-12) which is expressed by thymus-derived $T_{REG}$ cells. IL-35 deficient $T_{REG}$ are less efficient in suppressing colitis and in *in vitro* suppression assays [71].

Another suppression mechanism is based on the fact that $T_{REG}$ cells are able to capture large amounts of IL-2 using high-affinity IL-2R on their surface, consisting of CD25, CD122 and CD132 subunits. Doing this they deprive other T cellsof IL-2, a lymphokine critical for effector T cell differentiation, thereby inducing apoptosis [72].

## 1.5  Thymus derived and Induced T<sub>REG</sub>

Apart from being generated in thymus, $T_{REG}$ cells can differentiate in periphery from naive T cells. the main factors which were identified to trigger FOXP3 expression and suppressive properties in naive T cells are TGF-β and IL-2 [73]. $T_{REG}$ can be differentiated in such a way *in vitro* and are then called induced regulatory T cell (i$T_{REGS}$). $T_{REGS}$ induced in a similar manner *in vivo* are referred to as peripherally generated regulatory T cell (p$T_{REGS}$). p$T_{REGS}$ are a minor population compared to t$T_{REG}$. However, they are enriched at mucosal sites such as intestine and lung. As mentioned above, FOXP3 induction in i$T_{REGS}$ and p$T_{REGS}$ is dependent on CNS1 enhancer regulatory element of *Foxp3*. Upon ligand binding, TGF-β receptor causes engagement of SMAD2 and SMAD3, which oligomerize with SMAD4. CNS1 contains two Sma/mothers against decapentaplegic homolog (SMAD)-binding sites confirmed to be functional [74]. Moreover, mice lacking CNS1 displayed $T_H2$-pathologies in the lung and intestine and a decline in p$T_{REG}$ numbers. p$T_{REG}$ also appear in the intestine upon exposure to retinoic acid (RA). RA binding to retinoic acid receptor (RAR) and retinoic X receptor (RXR) and binding of these nuclear receptors to CNS1 facilitates SMAD proteins recruitment to their *Foxp3* CNS1 sites [75, 44]. Short chain fatty acids (SCFA) are abundant in the intestine, as they are products of dietary fiber fermentation by commensal bacteria. Mice with no gut microbiota displayed a decline in p$T_{REG}$ population, whereas SCFA treatment of these mice restored gut $T_{REG}$ numbers. SCFA feeding also protects mice from experimental colitis. Colonic $T_{REG}$ express GPR43, a receptor for SCFA, which is involved in the process of protection against colitis by SCFA. SCFA butyrate and propionate are capable of promoting p$T_{REG}$ generation through through H3 acetylation in *Foxp3* promoter and CNS via HDAC inhibition [76]. On the other hand, SCFA cannot induce i$T_{REG}$ *in vitro*. It is likely that CD103$^+$DC in the *lamina propria* of intestine are one of the main p$T_{REG}$ inducers. They provide antigens and signals such as TGF-β and RA needed for p$T_{REG}$ generation. It has been reported, that p$T_{REG}$ may be distinguished from t$T_{REG}$ by expression of NRP1 and HELIOS on the surface of the latter. p$T_{REG}$ are thought to possess less stable FOXP3 expression than t$T_{REG}$. This is dependent on CNS2 CpG islands demethylation, to a greater extent in t$T_{REG}$. However, p$T_{REG}$ may display stable FOXP3 expression often accompanied by RORγt expression. Mechanisms accounting for CNS2 demethylation include binding of FOXP3-CBF-β-RUNX-1 or CREB/ATF complexes to CNS2

[77], as well as facilitated by ten-eleven-translocation (TET) enzymes which mediate demethylation and may be aided by vitamin C and H$_2$S [78, 79].

## 1.5.1   Non-Foxp3 regulatory cells

Some subsets of regulatory T cells do not express FOXP3.

Tr1 cells are CD4$^+$FOXP3$^-$ T cells which express IL-10 and involved in graft tolerance and allergic responses. These cells may also secrete TGF-β, IL-5 and IFN-γ as well express molecules such as LAG3 on their surface [80]. T$_H$3 cells are regulatory cells which are characterized by expression of latency-associated peptide (LAP) and production of TGF-β, IL-4 and IL-10. They facilitate oral tolerance and are also capable of preventing EAE induction. These suppressive effects are mainly realized through TGF-β. T$_H$3 are thought to differentiate in the presence of high levels of IL-4, IL-10 and TGF-β commonly observed in the intestine. That was also confirmed *in vitro.* [81]

Among CD8$^+$ T cells there are at least two known subsets of T$_{REG}$ . The first type are cells bearing TCR against antigens presented by MHC class lb Qa-1 protein. Peptides of host and foreign origin may be presented by this molecule. The interaction of CD94/NKG2 inhibitory molecules on these cells with lb Qa-1 is necessary for controlling T$_{FH}$ and preventing lupus-like autoimmune reaction. The control of T$_{FH}$ cells is realized through perforin expression [82].

The second type of CD8$^+$ T$_{REG}$ are CD8$^+$CD28$^-$ T$_{REG}$ directly interact with DC and inhibit activation of effector T cells by the latter [83].

A minor population of CD4$^-$CD8$^-$ double-negative T$_{REG}$ were also found, which could suppress T cell proliferation *in vivo* and *in vitro* in an antigen-specific manner. These cells express αβTCR, but not CD4, CD8 or NK cell markers. These cells can acquire MHC molecules from the antigen presenting cells by trogocytosis. Thus, they can later present fragments of extracted peptides to other T cells without a costimulatory signal, which possibly causes apoptosis. In addition, they may express CTLA-4 and thereby suppress APCs [83, 84].

Regulatory functions of γδT cells were also identified. Their presence was shown that mice lacking γδT cells did not manage to control reactions to pathogens and developed excessive immune responses. Autoimmune reactions were also present in these mice as shown in the model of systemic lupus erythematosus (SLE) and by spontaneous dermatitis development in some cases. Whatever context, regulatory γδT cells usually inhibit processes triggered by αβT cells [85]. Potential mechanisms of immunoregulation by γδT cells may rely on high mRNA-expression or secretion of some molecules associated with suppression in other cells (IL-4, IL-10, TGF-β). γδT cells also express cytotoxic granzymes A, B, which together with FAS-ligand allow them to achieve killing of effector cells expressing FAS [86, 87]. One more γδT cells -expressed molecule associated with immune regulation by unknown mechanism is thymosin-β4 [88, 89].

NKT cells are subdivided in two subcategories: IFN-γ-inducing proinflammatory cells or IL-4, IL-10, IL-13-inducing anti-inflammatory cells [90, 91]. NKT cells might provide tolerance in allergy, involved in protection from autoimmunity and graft allograft tolerance during transplantation [92, 93]. Of note, NKT cells may express CD25, like CD4$^+$ T$_{REG}$, in humans and likely in mice during activation [94].

# Chapter 2

# Immune system of non-lymphoid tissues

## 2.1 Lymphocytes in NLT

In addition to blood and lymphatic vessels and lymphoid organs, NLT contain large amount of immune cells [95].

Tissue-resident immune cells, in particular T cells, were widely studied in the context of immune memory. For instance, most of activated antigen-specific T cells are eliminated after successful destruction of tissue pathogens, but a small proportion of memory cells is kept to mount a faster antigen-specific immune response should infection reoccur [96]. Antigen-specific T lymphocytes recirculate and reach tissue-draining lymph nodes through afferent lymphoid vessels. They then become able to (re)populate the same non-lymphoid tissue presumably through the blood. even when experimentally isolated from local lymphatic vessels and injected back into the blood [97]. Surface adhesion molecules and chemokine receptors drive antigen-specific T lymphocyte migration to various tissues. Cutaneous lymphocyte antigen (CLA) is required for cells to migrate to inflammed skin, CCR9, $\alpha_4\beta_7$ and some others – to the intestine and CCR7 is a marker for migration to spleen and other secondary lymphoid organs (SLO) [98, 99]. Naive T cells migrate in a CD62L-dependent manner to lymph nodes where they might encounter their cognate antigen [100, 101]. Two subtypes of recirculating antigen-experienced memory T cells are distinguished in humans based on expression of CCR7. They differ for homing to SLO as well asign effector function and proliferation ability. Central memory T cell ($T_{CM}$) express CCR7, while effector memory T cell ($T_{EM}$) do not. By contrast, resident memory T cell ($T_{RM}$) do not migrate but stayed inside non-lymphoid tissues [102, 103]. $T_{RM}$ cells are potent effectors and might be confused with effector cells, recently migrated to a tissue. A T cell population of displaying surface effector phenotype including CD69 and expressing high levels of cytolytic molecules and remains present in the intestine and in the skin after infection is resolved. Interestingly, $T_{RM}$ do not migrate to their organ of origin after transfer into a new host [104]. Full understanding of $T_{RM}$ and other non recirculating T cell biology in general is not yet well established.

Regarding $T_{RM}$ subsets, mouse intestinal CD8$^+$ T cells express high levels of CD103 and β7 (as well as CD69) integrin expression upon viral infection. Expectedly, these cells are not found in either spleen or blood, thus are likely not circulating [105]. Intestinal T cells adoptively transferred into new host do migrate back to the intestine [106].

Likewise, in parabiosis experiments resident T cells from partners neither mix, nor are found in the joined circulation [95, 107]. These transfer and parabiosis methods, however, are vulnerable to artifacts. engraftment of biopsy from psoriasis patients into immunocompromised mouse displayed

spontaneous development of T cells-driven psoriasis-like symptoms with no T cells migration observed [108]. However, *in vivo* intravascular T cells staining and *in situ* labeling for imaging brought the very "concept" of $T_{RM}$ into question by demonstrating that 96% of CD8$^+$ T cells isolated from lung tissue, for instance, were actually from alveolar microvasculature even after perfusion [109, 95]. Only small population of CD8$^+$ cells was not labelled intravascularly and displayed CD103$^+$ phenotype.

It is not clear whether resident T cells are found because of retention of circulating cells in NLT or emerge separately [110].

## 2.2 Regulatory T cell in non-lymphoid tissue

Similarly to memory T cells $T_{REG}$ circulate in the blood and lymphoid system and home to NLT. $T_{REG}$ are subdivided into:

**Central or naive CD62L$^+$CD44$^-$CCR7$^+$ $T_{REG}$** found in lymphoid tissues;

**Effector or activated CD62L$^{lo}$CD44$^{high}$CCR7$^{lo}$CD25$^{high}$$T_{REG}$** which temporarily infiltrate sites of inflammation and NLT, often also characterized as KLRG-1$^+$;

**Tissue-resident $T_{REG}$** which are non-recirculating long-term NLT residents [111]. Their markers include those of effector $T_{REG}$ and additional tissue-specific molecules.

As for memory T cells, distinction between these is quite blurry,and is still evolving. In the next section we will mainly focus on tissue-resident $T_{REG}$, whereas effector $T_{REG}$ will be described in more detail in the context of specific pathologies. Of note, the term "tissue" when used in conjunction "tissue $T_{REG}$" is not fully analogous to that of "tissue-resident" or "resident memory", the two latter being largely synonyms of "non-recirculating". "Tissue $T_{REG}$" is rather used with the meaning of NLT.

Tissue $T_{REG}$ exert pleiotropic activities. They control metabolic properties of VAT, tissue repair in the skin and lungs, regeneration processes in skeletal muscle and microbial content of the large intestine [112, 113, 114, 76]. Tissue $T_{REG}$ display profound differences in gene expression profiles compared to $T_{REG}$ from SLO, and to some extent differ between different NLT. For instance, "specific" master transcription factors have been identified for several tissue $T_{REG}$ subsets, including peroxisome proliferator associated receptor gamma (PPARγ) for VAT $T_{REG}$ and Amphiregulin for muscle $T_{REG}$. A first highly characteristic tissue Treg population identified in the lean mouse VAT consists of thymus-derived non-recirculating (resident) cells. VAT $T_{REG}$ act to promote local and systemic metabolic homeostasis [112]. However, less characteristic subsets of tissue Treg also play a homeostatic role previously attributed to SLO $T_{REG}$ in some inflammatory context [115, 116, 70]. Indeed, skin and lung Treg are involved in the control of allergic inflammation; colonic Treg include at least two Treg populations of different origins that regulate colitis. Several tissue $T_{REG}$ subsets consist of both resident and recirculating cells. Overall, tissue $T_{REG}$ diversity resembles that of conventional memory T cells. The latter are antigen-experienced T cells, located in NLT and peripheral lymphatics, and are divided into central-, effector- and resident-memory cells based on function and migration patterns [117].

Despite differences, tissue $T_{REG}$ from various NLT display substantial similarities: a highly effector phenotype (CD25, CTLA4, KLRG1, CD44, Gramzyme B..) and $T_H$2-like transcriptional profile. But they express distinct sets of tissue-specific homing molecules and T cell-receptor (TCR) repertoires [118, 119, 120, 121]. These characteristics of tissue $T_{REG}$ are being investigated in depth using single-cell RNA sequencing (scRNA-seq), Assay for Transposase-Accessible Chromatin using sequencing (ATAC-seq) and other whole-genome techniques [122, 120, 119]. Some genes and open chromatin region (OCR) from ATAC-seq, like *Fos2* and *Irf4* also fall into "pan-$T_{REG}$" category, meaning that they are expressed in all the $T_{REG}$ no matter if they are found in SLO or NLT. It is suggested that such genes may participate in "priming" of $T_{REG}$ in SLO before they home and reside in NLT. The

two other types of gene signatures tissue $T_{REG}$ are sometimes referred to as "pan-tissue" and "tissue specific", depending if they are common between $T_{REG}$ from different NLT or are only found in $T_{REG}$ from some NLT, but not others [120]. Also, $T_{REG}$ from spleen and from NLT have OCR associated with dedicated super-enhancers (600-1000), different for different subsets. Signatures of $T_{REG}$ also include the landscape of monovalently (permissive histone marks) or bivalently (both permissive and repressive histone marks) marked enhancers, which vary between NLT. This was already shown on other tissue resident immune cells like macrophages. These key epigenetic processes thus seem to be a general mechanism of immune cell adaptation to tissue environment [122]. Investigation of tissue $T_{REG}$ chromatin for TF family motif-associated OCR also identified some families like RFX, bZIP, ETS, which may be conductors of pan-tissue $T_{REG}$ transcriptional program [120].

## 2.2.1 Visceral adipose tissue

The most distinctive context, in which tissue $T_{REG}$ are being studied is homeostatic conditions. First and best described population of tissue $T_{REG}$ to date is murine VAT $T_{REG}$. $T_{REG}$ cells in the VAT of chow diet (CD) fed mice are abundant, making up to 40% of $CD4^+T$ cells compared to roughly 10% in the immune tissues [112]. The population size of VAT $T_{REG}$ changes throughout the lifespan with the maximum at around 22-25 weeks of age followed by a gradual decline. These cells are not converted into $T_{REG}$ from $T_{CONV}$ and do not represent circulating $T_{REG}$, but are a resident population, as shown by various labeling and parabiosis techniques [123]. Thymectomy experiments and $T_{REG}$ depletion using diphtheria toxin-based systems, together with VAT $T_{REG}$ proliferation assessment revealed that $T_{REG}$ likely seed VAT during the first (three) weeks of life and then undergo "indolent" homeostatic proliferation (microexpansion) of certain clones (different between individual mice) to reach peak frequency at around 25 weeks of age [112]. As a result, VAT $T_{REG}$ niche shows particular dynamics in the numbers provided above, together with limited TCR repertoire diversity compared to SLO $T_{REG}$. These TCR allow $T_{REG}$ to stay in VAT via interaction with MHC-II on the surface of local APC, most likely DC and macrophage (MF) [123]. High surface expression of ST2 is important for $T_{REG}$ accumulation in VAT. ST2 is a receptor for interleukin-33 (IL-33), an alarmin, which improves metabolic parameters in obese mice and drives VAT $T_{REG}$ expansion [124]. IL-33 depletion, by contrast, results in VAT $T_{REG}$ paucity. Under physiological conditions IL-33 is presumably expressed in the VAT by fibroblast reticular cells or endothelial cells and maintains a constant $T_{REG}$ population. In agreement with T helper-like paradigm for $T_{REG}$ functional specialization PPARγ controls the distinct VAT $T_{REG}$ transcriptional profile. Interestingly, PPARγ is also the master regulator of adipogenesis [125]. When conventional $CD4^+T$ cells are cotransduced with *Foxp3* and *Pparg* constructs, they acquire a gene expression profile akin to that of VAT $T_{REG}$. As $T_{RM}$ cells, tissue $T_{REG}$ constitutively display effector phenotype. That holds true for VAT $T_{REG}$. Indeed, apart from *Foxp3* and *Pparg* they express high levels of genes encoding suppressive molecules including *Il10*, *Il2ra* (CD25) and *Tnfrsf18* (GITR) [126, 127], as well as genes facilitating accumulation in VAT such as *Il1rl1* (IL-33 receptor) and *Ccr2*. Finally, VAT $T_{REG}$ express genes involved in regulation of lipid metabolism, likely using them to adapt for local lipid-rich microenvironment. In addition to PPARγ, IRF4 and BATF TF play key roles in VAT $T_{REG}$ differentiation and function [124]. By contrast, interleukin-21 (IL-21) and STAT-3 are the two negative regulators of VAT $T_{REG}$ accumulation in contrast to the factors listed above [128, 129].

In line with VAT $T_{REG}$ homeostatic role, obesity and insulin resistance negatively correlate with VAT $T_{REG}$ in mouse models. Whole-body depletion of $T_{REG}$ induces VAT inflammation and in turn leads to worsening of most parameters of glucose metabolism [127, 130]. These include higher fasting glycemia, slower glucose clearence in glucose-tolerance tests and decreased phosphorylation of insulin receptor in the VAT. $T_{REG}$-specific deficiency in PPARγ leads to shrinkage of VAT $T_{REG}$ compartment and induces VAT inflammation, compromising insulin sensitivity, while administration of PPARγ agonists improves the metabolic status [125]. It was also shown that in obesity VAT $T_{REG}$ change their phenotype

dependent on specific phosphorylation of PPARγ [131, 132, 133].

## 2.2.2   Skeletal muscle

Skeletal muscle $T_{REG}$ population has been so far mostly studied in the context of regeneration upon injury. $T_{REG}$-depletion using dyphteria toxin receptor (DTR) expressing construct or anti-CD25 antibody at the time of injury compromises muscle repair [114]. By contrast, injection of IL-2/anti-IL-2 complexes into dystrophic mice and resulting increase in $T_{REG}$ numbers reduces inflammation in the muscle and leads to a decrease in myofiber injury [134]. $T_{REG}$ resident in the skeletal muscle are a minor population which expands (upto 60% of CD4$^+$T cells) in acutely injured muscle and maintains it's size for up to a month afterwards. Muscle $T_{REG}$ numbers also increase with age, although not rescuing declining regeneration ability of the tissue. Muscle $T_{REG}$ also accumulate in the muscle tissue in the genetic mouse models of dystrophy. Muscle $T_{REG}$ possess highly restricted TCR sequence pool, which is even less diverse than that of VAT $T_{REG}$, likely reflecting dependency on a local – yet unidentified – tissue antigen often important for T cells retention. Transcriptionally, muscle $T_{REG}$ are quite close to VAT $T_{REG}$ with *Ccr2*, *Il10*, *Klrg1* and *Il1rl1* transcripts being overrepresented in addition to *bona fide* $T_{REG}$ signature [114, 134, 135]. Importantly, some genes induced in muscle $T_{REG}$ compaired to SLO $T_{REG}$ seem to distinguish them from their VAT counterparts. These include growth factors *Pdgf* and *Areg*, chemokine receptors *Cxcr5* and *Ccr7* and Wnt signaling-associated genes *Tcf7*, *Satb1*, *Lef1*. As for VAT $T_{REG}$, muscle $T_{REG}$ similarly expand in response to IL-33 injection and contract upon ST2 deficiency [114]. Muscle regeneration is facilitated by satellite cells, which are muscle cell progenitors located beneath the basal membrane of myofibers. Satellite cells are activated when the muscle is damaged, they proliferate and yield new muscular fibers. The process of regeneration goes in parallel with local inflammation, mounted after injury to clear damaged cell debris and then restore disturbed structure of the tissue[136, 137, 138]. Immediately following injury, inflammatory environment displays traits of type 1 inflammation with proinflammatory (M1) MF being central players. However, an anti-inflammatory (M2) macrophage-driven response promptly takes place. Besides MF, conventional CD4$^+$ and CD8$^+$ T lymphocytes also contribute to inflammation [139]. $T_{REG}$ play a decisive role in the M1-M2 switch mentioned above by contributing to anti-inflammatory environment and inflammation resolution [140]. Furthermore, muscle $T_{REG}$ overexpress *Areg* gene encoding Amphiregulin sensed by epidermal growth factor receptor (EGFR) expressed by satellite cells, thereby inducing proliferation *in vitro* and promoting muscle repair *in vivo* upon injection [113]. However, Amphiregulin affects both wild type and $T_{REG}$-deficient mice, questioning the importance of $T_{REG}$-expressed Amphiregulin in muscle repair [114].

## 2.2.3   Intestine

A population of colonic $T_{REG}$ represents another widely discussed subset of NLT $T_{REG}$ [141, 142]. Mucosal tissues have an abundant immune compartment often referred to as MALT, with gut-associated lymphoid tissue (GALT) playing a prominent role in tolerance and immune response against food allergens, commensal microbiota and intestinal pathogens [143]. As for other tissues, $T_{REG}$ in the intestine play a homeostatic and anti-inflammatory roles triggered by cognate antigens cognate antigens including the microbial ones and sensing metabolites produced by the symbionts [141] Figure 2.1. Intestinal $T_{REG}$ make up to 40% of CD4 T cells in the colon at steady state and may be divided into two subpopulations: RORγt$^+$ and RORγt$^-$[144]. The latter are widely accepted to also co-express GATA-3 and Helios. While some of the data from the large number of publication on the topic are controversial, it is commonly admitted that colonic RORγt $T_{REG}$ are more dependent on the microbiota, as they display a decline in antibiotic treated mice [145, 146, 147]. On the other hand, RORγt$^-$GATA-3$^+$ $T_{REG}$ also show ST2 expression and specifically expanded in response to

IL-33 treatment [148]. RORγt$^+$ and RORγt$^-$ $T_{REG}$ can be considered respectively as t$T_{REG}$ and p$T_{REG}$. RORγt$^+$ cells are induced in response to TGF-β abundant in the intestine. However, p$T_{REG}$ are clearly present in the intestine as CNS1 mutation causes pathologies in the colon, again, likely dependent on RORγt$^+$ $T_{REG}$ [149].

### 2.2.4  Skin

The skin is another barrier tissue with abundant immune system. Mouse dermis houses a population of CD4$^+$ T cells, 20-60% of which are $T_{REG}$ cells [144, 150]. Seeding of skin with thymus-derived $T_{REG}$ takes place early in life and is dependent on CCL20 and possibly skin-resident microbiota[150]. The receptor for CCL20 is CCR6, which is indeed highly expressed on skin $T_{REG}$ [151]. At least in humans, skin $T_{REG}$ also display CLA expression [98]. $T_{REG}$ which home to skin are also defined by expression of CCR4 (itsligands are CCL17 and CCL22) and CD103 (ligand E-cadherin) [152, 153]. CCL17 is expressed by endothelial cells of dermal post-capillary venules and CCL22 is secreted by cutaneous myeloid cells, whereas keratinocytes express E-cadherin [154, 155]. Most of skin $T_{REG}$ (up to 80%) are t$T_{REG}$ and express GATA3 and Helios [156, 121, 157]. A Helios$^+$RORα$^+$ $T_{REG}$ population was identified in the skin[116]. GATA3 deficiency in $T_{REG}$ leads to spontaneous type 2 inflammation in the skin [158]. Skin $T_{REG}$ cells accumulate in wounds on in an EGFR-dependent manner and contribute to healing [159]. In non-inflamed human and likely mouse skin, $T_{REG}$ reside near to hair follicles and promote their regeneration via proliferation and differentiation of stem cells [160]. Skin $T_{REG}$ cells proliferation is induced by Langerhans cells and fibroblasts in an IL-2 dependent manner *in vitro*. Very intriguingly, skin $T_{REG}$ cells expand and deploy suppressive activity upon UVB-irradiation – a method of treatment for atopic dermatitis and psoriasis. It is facilitated by dermal DC and vitamin D being converted to D3, likely acting on it's receptors expressed by many immune cells [161, 156].

In response to inflammation, $T_{REG}$ cells were shown to migrate to skin with the help of P-selectin glycoprotein ligand-1n (PSGL-1) expression [98, 162, 152]. Allergic inflammation in the challenged skin is controlled by RORα$^+$ $T_{REG}$, disease is exacerbated upon $T_{REG}$-specific deletion of RORα [116].

## 2.3  $T_{REG}$ in pathologies

### 2.3.1  Asthma

Asthma is a chronic inflammatory disease of the lung, characterized by airway hyperresponsiveness, excessive mucus production and airway remodeling. Asthma affects up to 10% of the general population Asthma has 2 main origins: allergic asthma is the prototypical allergic disease classically associated to type 2 immune response while origin ofnonallergic (or intrinsic) asthma is less clear [163]. Allergic asthma usually develops upon sensitization to common environmental antigens (allergens) such as including house dust mite (HDM), dander of animals, pollen, fungal spores. It is s defined by the presence of serum immunoglobulin E (IgE) and eosinophilia During the so called "atopic march", a large proportion of children are sensitized to allergens early on and develop atopic eczema and allergic rhinitis of increasing intensity than evolves towards asthma. Non-allergic asthma, on the other hand, develops without known reactivity to allergens or elevated IgE levels [164].

Several immune cell types are involved in allergic asthma [165, 166, 167]. Numerous allergens such as House Dust Mite (HDM) major protein (Derp 1 –Dermatophagoides pteronyssinus 1-) possess protease activity, so they are able to cleave proteins from epithelial tight junctions and engage protease-activated receptors. Stressed/damage epithelial cells secrete alarmins: IL-33, IL-25 and TSLP whih activate Type 2 Innate lymphoid cells (ILC2) and ILC2 synthetize, as Th2 cells, IL-4, IL-5 and IL-13 driving (among other) eosinophil infiltration [168] They also contribute to alternative activation macrophages and affect TH differentiation and function via secretion of cytokines. Mice lacking RORα

in hematopoietic cells, are lacking ILC2 and display milder HDM-induced lung inflammation than wild-type mice. DCs are also central to for the development of the T cell-mediated allergic response. They can sample antigens/allergens through the lung epithelium REF or as a result of damaged epithelial barrier. Increased synthesis of mostly CD4+ T-derived interleukin-4 (IL-4), promotes isotypic swich leading to IgE production by B cells, and -interleukin-5 (IL-5) [169, 170, 171]. FcεRI expressed by human DCs binds IgE and causes a release of CCL28, which attracts TH 2 [172] ILC2 also contributes to DC activation REF.. Conventional and plasmacytoid DCs (cDC and pDC) are the two subsets of DCs described in the lung. A cDC subset, which depend on IRF4 TF, induce sensitization to allergen. IRF8- and BATF3-dependent cDCs and pDC, however, provide tolerance to harmless antigens through TREG [173, 168]. So did genetic deficiencies of those cytokines in the mice. Common mouse models of allergic asthma include ovalbumin (OVA)-driven or HDM-driven AAI. In general, this models mimic mechanisms of development of human allergic asthma, with OVA being more T cells-skewed and HDM inducing a broader, thus more physiologically relevant, spectrum of innate and adaptive immune cell responses. Apart from eosinophil (EOS) and T cells, some other immune cells are involved in allergic asthma [174, 172]. Eotaxins CCL11, CCL24 and, in humans, CCL26, produced by epithelial cells also facilitate eosiophil chemotaxis to the lung mucosa. By secreting specific cytotoxic molecules such as eosinophil peroxidase (Epx), eosinophil-derived neurotoxin (EDN), eosinophil cationic protein (ECP) and major basic protein (MBP), eosinophils are able to directly cause airway hyperreactivity, damage lung structures and/or induce DC "polarization" towards priming of Th2 response.. According to some studies, eosinophils may also serve as APCs themselves [165, 166, 167]. eosinophil-derived TGF-β leads to airway wall remodeling and thickening of subepithelial membrane. Serum levels of IL-4, IL-5, interleukin-13 (IL-13) and interleukin-25 (IL-25) are also often elevated [169, 170]

$T_{REG}$ cells are critical for the regullation of allergic asthma, their numbers are reduced in sputum and in the blood of asthmatic patients. $T_{REG}$ control asthma by regulating DC activation through secretion of IL-10 and TGF-β. They also may inhibit angiogenesis via direct interaction with endothelial cells. Both $tT_{REG}$ and $pT_{REG}$ are found in the lung [175, 149]. The importance of the latter was demonstrated by exacerbation of airway $T_H2$ responses in CNS1 mutated mice. A well-known property of $T_{REG}$ in asthma and allergic diseases in general is a pathogenic $T_H2$-reprogramming [176]. During this process observed in both mice and humans, $T_{REG}$ cells acquire an effector phenotype with increased GATA3 expression and secretion of IL-4 while keeping FOXP3 expression. A recent study also associated this reprogramming with IL-33 acting on lung $T_{REG}$ which express ST2 during allergic AAI [115]. A similar phenomenon is caused by a mutation of IL-4 receptor gene, altering it's downstream signaling and leading to the emergence of a $T_H2$-$T_H17$ $T_{REG}$ population and associated with asthma in both mice and humans [177, 178].

## 2.3.2 Obesity

Obesity in humans results from excessive caloric intake compared to energy expenditure. It is defined a body mass index (BMI) equal or greater than 30 $kg/m^2$. Obesity causes comorbidities and alters multiple parameters of the organism, which includes: large waist circumference, high triglyceride and fasting glucose concentrations, low high density lipoproteins (HDL) cholesterol and hypertension. Large waist or waist/hip ratio represent fat deposition in the abdominal cavity, such adipose tissue is called visceral fat. VAT adipocytes found in the peritoneum, especially those in the greater omentum (a fold of visceral peritoneum), are not adapted to store large amounts of fat and normally are almost devoid of it. During obesity, they generate abnormal quantities of fatty acids, cytokines and hormones, which are brought into the liver with the blood flow. This in turn alters lipoproteins production and lowers insulin sensitivity of the cells in peripheral tissues [179]. Upon obesity development, a chronic inflammatory process is induced within the VAT. Adipose produces tumor necrosis factor alpha (TNFα). This finding was the first mechanistic link between obesity and inflammation.

Obesity often leads to insulin resistance (IR). IR is characterized by a decrease in insulin-induced glucose uptake in the adipose tissue and skeletal muscle, as well as insufficient insulin-dependent suppression of glucose production by the liver. The key molecules linking inflammatory signals to metabolism are insulin receptor (IR) and insulin receptor substrate-1 (IRS-1). TNFα causes a decrease of Tyr phosphorylation of IR β-subunit, but increases Ser phosphorylation of IRS-1 at multiple sites. This is mediated by IKK and JNK1 respectively and causes subsequent impairment of insulin sensitivity [180, 181]. Fatty acids (FA) are also involved in inhibitory IRS-1 Ser phosphorylation through protein kinase C theta (PKC-θ) (lipotoxicity). Thus, links of inflammation and IR were also established [182]. Adipose tissue contains a wide range of immune cells with striking differences between lean and obese adipose tissue. Accumulation of macrophages in VAT, their organization into crown-like structures around dead adipocytes during efferocytosis and installation of an M1 inflammatory polarization are considered as hallmark of obesity, at least in mouse models [183, 184]. M1 macrophages differentiate in response to lipopolysaccharide (LPS) and IFN-γ, bear CD11b$^+$CDD11c$^+$F4/80$^+$ on their surface and produce TNFα, IL-6, interleukin-1 beta (IL-1β), IL-12, nitric oxide (NO). In line with increase of TNFα, IL-1β and IL-6 in plasma of obese humans and mice [181, 185, 186]. In lean VAT, MF display mainly M2 anti-inflammatory polarization profile with CD11c$^-$CD11b$^+$F4/80$^+$CD206$^+$CD301$^+$ surface phenotype [187, 188, 189]. M2 macrophages develop in the presence of type 2 cytokines IL-4 and IL-13 and secrete IL-10 and interleukin-1 receptor antagonist (IL-1Ra) thereby attenuating inflammation and promoting insulin sensitivity. In addition to macrophages, other immune cells are known to contribute to obesity and associated metabolic dysfunction. Various other innate immune cells, on one hand, promote inflammationin, particular neutrophil (NΦ) and mast cells. NΦ and mast cells normally activated upon injury, accumulate in adipose tissue during obesity and contribute to inflammation by secreting IL-6 and IFN-γ and by degranulating, which results in the recruitment of other immune cells. Ablation of mast cells or blocking the release of their granules reduces weight gain in mice with DIO, reduces the number of VAT macrophages and circulating pro-inflammatory molecules in turn improving insulin sensitivity [190]. Neutrophils are also enriched in VAT during DIO [191]. They secrete elastase, which induces glucose intolerance even when injected into lean mice. Conversely, genetic ablation of elastase gene improved inflammation and lowered VAT macrophage and neutrophil content [192]. On the other hand beyond anti-inflammatory macrophages, various innate immune cell types associated to type 2 immunity, as found in allergic asthma, foremost ILC2 and eosinophils, are mostly present in lean adipose tissue and exert an homeostatic role by largely skewing VAT macrophages towards M2 polarization through type 2 cytokine production. ILC2 also promote eosinophil maturation via IL-5. In line, ILC2 content in VAT decreases during DIO [193]. Eosinophils, secrete IL-4 and IL-13 preserving glucose tolerance during DIO [194]. EOS depletion of leads to greater body weight gain and impaired glucose tolerance, whereas helminth-induced or IL-4 infusion induced VAT eosinophilia increases insulin sensitivity, although EOS numbers are very low [195]. Adaptive immune cells, T and B lymphocytes, infiltrate VAT during DIO [196] CD8$^+$ T cells worsen inflammation and insulin resistance in mouse models of DIO likely due to their effect on macrophages. VAT CD8$^+$ T cells in have restricted TCR repertoire and may be stimulated by adipocytes during DIO [197, 198]. Paradigmatically, VAT CD4$^+$ T$_H$ cells favor or inhibit obesity development according to their polarization and cytokine profile [127, 199, 200]. However, T$_H$2 cells were not very well defined during these studies in VAT, likely due to their resemblance to VAT T$_{REG}$, which play an important part in VAT homeostasis and express type 2-associated genes like *Gata3*, *Irf4 Il1rl1*, *Il10*. Expansion of a VAT-resident population of T cells during DIO was also associated with higher vulnerability to viral infection [201]. CD4$^-$CD8$^-$ γδT cells also probably contribute to VAT inflammation by producing IL-17, however, their role is likely redundant. Mice lacking IL-17 displayed increased adiposity on CD and high fat diet (HFD), and the main producers of IL-17 in VAT are thought to be γδT cell . But depletion of γδT cell did not cause the same phenotype as IL-17 deficiency [199]. NKT are T cells, which recognize lipids and glycolipids in complex with CD1d,

but not MHC, as other T cells [202]. The role of NKT cells in obesity and metabolic syndrome is rather controversial. But it is likely, that NKT cells promote VAT inflammation and insulin resistance, especially the invariant NKT cells population, activated by lipid excess during obesity [203, 204]. B cells exacerbate VAT inflammation and insulin resistance [205]. VAT upon HFD is infiltrated mainly by IgG-producing B cells. Particular repertoire of IgG molecules correlates with insulin resistance in both humans and mice. The effect of IgG on VAT inflammation was demonstrated to be independent of Fcγ receptor [206]. Another subset of regulatory B cells negatively controls adipose tissue inflammation via production of IL-10 [207]

VAT $T_{REG}$ are negative regulators of immune response and preserve glucose homeostasis. VAT $T_{REG}$ numbers are reduced upon HFD. When $T_{REG}$ in VAT are expanded or removed experimentally, insulin sensitivity follows the same dynamics [127]. Recently, a mechanism was proposed, in which adipocytes influence $T_{REG}$ frequencies through secretion of prostaglandin E2 (PGE2). Activation of mammalian target of rapamycin complex 1 (mTORC1) in adipocytes during obesity led to phosphorylation of CREB regulated transcription coactivator 2 (CRTC2) and suppressed cyclooxygenase 2 (COX-2) expression and PGE2 secretion. Treatment by PGE2 expanded $T_{REG}$ cells both *in vivo* and *in vitro*[208]. Important traits of VAT-resident $T_{REG}$ are discussed above. As $T_{REG}$ may establish type 2 immune environment in the adipose tissue, it is possible, that they are involved in control of white adipose tissue beiging [209]. Moreover, a distinct population of $T_{REG}$ was found in brown adipose tissue (BAT) and are required for thermogenesis [210].

### 2.3.3   Intestinal inflammation

Intestinal homeostasis is a balance between commensal microbiota, immune responses they trigger and regulatory mechanisms controlling these responses. Intestinal inflammation occurs, among other causes, when either of the three components fail [211]. inflammatory bowel disease (IBD) is subdivided into Crohn's disease with substantial transmural inflammation and ulcerative colitis where the lesions are more superficial. They also are found different segments of the intestine, but all occur where microbiota is the most abundant: in ileum, colon and rectum. This supports a general consensus, that IBD is largely driven by commensal microorganisms in addition to nutritional and genetics factors [212]. Several murine models of intestinal inflammation have been developed. Colitis can be induced by haptenizing agents like trinitrobenzene sulfonic acid (TNBS) or oxazolone colitis. They disrupt epithelial layer and induce acute immune reaction against haptenized self-proteins. These models are often used when studying type 2-driven inflammation and largely depend on IL-4 and IL-13 and NKT cells [213, 214, 215]. Dextran sulfate sodium (DSS) induced colitis only disrupts epithelial layer and allows for entry of commensal bacteria into the mucosa, leading to immune system activation more akin to naturally occuring pathology (mainly ulcerative colitis). Immune response triggered upon DSS colitis induction is also more complex, involving interleukin-23 (IL-23) and IL-22 dependent control of intestinal epithelial cells, TNFα secreted by macrophages and contribution from $T_H1$ and $T_H17$ lymphoid cells, as well as [216, 217, 218]. Finally, another model of experimental colitis is achieved upon adoptive transfer of naive CD4$^+$ T cells into lymphopenic hosts. It is based on activation of transferred T cells in response to microbiota (and other intestinal antigens) and subsequent development of intestinal inflammation [219]. This model allows the assessment of T cells responses *in vivo*, as well as $T_{REG}$ suppressive activity when the latter are cotransferred with conventional T cells. Naive T cells preferentially differentiate into $T_H1$ and $T_H17$ cells.

IL-10 secreted by $T_{REG}$ (and by many other immune cells) is an anti-inflammatory cytokine and is particularly important in the intestine, as IL-10 deficient mice do not develop systemic autoimmunity, but only microbiota-triggered spontaneous colitis driven by CD4$^+$ T cells. $T_{REG}$-specific IL-10 deficiency possesses similar phenotypic traits, suggesting that $T_{REG}$ are a major source of IL-10 in the intestine [70]. Furthermore, $T_{REG}$ require IL-10 stimulation for suppression of inflammation [220]. IL-10 is also
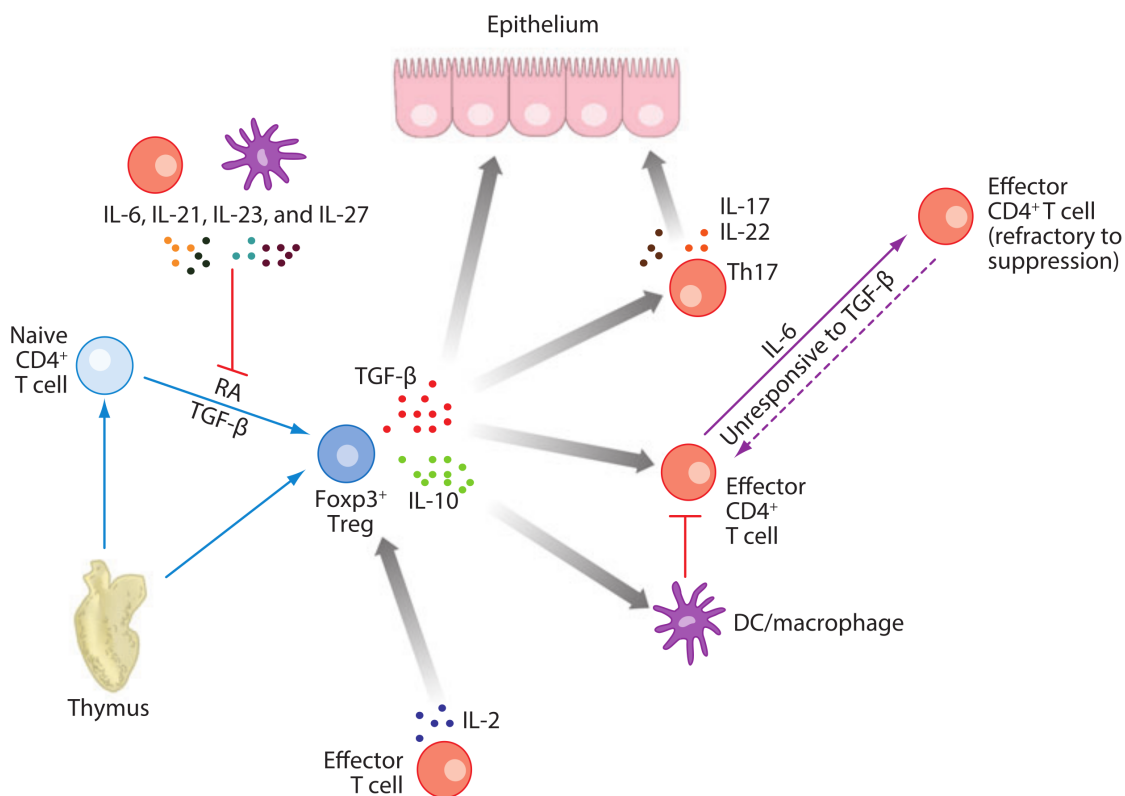
Figure 2.1 – Cytokines in the T$_{REG}$ network in the intestine [211].

able to reduce antigen presentation by DC and monocytes [221]. TGF-β deficiency in T cells also leads to early onset spontaneous colitis in the mice [222]. T$_{REG}$ also produce TGF-β, which may further promote development of both pT$_{REG}$ and T$_H$17 cells Figure 2.1. That is probably one of the reasons why both beneficial and detrimental effects of this cytokine were demonstrated in colitis models [223, 224]. Interestingly, T$_H$17 cells may also produce IL-22, which contributes to reinforce mucosal barrier and promotes epithelial cells regeneration [225]. CTLA-4-dependant induction of IDO in DC by T$_{REG}$ is also at play, with RORγt$^+$ T$_{REG}$ being the most active drivers [147, 226]. A special trait of T$_{REG}$ in colitis is that they are prone to dedifferentiate and lose their suppressive capacity and start producing IL-17 in these inflammatory conditions. It was shown that T$_{REG}$ expand in patients with Crohn's disease, however became pathogenic T$_H$17-like cells, which was also found in the mice [227, 228, 69].

# Chapter 3

# Nuclear receptor RORα

## 3.1 Superfamily of nuclear receptors

The superfamily of nuclear receptors is the largest group (48 receptors in human) of eukaryotic TF, which share structural similarities. Their main feature is ligand-activated regulatory activity on gene transcription [229]. These molecules sense signals of lipophilic hormones: steroids, retinoids, thyroid hormones and vitamin D to regulate an extremely broad set of processes [230]. These include organismal development, reproduction, cell differentiation, cholesterol, bile acids and fatty acids homeostasis, xenoprotection and circadian rhythmicity. Ligand binding potential makes some of the receptors capable of both repressing and activating target genes via respective chromatin modifications. Thanks to their regulatory power, nuclear receptors include many examples of successfully harnessed therapeutic targets for treatment of cancer, hyperlipidemia, type 2 diabetes, nonalcoholic steatohepatitis (NASH) and atherosclerosis [231].

Nuclear receptor research was born when it was noticed that [$^3$H]-labeled steroid hormones accumulate in the reproductive organs of immature female goats and sheep upon injection [232]. It was proposed that a putative receptors should exist in the cells of respective tissues and drive this retention. Another evidence came from incubation of salivary glands of *Drosophila* with a molting hormone 20-hydroxyecdysone, which led to puffing at specific sites of polytene chromosome. This one demonstrated an effect of steroids on transcriptional level, again indicating presence of a potential sensing intermediary protein [233]. Soon after, cDNAs of estrogen and glucocorticoid receptors were isolated, allowing to elucidate a conserved genetic template, further used to decipher structural features of the emerging superfamily [234, 235]. The sequences showed homology with known erb-A oncogen of avian erythroblastosis virus. Commonly, nuclear receptors derive their names from their ligands. Nuclear receptora are referred to as "orphan" when they are identified independently of its ligand. Once a physiological ligand is found and the receptor is "adopted". A prototypical specimen of the nuclear receptor superfamily encompasses an N-terminal A/B region also called ligand-independent activation function 1 (AF-1), a conserved DNA binding domain (DBD) with two zinc finger motifs (C region), a short flexible hinge (D region), conserved ligand binding domain (LBD) with ligand-dependent activation domain 2 (AF-2), a variable C-terminal region. Nuclear receptors bind to respective DNA half-sites called response elements, usually hexameric repeats, serving as determinants of specificity for binding to the target genes. The receptors are often divided into steroid and nonsteroid. Steroid receptors bind to two palindromic half-sites separated by three base pairs as homodimers [236, 235]. All nonsteroid receptors bind to tandem (direct) repeats, but differ regarding spacer length between

their half-sites [237, 238, 239]. This difference was summarized as a 3-4-5 rule standing for the spacing length of vitamin D, thyroid hormone and retinoic acid receptor sites respectively. Importantly, nonsteroid receptors bind to DNA forming heterodimers with either of RXR (RXRα, RXRβ or RXRγ depending on the cell type) in contrast to steroid receptor homodimers [240, 241, 242, 243]. It is interesting, that such dimerisation creates another level of regulatory potential, as two different nuclear receptors bound together means two LBD with distinct ligand specificity. Nonsteroid nuclear receptor heterodimers fall into two categories depending on their activation schemes. Permissive dimers may be activated by either RXR or partner protein, whereas nonpermissive dimers are only activated by the ligand of the partner, without involvement of RXR. Permissive partners include liver X receptor (LXR), farnesoid X receptor (FXR), pregnane X receptor (PXR), constitutive androstane receptor (CAR), peroxisome proliferator associated receptor (PPAR). Some orphan nuclear receptors, however, show another mode of action regarding ligand binding [244, 245, 246]. Their ligand binding pocket of LBD may be absent or occupied by a lipid, phospholipid or another molecule such as heme, thereby interfering with the traditional binding of a ligand. Accordingly, these orphan receptors are generally repressors. They also tend to act as monomers or homodimers.

One central and intensively studied physiological role of several RXR-partnered nuclear receptors is their control of systemic metabolism by regulating distribution and use of ingested (and some for processed) nutrients and energy throughout the body. For instance, feeding-induced increase of bile acids in the intestine activates FXR. FXR triggers induction of nutrient transporters expression and production of fibroblast growth factor 19 (FGF19), promoting glycogen synthesis and bile acid pool regulation in response to a meal [247, 248]. LXR is activated by dietary cholesterol and contributes to liver production of triglycerides, which are directed to periphery to nurture tissues. Additionally, LXR participates in clearance of excess cholesterol via regulation of it's reverse transport by HDL as well as in the control of hepatic bile acid synthesis from cholesterol [249]. Engagement of FXR activates a negative feedback loop, which inhibits LXR and thus prevents increase in bile acids, when they are already detected by FXR in the intestine and liver. PPAR, whose ligands are FA in turn are responsible for the storing or mobilization of energy gained from food in the form of lipids. PPARα and PPARδ are activated when free FA levels rise. These receptors promote β-oxidation in muscles [250, 251]. PPARγ controls adipocyte differentiation and provides storage of extra energy in the form of triglycerides in the adipose tissue. PPARγ also has effects on glucose metabolism, and promotes systemic insulin sensitivity [252]. This is achieved by 2 distinct mechanisms. First, PPARγ lowers blood free FA concentration by directing them into lipogenesis. Lower free FA concentration reduces lipotoxicity-induced impairment of insulin signaling in the tissues including liver and muscles. Lipotoxicity also decreases insulin secretion by islets in the pancreas [253]. Second, PPARγ promotes expression of adipokines leptin and adiponectin, which improve insulin sensitivity in skeletal muscles and liver [254].

## 3.2   Nuclear receptor RORα

RORα (NR1F1) is an orphan nuclear receptor structurally similar to RAR and RXR which was identified in 1993 [255, 256]. RORα belongs to a ROR subfamily consisting of RORα, RORβ, RORγ. RORs bind as monomers or (according to some data) homodimers to ROR response element (RORE), short AT-rich part followed by a single half-site of a sequence TAAA /TNTAGGTCA, PuGGTCA sequence being a core motif [257]. On the basis of a RORα LBD co-crystal structure bound to cholesterol, it was proposed that cholesterol, cholesterol sulfate and 7-oxygenated sterols may be physiological RORα ligands, but no direct evidence of their action on the receptor has been obtained yet. When bound to a promoter of a target gene in a transcriptionally active conformation, RORs recruit coactivators or corepressors via their AF2 domain, causing activation or inhibition of transcription. Among RORs

coactivators are NCOA1 (SRC1), NCOA2 (TIF2 or GRIP1), PGC-1α, p300, and CBP; corepressors – NCOR1, NCOR2, RIP140, NIX1 [258, 259, 260, 261]. ROR-mediated transcriptional activity is repressed by direct interaction with FOXP3 [48]. RORα is expressed in the liver, skin, adipose tissue, lung, skeletal muscle, kidney, thymus, mature leukocytes and brain [262, 263]. In the central nervous system it is expressed in cerebellar Purkinje cells, the thalamus, the suprachiasmatic nuclei and retinal ganglion cells. Alternative splicing and promoter usage result in 4 RORα isoforms of RORα (RORα1, 2, 3, 4), which differ only in N-terminal domains. RORα1 and RORα4 are expressed in mouse cerebellum. In other mouse tissues only RORα4 is found, RORα3 is characterized by expression in human testis [264]. In most of mouse tissues including leukocytes, the fourth isoform is expressed. Interestingly, liver mRNA of RORα1 isoform shows an oscillatory pattern of expression (and peaks at circadian time (CT)16-CT0), in contrast to RORα4, which is stable all over the 24 hour period [265]. Furthermore, different isoforms of RORα displayed different binding behavior, likely regulated through N-terminal domain, as shown *in vitro*. ROREα1 consensus site, to which RORα1 binds with high affinity, was only weakly bound by RORα2 and RORα3 isoforms. A deletion of residues 23-71 of N-terminal domain of RORα1 inhibits it's ability to bind with ROREα1, but does the opposite when it comes to RORα2 (depending on residues 46-71) [256].

*sg* mutation of *Rora* removes the start of LBD. Deletion affects one exon, where it causes a reading frame shift and emergence of a stop codon after 27 amino acids. As a consequence, the protein translated from *sg* gene preserves DNA-binding capacity losing, however, it's transactivational activity. *Staggerer* (*sg/sg*) mice homozygous for a spontaneous deletion in *Rora* gene, preventing translation of LBD display ataxia due to defect in Purkinje cells development and, as well as thin bones [263, 262, 266]. The mechanism for deficient Purkinje cells maturation in *sg/sg* mice is attributed to dysfunctional glutamate transport and reception systems. RORα deficiency causes a decrease in expression of glutamate receptor *Grm1*, and a glutamate trnsporter *Slc1a6*. This may contribute to the fact, that parallel fibers of granule cells, being an exitatory input for Purkinje cells and vital for their maturation are not properly formed. Some other genes associated with Purkinje cells maturation are also downregulated in *sg/sg* mice [260, 267]. They were involved in calcium signaling (*Pcp4*, *Itpr1*, *Cals1*, *Atp2a2*, *Calb1*). *In vivo* binding of RORα to RORE in promoter regions was demonstrated for some of those genes (*Pcp2*, *Pcp4*, *Itpr1*, *Shh*, *Slc1a6*). While acting on these genes a RORα transactivation complex is formed with one of the proteins: TIP60, SRC-1, CBP, GRIP-1, β-catenin, p300. β-catenin participation in RORα transactivation may be revealing a link with Wnt signaling pathway, which is consistently important in cerebellar development. Purkinje cells differentiation depends on granule cells, while granule cells proliferation depends on some factors produced by Purkinje cells. One of them is Sonic hedgehog (Shh), whose expression in Purkinje cells is reduced by several fold in *sg/sg* mice. Shh interacts with Patched (Ptch) receptors on granule precursors and activates GLI Krüppel-like zink finger proteins, which transactivate N-Myc and some other cell cycle regulation proteins. The latter are decreased in granule cells of *sg/sg* mice along with Shh [260, 267].

RORα and retinoic acid receptor-related orphan receptor gamma (RORγ) play redundant roles in the liver. They control expression of many genes including *Ccl5* (RANTES), one of pivotal factors of $T_{CONV}$ and $T_{REG}$ differentiation as well as a long list of genes involved in lipid metabolism, particularly cytochrome P450 genes (*Cyp*) with *Cyp7b1* being preferentially regulated by RORα. The latter regulate bile acids biosynthesis and *sg/sg* mice have lower serum cholesterol level (as well as that of triglycerides). A gene potentially specifically repressed by RORα in the liver is *Sult1e1*. RORα is involved in organismal circadian clock molecular machinery by activating *Arntl* gene transcription of BMAL1 protein. RORα competes with another nuclear receptors REV-ERBα/β for the RORE response element in *Arntl* promoter. Acting together, RORα and REV-ERBs maintain circadian pattern of *Arntl* transcription[268, 269]. BMAL1-CLOCK complex drives *Per* expression further transmitting rhythmicity signal. RORα is important in allergy, as *sg/sg* develop less severe phenotype in the OVA-induced AAI, with less eosinophils, neutrophils and lymphocytes infiltration in the lungs

and bronchoalveolar lavage (BAL), as well as less IL-4, IL-5 and IL-13 production. Very recently, RORα was identified as an important molecule in intestinal homeostasis, as demontrated by increased inflammation in mice with RORα deficiency in intestinal epithelial cells [270].

Several functions of RORα have been studied in the liver. However it is expressed and has known effects in immune cells. LPS-activated *sg/sg* macrophages or mast cells produced higher levels of TNFα and IL-6 than controls [271]. One proposed mechanism of repression of cytokine expression by RORα is through IKBα, directly transactivated by the protein. A study on THP-1 cell line demonstrated hyperactivated state of cells deficient for RORα with increased levels of TREM1, TNF,IL1B, IL6, clearly stressing involvement of the NFκB-regulated genes and resulting in an M1 bias in deficient cells [272]. According to another study, RORα promotes M2 polarization of macrophages in the liver, which is dependent on KLF4, and protects mice against NASH [273]. Based on these studies RORα is sometimes considered a negative regulator of inflammation.

RORα is required for the development of ILC2 and for allergic inflammation largely mediated by these cells [274]. RORα also controls a population of ILC3, which was shown to drive fibrosis in the mouse model of Crohn's disease [275].

In *sg/sg* mice the spleen and the thymus are decreased in size, as well as in total numbers of thymocytes and splenocytes. RORα mRNA is increased during development of T cells in the thymus from DP up to a SP state and is preserved at relatively high level in mature CD4$^+$ lymphocytes compared to CD8$^+$T cells and B cells. B cells, however, do express RORα and a knockdown of it's gene in IgA$^+$ B cells strongly reduces IgA BCR transcription [276]. Proliferation of *sg/sg* T cells in response to anti-CD3 or LPS treatment was normal. RORα participates in the development of T$_H$17 cells together with RORγt. However is dispensable for this process and it's deletion leads to only partial reduction in IL-17 and IL-23R in T$_H$17 cells [198]. A new study investigating RORα role in CD4$^+$T cells and shows the broad expression of the receptor in activated T$_H$ cells, (Only pre-print version available https://www.biorxiv.org/content/10.1101/709998v2.full). *Rora* deficiency in CD4$^+$ T cells exacerbates allergic asthma caused by *N. brasiliensis* infection. Also, RORα was highly expressed in T$_H$ cells during *Schistosoma mansoni* worm infection. IL-33 and CCL7 promote *Rora* expression in CD4$^+$ T cells and CCL22 and SDF1a inhibit it. RORα downstream genes highlighted in the study were *Tnfrsf25*, *Arntl*, *S100a4*, *Cxcr6*, *Alox8*, *St6galnac3*.

Recently, RORα role in T$_{REG}$ was shown during atopic dermatitis. Mice with T$_{REG}$-specific deficiency of RORα developed a stronger skin inflammation with increased T$_H$2 cytokines levels and ILC2 numbers. The proposed mechanism implies that RORα action is mediated through *Tnfrsf25*, which restrains ILC2 and EOS infiltration [116].

# Chapter 4

# Aims

With this work we expect to obtain an understanding of the role of RORα in $T_{REG}$ cells. The objectives of this work are:

1. To identify a role of RORα in VAT $T_{REG}$ in the steady state and DIO;

2. To test participation of RORα$^+$ $T_{REG}$ in type 2 immunity-associated pathologies: DIO and HDM-induced AAI model;

3. To elucidate molecular mechanisms of potential $T_{REG}$ control by RORα.

# Chapter 5

# Results

## 5.1 Generation and characterization of RORα$^{\text{Foxp3/Foxp3}}$ mice

In order to study the potential contribution of RORα to T$_{\text{REG}}$ development and function, we generated mice with T$_{\text{REG}}$-specific *Rora* deficiency by crossing *Rora* $^{\text{fl/fl}}$ mice harboring loxP sites flanking a short sequence in the third exon of *Rora* gene (Figure 5.1a) with FOXP3YFP-Cre mice. Gene targeting led to the deletion of a 86 bp sequence encoding part of DNA-binding domain in RORα$^{\text{Foxp3/Foxp3}}$ mice. Mice obtained by breeding *Rora*$^{\text{WT/WT}}$ mice with FOXP3YFP-Cre mice were used as control (referred to as RORα$^{\text{WT/WT}}$ mice). PCR-based tests for WT and mutant allele as well as for potential *Rora* δ allele recombination were performed in sorted YFP$^+$CD4$^+$ and YFP$^-$CD4$^+$ cells from RORα$^{\text{Foxp3/Foxp3}}$ mice and RORα$^{\text{WT/WT}}$ mice. Deletion was observed only in YFP$^+$CD4$^+$ cells from RORα$^{\text{Foxp3/Foxp3}}$ mice (Figure 5.1b). *Rora* deletion was neither detected in YFP$^-$CD4$^+$ (referred to as Tconv) cells from RORα$^{\text{Foxp3/Foxp3}}$ mice nor in CD4$^+$ cells from RORα$^{\text{WT/WT}}$ mice regardless of YFP expression (Figure 5.1b). At mRNA level, quantitative polymerase chain reaction (qPCR) performed on sorted YFP$^+$CD4$^+$ and YFP$^-$CD4$^+$ cells showed a 10-fold decrease of *Rora* gene expression in YFP$^+$CD4$^+$ cells from RORα$^{\text{Foxp3/Foxp3}}$ mice compared to those from RORα$^{\text{WT/WT}}$ mice while no significant decrease was observed for *Rora* mRNA expression in Tconv (Figure 5.2a). These data suggests that RORα deletion in RORα$^{\text{Foxp3/Foxp3}}$ mice is T$_{\text{REG}}$-specific.

## 5.2 RORα does not affect development and functional activity of T$_{\text{REG}}$ in homeostatic conditions but promotes type 2 cytokine genes expression

RORα$^{\text{Foxp3/Foxp3}}$ mice were viable, displayed normal appearance and weight (Figure 5.1c-d). Both male and female RORα$^{\text{Foxp3/Foxp3}}$ mice were born at the expected Mendelian frequencies and did neither show any detectable autoimmune pathology nor the staggerer phenotype observed in *Rora*$^{sg/sg}$ mice during at least one year of life. In line, histological assessment of various tissues did not reveal any signs gross tissue alterations (Figure 5.1l). Compared with RORα$^{\text{WT/WT}}$ mice, numbers of CD4$^+$ and CD8$^+$ T cell subsets were unaltered in thymic and peripheral immune compartments from RORα$^{\text{Foxp3/Foxp3}}$ mice (data not shown). By contrast, differences in T$_{\text{REG}}$ proportions were found in some non-immune tissues. Indeed, in colon, but not in spleen, the percentage of total FOXP3$^+$ T$_{\text{REG}}$ (Figure 5.2b and S1e-g), as well as RORγt$^+$subpopulations (data not shown), were lower in

ROR$\alpha^{\text{Foxp3/Foxp3}}$ mice. In spleen and lungs, a slight decrease in CD44$^+$FOXP3$^+$ cells was found in ROR$\alpha^{\text{Foxp3/Foxp3}}$ mice suggesting the effect of ROR$\alpha$ on T$_{\text{REG}}$ activation or their accumulation in tissues (Figure 5.2c-f). However, expression of function-associated molecules CD25, CD69 and T-BET was unaltered (Figure 5.1h-j). In agreement, *in vivo* suppression assay, using a model of T cell-induced colitis [277], revealed a slightly improved, but not compromised suppressive capacity of ROR$\alpha^{\text{Foxp3/Foxp3}}$ T$_{\text{REG}}$ compared to their ROR$\alpha^{\text{WT/WT}}$ counterparts as shown by less pronounced weight loss in animals injected by ROR$\alpha^{\text{Foxp3/Foxp3}}$ T$_{\text{REG}}$ (Figure 5.2h), without major differences regarding histological inflammation (Figure 5.2g, i). Yet, IL-4 and IL-13 expression was higher upon injection of ROR$\alpha^{\text{Foxp3/Foxp3}}$ T$_{\text{REG}}$ (Figure 5.2j). The results suggest ROR$\alpha$ expression in T$_{\text{REG}}$ is not critical for their normal development and function in homeostatic conditions. However, in inflammatory conditions, absence of ROR$\alpha$ in T$_{\text{REG}}$ leads to an increase in type 2 cytokine expression in the intestine.
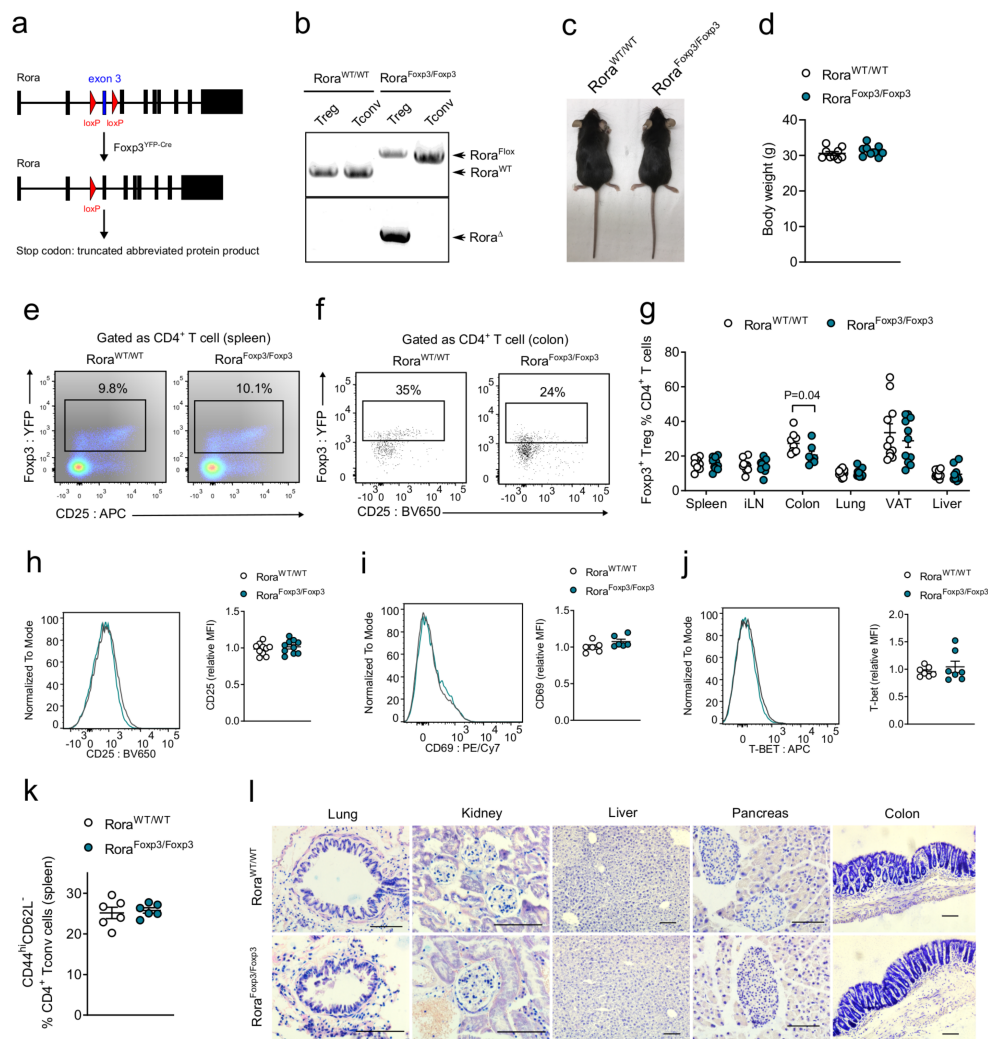
Figure 5.1 – **Characterization of unmanipulated RORα<sup>Foxp3/Foxp3</sup> mice**
**a.** Scheme of targeted *Rora* allele, and localization of Cre-mediated deletion; **b.** DNA analysis showing presence of floxed allele in RORα<sup>Foxp3/Foxp3</sup> mice and specificity of Cre-mediated *Rora* deletion in RORα<sup>Foxp3/Foxp3</sup> T<sub>REG</sub> but not in Tconv cells sorted from spleens from unmanipulated from RORα<sup>WT/WT</sup> and RORα<sup>Foxp3/Foxp3</sup> mice; **c.** Representative photographs of unmanipulated 12 week old female RORα<sup>WT/WT</sup> and RORα<sup>Foxp3/Foxp3</sup> mice ; **d.** Body weight (groups as in c.), n = 9; **e-g.** T<sub>REG</sub> proportions in tissues (groups as in c.). Flow cytometry dot plot from spleen (e.), colon (f.) percentages in indicated tissues (groups as in c.) (g.), n = 8-12; Student t-test; h-j. Expression of T cell activation or differentiation markers by splenic T<sub>REG</sub>s. CD25 (h.), CD69 (i.) and Tbet (j.) Histogram plots (left panels) and MFI (right panels), n = 6-7; **k.** Proportions of CD44<sup>high</sup>CD62L<sup>−</sup>CD4<sup>+</sup> T cells (groups as in c.), n = 6; **l.** Histology of various non-lymphoid tissue (NLT) (groups as in c.), MGG staining Scale bar 100 μm.
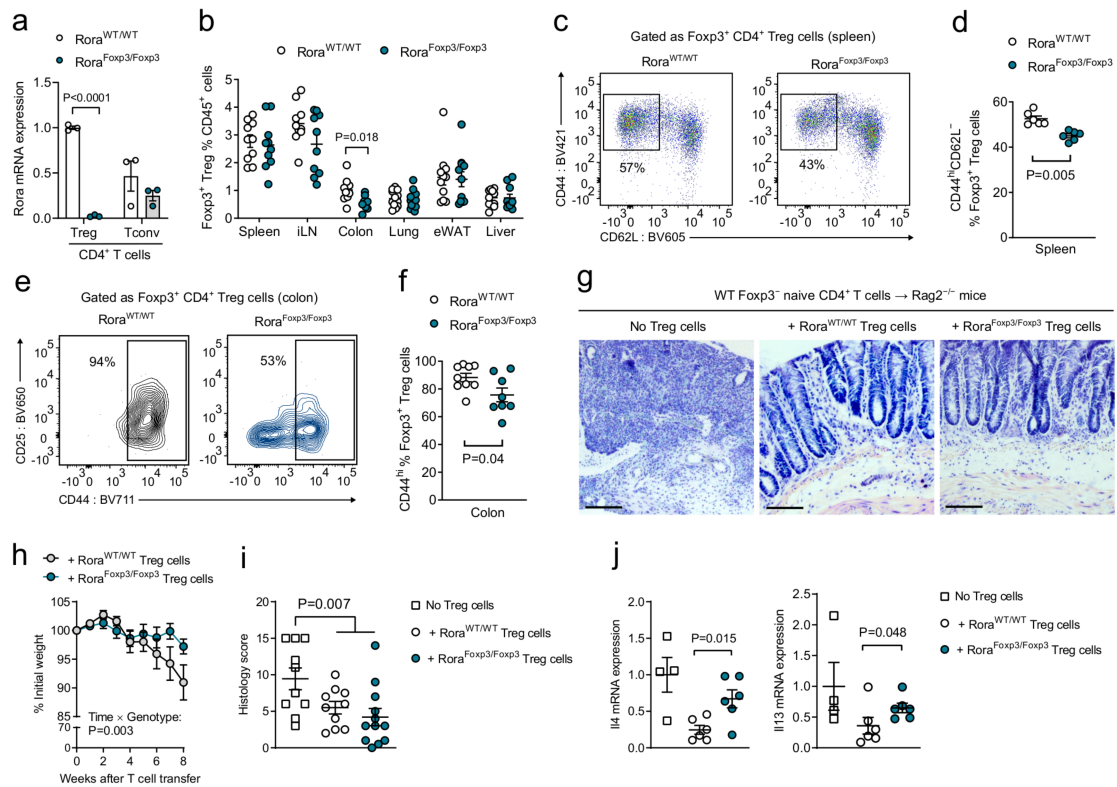
Figure 5.2 – **RORα expression and selective inactivation in $T_{REG}$**

**a.** mRNA expression level of *Rora* in forkhead box P3 (FOXP3)$^+$ and FOXP3$^-$ CD4$^+$ T cells sorted form RORα$^{WT/WT}$ or RORα$^{Foxp3/Foxp3}$ mice, n = 3. Student t-test; **b.** Proportions of $T_{REG}$ cells in tissues of RORα$^{WT/WT}$ and RORα$^{Foxp3/Foxp3}$ mice, n = 9-10, Student t-test; **c-f.** CD44 and CD62L expression in splenic **(c-d)** and colonic **(e-f)** $T_{REG}$. Representative dot plot of CD44 and CD62L expression **(c, e)**. $T_{REG}$ were gated as CD45$^+$TCRβ$^+$CD4$^+$YFP$^+$, numbers represent mean percentages, n = 6(c)-9(e); Proportions of CD44$^{high}$CD62L$^-$$T_{REG}$ **(d, f)**; n = 9; **g-j.** $T_{REG}$ regulation of naïve T cell-induced colitis in Rag2$^{-/-}$ mice. Histological analysis of colons upon MGG staining **(g)** No $T_{REG}$ cotransferred (left panel), RORα$^{WT/WT}$ $T_{REG}$ cotransferred (middle panel), RORα$^{Foxp3/Foxp3}$ $T_{REG}$ cotransferred (right panel). Scale bar 100 μm; **h.** Body weight (groups as in **g**).n = 10-11, repeated measures ANOVA; **i.** Histological severity scoring (groups as in g). n = 10-11, Unpaired two-tailed t-test; **j.** mRNA expression of IL-4 (left panel) and IL-13 (right panel) (groups as in **g**). n = 4-6, Student t-test.

## 5.3  RORα deletion in $T_{REG}$ aggravates type 2-mediated allergic airway inflammation

To further examine a potential role for $T_{REG}$-expressed RORα in the regulation of type 2 inflammation, we used an established of model of HDM-induced allergic aiway inflammation (AAI) model (Figure 5.3a) [163]. HDM-induced AAI was more pronounced in RORα$^{Foxp3/Foxp3}$ mice compared with RORα$^{WT/WT}$ mice as shown by increased inflammatory infiltrates in lung (Figure 5.3b). In line, analysis of bronchoalveolar lavage fluid, lungs and mediastinal lymph node (mLN) revealed an
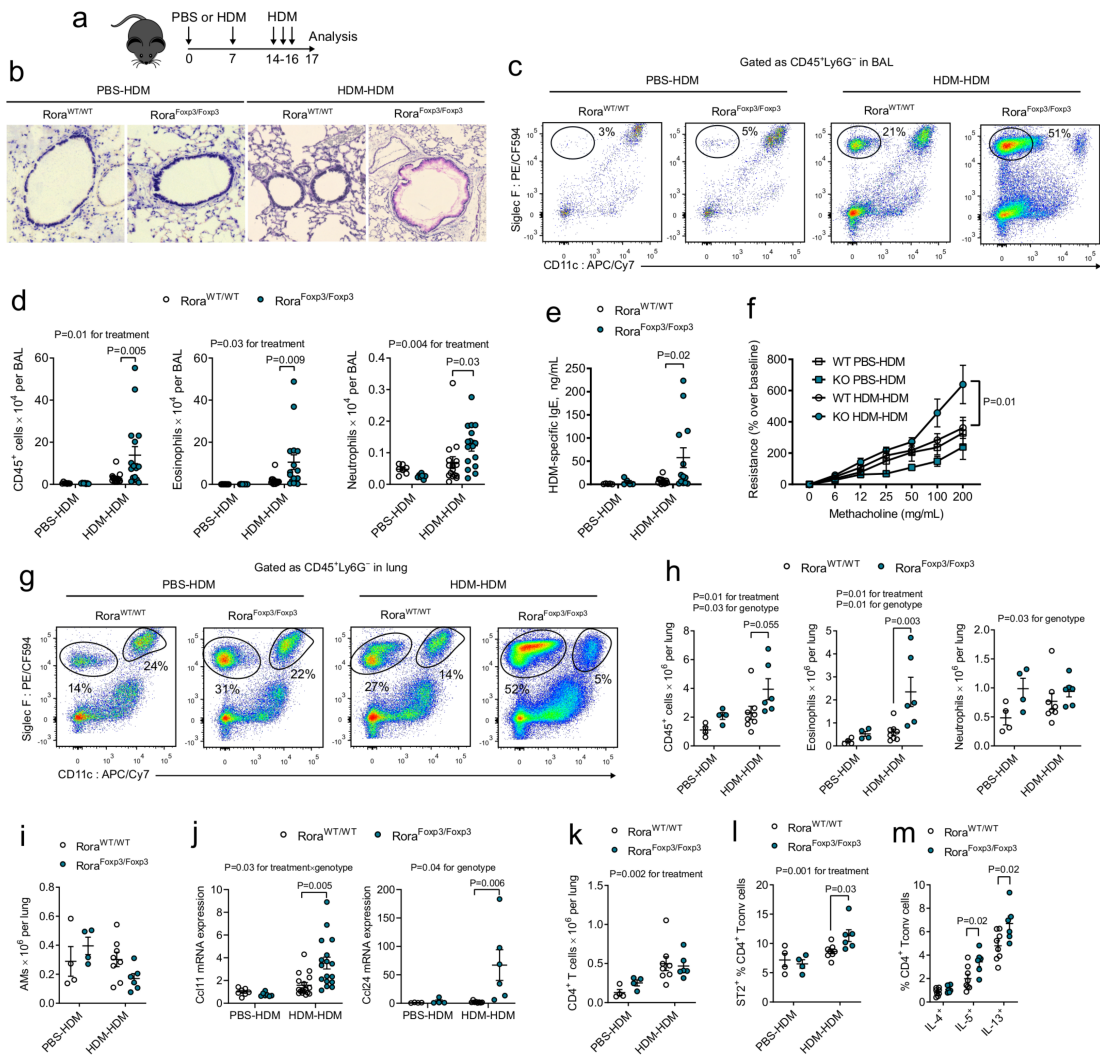
**Figure 5.3 – Increased Allergic Airway Inflammation in RORα$^{Foxp3/Foxp3}$ mice**
**a.** Scheme of HDM-induced AAI model in RORα$^{WT/WT}$ and RORα$^{Foxp3/Foxp3}$ mice; **b.** Histological analysis of airways upon MGG staining. PBS-HDM: Vehicle-sensitized and antigen-challenged animals. HDM-HDM: antigen-sensitized and -challenged animals. Scale bar 100 μm **c.** Eosinophilia (SiglecF$^+$CD11c$^-$ cells) in bronchoalveolar lavage fluid (BALF). Representative dot plot (groups as in b). Numbers are mean percentages, n = 9-15; **d.** Numbers of immune cells (left panel), eosinophils (middle panel) and neutrophils (right panel) in BALF (groups as in b). Student t-test; **e** HDM-specific IgE plasmatic concentrations (groups as in b); **f.** Airway resistance upon increasing methacholine concentrations. Student t-test; **g.** Lung eosinophilis (SiglecF$^+$CD11c$^-$ cells) and alveolar macrophages (SiglecF$^+$CD11c$^+$ cells),Representative dot plot n = 4-8; **h-i.** Numbers of lung immune cells (h. left panel), eosinophils (h. middle panel), neutrophils (h. right panel) and macrophages (i). Student t-test. n = 4-8 (groups as in b) ; **j.** Lung mRNA expression of CCL11 (left panel) and CCL24 (right panel) Student t-test; n = 4-16 (groups as in b); **k-m.** Numbers of lung CD4$^+$ T cells (k);. proportion of lung ST2$^+$ CD4$^+$ T conv (l); proportion of lung IL-4$^+$, IL-5$^+$, IL-13$^+$ CD4$^+$ T conv (m). Student t-test. n = 6-8 (groups as in b).
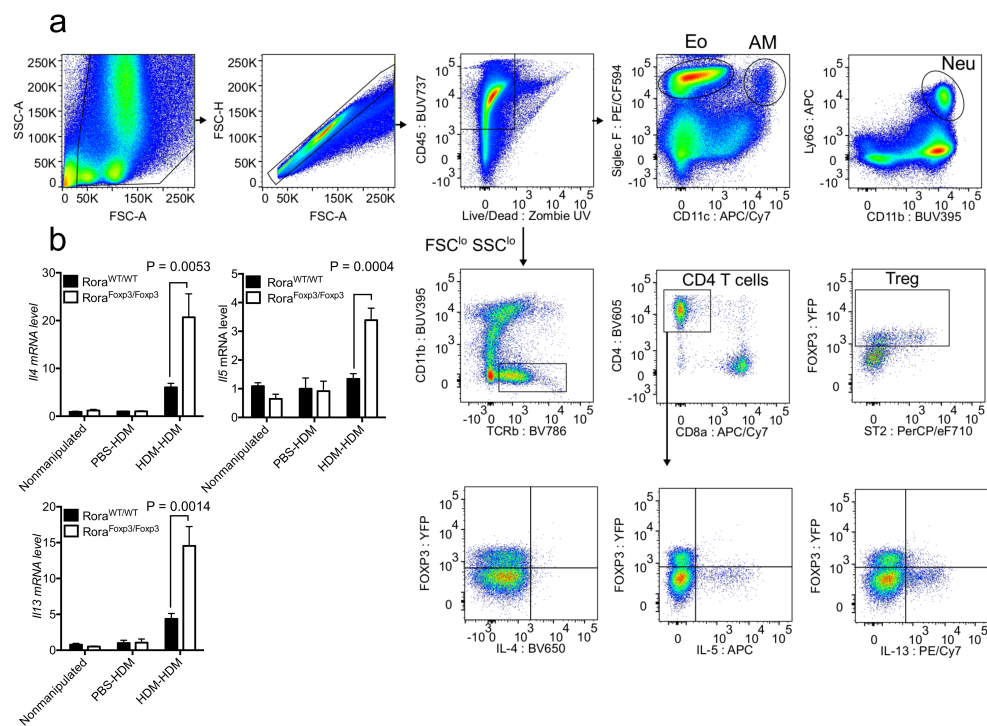
Figure 5.4 – **Allergic Airway Inflammation in RORα$^{\text{Foxp3/Foxp3}}$ mice**
**a.** Gating strategy for immune cells in RORα$^{\text{Foxp3/Foxp3}}$ mice. Eo: eosinophils, AM: alveolar macrophages, Neu: neutrophils, T$_{\text{REG}}$: Regulatory T cells; **b.** mRNA expression levels in lung tissue during HDM-induced AAI model, Student t-test; n = 6-8

increase in total CD45$^+$ cells, with pronounced eosinophilia in RORα$^{Foxp3/Foxp3}$ mice compared with RORα$^{WT/WT}$ mice in both lung and BALF (Figure 5.3c-d, g-h). We also observed higher HDM-specific IgE concentrations (Figure 5.3e), characteristic of increase type 2 response. Futhermore airway resistance (AR) upon increasing methacholine concentrations was increased in RORα$^{Foxp3/Foxp3}$ mice (Figure 5.3f). RORα$^{Foxp3/Foxp3}$ mice also displayed slightly lower number of alveolar macrophages (AM) (not satistically significant) (Figure 5.3i). Lung expression of type 2-associated cytokines IL-4 and IL-13 (controlling IgE synthesis), IL-5 (controlling eosinophil differentiation (Figure 5.4b) and chemokines (CCL11 and CCL24) (Figure 5.3j), associated to eosinophil recruitment was increased in RORα$^{Foxp3/Foxp3}$ mice. In line, increased numbers of CD4$^+$ T cells expressed ST2/IL-33R, IL-5 and IL-13 in RORα$^{Foxp3/Foxp3}$ mice (Figure 5.3k-m). By contrast, there were no differences in expression T$_H$1- or T$_H$17-associated molecules at mRNA (data not shown). These results suggest that T$_{REG}$-expressed RORα restricts type 2 response in allergic lung.

## 5.4  RORα deletion in T$_{REG}$ alters intrinsic transcriptomic program and cell cycle progression

Regarding T$_{REG}$ themselves, proportion of FOXP3$^+$ T$_{REG}$ was decreased in allergic lungs and mLN in RORα$^{Foxp3/Foxp3}$ mice compared with RORα$^{WT/WT}$ mice (Figure 5.5a, b, d). As lung T$_{REG}$ increase expression of ST2 in inflammatory conditions [115], we examined its expression in AAI but found no differences in ST2$^+$ T$_{REG}$ between the 2 genotypes (Figure 5.5c). However, an increase in IL-5$^+$FOXP3$^+$CD4$^+$ T$_{REG}$ cells in lungs and mLN in RORα$^{Foxp3/Foxp3}$ mice (Figure 5.5e) suggests potentially compromised stability of the "regulatory phenotype" of RORα-deficient T$_{REG}$ cells and their acquisition of a more T$_H$2-like phenotype in AAI. Transcriptomic profiling of sorted lung and mLN T$_{REG}$ from allergic mice showed that these two populations were transcriptionally distinct, in line with their respective non lymphoid and lymphoid tissue localization (Figure 5.5f). Indeed, an overlap with tissue-T$_{REG}$ gene set from a recent publication showed a robust induction of these genes in lung T$_{REG}$ (Figure 5.6a). Furthermore, RORα deficiency had a broader impact on lung T$_{REG}$ transcriptome than on mLN T$_{REG}$ transcriptome, suggesting a major role for this nuclear receptor in non lymphoid tissue T$_{REG}$ (Figure 5.5f). Among down-regulated genes in both mLN and lung RORα$^{Foxp3/Foxp3}$ T$_{REG}$, several genes from the core circadian clock machinery (*Arntl, Cry1, Nr1d2*), in agreement with the known regulatory role of RORα in these processes (Figure 5.5g-h).

Further analysis of gene expression profile in T$_{REG}$ cells isolated from lungs and mLN during HDM-induced AAI model revealed substantial alterations of cell cycle associated transcripts (Figure 5.5g-h). In both lung and mLN T$_{REG}$ an enrichment was seen in targets of dimerization partner, RB-like, E2F and multi-vulval class B (DREAM) complex, the most potent RB-independent controller of the cell cycle, in particular its late phases [278] (Figure 5.6f). Indeed, no differences of RB phosphorylation in lung T$_{REG}$ was observed between RORα$^{WT/WT}$ and RORα$^{Foxp3/Foxp3}$ mice, suggesting that observed effects are RB-independent (Figure 5.6c). Only few genes were weakly downregulated, while upupregulated genes included *Cenpp, Prr11, Nuf2, Cep55*, which are centromere and kinetochore proteins as well as cyclins-associated genes like *Cdc25b, Cdkn3* (Figure 5.5g-h). Differentially expressed gene sets between RORα$^{WT/WT}$ and RORα$^{Foxp3/Foxp3}$ T$_{REG}$ confirmed cell cycle dysregulation, in particular gap 2 - mitosis checkpoint (G2-M) checkpoint, E2F targets and Mitotic spindle gene sets, associated with late cell cycle regulation (Figure 5.5i-j). Other differentially expressed gene sets included IL2/STAT5 signaling, IFNγ response and mTORC1 signaling (Figure 5.5i-j), strongly suggesting defective activation and proliferation. The latter might account for smaller numbers of T$_{REG}$ in lung and mLN. To further assess alteration in cell cycle, we determined cycle distribution of RORα$^{WT/WT}$ and RORα$^{Foxp3/Foxp3}$ T$_{REG}$ *in vivo* by injecting mice with 5-ethynyl-2'-deoxyuridine (EdU) during antigen challenge. We observed increased numbers of EdU$^+$ lung T$_{REG}$ cells with a 4n DNA-content and slightly decreased
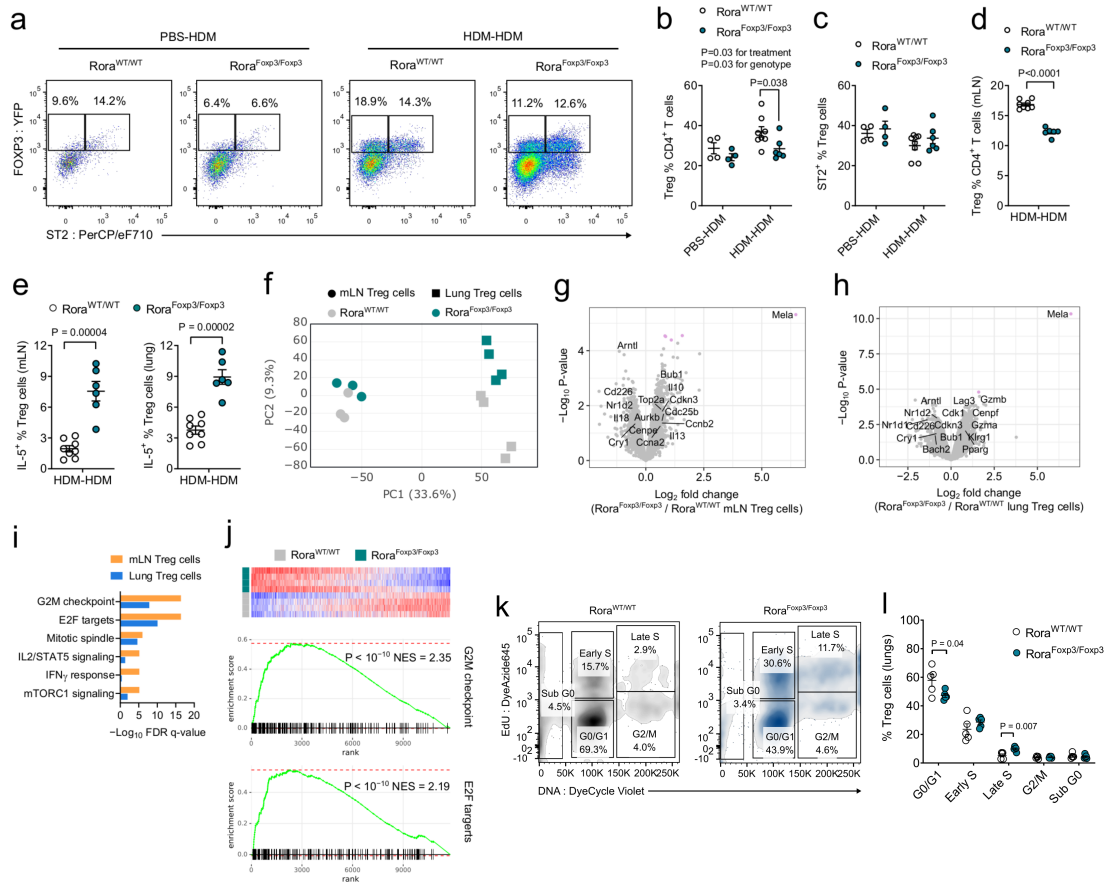
**Figure 5.5 – Altered transcriptional program and cell cycle in T$_{REG}$ from allergic RORα$^{Foxp3/Foxp3}$ mice**

Allergic airway inflammation (AAI) in RORα$^{WT/WT}$ and RORα$^{Foxp3/Foxp3}$ mice was induced as in Figure 5.3a. **a.** ST2 expression on lung T$_{REG}$. Numbers are mean percentages, n = 4-7; (groups as in Figure 5.2b); **b-d.** Proportions lung T$_{REG}$ (b.), lung ST2$^+$ T$_{REG}$(c.) and mLN T$_{REG}$ (d) Student t-test, n = 6-8. (groups as in Fig 1b); **e.** Proportion of IL-5$^+$ mLN (left panel) and lung (right panel) in allergen-sensitized and -challenged mice. Student t-test, n = 6-8; **f.** Principal component analysis (PCA) analysis of gene expression data from mLN and lung T$_{REG}$ microarray. n = 4 (mLN)-4 (lungs) (groups as in e.); **g-h.** Volcano plots of gene expression data analysis of mLN (g.) and lungs (h) T$_{REG}$ (groups as in e.); **i.** Gene sets enriched in differentially expressed genes between mLN and lung T$_{REG}$ from RORα$^{WT/WT}$ and RORα$^{Foxp3/Foxp3}$ mice; **j.** Gene set enrichment analysis (GSEA) plots of the two top enriched gene sets in lung T$_{REG}$; **k.** Cell cycle analysis by flow cytometry of lung T$_{REG}$. Numbers are mean values, n = 5, data representative ofr two independent experiments (groups as in e.); **l.** Proportions of lung T$_{REG}$ cells in different phases of cell cycle, n = 5, data representative for two independent experiments(groups as in e.).
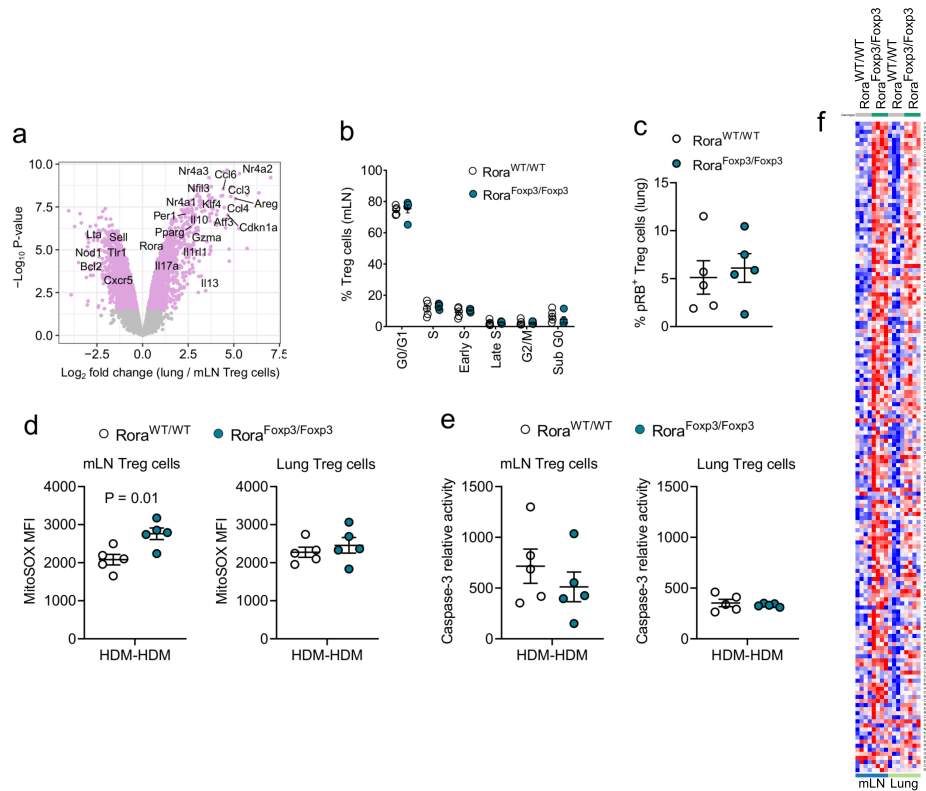
**Figure 5.6 – T_REG analysis in allergic RORα^Foxp3/Foxp3 mice**

**a.** Volcano plot for differential gene expression profiles in lung and mLN T_REG from RORα^WT/WT vs RORα^Foxp3/Foxp3 mice in HDM-induced allergic airway inflammation n = 5; **b.** Proportions of mLN T_REG from RORα^WT/WT and RORα^Foxp3/Foxp3 mice in different phases of cell cycle measured by flow cytometry. n = 5; **c.** RB protein phosphorylation in lung T_REG cells (groups as in b.). n = 5; **d.** mtROS content in mLN and lung T_REG (groups as in b.) using in MitoSOX staining. Student's t-test? n = 5 ; **e.** Caspase-3/7 activity in mLN and lung T_REG (groups as in b.). n = 5; **f.** Genes from gene set "DREAM complex targets", significantly differentially regulated in mLN and lung T_REG during HDM-induced AAI model.

number of EdU$^-$ lung $T_{REG}$ with a 2n DNA in $T_{REG}$ from ROR$\alpha^{Foxp3/Foxp3}$ mice (Figure 5.5k-l), but not in mLN $T_{REG}$. This indicates that ROR$\alpha^{Foxp3/Foxp3}$ $T_{REG}$ in allergic lung may be blocked before G2-M checkpoint and S phase completion and, harbor a smaller proportion of quiescent cells. As altered cell cycle progression and checkpoint control induce reactive oxygen species (ROS) [279], we evaluated mitochondrial ROS production and found that mLN but not lung $T_{REG}$ in ROR$\alpha^{Foxp3/Foxp3}$ mice showed higher ROS content (Figure 5.6d). However, this did not affect apoptosis levels as measured by caspase activity (Figure 5.6e). These results suggests that ROR$\alpha$ deficiency in $T_{REG}$ leads to cell cycle alterations impacting on $T_{REG}$ pool with a stronger effect on lung (non lymphoid) tissue $T_{REG}$ than on mLN $T_{REG}$.

## 5.5 ROR$\alpha$ deletion in $T_{REG}$ improves metabolic parameters in diet-induced obesity by type 2 response

In contrast to allergic diseases [280], type 2 immune response is beneficial for the adipose tissue homeostasis, as well as for local and systemic glucose tolerance and insulin sensitivity. Adipose tissue-resident $T_{REG}$ cells participate in adipose tissue homeostasis and obesity is associated with paucity of the resident $T_{REG}$ as well as to a switch from a type 2 to a type 1/17 local environment [127]. We thus investigated the contribution of $T_{REG}$-expressed ROR$\alpha$ to adipose tissue and metabolic homeostasis at steady state and in DIO. Unmanipulated 20-25-week-old male ROR$\alpha^{Foxp3/Foxp3}$ mice fed with CD displayed no significant differences in body weight or proportions of the white adipose tissue compared with ROR$\alpha^{WT/WT}$ mice (Figure 5.7a-b). However, induction of DIO upon feeding a HFD led to lower body weight gain and lower adipose tissues proportion in ROR$\alpha^{Foxp3/Foxp3}$ mice (Figure 5.7a-c) without difference in food intake (Figure 5.8a). Expansion of the adipose tissue depends on both adipogenesis and accumulation of lipids within adipocytes [281], leading to both adipocyte hyperplasia and hypertrophy. To investigate whether lower body weight and adiposity in ROR$\alpha^{Foxp3/Foxp3}$ mice resulted from adipocyte hyperplasia or hypertrophy, we measured adipocyte diameter in VAT and analyzed proportions of adipocyte progenitors, CD24$^+$ adipose-derived stem cell (ASC) and CD24$^-$ preadipocytes by flow cytometry. Mice from either genotype fed with CD or HFD had similar microscopic structure of epididymal white adipose tissue (eWAT) with no changes in adipocyte size (Figure 5.7d, e). HFD feeding resulted in increased proportion of ASC in stromal vascular fraction regardless of the genotype. By contrast, in inguinal white adipose tissue (iWAT) it reduced preadipocytes proportion of in ROR$\alpha^{WT/WT}$ mice but increased it in ROR$\alpha^{Foxp3/Foxp3}$ animals suggesting that ROR$\alpha$ deficiency in $T_{REG}$ might have an effect on adipogenesis in subcutaneous adipose tissue (Figure 5.8b).

Gene expression profiling of eWAT from ROR$\alpha^{Foxp3/Foxp3}$ and ROR$\alpha^{WT/WT}$ mice upon DIO showed an enrichment of fatty acid metabolism, adipogenesis, mTORC1 signaling, hypoxia and glycolysis pathways among the most up-regulated genes in ROR$\alpha^{Foxp3/Foxp3}$ eWAT (Figure 5.7f). These signs are usually considered detrimental, however, downstream of gene expression, plasma adipokines (leptin and adiponectin) (Figure 5.10a-b) as well as triglycerides (TG) (Figure 5.10c) and ketone bodies (Figure 5.10e) concentrations were similar for both genotypes. Importantly, cholesterol concentrations were lower in HFD-fed ROR$\alpha^{Foxp3/Foxp3}$ mice than in ROR$\alpha^{WT/WT}$ mice (Figure 5.10d). In line, Retnla, an adipokine with a cholesterol lowering effect [282], several genes associated to insulin sensitivity, some of them controlling lipid metabolism (*Fasn, Dgat1, Pnpla3, Acaca*) [283, 284, 285] and adipocyte differentiation associated *Lpin1* [286] were upregulated (Figure 5.7f). Down-regulated genes were largely associated with inflammation, including KRAS-signaling, inflammatory response, TNF$\alpha$ signaling via nuclear factor kappa-B (NF$\kappa$B) (Figure 5.7f, h). Among the most downregulated genes, *Spp1* and *Ctsk* repectively encoding for osteopontin and cathepsin K are associated with obesity and IR [287, 288] (Figure 5.7h). Anti-inflammatory changes in ROR$\alpha^{Foxp3/Foxp3}$ eWAT are further
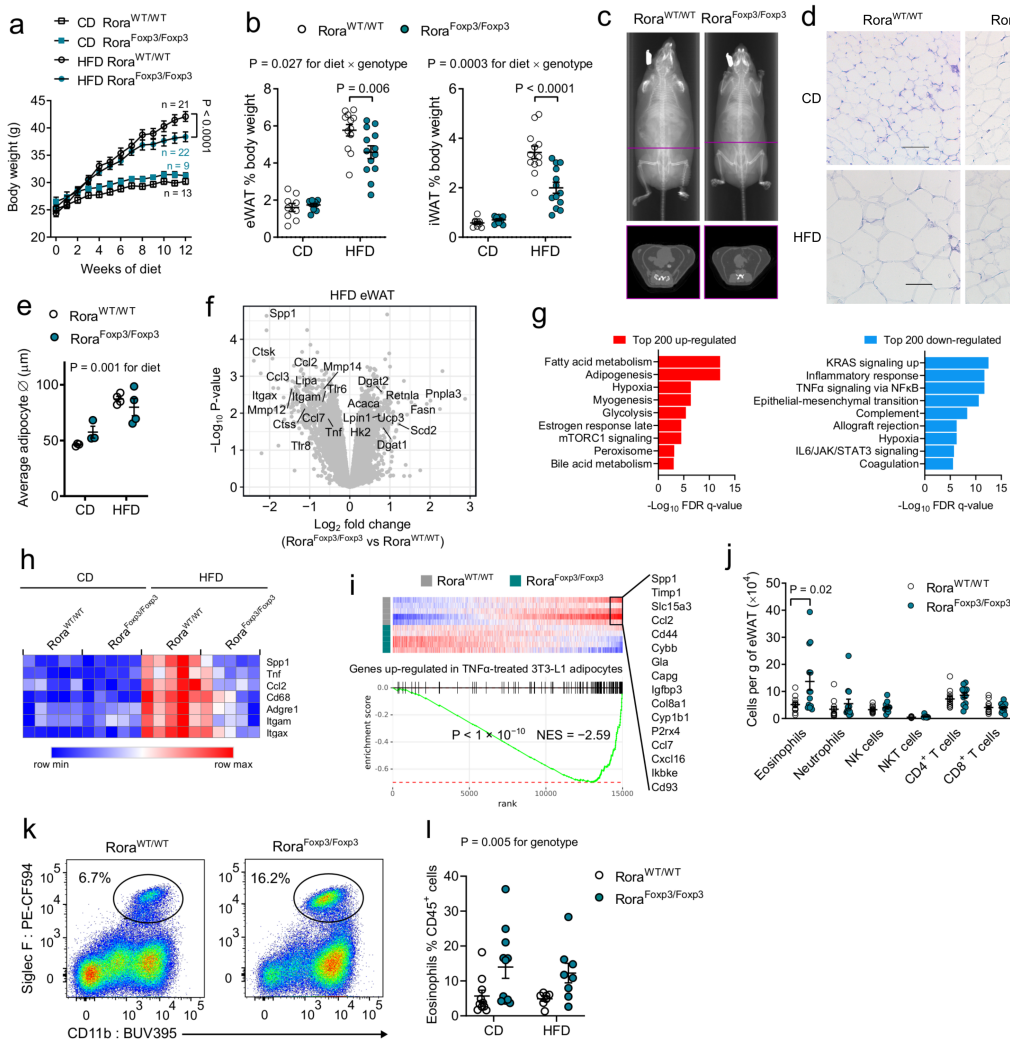
Figure 5.7 – **Improvement of weight gain and adipose tissue inflammation in RORα$^{Foxp3/Foxp3}$ mice in diet-induced obesity**
**a.** Body weight of RORα$^{WT/WT}$ and RORα$^{Foxp3/Foxp3}$ mice mice upon high fat diet (HFD) or Chow diet (CD) feeding for 12 weeks. repeated measures ANOVA ; **b.** Proportions of epididymal white adipose tissue (eWAT) and inguinal white adipose tissue (iWAT) as percentage of body weight. Student t-test and 2-way ANOVA, n = 9-22; **c.** Computerized tomography upon HFD feeding; **d.** Histological analysis of eWAT upon MGG staining. Scale bar 100 μm; **e.** Adipocyte diameter, 2-way ANOVA; **f.** Volcano plot of gene expression data analysis from eWAT of RORα$^{WT/WT}$ and RORα$^{Foxp3/Foxp3}$ mice, n = 3-4; **g.** Top up- and down-regulated gene sets in gene expression data from eWAT; **h.** Heat map of selected immune-related genes in eWAT; **i.** GSEA plot comparing gene expression profiles of eWAT of RORα$^{WT/WT}$ and RORα$^{Foxp3/Foxp3}$ mice with top 100 up-regulated genes in tumor necrosis factor alpha (TNFα)-treated mouse 3T3-L1 cells; **j-l.** Proportions of eWAT immune cells (j.) and eosinophils (k-l) with a representative dot plot analysis (k.) in RORα$^{WT/WT}$ and RORα$^{Foxp3/Foxp3}$ mice, Student t-test or 2-way ANOVA.
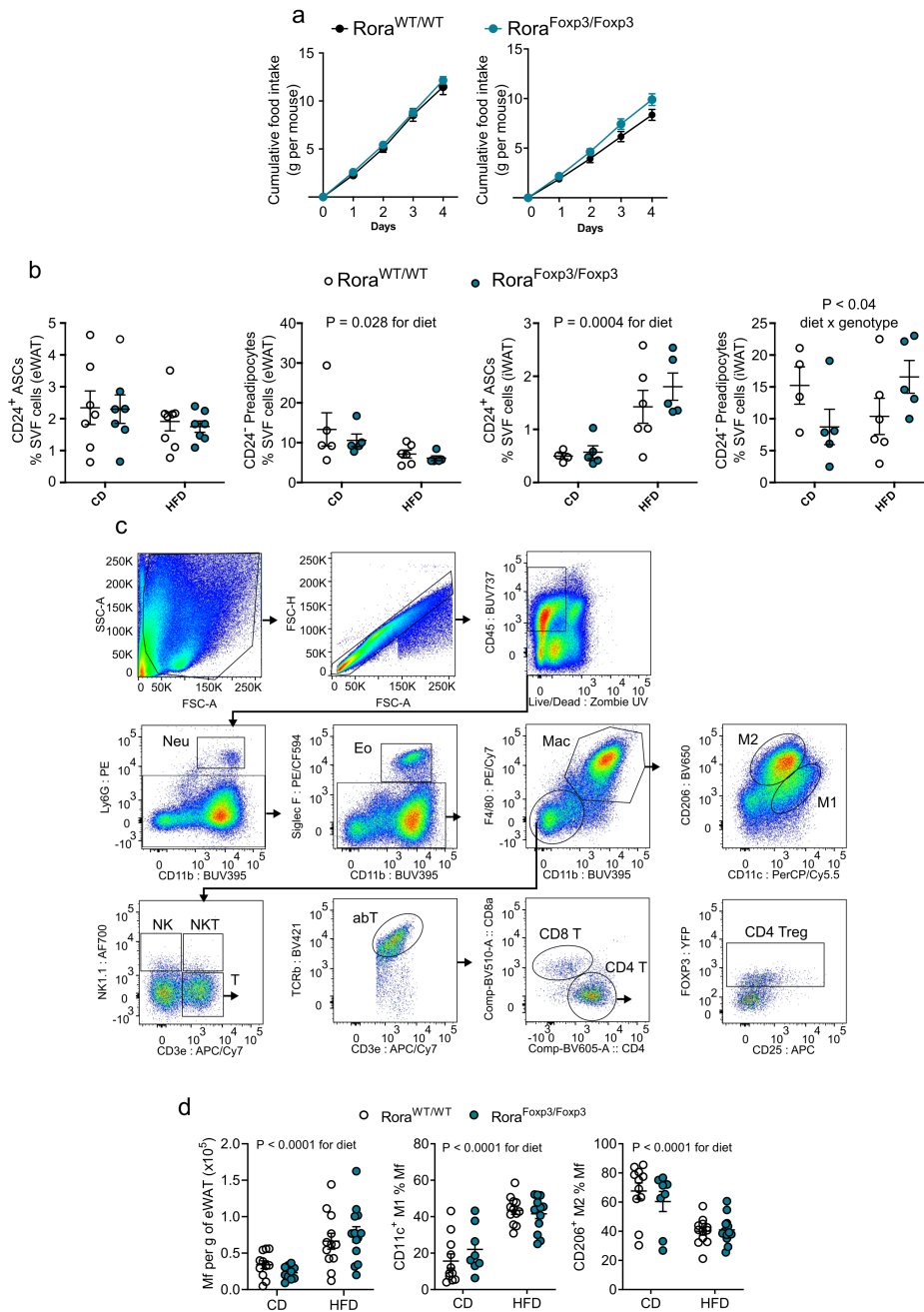
Figure 5.8 – **Metabolic and immune parameters in RORα^Foxp3/Foxp3 mice in diet-induced obesity**
**a.** Cumulative food intake of RORα^WT/WT and RORα^Foxp3/Foxp3 mice upon CD (left panel) and HFD (right panel) feeding for 12 weeks n = 4-9; **b.** Proportions of CD24^- preadipocytes and CD24^+ adipose-derived stem cell in eWAT and iWAT (groups as in a.); **c.** Gating strategy for identification of immune cells in murine eWAT and iWAT. Neu: neutrophils, Eo: eosinophils, Mac: macrophages (M1 and M2 subpopulations); **d.** Proportions of total (left panel), M1 (central panel) and M2 (right panel) macrophage subpopulations in eWAT (groups as in a.), 2-way ANOVA. n = 12

underscored by downregulation of genes, associated with TNFα activation of adipocytes (Figure 5.7i). In agreement with decreased expression levels of proinflammatory genes, immunophenotyping of eWAT revealed an increased number of EOS, which inhibit adipose tissue inflammation via secretion of type 2 cytokines, with no changes in the majority of other immune cell types (Figure 5.7j-l). As adipose tissue inflammation results in IR, we measured parameters connected to insulin sensitivity in CDor HFD-fed RORα$^{WT/WT}$ and RORα$^{Foxp3/Foxp3}$ mice. Although fasting levels of glucose and insulin were similar between CD-fed RORα$^{Foxp3/Foxp3}$ mice and RORα$^{WT/WT}$ mice, both parameters where significantly improved in HFD fed RORα$^{Foxp3/Foxp3}$ mice (Figure 5.9a-b). Furthermore, intraperitoneal glucose tolerance test (IPGTT) revealed that RORα$^{Foxp3/Foxp3}$ mice had significantly improved glucose tolerance (Figure 5.9c-d). Plasma insulin levels measured during IPGTT (Figure 5.9e) revealed that RORα$^{Foxp3/Foxp3}$ mice keep lower insulin levels while managing to provide faster glucose clearance, further underscoring the increased systemic insulin sensitivity together with insulin tolerance test (ITT) (Figure 5.9f). Furthermore, insulin-dependent AKT phosphorylation was increased in both eWAT and iWAT of RORα$^{Foxp3/Foxp3}$ mice, as shown by western-blotting (Figure 5.9g), suggesting an increased signaling downstream the insulin receptor. Overlapping the transcripts changed between RORα$^{WT/WT}$ and RORα$^{Foxp3/Foxp3}$ eWAT with human genes associated with IR in the adipose tissue also demonstrated an underrepresentation of IR-signature transcripts in RORα$^{Foxp3/Foxp3}$ mice (Figure 5.9h). In line with improved adipose tissue inflammation and metabolic parameters upon DIO, numbers of eWAT T$_{REG}$, were increased in RORα$^{Foxp3/Foxp3}$ mice (Figure 5.11a-b), whereas they remained comparable in both genotypes in CD-fed mice (Figure 5.11a-b) [127]. However, total numbers and proportions of classically and alternatively activated eWAT macrophages, which are also major contributors to inflammation were similar between genotypes (Figure 5.8d). Similarly to lungs and mLN, gene expression profiling of T$_{REG}$ sorted from RORα$^{Foxp3/Foxp3}$ mice and RORα$^{WT/WT}$ mice upon HFD feeding revealed a decreased expression in circadian clock genes in RORα$^{Foxp3/Foxp3}$ cells (Figure 5.11c). Pathways enriched among the genes up-regulated in RORα$^{Foxp3/Foxp3}$ T$_{REG}$ point towards a more activated phenotype with interferon γ response suggesting an improved ability to suppress type 1 response [289] and cytotoxicity as suggested by dowregulation of *Gzmb* (Figure 5.11d). Type 1 response in the adipose tissue is associated with obesity and IR with T$_H$1 cells activating M1 macrophage (MF). Fatty acid metabolism genes, induced in RORα$^{Foxp3/Foxp3}$ T$_{REG}$ might represent a sign of a metabolic switch towards fatty acid oxidation, which is a characteristic trait of T$_{REG}$ compared to activated conventional T cells, mostly relying on glycolysis [290]. Such a switch might be beneficial for T$_{REG}$ function. Taken together these results suggest that as in AAI, RORα controls the development of type 2 response thereby impacting on adipose tissue inflammation and glucose and insulin metabolism.

## 5.6 RORα-deficient T$_{REG}$ display a T$_H$2-like phenotype akin to non lymphoid tissue T$_{REG}$ *in vitro*

To further investigate the molecular mechanisms by which RORα control T$_{REG}$ function, we designed an *in vitro* model mimicking T$_H$2 conditions found for in non lymphoid tissues. In vitro suppression assay under T$_H$0 and T$_H$2 conditions (Figure 5.12a-b) showed results similar to those obtained *in vivo* (Figure 5.2g-i). RORα$^{Foxp3/Foxp3}$ T$_{REG}$ had slightly, but not significantly, increased suppressive capacity compared to RORα$^{WT/WT}$ T$_{REG}$, suggesting, that RORα-deficient T$_{REG}$ have normal suppressive functions *in vitro*. Proliferation of RORα$^{Foxp3/Foxp3}$ T$_{REG}$ was also unaffected in T$_H$0 conditions when activated by anti-CD3/CD28 beads and IL-2. However, proliferation in T$_H$2-polarizating conditions was lower in RORα$^{Foxp3/Foxp3}$ T$_{REG}$ (Figure 5.12c-e). This might account for decreased proportion of T$_{REG}$ in lung and mLN of RORα$^{Foxp3/Foxp3}$ mice in HDM-induced AAI model (Figure 5.5b,d). Additionally, in T$_H$2-polarizating conditions, RORα$^{Foxp3/Foxp3}$ T$_{REG}$ displayed increased induction of
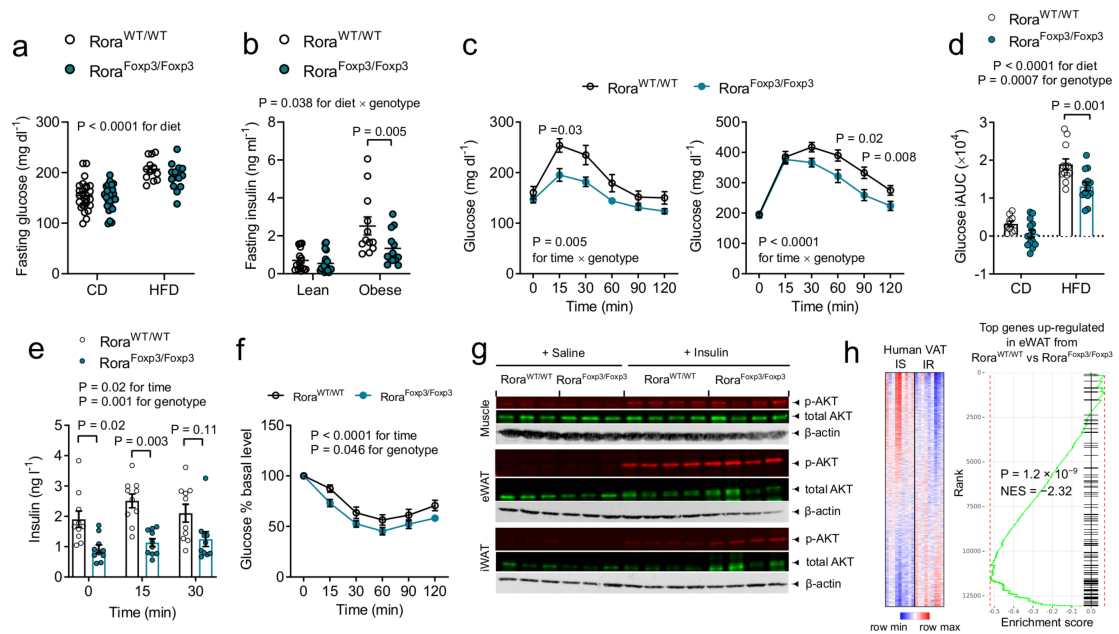
Figure 5.9 – **Improvement of glucose metabolism in RORα$^{\text{Foxp3/Foxp3}}$ mice in diet-induced obesity**
**a.** Fasting plasma glucose concentration weight of RORα$^{\text{WT/WT}}$ and RORα$^{\text{Foxp3/Foxp3}}$ mice mice upon high fat diet (HFD) or Chow diet (CD) feeding for 12 weeks , 2-way ANOVA, n = 12-28; **b.** Fasting plasma insulin concentration (groups as in a.), 2-way ANOVA or Student t-test n = 12-19; **c-d.** Intraperitoneal glucose tolerance test (IPGTT) in animals CD (left panel) or HFD (right panel) fed mice for 10 weeks. Blood glucose concentration over time **(c)**. Incremental area under the curve (iAUC) **(d)** n = 12-19, **e.** Blood insulin concentration during IPGTT, 2-way ANOVA, n = 10; **f.** Insulin tolerance test (ITT) upon HFD; g. Insulin-induced Akt phosphorylation in muscle, eWAT and iWAT upon HFD; h. GSEA plot showing up-regulation of top 100 up-regulated genes in human insulin resistant (IR) visceral adipose tissue (VAT) (compared to insulin sensitive (IS) VAT) in eWAT from HFD-fed RORα$^{\text{WT/WT}}$ mice compared to RORα$^{\text{Foxp3/Foxp3}}$ mice (right panel).
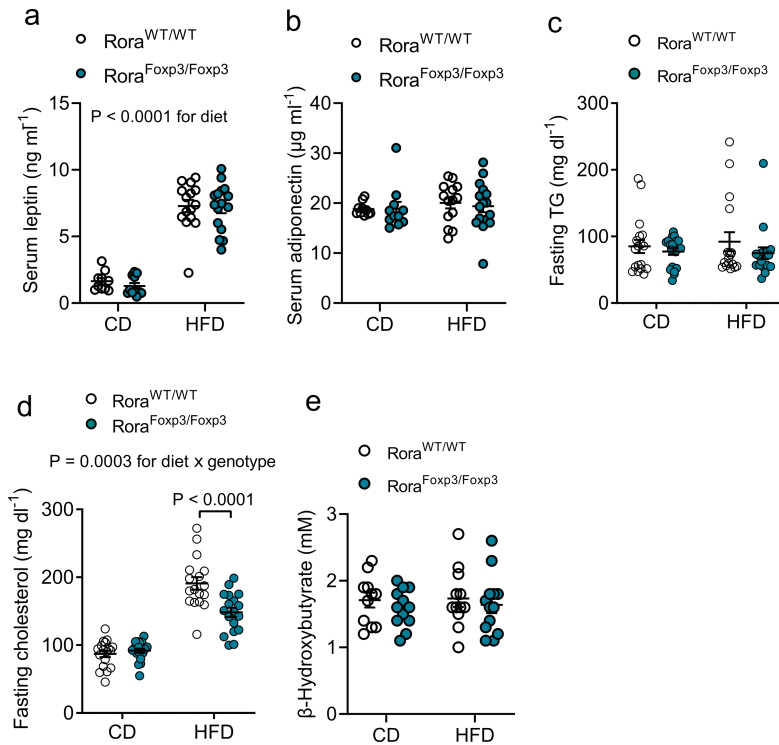
Figure 5.10 – **Circulating adipokine, cholesterol, triglyceride and ketone bodies concentrations in RORα$^{Foxp3/Foxp3}$ mice in diet-induced obesity**
**a.-c.** Plasma concentrations of adipokines in RORα$^{WT/WT}$ and RORα$^{Foxp3/Foxp3}$ mice measured by multiplex analysis Leptin (a.). Adiponectin (b.); **c.** Fasting triglycerides concentrations (TG); **d.** Cholesterol concentrations; **e.** β-hydroxybutyrate concentrations, 2-way ANOVA. n = 11
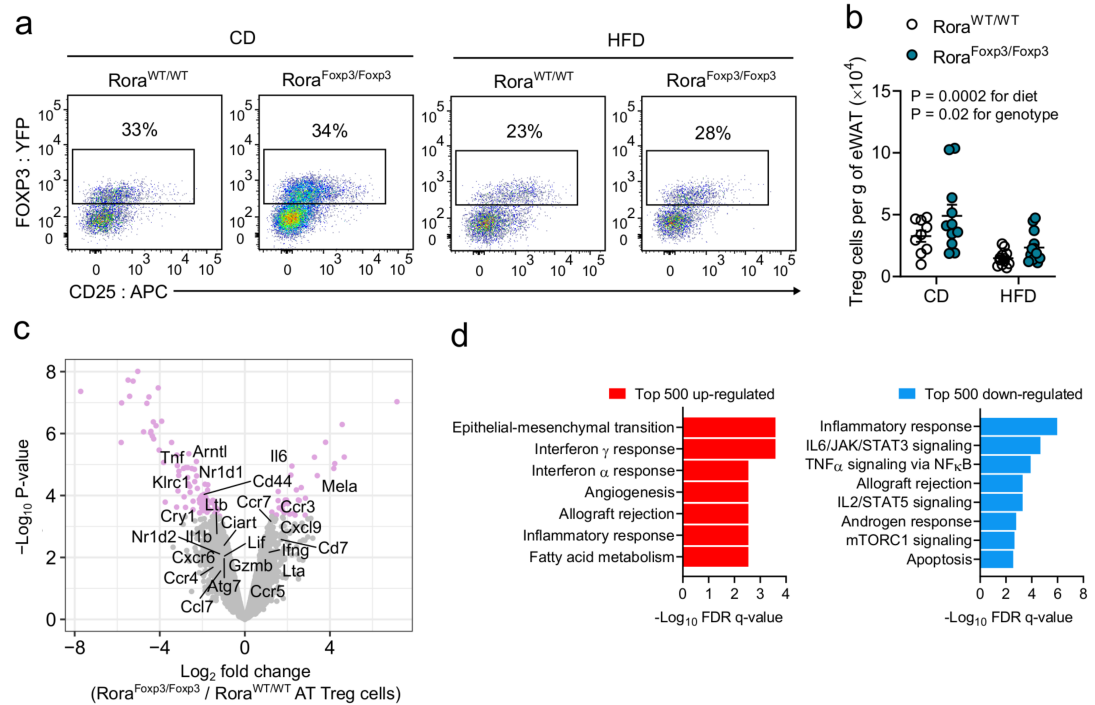
Figure 5.11 – **Altered transcriptional program in adipose tissue T$_{REG}$ from ROR$\alpha^{Foxp3/Foxp3}$ mice in diet-induced obesity**
**a.** Proportion of T$_{REG}$ in eWAT from ROR$\alpha^{WT/WT}$ and ROR$\alpha^{Foxp3/Foxp3}$ mice mice upon HFD or Chow diet (CD) feeding for 12 weeks. numbers are mean values, n = 9-13; **b.** T$_{REG}$ number per gramm of eWAT, 2-way ANOVA, n = 9-13 (groups as in a.); **c.** Volcano plot representing gene expression profile of eWAT T$_{REG}$ from HFD fed mice; **d.** Gene sets ("Hallmark") enriched in top up- and down-regulated genes in eWAT T$_{REG}$ from ROR$\alpha^{Foxp3/Foxp3}$ vs ROR$\alpha^{WT/WT}$ HFD-fed mice.

T<sub>H</sub>2-associated genes including *il5, Il4, Il10, Il13*, compared to RORα$^{WT/WT}$ T<sub>REG</sub> (Figure 5.12f), in line with the T<sub>H</sub>2-like phenotype of RORα$^{Foxp3/Foxp3}$ T<sub>REG</sub> observed in HDM-induced AAI model (Figure 5.3j-m, Figure 5.4b). While expression *Gata3*, controlling T<sub>H</sub>2 polarization was similar, *Bach2*, a suppressor of T<sub>H</sub>2 transcriptionnal program [291, 292], was downregulated in RORα$^{Foxp3/Foxp3}$ . Furthermore, gene expression profile of *in vitro* T<sub>H</sub>2-polarized T<sub>REG</sub> showed an enrichment of gene set associated with "tissue T<sub>REG</sub>" phenotype seen in T<sub>REG</sub> cells in NLT (Figure 5.12g) [120]. T<sub>H</sub>1 and T<sub>H</sub>17 TF genes *Tbx21, Rorc* were similar between genotypes. As for lung and mLN T<sub>REG</sub>, gene expression profiling of T<sub>REG</sub> activated *in vitro* in T<sub>H</sub>2 conditions confirmed that RORα$^{Foxp3/Foxp3}$ T<sub>REG</sub> upregulated G2-M checkpoint, E2F targets and DREAM targets associated genes (Figure 5.12h). We next investigated proportions of RORα$^{WT/WT}$ vs RORα$^{Foxp3/Foxp3}$ T<sub>REG</sub> cells in different phases of cell cycle by flow cytometry. In T<sub>H</sub>0-polarizing conditions, cell cycle analysis revealed differences in RORα$^{Foxp3/Foxp3}$ T<sub>REG</sub> which included a lower percentage in G2-M phase and a higher percentage of cells with fragmented DNA (Sub G0 phase). In T<sub>H</sub>2-polarizing conditions, in addition to the decrease in G2-M a lower percentage of RORα$^{Foxp3/Foxp3}$ T<sub>REG</sub> was found in G0/G1 phase in agreement with lower proliferation of RORα$^{Foxp3/Foxp3}$ T<sub>REG</sub> only in a T<sub>H</sub>2 cytokinic environment (Figure 5.12i-j) and similar to T<sub>REG</sub> in allergic lung (Figure 5.5l). Taken together these results suggest that splenic T<sub>REG</sub> cultured in T<sub>H</sub>2-polarizing conditions mimic well the phenotype of non lymphoid tissue T<sub>REG</sub>, especially lung T<sub>REG</sub> during HDM-induced AAI model.

## 5.7 RORα contributes to epigenetic regulation in T<sub>REG</sub>

In addition to being transcription factors, nuclear receptors may act as chromatin remodelers to alter gene expression [293]. To evaluate whether RORα might in part regulate gene expression through epigenetic modifications of chromatin in T<sub>REG</sub>, we performed H3K27Ac chromatin immunoprecipitation-sequencing (ChIP-seq) of T<sub>REG</sub> in T<sub>H</sub>2-polarizing conditions *in vitro*. H3K27Ac is a histone modification mark, indicating open state of chromatin. As T<sub>REG</sub> stability is largely controlled by activity of FOXP3 promoter [42, 121], we examined the state of regulatory regions of T<sub>REG</sub>-specific genes including *Foxp3* in terms of chromatin activity. Most of these regions showed strong signals of H3K27Ac binding in both RORα$^{WT/WT}$ and RORα$^{Foxp3/Foxp3}$ T<sub>REG</sub> (Figure 5.13a), suggesting that T<sub>REG</sub> remain committed to T<sub>REG</sub> lineage, in line with the broad conservation of T<sub>REG</sub> identity in RORα-deficient T<sub>REG</sub>. Differential binding analysis identified 50 statistically significant differentially bound regions between RORα$^{WT/WT}$ and RORα$^{Foxp3/Foxp3}$ cells (Table 5.1). We mapped these regions to the closest genes and sought for enriched gene sets. Several of the identified pathways were associated to STAT-signaling with *Il20, Il24, Il6r, Parp9, Parp14* genes mainly responsible for that. PARP9/PARP14 act together to inhibit STAT1 activation [294] (Figure 5.13b). Involvement of these genes in STAT3 and STAT6 signaling, together with inhibition of STAT1, is in agreement with the notion that RORα-deficient T<sub>REG</sub> develop a T<sub>H</sub>2-like dedifferentiated phenotype [294]. In addition to their association to STAT-signaling, *Il20* and *Il24* form a cluster with *Il10*, although functions of *il20* and *il24* are poorly studied. Nevertheless, differential binding in this region may also lead to altered IL-10 regulation in RORα$^{Foxp3/Foxp3}$ T<sub>REG</sub> and explain the slight differences in their suppressive capacity [295]. Another pathway enriched in the genes mapped to regions differentially bound by H3K27Ac in RORα$^{Foxp3/Foxp3}$ T<sub>REG</sub> was Ataxia telangiectasia mutated (ATM) network. ATM is one of the three main serine/threonine protein kinases, controlling DNA-damage response (DDR) and checkpoint activation for cell cycle progression. It activates checkpoint signaling in response to double-strand DNA breaks, apoptosis and genotoxic stresses [296, 297] in line with a higher DNA fragmentation (**??**) and apoptosis level (Figure 5.13c) in RORα$^{Foxp3/Foxp3}$ T<sub>REG</sub> *in vitro*, although the latter was only seen in T<sub>H</sub>0-polarizing conditions. As differential acetylation of histones allows for but does not necessarily leads to transcription, this might reflect a globally increased susceptibility of RORα$^{Foxp3/Foxp3}$ T<sub>REG</sub> to apoptosis. ATM phosphorylates
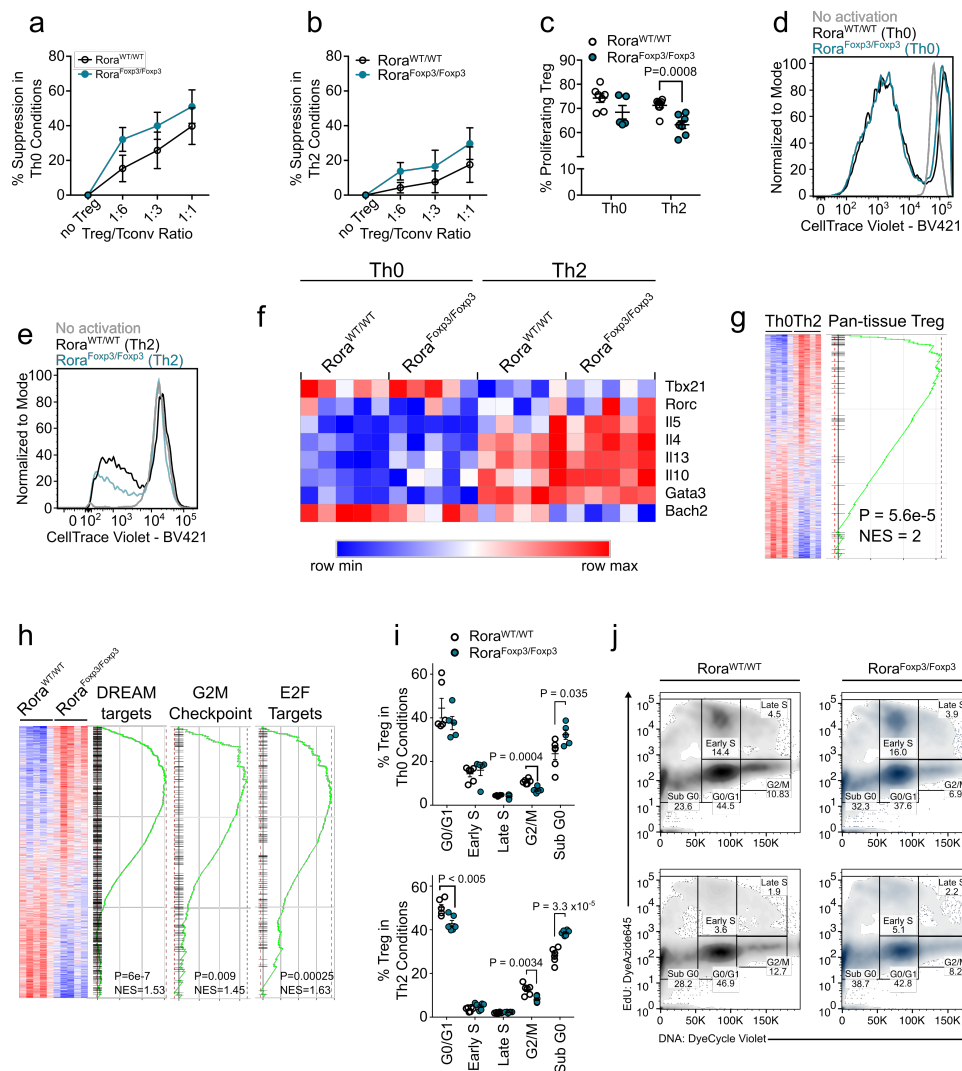
Figure 5.12 – **Altered transcriptional program and cell cycle in T$_H$2-polarized T$_{REG}$ from RORα$^{Foxp3/Foxp3}$ mice *in vitro***

**a.-b.** *In vitro* immunosuppression assay with anti-CD3- and anti-CD28 and IL-2 (T$_H$0) or IL-2, IL-4, anti-IFN-γ (T$_H$2) and splenic T$_{REG}$ from RORα$^{WT/WT}$ and RORα$^{Foxp3/Foxp3}$ mice, data pooled from 4 independent experiments; **c.-e.** anti-CD3- and anti-CD28 and IL-2 or IL-2, IL-4, anti-IFN-γ-treated T$_{REG}$ cells proliferation in T$_H$0- (c.-d.) and T$_H$2 (c., e.)-polarizing conditions. Percentage of proliferating cells (c.) and dye dilution profile (d.-e.) n = 5-7 or data pooled from 5 experiments, Student t-test; **f.** Heat map of expression of TH polarization-associated genes in T$_{REG}$ *in vitro* measured by microarray; **g.** GSEA plot showing an enrichment of pan-tissue T$_{REG}$ gene signature in T$_H$2-polarized T$_{REG}$; **h.** GSEA plot showing enrichment of cell cycle-associated gene sets in T$_H$2-polarized T$_{REG}$ from RORα$^{Foxp3/Foxp3}$ mice; **i.** Proportions of splenic T$_{REG}$ from RORα$^{WT/WT}$ and RORα$^{Foxp3/Foxp3}$ mice in different phases of the cell cycle cultured in T$_H$0- (upper panel) and T$_H$2 (lower panel)-polarizing conditions , 2-way ANOVA, Student t-test, n = 5; **j.** Representative flow cytometry analysis of cell cycle (groups as in i.).

several cell cycle associated proteins and is involved in establishing G2-M checkpoint (which is sometimes referred to as "DNA-damage checkpoint"). Some of its coexpressed genes such as *Hdac1, Lair1, Ncapd2* were differentially regulated transcriptionally in RORα$^{\text{Foxp3/Foxp3}}$ T$_{\text{REG}}$. Thus chromatin alterations identified in in RORα$^{\text{Foxp3/Foxp3}}$ T$_{\text{REG}}$ might in part account for their decreased stability in T$_{\text{H}}$2-polarizing conditions and altered progression through cell cycle. It also further connects described alterations with potentially defective STAT signaling, as well as susceptibility to apoptosis and DNA damage due differences in DDR system between RORα$^{\text{Foxp3/Foxp3}}$ and RORα$^{\text{WT/WT}}$ T$_{\text{REG}}$.
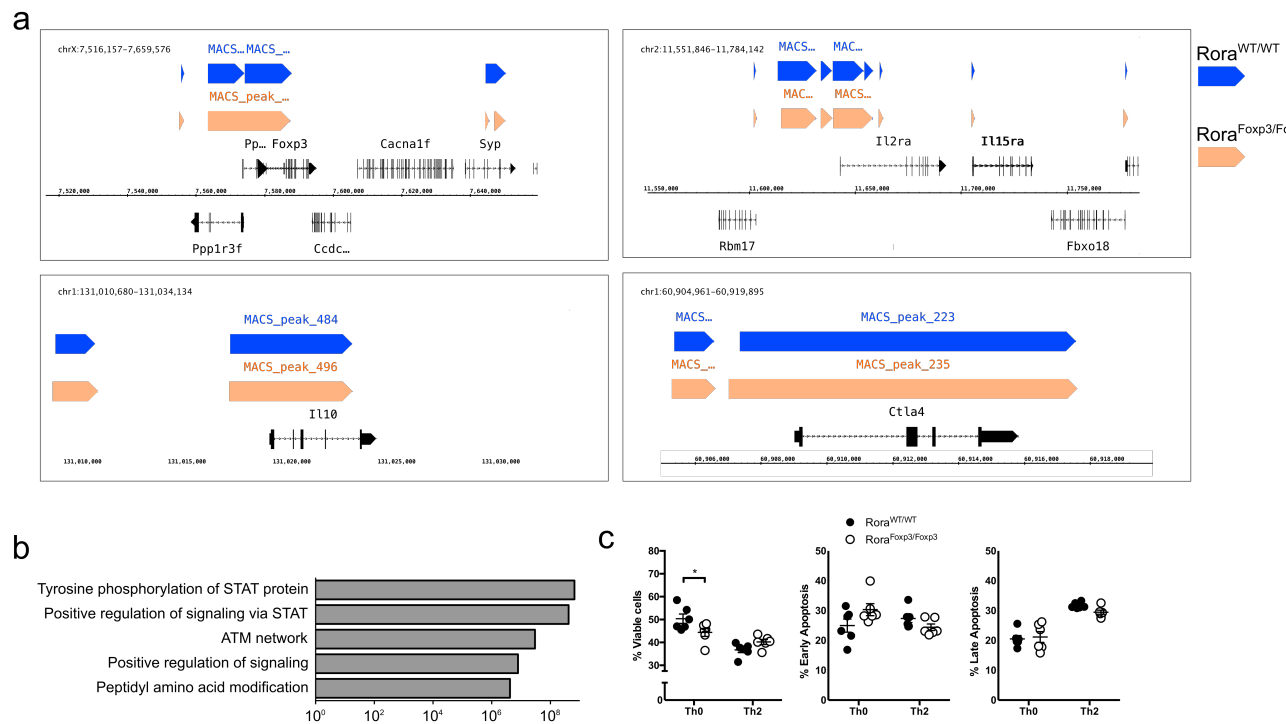
Figure 5.13 – **Epigenetic modifications in T$_H$2-polarized T$_{REG}$ from ROR$\alpha^{Foxp3/Foxp3}$ mice *in vitro***

**a.** H3K27Ac marks identified in the vicinity of T$_{REG}$ identity-associated genes in T$_H$2-polarized splenic T$_{REG}$ from ROR$\alpha^{WT/WT}$ and ROR$\alpha^{Foxp3/Foxp3}$ mice; **b.** Top enriched gene sets in genes mapped to H3K27Ac-enriched regions, differentially bound between ROR$\alpha^{WT/WT}$ and ROR$\alpha^{Foxp3/Foxp3}$ T$_{REG}$, X-axis is enrichment p-value in reverse logarithmic scale; **c.** Apoptosis *in vitro* in splenic T$_{REG}$ from ROR$\alpha^{WT/WT}$ and ROR$\alpha^{Foxp3/Foxp3}$ mice in T$_H$0- and T$_H$2-polarizing conditions assessed by annexin binding. Percentage of viable (left panel), early (central panel) and late (right panel) apoptotic cells. 2-way ANOVA, Student t-test n = 6

| chromosome | start | end | regionname | enrichment |
|---|---|---|---|---|
| 1 | 36939550 | 36939950 | region1 | 7.8094280059788 |
| 1 | 130903350 | 130903700 | region2 | 6.16192000124634 |
| 10 | 33950950 | 33951150 | region3 | 6.86075199330079 |
| 11 | 53300000 | 53301350 | region4 | 7.24839650895041 |
| 11 | 61648550 | 61649250 | region5 | 7.24839650895041 |
| 11 | 97007250 | 97007400 | region6 | 6.44890860649061 |
| 11 | 98795850 | 98796050 | region7 | 17.167321027224 |
| 11 | 106535500 | 106537550 | region8 | 6.03618972407289 |
| 11 | 106787700 | 106789450 | region9 | 9.7121908690573 |
| 12 | 69184500 | 69184800 | region10 | 6.86390351694618 |
| 12 | 107131900 | 107132150 | region11 | 6.86075199330079 |
| 13 | 52168900 | 52169100 | region12 | 6.16192000124634 |
| 14 | 56274850 | 56276150 | region13 | 7.57128114078888 |
| 15 | 81585400 | 81586600 | region14 | 6.86390351694618 |
| 15 | 82899250 | 82899400 | region15 | 7.2514290656058 |
| 15 | 100615650 | 100616050 | region16 | 6.83106082668213 |
| 16 | 35919000 | 35919150 | region17 | 9.7121908690573 |
| 16 | 89835400 | 89837100 | region18 | 7.57128114078888 |
| 17 | 35439200 | 35439400 | region19 | 6.16192000124634 |
| 17 | 52163650 | 52164500 | region20 | 6.86075199330079 |
| 18 | 7868450 | 7868650 | region21 | 6.86075199330079 |
| 18 | 35562400 | 35562550 | region22 | 9.7121908690573 |
| 18 | 65008050 | 65009100 | region23 | 7.57128114078888 |
| 18 | 84685000 | 84685500 | region24 | 7.57128114078888 |
| 19 | 4842200 | 4843700 | region25 | 6.15701275347152 |
| 19 | 7017600 | 7020000 | region26 | 7.57128114078888 |
| 2 | 154791050 | 154791750 | region27 | 7.24839650895041 |
| 2 | 155047550 | 155048200 | region28 | 7.8094280059788 |
| 2 | 155381850 | 155382150 | region29 | 7.24839650895041 |
| 3 | 89871350 | 89871500 | region30 | 6.86075199330079 |
| 4 | 97996550 | 97996700 | region31 | 9.7121908690573 |
| 4 | 151057650 | 151058000 | region32 | 6.86075199330079 |
| 5 | 31193500 | 31193650 | region33 | 7.57128114078888 |
| 5 | 103753150 | 103754250 | region34 | 7.57128114078888 |
| 5 | 123015450 | 123015700 | region35 | 6.86075199330079 |
| 5 | 124035400 | 124035650 | region36 | 7.24839650895041 |
| 6 | 125222600 | 125222800 | region37 | 6.86075199330079 |
| 7 | 13034300 | 13034550 | region38 | 6.65825549246246 |
| 7 | 24884850 | 24885000 | region39 | 7.82283249359777 |
| 7 | 46795850 | 46796150 | region40 | 7.57128114078888 |
| 7 | 100674650 | 100674800 | region41 | 35.773461638539 |
| 7 | 106235400 | 106237700 | region42 | 104.277611106135 |
| 7 | 106528750 | 106528900 | region43 | 11.7010826382223 |
| 7 | 125485400 | 125496850 | region44 | 9.7121908690573 |
| 7 | 126199900 | 126200300 | region45 | 6.86075199330079 |
| 7 | 140320650 | 140322250 | region46 | 6.88226680441404 |
| 8 | 64947400 | 64947600 | region47 | 7.33976070886193 |
| 9 | 101074900 | 101075650 | region48 | 6.16192000124634 |
| 9 | 107554950 | 107555100 | region49 | 7.57128114078888 |
| 9 | 115309800 | 115309950 | region50 | 6.65825549246246 |

Table 5.1 – **Coordinates of regions, differentially bound between RORα$^{WT/WT}$ and RORα$^{Foxp3/Foxp3}$ T$_{REG}$ in H3K27Ac chromatin immunoprecipitation-sequencing (ChIP-seq) analysis and relative enrichment within this region**, FDR = 0.2.

# Chapter 6

# Discussion and conclusion

## 6.1 General considerations and metabolic phenotype of ROR$\alpha^{\text{Foxp3/Foxp3}}$ mice

We have demonstrated a major role of nuclear receptor ROR$\alpha$ in the function of T$_{\text{REG}}$ cells. Although naive mice do not require T$_{\text{REG}}$-expressed ROR$\alpha$ to maintain immune homeostasis, we found that this nuclear receptor is a pivotal regulator of T$_{\text{REG}}$ adaptation to the local environment and a major controller of inflammation. Minor immunological changes in untreated ROR$\alpha^{\text{Foxp3/Foxp3}}$ mice (such as decreased proportion of ROR$\gamma$t$^+$, CD44$^+$or total T$_{\text{REG}}$ number in some tissues) rather point towards of ROR$\alpha$ for highly active effector T$_{\text{REG}}$ compartment. Yet, this impact on active effector T$_{\text{REG}}$ compartment doesn't lead by *per se* to any apparent spontaneous pathology. Interestingly, so-called "tissue T$_{\text{REG}}$" cells possess an effector-like phenotype. The field of tissue T$_{\text{REG}}$ research strongly relies on high-throughput data. As a result, sets of genes defining NLT T$_{\text{REG}}$ and distinguishing them from lymphoid organ T$_{\text{REG}}$ are quite large and differ from study to study. However, most of the publications are in agreement regarding the importance of effector molecules such as *Ctla4*, *Klrg1*, *Gzmb*; chemokine receptors like *Ccr4*, *Ccr6*, *Ccr9* and some transcription factors, many of which turned out to be involved in the control of type 2 response: *Gata3*, *Irf4*, *Gata3*, *Rora* [118, 120]. Further investigation of the steady-state phenotype in ROR$\alpha^{\text{Foxp3/Foxp3}}$ mice strikingly revealed an improvement of glucose metabolism. This benefit is preserved in obese animals in a model of DIO conditions and is accompanied by a reduced weight gain in ROR$\alpha^{\text{Foxp3/Foxp3}}$ mice. Glucose intolerance during DIO largely results from inflammation taking place in the adipose tissue. Adipose tissue-resident T$_{\text{REG}}$ cells are a central link in restraining this inflammation and in turn, maintaining metabolic homeostasis. Of note, all the phenotype observed in untreated mice disappeared with age. Indeed, 50-60 week old ROR$\alpha^{\text{Foxp3/Foxp3}}$ mice mice were not metabolically different from wild type mice of the same age (data not shown). This suggests that the protective mechanisms, at play in ROR$\alpha^{\text{Foxp3/Foxp3}}$ mice at a young and intermediate age stop working with aging. This might be due to senescence of T$_{\text{REG}}$ cells, perhaps in relationship with cell cycle alterations that will be discussed below.

Obese ROR$\alpha^{\text{Foxp3/Foxp3}}$ mice also displayed milder liver steatosis than their wild type counterparts in line with lower liver TG. ROR$\alpha^{\text{Foxp3/Foxp3}}$ mice also displayed decreased circulating cholesterol concentrations, a parameter controlled by by insulin sensitivity and obesity [298]. Furthermore, we also evaluated the phenotype of ROR$\alpha^{\text{Foxp3/Foxp3}}$ mice in a model of diet-induced NASH (high fat, high cholesterol, high sugar diet) [299]. Interestingly, after 24 weeks of diet, ROR$\alpha^{\text{Foxp3/Foxp3}}$ mice displayed similar fat mass and or liver lipid content compared to wild type mice. However, glucose

tolerance was still improved in ROR$\alpha^{\text{Foxp3/Foxp3}}$ mice (data not shown). This finding suggests that major components of glycaemia and steatosis might be differently controlled by ROR$\alpha$ in T$_{\text{REG}}$ once an hyperglycemic and hypercholestrolemic diet is provided. The underlying mechanisms of these complex gene-diet interactions remains to be established. The two genes displaying the strongest downregulation in eWAT from ROR$\alpha^{\text{Foxp3/Foxp3}}$ mice upon HFD feeding are Ctsk and Spp1 respectively encoding cathepsin K and osteopontin. Mouse models of *Spp1* or *Ctsk* deficiency are characterized by reduced body weight gain in DIO models and improved glucose metabolism [287, 288]. These genes also regulate liver steatosis, blood cholesterol concentrations, macrophage-induced VAT inflammation and adipocyte differentiation. We did not observe any difference in adipocyte size or in proportions of early adipocyte progenitors and preadipocytes. By contrast, expression of proinflammatory genes such as *Tnf* were reduced in VAT and in VAT macrophages of ROR$\alpha^{\text{Foxp3/Foxp3}}$ mice. This decrease was accompanied by improved glucose clearance during IPGTT, increased Akt signaling in eWAT and iWAT and lower plasma insulin concentration. In VAT from ROR$\alpha^{\text{Foxp3/Foxp3}}$ mice, proportions of macrophages – major regulators of local inflammation – were unchanged. However, ROR$\alpha^{\text{Foxp3/Foxp3}}$ mice had increased numbers of VAT T$_{\text{REG}}$, in line with the positive correlation existing between this parameter and which insulin sensitivity [127]. Eosinophils were also more abundant. Eosinophilia is a hallmark of type 2 immunity associated to VAT homeostasis. In this work, we did not examine ILC2, also associated to metabolic homeostasis and acting upstream eosinophils. It is likely that T$_{\text{REG}}$-expressed ROR$\alpha$ controls VAT homeostasis in an ILC2-dependent manner. Indeed, in mouse skin, T$_{\text{REG}}$-specific ROR$\alpha$ deficiency failed to restrain inflammation due to lower expression of *Tnfrsf25*, a receptor for TL1A expressed by T$_{\text{REG}}$, resulting in an increased TL1A availability for ILC2 and higher activation and cytokine secretion by T$_{\text{H}}$2 [116].

## 6.2   Allergic airway inflammation in ROR$\alpha^{\text{Foxp3/Foxp3}}$ mice and T$_{\text{REG}}$ cell cycle regulation

In light of our findings revolving around type 2 immunity, we evaluated the development of AAI, a prototypical type 2-associated pathology, in ROR$\alpha^{\text{Foxp3/Foxp3}}$ mice in the classical HDM-induced AAI model. As in DIO model (and in atopic dermatitis, as was published earlier [116]), T$_{\text{REG}}$-specific ROR$\alpha$ deficiency promoted type 2 response during HDM-induced AAI model. This resulted in exacerbating the cardinal features of AAI. Indeed, ROR$\alpha^{\text{Foxp3/Foxp3}}$ mice displayed increased airway hyper-responsiveness and lung immune inflammation with prominent eosinophilia. Antigen-specific immunoglobulin E (IgE) concentrations reflected the increased humoral response. Interestingly, ROR$\alpha$-deficient T$_{\text{REG}}$ cells themselves expressed increased levels of type 2 cytokines. Inflammation was also increased due to the lower proportion of T$_{\text{REG}}$. We evaluated *in vivo* proliferation of T$_{\text{REG}}$ in lungs in AAI and found major alterations in proportions of cells in the different phases of the cell cycle. Lung ROR$\alpha$-deficient T$_{\text{REG}}$ cells did replicated their DNA, but accumulated in late S phase presumably failing to proceed beyond G2-M checkpoint to reach G1 phase. To further delve into the fine details of cell proliferation we next investigated proliferation *in vitro*. ROR$\alpha$-deficient T$_{\text{REG}}$ displayed an impaired ability to proliferate in a type 2 cytokinic environment. Less ROR$\alpha$-deficient T$_{\text{REG}}$ cells reached mitotic state in both non-polarized and in type 2 conditions. Only upon type 2 polarization, however significantly less ROR$\alpha$-deficient T$_{\text{REG}}$ were found in both G0/G1 and mitotic (G2-M) phases. Additionally, a larger proportion had fragmented DNA (Sub G0) upon type 2 activation, suggesting either controlled apoptotic fragmentation or an indication of oxidative stress. Annexin V or ADP/ATP ratio (data not shown) apoptosis assays showed that ROR$\alpha$-deficient T$_{\text{REG}}$ were more apoptotic, although only in T$_{\text{H}}$0, but not type 2 conditions. Apoptosis measured as caspase 3/7 activity in lung T$_{\text{REG}}$ in AAI demonstrated even slightly improved condition ROR$\alpha$-deficient T$_{\text{REG}}$. Stress, evaluated by mitochondrial reactive oxygen species (mtROS) production, was increased in mediastinal lymph node

$T_{REG}$ upon AAI. The fairly minor differences between *in vivo*and *in vitro* phenotypes may be due to the heterogenity of lung $T_{REG}$ populations found in AAI, for instance, due to migration of $T_{REG}$ during inflammation. Cell cycle alterations in ROR$\alpha$-deficient $T_{REG}$ are supported by the fact that ROR$\alpha$ is often associated with cancer and checkpoint control. Furthermore, *sg/sg* phenotype is partly due to defective cell cycle in Purkinje and glial cells in mouse cerebellum [260, 267].

Based on the analysis of gene expression profiling data from lung ROR$\alpha$-deficient in AAI combined with known binding sites of ROR$\alpha$ published ChIP-seq, it is likely that ROR$\alpha$ regulates numerous cell cycle-associated genes including E3-ubiquitin ligases and cyclin-dependent kinases. A recent study addressed the acquisition of tissue phenotype by $T_{REG}$ cells during their recruitment to NLT [300]. A phenotypic/transcriptomic continuum was unraveled by single-cell transcriptomic analysis from lymphoid tissue, skin and colonic $T_{REG}$. Based on transcriptomic analysis, results show that majority of cells is moving through cell cycle while migrating to NLT, starting from S phase through G2-M to G1. Interestingly, *Rora* expression starts on just about the time when cells are "passing" S-G2-M checkpoint. Our data provide *in vivo*and *in vitro* functional evidence of ROR$\alpha$ involvement in this process. *Rora* deletion thus hinders the shift in the prevailing cell cycle phase during $T_{REG}$ recruitment to tissue upon AAI or *in vitro* activation by IL-4. ROR$\alpha$ deficiency thus prevents acquisition of tissue phenotype and compromises adaptation to local environment or inflammatory condition. Indeed, $T_{REG}$ cells lacking ROR$\alpha$ fail to balance DNA replication and cell division, causing accumulation at G2-M checkpoint, preventing rapid expansion during inflammation resolution. TCR and IL-2 signaling play critical roles in $T_{REG}$ activation, suppressor function, metabolic reprogramming and tissue adaptation. ROR$\alpha^{Foxp3/Foxp3}$ $T_{REG}$ showed decreased Akt phosphorylation in *in vitro* model of activation and increased STAT5 phosphorylation in conditions of short *ex vivo* stimulation with cytokines (data not shown). These effects were dynamic in time and need to be further investigated using extended time-course design. Altered Akt signaling might be another underlying cause of altered cell cycle (via cyclins and cyclin-dependent kinases), glycolysis (through mTOR) and senescence (via FoxO proteins) [301, 302, 303]. Increased STAT5 activation may reveal an increased responsiveness to IL-2 and be involved in marginally improved suppressive abilities in ROR$\alpha$-deficient $T_{REG}$.

## 6.3 Regulation of $T_{REG}$ identity by ROR$\alpha$

As the expression of *Rora* is higher in tissue $T_{REG}$ than in their lymphoid organs counterparts, it is tempting to consider ROR$\alpha$ as a NLT environmental sensor in $T_{REG}$. ROR$\alpha$ appears to act as a switch restraining activation of effector cell pathways in $T_{REG}$ in inflammatory conditions. ROR$\alpha$ allows $T_{REG}$ to preserve their identity, while adapting to external polarizing stimuli, likely acting via (a) negative feedback loop(s) such as BACH2-mediated. BACH2 was identified as a regulator of $T_{REG}$ stability [304] and we show that it's expression level was decreased in ROR$\alpha$-deficient lung $T_{REG}$ during HDM-induced AAI model and *in vitro* activation. While ROR$\alpha$ transcriptionally regulates several genes involved in Th polarization, the most pronounced functional effect were observed on the $T_H2$ component. This might be due to the fact that transcriptional networks acting in tissue $T_{REG}$ are closer to those of $T_H2$ cells than other populations and thus ROR$\alpha$ deficiency rather favors a shift toward $T_H2$. In line with detrimental role of type 2 immunity in allergic diseases and its protective homeostatic role in VAT, ROR$\alpha$ expression in VAT $T_{REG}$ weakens their regulatory ability, impacting on insulin sensitivity in CD or HFD fed animals. A similar observation was made when studying suppressive capacity of $T_{REG}$. Both *in vivo*(in a T cell-induced colitis model) and *in vitro*, ROR$\alpha$-deficient $T_{REG}$ tend to be slightly better suppressors than wild type cells. However, these differences were either not significant or very small. Gene expression analysis of published and new data reveals that ROR$\alpha$ regulates a wide range of gene and activities in various tissues (skin, lung, adipose tissue, colon, muscle) and conditions (homeostatic or inflammatory). This paradigm of broad multifunctional regulators is often seen in

immune control circuits such as that of NFκB, which alone may potentially activate transcription of hundreds of genes, but provides highly specific action which depends on the input [305, 190].

In line with this broad regulatory pattern, $T_{REG}$ activation of RORα$^{Foxp3/Foxp3}$ $T_{REG}$ in the presence of IL-4 is sufficient to drive a significant part of transcriptional changes caused by RORα deficiency seen in lung $T_{REG}$ in AAI. At the same time, $T_{REG}$ from VAT show gene signature distinct from that of lung of *in vitro* activated $T_{REG}$, although VAT $T_{REG}$ are also controlled by RORα. These pleiotropic but differential effects are actually in agreement with known roles of RORα in immune cells. Effect of RORα in $T_{REG}$ may be facilitated through other major TF [274]. For instance, *Pparg*, a gene of a major regulator of VAT $T_{REG}$ (as well as for other tissue $T_{REG}$) is upregulated in most gene expression profiles of RORα-deficient $T_{REG}$, and *Bach2*, important for $T_{REG}$ stability and highly expressed in tissue $T_{REG}$, is decreased. However other genes shown to be critical for $T_{REG}$ development and function such as *Gata3* or *Irf4* seem unaffected by RORα expression. Our data together with published reports suggest, that in contrast to PPARγ or RORγt, RORα is rather a (pan-tissue) regulator with broad-specificity for $T_{REG}$ from various NLT.

## 6.4  Colonic $T_{REG}$ and inflammation in RORα$^{Foxp3/Foxp3}$ mice

$T_{REG}$ cells may loose their identity in favor of effector $T_H17$ phenotype. Indeed, ex-$T_{REG}$ start to express IL-17 and have reduced suppressive activity as observed in mice and humans during intestinal inflammation [69, 228]. We thus examined $T_{REG}$ subpopulations of in colon to test whether RORα had a role in ex-$T_{REG}$ generation. We found in both steady state and DSS-induced colitis model, that RORα-deficient $T_{REG}$ had lower proportions of RORγt$^+$ and CCR6$^+$ $T_{REG}$ cells (data not shown). $T_{REG}$ showing such surface phenotype were described as susceptible to dedifferentiation into pathogenic effectors (ex-$T_{REG}$). Furthermore, intestinal $T_{REG}$ with the highest suppressive capacity are RORγt$^+$CCR6$^+$CD44$^+$[146, 306] and the greatest reduction observed in RORα-deficient $T_{REG}$ subsets affected cells co-expressing these markers However, we were unable to show any disease improvement in RORα$^{Foxp3/Foxp3}$ mice: animals lost same amount of weight and had only slightly and not significantly reduced intestinal inflammation. Another trait of colon RORγt$^+$ $T_{REG}$ their reported extrathymic origin (peripherally activated p$T_{REG}$) in contrast to colonic GATA3$^+$ $T_{REG}$ of thymic origin [211]. We thus tested whether RORα affected i$T_{REG}$ generation *in vitro* by culturing naive T cells in the presence of tumor growth factor beta (TGF-β). We didn't observe any differences between $T_{REG}$ from wildtype and RORα$^{Foxp3/Foxp3}$ mice, regardless of strength of TCR costimulation and concentration of TGF-β (data not shown). By contrast, preliminary data obtained using TNBS-induced colitis associated to type 2 response showed an exacerbated pathology in RORαFoxp3/Foxp3 mice. This was accompanied by increased expression of type 2 cytokines (data not shown), similarly to the other model of type 2 inflammation. These results further confirm that RORα expression in $T_{REG}$ controls type 2 rather than Th17 response.

## 6.5  Conclusion and perspectives

Although several characteristics of RORα-deficient $T_{REG}$ were addressed in this study, the underlying molecular mechanisms of RORα regulation still require full investigation. Taking into account the diversity and complexity of RORα effects in $T_{REG}$, we examined how RORα might affect $T_{REG}$ genome-wide. For these studies, we were unable to successfully use VAT $T_{REG}$ directly due to very low cell numbers. To overcome this issue, we used a model of *in vitro* $T_{REG}$ activation in the presence of IL-4, which induced, in splenic $T_{REG}$, a phenotype closely resembling those of tissue $T_{REG}$ and $T_{REG}$ activated during type 2-mediated responses. We first sought for binding sites of RORα in $T_{REG}$ cells by ChIP-seq. We tested 3 different anti-RORα antibodies, but none provided a specific signal. We

then searched for the RORα-dependent chromatin changes in $T_{REG}$ and thus focused on histone modifications and DNA methylation. Indeed, several recent studies showed that chromatin profiles of tissue $T_{REG}$ are distinct from those of other cell types [120, 121] Thus, we performed ChIP-seq for the acetylated or methylated histones: H3K27Ac, H3K27me3 and H3K4me1 to localize open and closed chromatin regions in RORα-deficient and proficient cells [307]. We also performed an Assay for Transposase-Accessible Chromatin using sequencing (ATAC-seq) [308], to complement histone modification data and, most importantly, to identify RORα binding sites using footprinting analysis. Additionally, we performed MeDIP-seq assay [309] to track the impact of RORα on DNA methylation profile as it was recently shown that tissue $T_{REG}$ possess an identifiable DNA methylation pattern [121]. Furthermore, methylation of regulatory regions of $T_{REG}$ master TF – forkhead box P3 (FOXP3) also plays an important regulatory role [44]. We have optimized protocol for $T_{REG}$ and experimental samples are now processed for these assays (with H3K27Ac ChIP-seq already completed). Data will be analysed within the next couple of months and integrated with transcriptomic analysis.

A more distant perspective is to consider RORα in $T_{REG}$ as a target for pharmaceutical intervention. The pleiotropic nature RORα action might be useful for at least 2 therapeutic applications. Targeted expansion or activation of RORα-expressing $T_{REG}$ or induction of RORA expression in these cells might be potentially be beneficial in case of allergic diseases such as asthma and atopic dermatitis. Whereas inhibition of the protein or downregulation of RORA expression may improve metabolic parameters in insulin-resistant individuals and reduce weight gain. This is, however, associated with many obstacles. First, the availability of specific RORα agonists and antagonists stays very limited. Second, the hypothetical treatment should be $T_{REG}$-specific as interference with whole-body RORA expression may cause numerous pathologies described in both humans and mice [310]. Third, even assuming that $T_{REG}$-restricted RORA targeting is possible, rigorous testing should be carried out to study outcomes of its highly pleiotropic effects. RORα role in $T_{REG}$ is substantial and complex, but might be summarized as an adaptive switch, sensing local cues and shaping a $T_{REG}$ phenotype, capable of controlling homeostasis and preserving functional integrity during (especially type 2) inflammation.

# Chapter 7

# Methods

## 7.1  Animals

Rora$^{fl/fl}$ mice were generated by Genoway using homologous recombination in C57BL/6 embryonic stem cells. Targeting vector contained insertion of two loxP sites flanking a fragment of Rora exon 3 sequence, as well neomycin positive selection marker and diphtheria toxin A negative selection marker. Recombination was validated by Southern blotting. Rora$^{fl/fl}$ mice were crossed with Foxp3YFP-Cre animals to obtain ROR$\alpha^{Foxp3/Foxp3}$ mice [70]. Cre-mediated recombination resulted in conditional deletion of 86 bp fragment in exon 3 of Rora gene coding DNA-binding domain. Dysregulated splicing results in a frame shift and creates premature stop codon. In case of translation, resulting mRNAs could give 88 or 32 amino acids-long truncated proteins for the two alternative splicing isoforms: Rora 1 and 2 respectively. Mice were maintained in specific pathogen-free animal facility (12:12 h light/dark cycle, 21-24°C) in Pasteur Institute of Lille in accordance with institutional guidelines. 6-20-week-old female mice were used for all but dietetary experiments with *ad libitum* access to food and water. Mice were randomized between experimental groups, equilibrated for body weight and age. All experiments were performed following approval by the Ethics Committee for Animal Experimentation from Nord-Pas de Calais Region CEEA75 №01-2002R and APAFIS # 7160- 2017040313471173.

## 7.2  PCR Confirmation of the Deletion of the Floxed Rora Allele

Genomic DNA from flow cytometry-sorted CD4$^+$YFP$^+$ or CD4$^+$CD62L$^+$CD44$^-$YFP$^-$ T cells was isolated using Trizol (ThermoFisher, USA) reagent and diluted in water. PCR reaction was made using Diamond Taq Polymerase with the following primer pairs:
5'-GCATCAAGTACCAAAGTCAGTGGTTACAGAAAAT-3';
5'-CTGCAAATGATGGTGGTGAACTGTGC-3' for Rora$^{WT}$ and Rora$^{fl}$ allele detection;
5'-GCATCAAGTACCAAAGTCAGTGGTTACAGAA-3';
5'-CCTTCTCATAAATCCAGTAATGGGCAACC-3' for detection of Rora allele lacking Cre-excised fragment.

## 7.3   Diets and Metabolic Tests

Mice were fed with either normal chow or high fat diet (HFD) with 60 % kcal from animal Fat (Research Diets, USA). All experiments about metabolism were performed on male mice. Measurements for intrapeitoneal glucose and insulin tolerance tests (IPGTT & ITT respectively) were performed using tail incision and Accu-Check glucometer. 1 g/kg of glucose was injected i.p for glucose tolerance cells. 0.4 U/kg of insulin was injected i.p. for insulin tolerance test [311].

## 7.4   Preparation of Single-Cell Suspensions of Immune Cells from Mouse Tissues

Splenic and lymph node cell suspensions were obtained by mechanical homogenisation of organs on a 40 μm cell strainer. For spleens, red blood cells were lysed using ammonium chloride containing buffer Composition, cells were washed with cold PBS. Lungs were minced and digested in DMEM containing 0.5% FCS and 0.1% Collagenase D (Gibco (ThermoFisher), USA) for 40 minutes at 37°C in a water bath under agitation. Cell pellets were incubated in ice cold ammonium chloride containing buffer, washed in cold PBS and filtered through 70μm cell strainer, centrifuged 400g in 20% Percoll (GE Healthcare, USA) solution in PBS (Gibco (ThermoFisher), USA) at room temperature. Mouse adipose tissues were minced, in DMEM containing 0.5% FCS and 0.1% Collagenase D (Gibco (ThermoFisher), USA) incubated at 37°C during 45 minutes. Cells from stromal vascular fraction were centrifuged, treated with ice cold red blood cell lysis buffer, filtered through strainer and resuspended in PBS with 0.5% FCS. Mouse colon was isolated as follows. Peyer's patches and mesenteric fat were removed, colon was cut longitudinally and washed with cold PBS. Colon was cut into pieces, washed and incubated in EDTA-containing buffer at 37°C for 40 minutes being shaken thoroughly. Colon pieces were vortexed and treated with Collagenase I-containing buffer for 1.5 hours at 37°C. Cells were filtered through a mesh (70 μm) and washed. Immune cells were separated by a two-phase 40-80% gradient of Percoll by a 1000g centrifugation for 20 minutes at room temperature with brake turned off. After either of the procedures, pellets were washed with cold PBS and resuspended in PBS with 0.5% FCS for flow cytometry analysis.

## 7.5   Flow Cytometry

Cells were stained with 1/500 Zombie UV (BioLegend, USA) viability dye in PBS for 10 minutes at room temperature, washed with 0.5% FCS in PBS and stained with antibodies (see Key resources table) for surface antigens for 20 minutes on ice with addition of Fc Block. Antibodies were purchased from BD, Biolegend of ThermoFisher (eBioscience). For staining of intracellular antigens, BD Fixation/Permeabilization Solution Kit or eBioscience FoxP3/Transcription Factor Staining Buffer set were used in accordance with manufacturer guidelines. For detection of cytokine levels, cells were washed with 0.5% FCS in PBS and analysed using BD LSR Fortessa X20 Cell Analyzer controlled by BD FACSDiva software. Data were analyzed using FlowJo software (TriStar).

## 7.6   Cell Sorting

$CD4^+TCR\beta^+YFP^+$ $T_{REG}$ cells were sorted from spleen and adipose tissue by flow cytometry. $CD45^+CD4^+NK1.1^-YFP^+$ cells were sorted from lungs and mediastinal lymph nodes. For culturing, cells were sorted into fetal calf serum (FCS)-coated tubes. For RNA isolation, cells were sorted directly into RLT buffer (Qiagen RNeasy Micro Kit). BD Influx Cell Sorter was used.

## 7.7   T$_{REG}$cell culture

Flow cytometry-sorted T$_{REG}$cells were washed with RPMI (ThermoFisher, USA) containing 10% FCS and cultured in 37°C CO2 incubator for 5 days in round-bottom 96-well plates. $5 \times 10^4$ cells were seeded per well in RPMI medium containing HEPES, 10% FCS, 4.5 g/L D-glucose, 4 mM L-glutamine, 1 mM non-essential amino acids, 1 mM sodium pyruvate (ThermoFisher, USA), 0.05 mM 2-mercaptoethanol (Sigma-Aldrich, USA) and gentamycin. Mouse T cell activator Dynabeads with 1:1 bead-cell ratio and 40 ng/mL of mouse recombinant IL-2 were added for cell activation. 40 ng/mL mouse recombinant IL-4 and 1 µg/mL anti-murine IFN$\gamma$ antibody (Peprotech, USA) were also added for Th2 polarization. For differentiation of induced T$_{REG}$cells (iT$_{REG}$), flat-bottom 96-well plates were coated with 2µg/mL anti-mouse CD3$\varepsilon$ antibody (BioLegend) during 2 hours at 37°C. 50 x 103 FACS-sorted CD4$^+$TCR$\beta^+$YFP$^-$CD62L$^+$CD44$^-$ naive T cells were seeded per well and cultured during 5 days in RPMI and containing HEPES, 10% FCS, 2 g/L D-glucose, 2 mM L-glutamine, 1 mM non-essential amino acids, 1 mM sodium pyruvate, 0.05 mM 2-mercaptoethanol, gentamycin, 1 µg/mL anti-murine CD28, 1 µg/mL anti-murine IFN$\gamma$, 1 µg/mL anti-murine IL-4, 10 ng/mL murine IL-2, 0.5 ng/mL human TGF$\beta$ (Peprotech).

## 7.8   In vitro Proliferation and Suppression Assays

For proliferation assays, cells were stained with CellTrace proliferation kit (Thermo), using manufacturer's protocol and analysed by flow cytometry after 5 days of culture. For in vitro suppression assays, FACS-sorted CD4$^+$TCR$\beta^+$YFP-CD62L$^+$CD44- naive T cells were stained with CellTrace proliferation kit. CD4$^+$TCR$\beta^+$YFP$^+$ T$_{REG}$cells were co-cultured with labeled naive T cells in Tnaive/T$_{REG}$ratios of 1:1, 1:3 and 1:6. After 4 days, proliferation of naive T cells was analysed by flow cytometry.

## 7.9   T cell-induced Colitis

Naive T cells (CD3$\varepsilon^+$CD4$^+$CD45RB$^+$CD25-) were sorted from spleens of 9 week old female C57BL/6 wild-type mice [219]. T$_{REG}$cells were sorted from spleens of female Rora$^+$/$^+$ (ROR$\alpha^{WT/WT}$) or ROR$\alpha^{Foxp3/Foxp3}$ mice ( 9 weeks old). Naïve T cells or mix of naïve T cells and T$_{REG}$cells were resuspended in sterile PBS. 100uL of solution per mouse were injected. Cells were injection into tail vein of female Rag2$^{-/-}$ mice ( 20 weeks old). Rag2$^{-/-}$ mice were divided into 3 groups: 1) Injected with $2 \times 10^6$ naïve T cells; 2) Injected with $2 \times 10^6$ naïve T cells and $5 \times 10^5$ T$_{REG}$cells sorted from ROR$\alpha^{WT/WT}$ mice; 3) Injected with $2 \times 10^6$ naïve T cells and $5 \times 10^5$ T$_{REG}$cells sorted from ROR$\alpha^{Foxp3/Foxp3}$ mice. Mice from different experimental groups were randomly co-housted. Body weight was monitored once weekly. Mice were sacrificed after 8 weeks and colitis intensity was assessed. (n = 6 mice per group).

## 7.10   Apoptosis Assessment

For in vivo analyses of apoptosis level, lung T$_{REG}$ cells were stained using FLICA Caspase 3/7 kit (Bio-Rad, USA). In this assay, staining intensity correlates with activity of caspases 3/7. In vitro cultured T$_{REG}$ were stained with Annexin V (BioLegend, USA) and Zombie UV. After staining cells were analyzed by flow cytometry.

## 7.11    RNA Isolation

Total RNA isolation for qPCR was performed using Trizol in accordance with manufacturer's guidelines. For microarray analyses, total RNA from tissues was isolated with RNeasy Mini Kit Qiagen (Germany), and from sorted and cultured cells with RNeasy Micro Kit Qiagen (Germany).

## 7.12    Reverse Transcription and Real-time PCR

Isolated total RNA was treated with DNAse I, cDNA was synthesized using High-capacity cDNA reverse transcription kit. Gene expression was analysed using 2x Brilliant II SYBR Green QPCR Master Mix (Agillent). $\Delta\Delta$Ct method was used [312], Ct values were normalized to those of Hprt1 housekeeping gene.

## 7.13    Western Blotting

Tissues were homogenized using Ultra Turrax (IKA). Cells or homogenates were lysed in Bolt LDS Sample Buffer (Life technologies). Electrophoresis and transfer were made using Bolt system (Thermo) according to manufacturer's guidelines. Nitrocellulose membranes were used. Non-specific protein binding by a membrane was blocked by incubation with 5% BSA in PBS for 2 hours at room temperature. Incubation with primary antibodies was made overnight at 4°C Membranes were scanned with Odyssey CLx (LI-COR), band intensities were analysed using Image Studio software (LI-COR).

## 7.14    Analysis of Mitochondrial Content

$T_{REG}$ cells cultured in vitro or single cell suspenions from lungs and mediastinsal lymph nodes were incubated with 1μM MitoTracker Deep Red (ThermoFisher) in DMEM at 37°C in CO2 incubator for 30 minutes, washed with PBS, stained for CD45, TCRβ and analyzed by flow cytometry.

## 7.15    Analysis of Mitochondrial ROS

Single cell suspensions from lungs and mediastinsal lymph nodes were incubated with 5μM MitoSOX Red in DMEM 37°C in CO2 incubator for 30 minutes, washed with PBS, stained for CD45, TCRβ and CD4 and analyzed by flow cytometry according to manufacturer's guidelines.

## 7.16    HDM-induced Allergic Asthma Model

6-10 weeks old mice were injected intratracheally, under anesthesia with isofluran, with 1μg of HDM (Greer, USA) on days 0 and 7. On the day 14, 15 and 16 5μg of HDM was injected, mice were sacrificed on day 18 (or on day 17 in case of EdU experiments) (adapted from [313]).

## 7.17    Invasive Plethysmography

Measurement of dynamic lung resistance (and compliance) were performed on mice using Flexivent (SCIREQ, emka technologies, France) described([314]). Mice were anesthetized with 0.5 mg/kg medetomidine (Domitor; Pfizer, New York, USA) and 50 mg/kg ketamine (Imalgene; Merial, Toulouse,

France), tracheotomized and intubated with a 20-gauge catheter (Introcan; B. Braun, Melsungen, Germany). Then they were paralyzed with curare and immediately connected to mechanical ventilation. Increasing concentrations of methacholine (0-200 mg/mL) were administered at the rate of 20 puffs per 10 s, with each puff of aerosol delivery lasting 10 ms, via a nebulizer aerosol system with a 2.5–4 nm aerosol particle size generated by a nebulizer head (Aeroneb, Aerogen). Respiratory frequency was set at 150 breaths/min with a tidal volume of 0.2 ml, and a positive-end expiratory pressure of 2 ml water was applied.

## 7.18   EdU Cell Cycle Experiments

On days 15 and 16 of HDM-induced asthma protocol mice were injected with 12,5 mg/kg EdU intraperitoneally. Live $CD3\varepsilon^+CD4^+YFP^+$ or $CD3\varepsilon^+CD4^+YFP^+$ $T_{REG}$ and $T_{CONV}$ cells were sorted from lungs and lymph nodes, stained for EdU and DNA content and analysed by flow cytometry. For in vitro experiments cells were incubated with 10µM EdU during 24 hours. Staining of cells was performed using BD EdU Proliferation Kit in accordance with manufacturer's guidelines. Vybrant DyeCycle Violet DNA-dye (ThermoFisher, USA) was used to quantify DNA content.

## 7.19   Histology

Mouse organs were dissected and fixed in ImmunoHistoFix (Gentaur, Belgium), followed by embedding in ImmunoHistoWax (Gentaur, Belgium) at 37°C. 5 µm sections were prepared and stained with May-Grünwald Giemsa (Sigma, USA) for assessment of general morphology and mucosal layer in the lungs, intestine and other tissues. Hematoxilin (Sigma, USA) staining was used for 7 µm adipose tissue sections.

## 7.20   ELISA and Multiplex Cytokine Analysis

Blood samples were collected from retroorbital vein of anesthetized with isofluran just before sacrifice. Samples were kept for two hours at room temperature to facilitate coagulation and spinned to discard coagulates. Concentration of HDM-specific IgE in mice sera were determined with Chondrex kits according to supplier's guidelines. Media from cultured cells were collected and stored -20°C. Concentrations of cytokines were measured using R&D ELISA kits in accordance with supplier's guidelines. Adipokine concentrations were assessed using Milliplex kits according to guidelines. Data were acquired with Bio-Plex Magipix Multiplex Reader (Bio-Rad, USA)

## 7.21   Microarray Analysis

12ng of RNA isolated from $T_{REG}$ cells sorted from lungs and mediastinal lymph nodes or 50ng of RNA isolated from in vitro cultured $T_{REG}$ cells was prepared for microarray using Ovation Pico WTA Systems V2 and Affymetrix GeneChip WT Terminal. cRNA was hybridized with Affymetrix GeneChip Mouse Gene 2.0 ST Arrays in accordance with manufacturer's protocol. Chips were scanned with GeneChip scanner (Affymetrix) Microarray data were normalized using RMA method [315] with the help of oligo R package. Probes were collapsed by utilizing MaxMed approach and annotated using affycoretools R package. Differentially expressed genes were identified using limma R package, p-values were adjusted for multiple comparisons with Benjamini-Hochberg method [316]. For gene set enrichment analysis GSEA software [317] was used with 1000 gene set permutations performed to assess statistical significance of the enrichment score.

## 7.22   ChIP-seq Sample Preparation and Data Analysis

T$_{REG}$ were sorted from spleens of mice. Cells were cultured in the presence of T cell-activation beads, IL-2, IL-4 and anti-murine IFNγ (Th2 polarising conditions). After 5 days, cells were washed and incubated in 1% formaldehyde in PBS for cross-linking of chromatin. Nuclei were isolated using hypotonic buffer and lysed in SDS-buffer. Chromatin was sonicated using Diagenode Bioruptor and incubated with 2ug anti-H3K27ac (Active Motif) overnight. Immune complexes were incubated with A/G magnaetic beads (Thermo) for 6 hours. Beads were washed with LiCl (Sigma) containing buffer and TE Composition. Cross-linking was reversed in SDS and NaHCO3 containing buffer at 65°C overnight. DNA was isolated using Qiagen MinElute PCR-purification kit. Libraries were prepared with Truseq kit (illumina) and sequenced using single-end NextSeq technology (illumina). All epigenetic assays were performed at least in triplicates [307]. Sequencing was performed on the Biomics hugh-throughput techniques platform of Paris Pasteur Institute reads were mapped to mm10 reference genome using Bowtie2 [318] with standard parameters. Peaks were called using MACS2 or SICER (for broad histone marks) [319, 320]. SICER or csaw R packages were used for differential binding analysis, various FDR thresholds were tested (0.05-0.2) [321]. Galaxy platform was used for some of the applications [322].

## 7.23   Data Analysis

Data were plotted either as individual values or arithmetic means $\pm SEM$. Experimental groups were compared using two-tailed non-paired Student t-test or non-parametric Mann-Whitney test in case values in the sample were not normally distributed (for two groups). ANOVA followed by Tukey HSD was calculated when comparing more than two experimental groups. Statistical analyses were performed using GraphPad Prism 6, Microsoft Excel and R software. p $<$ 0.05 was considered to be statistically significant.

## 7.24   Key Resources

| REAGENT or RESOURCE | SOURCE | IDENTIFIER |
|---|---|---|
| Rat monoclonal anti-CD4 BV605 | Biolegend | Cat-100548 |
| Brilliant Violet 510 anti-mouse CD8a Antibody | Biolegend | Cat-100752 |
| Hamster monoclonal anti-TCR beta APC | BD Biosciences | Cat-553174 |
| Rat monoclonal anti-CD45 BV510 | Biolegend | Cat-103138 |
| BUV737 Mouse Anti-Mouse CD45.2 | BD Biosciences | Cat-564880 |
| Mouse monoclonal anti-NK1.1 AF700 | Biolegend | Cat-108730 |
| Rat monoclonal anti-CD62L PE | BD Biosciences | Cat-553151 |
| Rat monoclonal anti-CD44 BV711 | Biolegend | Cat-103057 |
| APC anti-mouse CD25 Antibody | Biolegend | Cat-101909 |
| Rat monoclonal anti-ST2 PercP-eF710 | eBioscience | Cat-46-9335-82 |
| Hamster monoclonal anti-CD3e PE-Cy7 | BD Biosciences | Cat-552774 |
| Rat Anti-Mouse IL-4 BV650 | BD Biosciences | Cat-564004 |
| Anti-mouse/human IL-5 APC | Biolegend | Cat-504306 |
| IL-10 Monoclonal Antibody (JES5-16E3) Alexa Fluor 700 | eBiosciences | Cat-56-7101-82 |
| IL-13 Monoclonal Antibody (eBio13A) PE-Cyanine7 | eBiosciences | Cat-25-7133-80 |
| Anti-mouse Ly-6A/E (Sca-1) APC/Cy7 | Biolegend | Cat-108126 |
| PE-CF594 Rat Anti-Mouse CD24 | BD Biosciences | Cat-562477 |
| PE Rat Anti-Mouse Ly-6G | BD Biosciences | Cat-551461 |
| BUV395 Rat Anti-CD11b | BD Biosciences | Cat-563553 |
| PE-CF594 Rat Anti-Mouse Siglec-F | BD Biosciences | Cat-562757 |
| PE/Cy7 anti-mouse F4/80 | Biolegend | Cat-123114 |
| Brilliant Violet 650 anti-mouse CD206 (MMR) | Biolegend | Cat-141723 |
| APC/Cyanine7 anti-mouse CD11c | Biolegend | Cat-117324 |
| APC anti-T-bet | Biolegend | Cat-644813 |
| PE/Cy7 anti-mouse CD69 | Biolegend | Cat-104512 |
| Goat polyclonal anti-ROR-alpha | Santa Cruz | Cat-sc-6062 |
| Mouse monoclonal anti-H3K27ac | Active Motif | Cat-39685 |
| Rat monoclonal CD16/CD32 | BD Biosciences | Cat-553141 |

Figure 7.1 – Key Resources

| | | |
|---|---|---|
| Alexa Fluor 647 Annexin V | Biolegend | Cat-640943 |
| NAD/NADH-Glo Assay | Promega | Cat-G9071 |
| ADP/ATP Ratio Assay Kit | Abcam | Cat-ab65313 |
| 647 EdU Proliferation Kit | BD Biosciences | Cat-565456 |
| eBioscience Foxp3 / Transcription Factor Staining Buffer Set | ThermoFisher Scientific | Cat-00-5523-00 |
| Transcription Factor Phospho Buffer Set | BD Biosciences | Cat-563239 |
| Mouse Anti-_House Dust Mite (HDM) IgE Antibody Assay Kit | Chondrex | CHO-3037 |
| Mouse Anti-House Dust Mite (HDM) IgG1 Antibody Assay Kit | Chondrex | CHO-3034 |
| Periodic Acid-Schiff (PAS) Kit | Sigma-Aldrich | 395B-1KT |
| Foxp3-Cre Mice | | |
| RoraFL/FL mice | Genoway | https://www.genoway.com/ |
| DIO (VHFD) 60 kcal% fat Diet | Research Diets | https://researchdiets.com/opensource-diets/dio-series-diets |
| House Dust Mite | Greer Laboratories | XPB70D3A25 |
| Pierce Protein A/G Magnetic Beads | Thermo Scientific | 88802 |
| RNeasy Micro Kit | Qiagen | Cat-74004 |
| MinElute PCR Purification Kit | Qiagen | Cat-28004 |

Figure 7.2 – Key Resources

| | | |
|---|---|---|
| Prism | GraphPad | https://www.graphpad.com/ |
| Excel | Microsoft | https://products.office.com/fr-fr/excel |
| R | R Foundation for Statistical Computing | https://www.R-project.org/ |
| limma | Ritchie M.E. Phipson B. Wu D. Hu Y. Law C.W. Shi W. and Smyth G.K. (2015). limma powers differential expression analyses for RNA-sequencing and microarray studies. Nucleic Acids Research 43(7) e47 | |
| oligo | Carvalho B. S. and Irizarry R. A. 2010. A Framework for Oligonucleotide Microarray Preprocessing. Bioinformatics. | |
| affycoretools | James W. MacDonald (2018). affycoretools: Functions useful for those doing repetitive analyses with Affymetrix GeneChips. R package version 1.52.2. | |
| Phantasus | Daria Zenkova Vladislav Kamenev Rita Sablina Maxim Artyomov Alexey Sergushichev | https://artyomovlab.wustl.edu/phantasus/ |
| GSEA | Subramanian Tamayo et al. (2005) PNAS 102 15545-15550 | http://www.broad.mit.edu/gsea/ |
| csaw | csaw: a Bioconductor package for differential binding analysis of ChIP-seq data using sliding windows. Lun AT1 Smyth GK2. Nucleic Acid Research 26578583 | https://bioconductor.org/packages/release/bioc/html/csaw.html |
| Bowtie2 | Fast gapped-read alignment with Bowtie 2. Ben Langmead and Steven L Salzberg. Nat Meth 2012, 3322381 | http://bowtie-bio.sourceforge.net/bowtie2/index.shtml |

Figure 7.3 − Key Resources

| | | |
|---|---|---|
| SICER | Spatial Clustering for Identification of ChIP-Enriched Regions (SICER) to Map Regions of Histone Methylation Patterns in Embryonic Stem Cells. Shiliyang Xu Sean Grullon Kai Ge and Weiqun Peng, Methods Mol Biol 2014 4152844 | https://github.com/ esebesty/sicer |
| Galaxy | The Galaxy platform for accessible, reproducible and collaborative biomedical analyses: 2018 update.Afgan E Baker D Batut B van den Beek M Bouvier D Cech M Chilton J Clements D Coraor N Grüning BA Guerler A Hillman-Jackson J Hiltemann S Jalili V Rasche H Soranzo N Goecks J Taylor J Nekrutenko A Blankenberg D. Nucleic Acid Research 2018, 6030816 | https://usegalaxy.org |
| MACS | Model-based Analysis of ChIP-Seq (MACS) Yong Zhang  Tao Liu  Clifford A Meyer  Jerome Eeckhoute  David S Johnson Bradley E Bernstein Chad Nusbaum Richard M Myers Myles Brown Wei Li and X Shirley Liu | http:// liulab.dfci.harvard.edu/ MACS/ |
| yathesis LaTeX package | Denis Bitouze | https://ctan.org/author/ bitouze |

Figure 7.4 – Key Resources

# Bibliography

[1]  S. A. Porcelli, C. T. Morita, and R. L. Modlin. "T-Cell Recognition of Non-Peptide Antigens". In: *Current Opinion in Immunology* 8.4 (Aug. 1996), pp. 510–516. ISSN: 0952-7915. DOI: 10.1016/s0952-7915(96)80039-2. pmid: 8794014.

[2]  Jean S. Marshall et al. "An Introduction to Immunology and Immunopathology". In: *Allergy, Asthma, and Clinical Immunology : Official Journal of the Canadian Society of Allergy and Clinical Immunology* 14 (Suppl 2 Sept. 12, 2018). ISSN: 1710-1484. DOI: 10.1186/s13223-018-0278-1. pmid: 30263032. URL: https://www.ncbi.nlm.nih.gov/pmc/articles/PMC6156898/ (visited on 10/29/2019).

[3]  Francisco A. Bonilla and Hans C. Oettgen. "Adaptive Immunity". In: *Journal of Allergy and Clinical Immunology* 125.2 (Feb. 1, 2010), S33–S40. ISSN: 0091-6749, 1097-6825. DOI: 10.1016/j.jaci.2009.09.017. URL: https://www.jacionline.org/article/S0091-6749(09)01405-5/abstract (visited on 08/09/2019).

[4]  Dale I. Godfrey et al. "The Biology and Functional Importance of MAIT Cells". In: *Nature Immunology* 20.9 (Sept. 2019), pp. 1110–1128. ISSN: 1529-2916. DOI: 10.1038/s41590-019-0444-8. URL: https://www.nature.com/articles/s41590-019-0444-8 (visited on 10/29/2019).

[5]  Sabrina Bianca Bennstein. "Unraveling Natural Killer T-Cells Development". In: *Frontiers in Immunology* 8 (Jan. 9, 2018). ISSN: 1664-3224. DOI: 10.3389/fimmu.2017.01950. pmid: 29375573. URL: https://www.ncbi.nlm.nih.gov/pmc/articles/PMC5767218/ (visited on 10/29/2019).

[6]  Benjamin E. Willcox and Carrie R. Willcox. "Γδ TCR Ligands: The Quest to Solve a 500-Million-Year-Old Mystery". In: *Nature Immunology* 20.2 (Feb. 2019), pp. 121–128. ISSN: 1529-2916. DOI: 10.1038/s41590-018-0304-y. pmid: 30664765.

[7]  Lars Kjer-Nielsen et al. "An Overview on the Identification of MAIT Cell Antigens". In: *Immunology and Cell Biology* 96.6 (July 2018), pp. 573–587. ISSN: 1440-1711. DOI: 10.1111/imcb.12057. pmid: 29656544.

[8]  Alex M. Abel et al. "Natural Killer Cells: Development, Maturation, and Clinical Utilization". In: *Frontiers in Immunology* 9 (2018). ISSN: 1664-3224. DOI: 10.3389/fimmu.2018.01869. URL: http://www.frontiersin.org/articles/10.3389/fimmu.2018.01869/full (visited on 10/29/2019).

[9]  David Artis and Hergen Spits. "The Biology of Innate Lymphoid Cells". In: *Nature* 517.7534 (Jan. 15, 2015), pp. 293–301. ISSN: 1476-4687. DOI: 10.1038/nature14189. pmid: 25592534.

[10] Ludger Klein, Ellen A. Robey, and Chyi-Song Hsieh. "Central CD4+ T Cell Tolerance: Deletion versus Regulatory T Cell Differentiation". In: *Nature Reviews. Immunology* 19.1 (Jan. 2019), pp. 7–18. ISSN: 1474-1741. DOI: 10.1038/s41577-018-0083-6. pmid: 30420705.

[11] S. Tonegawa. "Somatic Generation of Antibody Diversity". In: *Nature* 302.5909 (Apr. 14, 1983), pp. 575–581. ISSN: 0028-0836. DOI: 10.1038/302575a0. pmid: 6300689.

[12] Hiroyuki Takaba and Hiroshi Takayanagi. "The Mechanisms of T Cell Selection in the Thymus". In: *Trends in Immunology* 38.11 (Nov. 1, 2017), pp. 805–816. ISSN: 1471-4906, 1471-4981. DOI: 10.1016/j.it.2017.07.010. pmid: 28830733. URL: https://www.cell.com/trends/immunology/abstract/S1471-4906(17)30148-5 (visited on 08/09/2019).

[13] David Nemazee. "Mechanisms of Central Tolerance for B Cells". In: *Nature Reviews. Immunology* 17.5 (May 2017), pp. 281–294. ISSN: 1474-1741. DOI: 10.1038/nri.2017.19. pmid: 28368006.

[14] F. W. Alt et al. "Synthesis of Secreted and Membrane-Bound Immunoglobulin Mu Heavy Chains Is Directed by mRNAs That Differ at Their 3' Ends". In: *Cell* 20.2 (June 1980), pp. 293–301. ISSN: 0092-8674. DOI: 10.1016/0092-8674(80)90615-7. pmid: 6771018.

[15] Jennifer E. Smith-Garvin, Gary A. Koretzky, and Martha S. Jordan. "T Cell Activation". In: *Annual Review of Immunology* 27 (2009), pp. 591–619. ISSN: 0732-0582. DOI: 10.1146/annurev.immunol.021908.132706. pmid: 19132916.

[16] Oreste Acuto and Frédérique Michel. "CD28-Mediated Co-Stimulation: A Quantitative Support for TCR Signalling". In: *Nature Reviews. Immunology* 3.12 (Dec. 2003), pp. 939–951. ISSN: 1474-1733. DOI: 10.1038/nri1248. pmid: 14647476.

[17] Jordy Saravia, Nicole M. Chapman, and Hongbo Chi. "Helper T Cell Differentiation". In: *Cellular & Molecular Immunology* 16.7 (July 2019), pp. 634–643. ISSN: 2042-0226. DOI: 10.1038/s41423-019-0220-6. pmid: 30867582.

[18] T. R. Mosmann et al. "Two Types of Murine Helper T Cell Clone. I. Definition According to Profiles of Lymphokine Activities and Secreted Proteins". In: *Journal of Immunology (Baltimore, Md.: 1950)* 136.7 (Apr. 1, 1986), pp. 2348–2357. ISSN: 0022-1767. pmid: 2419430.

[19] Laurie E. Harrington et al. "Interleukin 17-Producing CD4+ Effector T Cells Develop via a Lineage Distinct from the T Helper Type 1 and 2 Lineages". In: *Nature Immunology* 6.11 (Nov. 2005), pp. 1123–1132. ISSN: 1529-2908. DOI: 10.1038/ni1254. pmid: 16200070.

[20] Thomas Duhen et al. "Production of Interleukin 22 but Not Interleukin 17 by a Subset of Human Skin-Homing Memory T Cells". In: *Nature Immunology* 10.8 (Aug. 2009), pp. 857–863. ISSN: 1529-2916. DOI: 10.1038/ni.1767. pmid: 19578369.

[21] M. H. Kaplan et al. "Impaired IL-12 Responses and Enhanced Development of Th2 Cells in Stat4-Deficient Mice". In: *Nature* 382.6587 (July 11, 1996), pp. 174–177. ISSN: 0028-0836. DOI: 10.1038/382174a0. pmid: 8700209.

[22] W. Zheng and R. A. Flavell. "The Transcription Factor GATA-3 Is Necessary and Sufficient for Th2 Cytokine Gene Expression in CD4 T Cells". In: *Cell* 89.4 (May 16, 1997), pp. 587–596. ISSN: 0092-8674. DOI: 10.1016/s0092-8674(00)80240-8. pmid: 9160750.

[23] Ivaylo I. Ivanov et al. "The Orphan Nuclear Receptor RORgammat Directs the Differentiation Program of Proinflammatory IL-17+ T Helper Cells". In: *Cell* 126.6 (Sept. 22, 2006), pp. 1121–1133. ISSN: 0092-8674. DOI: 10.1016/j.cell.2006.07.035. pmid: 16990136.

[24] Roza I. Nurieva et al. "Bcl6 Mediates the Development of T Follicular Helper Cells". In: *Science (New York, N.Y.)* 325.5943 (Aug. 21, 2009), pp. 1001–1005. ISSN: 1095-9203. DOI: 10.1126/science.1176676. pmid: 19628815.

[25] K. R. Mcintire, S. Sell, and J. F. Miller. "PATHOGENESIS OF THE POST-NEONATAL THYMECTOMY WASTING SYNDROME". In: *Nature* 204 (Oct. 10, 1964), pp. 151–155. ISSN: 0028-0836. DOI: 10.1038/204151a0. pmid: 14222260.

[26]  Y. Nishizuka and T. Sakakura. "Thymus and Reproduction: Sex-Linked Dysgenesis of the Gonad after Neonatal Thymectomy in Mice". In: *Science (New York, N.Y.)* 166.3906 (Nov. 7, 1969), pp. 753–755. ISSN: 0036-8075. DOI: 10.1126/science.166.3906.753. pmid: 5823314.

[27]  H. Ohki et al. "Implants of Quail Thymic Epithelium Generate Permanent Tolerance in Embryonically Constructed Quail/Chick Chimeras". In: *Development (Cambridge, England)* 104.4 (Dec. 1988), pp. 619–630. ISSN: 0950-1991. pmid: 3268407.

[28]  G. Plitas and A. Y. Rudensky. "Regulatory T Cells: Differentiation and Function". In: *Cancer Immunology Research* 4.9 (Sept. 2, 2016), pp. 721–725. ISSN: 2326-6066, 2326-6074. DOI: 10.1158/2326-6066.CIR-16-0193. URL: http://cancerimmunolres.aacrjournals.org/cgi/doi/10.1158/2326-6066.CIR-16-0193 (visited on 08/22/2019).

[29]  Marc A. Gavin et al. "Homeostasis and Anergy of CD4(+)CD25(+) Suppressor T Cells in Vivo". In: *Nature Immunology* 3.1 (Jan. 2002), pp. 33–41. ISSN: 1529-2908. DOI: 10.1038/ni743. pmid: 11740498.

[30]  Shohei Hori, Takashi Nomura, and Shimon Sakaguchi. "Control of Regulatory T Cell Development by the Transcription Factor Foxp3". In: *Science (New York, N.Y.)* 299.5609 (Feb. 14, 2003), pp. 1057–1061. ISSN: 1095-9203. DOI: 10.1126/science.1079490. pmid: 12522256.

[31]  Roli Khattri et al. "An Essential Role for Scurfin in CD4+CD25+ T Regulatory Cells". In: *Nature Immunology* 4.4 (Apr. 2003), pp. 337–342. ISSN: 1529-2908. DOI: 10.1038/ni909. pmid: 12612581.

[32]  Kimito Kawahata et al. "Generation of CD4(+)CD25(+) Regulatory T Cells from Autoreactive T Cells Simultaneously with Their Negative Selection in the Thymus and from Nonautoreactive T Cells by Endogenous TCR Expression". In: *Journal of Immunology (Baltimore, Md.: 1950)* 168.9 (May 1, 2002), pp. 4399–4405. ISSN: 0022-1767. DOI: 10.4049/jimmunol.168.9.4399. pmid: 11970982.

[33]  Sven Malchow et al. "Aire Enforces Immune Tolerance by Directing Autoreactive T Cells into the Regulatory T Cell Lineage". In: *Immunity* 44.5 (May 17, 2016), pp. 1102–1113. ISSN: 1097-4180. DOI: 10.1016/j.immuni.2016.02.009. pmid: 27130899.

[34]  Takashi Sekiya et al. "Nr4a Receptors Are Essential for Thymic Regulatory T Cell Development and Immune Homeostasis". In: *Nature Immunology* 14.3 (Mar. 2013), pp. 230–237. ISSN: 1529-2916. DOI: 10.1038/ni.2520. pmid: 23334790.

[35]  Chan-Wang Joaquim Lio and Chyi-Song Hsieh. "A Two-Step Process for Thymic Regulatory T Cell Development". In: *Immunity* 28.1 (Jan. 2008), pp. 100–111. ISSN: 1074-7613. DOI: 10.1016/j.immuni.2007.11.021. pmid: 18199417.

[36]  Marc A. Gavin et al. "Foxp3-Dependent Programme of Regulatory T-Cell Differentiation". In: *Nature* 445.7129 (Feb. 15, 2007), pp. 771–775. ISSN: 1476-4687. DOI: 10.1038/nature05543. pmid: 17220874.

[37]  Yongqiang Feng et al. "Control of the Inheritance of Regulatory T Cell Identity by a Cis Element in the Foxp3 Locus". In: *Cell* 158.4 (Aug. 14, 2014), pp. 749–763. ISSN: 1097-4172. DOI: 10.1016/j.cell.2014.07.031. pmid: 25126783.

[38]  Wonyong Lee and Gap Ryol Lee. "Transcriptional Regulation and Development of Regulatory T Cells". In: *Experimental & Molecular Medicine* 50.3 (Sept. 3, 2018), e456. ISSN: 2092-6413. DOI: 10.1038/emm.2017.313. pmid: 29520112.

[39]  Naganari Ohkura, Yohko Kitagawa, and Shimon Sakaguchi. "Development and Maintenance of Regulatory T Cells". In: *Immunity* 38.3 (Mar. 21, 2013), pp. 414–423. ISSN: 1097-4180. DOI: 10.1016/j.immuni.2013.03.002. pmid: 23521883.

[40] C. L. Bennett et al. "The Immune Dysregulation, Polyendocrinopathy, Enteropathy, X-Linked Syndrome (IPEX) Is Caused by Mutations of FOXP3". In: *Nature Genetics* 27.1 (Jan. 2001), pp. 20–21. ISSN: 1061-4036. DOI: 10.1038/83713. pmid: 11137993.

[41] Ethan M. Shevach. "The Resurrection of T Cell-Mediated Suppression". In: *Journal of Immunology (Baltimore, Md.: 1950)* 186.7 (Apr. 1, 2011), pp. 3805–3807. ISSN: 1550-6606. DOI: 10.4049/jimmunol.1100364. pmid: 21422250.

[42] Yohko Kitagawa et al. "Guidance of Regulatory T Cell Development by Satb1-Dependent Super-Enhancer Establishment". In: *Nature Immunology* 18.2 (Feb. 2017), pp. 173–183. ISSN: 1529-2916. DOI: 10.1038/ni.3646. pmid: 27992401.

[43] Hyoung-Pyo Kim and Warren J. Leonard. "CREB/ATF-Dependent T Cell Receptor-Induced FoxP3 Gene Expression: A Role for DNA Methylation". In: *The Journal of Experimental Medicine* 204.7 (July 9, 2007), pp. 1543–1551. ISSN: 0022-1007. DOI: 10.1084/jem.20070109. pmid: 17591856.

[44] Ye Zheng et al. "Role of Conserved Non-Coding DNA Elements in the Foxp3 Gene in Regulatory T-Cell Fate". In: *Nature* 463.7282 (Feb. 11, 2010), pp. 808–812. ISSN: 1476-4687. DOI: 10.1038/nature08750. pmid: 20072126.

[45] Lili Xu et al. "Positive and Negative Transcriptional Regulation of the Foxp3 Gene Is Mediated by Access and Binding of the Smad3 Protein to Enhancer I". In: *Immunity* 33.3 (Sept. 24, 2010), pp. 313–325. ISSN: 1097-4180. DOI: 10.1016/j.immuni.2010.09.001. pmid: 20870174.

[46] Hozefa S. Bandukwala et al. "Structure of a Domain-Swapped FOXP3 Dimer on DNA and Its Function in Regulatory T Cells". In: *Immunity* 34.4 (Apr. 22, 2011), pp. 479–491. ISSN: 1097-4180. DOI: 10.1016/j.immuni.2011.02.017. pmid: 21458306.

[47] Dipayan Rudra et al. "Transcription Factor Foxp3 and Its Protein Partners Form a Complex Regulatory Network". In: *Nature Immunology* 13.10 (Oct. 2012), pp. 1010–1019. ISSN: 1529-2916. DOI: 10.1038/ni.2402. pmid: 22922362.

[48] Jianguang Du et al. "Isoform-Specific Inhibition of ROR Alpha-Mediated Transcriptional Activation by Human FOXP3". In: *Journal of Immunology (Baltimore, Md.: 1950)* 180.7 (Apr. 1, 2008), pp. 4785–4792. ISSN: 0022-1767. DOI: 10.4049/jimmunol.180.7.4785. pmid: 18354202.

[49] Liang Zhou et al. "TGF-Beta-Induced Foxp3 Inhibits T(H)17 Cell Differentiation by Antagonizing RORgammat Function". In: *Nature* 453.7192 (May 8, 2008), pp. 236–240. ISSN: 1476-4687. DOI: 10.1038/nature06878. pmid: 18368049.

[50] Bin Li et al. "FOXP3 Interactions with Histone Acetyltransferase and Class II Histone Deacetylases Are Required for Repression". In: *Proceedings of the National Academy of Sciences of the United States of America* 104.11 (Mar. 13, 2007), pp. 4571–4576. ISSN: 0027-8424. DOI: 10.1073/pnas.0700298104. pmid: 17360565.

[51] Fred Ramsdell and Steven F. Ziegler. "FOXP3 and Scurfy: How It All Began". In: *Nature Reviews Immunology* 14.5 (May 2014), pp. 343–349. ISSN: 1474-1741. DOI: 10.1038/nri3650. URL: http://www.nature.com/articles/nri3650 (visited on 08/31/2019).

[52] Wenxian Fu et al. "A Multiply Redundant Genetic Switch 'locks in' the Transcriptional Signature of Regulatory T Cells". In: *Nature Immunology* 13.10 (Oct. 2012), pp. 972–980. ISSN: 1529-2916. DOI: 10.1038/ni.2420. pmid: 22961053.

[53] Guillaume Oldenhove et al. "Decrease of Foxp3+ Treg Cell Number and Acquisition of Effector Cell Phenotype during Lethal Infection". In: *Immunity* 31.5 (Nov. 20, 2009), pp. 772–786. ISSN: 1097-4180. DOI: 10.1016/j.immuni.2009.10.001. pmid: 19896394.

[54] Xuyu Zhou et al. "Instability of the Transcription Factor Foxp3 Leads to the Generation of Pathogenic Memory T Cells in Vivo". In: *Nature Immunology* 10.9 (Sept. 2009), pp. 1000–1007. ISSN: 1529-2916. DOI: 10.1038/ni.1774. pmid: 19633673.

[55] Shimon Sakaguchi et al. "Regulatory T Cells: How Do They Suppress Immune Responses?" In: *International Immunology* 21.10 (Oct. 2009), pp. 1105–1111. ISSN: 1460-2377. DOI: 10.1093/intimm/dxp095. pmid: 19737784.

[56] Ethan M. Shevach. "Mechanisms of Foxp3+ T Regulatory Cell-Mediated Suppression". In: *Immunity* 30.5 (May 2009), pp. 636–645. ISSN: 1097-4180. DOI: 10.1016/j.immuni.2009.04.010. pmid: 19464986.

[57] A. M. Thornton and E. M. Shevach. "CD4+CD25+ Immunoregulatory T Cells Suppress Polyclonal T Cell Activation in Vitro by Inhibiting Interleukin 2 Production". In: *The Journal of Experimental Medicine* 188.2 (July 20, 1998), pp. 287–296. ISSN: 0022-1007. DOI: 10.1084/jem.188.2.287. pmid: 9670041.

[58] Yasushi Onishi et al. "Foxp3+ Natural Regulatory T Cells Preferentially Form Aggregates on Dendritic Cells in Vitro and Actively Inhibit Their Maturation". In: *Proceedings of the National Academy of Sciences of the United States of America* 105.29 (July 22, 2008), pp. 10113–10118. ISSN: 1091-6490. DOI: 10.1073/pnas.0711106105. pmid: 18635688.

[59] Cecilia Oderup et al. "Cytotoxic T Lymphocyte Antigen-4-Dependent down-Modulation of Costimulatory Molecules on Dendritic Cells in CD4+ CD25+ Regulatory T-Cell-Mediated Suppression". In: *Immunology* 118.2 (June 2006), pp. 240–249. ISSN: 0019-2805. DOI: 10.1111/j.1365-2567.2006.02362.x. pmid: 16771859.

[60] Omar S. Qureshi et al. "Trans-Endocytosis of CD80 and CD86: A Molecular Basis for the Cell-Extrinsic Function of CTLA-4". In: *Science (New York, N.Y.)* 332.6029 (Apr. 29, 2011), pp. 600–603. ISSN: 1095-9203. DOI: 10.1126/science.1202947. pmid: 21474713.

[61] Ursula Grohmann et al. "CTLA-4-Ig Regulates Tryptophan Catabolism in Vivo". In: *Nature Immunology* 3.11 (Nov. 2002), pp. 1097–1101. ISSN: 1529-2908. DOI: 10.1038/ni846. pmid: 12368911.

[62] Jens Hänig and Manfred B. Lutz. "Suppression of Mature Dendritic Cell Function by Regulatory T Cells in Vivo Is Abrogated by CD40 Licensing". In: *Journal of Immunology (Baltimore, Md.: 1950)* 180.3 (Feb. 1, 2008), pp. 1405–1413. ISSN: 0022-1767. DOI: 10.4049/jimmunol.180.3.1405. pmid: 18209035.

[63] *A20 Is an Antigen Presentation Attenuator, and Its Inhibition Overcomes Regulatory T Cell–Mediated Suppression | Nature Medicine.* URL: https://www-nature-com.gate2.inist.fr/articles/nm1721 (visited on 08/26/2019).

[64] Milka Sarris et al. "Neuropilin-1 Expression on Regulatory T Cells Enhances Their Interactions with Dendritic Cells during Antigen Recognition". In: *Immunity* 28.3 (Mar. 2008), pp. 402–413. ISSN: 1097-4180. DOI: 10.1016/j.immuni.2008.01.012. pmid: 18328743.

[65] Youg Raj Thaker et al. "Treg-Specific LAG3 Deletion Reveals a Key Role for LAG3 in Regulatory T Cells to Inhibit CNS Autoimmunity". In: *The Journal of Immunology* 200 (1 Supplement May 1, 2018), pp. 101.7–101.7. ISSN: 0022-1767, 1550-6606. URL: https://www.jimmunol.org/content/200/1_Supplement/101.7 (visited on 10/29/2019).

[66] Clare Baecher-Allan, Elizabeth Wolf, and David A. Hafler. "MHC Class II Expression Identifies Functionally Distinct Human Regulatory T Cells". In: *Journal of Immunology (Baltimore, Md.: 1950)* 176.8 (Apr. 15, 2006), pp. 4622–4631. ISSN: 0022-1767. DOI: 10.4049/jimmunol.176.8.4622. pmid: 16585553.

[67] *Foxp3+ T Cells Induce Perforin-Dependent Dendritic Cell Death in Tumor-Draining Lymph Nodes - ScienceDirect*. URL: `https://www.sciencedirect.com/science/article/pii/S1074761310000397` (visited on 08/26/2019).

[68] Sadna Budhu et al. "Blockade of Surface-Bound TGF-β on Regulatory T Cells Abrogates Suppression of Effector T Cell Function in the Tumor Microenvironment". In: *Science Signaling* 10.494 (Aug. 29, 2017). ISSN: 1937-9145. DOI: `10.1126/scisignal.aak9702`. pmid: 28851824.

[69] Erica G. Schmitt et al. "IL-10 Produced by Induced Regulatory T Cells (iTregs) Controls Colitis and Pathogenic Ex-iTregs during Immunotherapy". In: *Journal of Immunology (Baltimore, Md.: 1950)* 189.12 (Dec. 15, 2012), pp. 5638–5648. ISSN: 1550-6606. DOI: `10.4049/jimmunol.1200936`. pmid: 23125413.

[70] Yuri P. Rubtsov et al. "Regulatory T Cell-Derived Interleukin-10 Limits Inflammation at Environmental Interfaces". In: *Immunity* 28.4 (Apr. 2008), pp. 546–558. ISSN: 1097-4180. DOI: `10.1016/j.immuni.2008.02.017`. pmid: 18387831.

[71] Lauren W. Collison et al. "The Inhibitory Cytokine IL-35 Contributes to Regulatory T-Cell Function". In: *Nature* 450.7169 (Nov. 22, 2007), pp. 566–569. ISSN: 1476-4687. DOI: `10.1038/nature06306`. pmid: 18033300.

[72] Pushpa Pandiyan et al. "CD4+CD25+Foxp3+ Regulatory T Cells Induce Cytokine Deprivation-Mediated Apoptosis of Effector CD4+ T Cells". In: *Nature Immunology* 8.12 (Dec. 2007), pp. 1353–1362. ISSN: 1529-2916. DOI: `10.1038/ni1536`. pmid: 17982458.

[73] Mitsuhiro Kanamori et al. "Induced Regulatory T Cells: Their Development, Stability, and Applications". In: *Trends in Immunology* 37.11 (Nov. 2016), pp. 803–811. ISSN: 1471-4981. DOI: `10.1016/j.it.2016.08.012`. pmid: 27623114.

[74] Tomohito Takimoto et al. "Smad2 and Smad3 Are Redundantly Essential for the TGF-Beta-Mediated Regulation of Regulatory T Plasticity and Th1 Development". In: *Journal of Immunology (Baltimore, Md.: 1950)* 185.2 (July 15, 2010), pp. 842–855. ISSN: 1550-6606. DOI: `10.4049/jimmunol.0904100`. pmid: 20548029.

[75] Janine L. Coombes et al. "A Functionally Specialized Population of Mucosal CD103+ DCs Induces Foxp3+ Regulatory T Cells via a TGF-Beta and Retinoic Acid-Dependent Mechanism". In: *The Journal of Experimental Medicine* 204.8 (Aug. 6, 2007), pp. 1757–1764. ISSN: 0022-1007. DOI: `10.1084/jem.20070590`. pmid: 17620361.

[76] Patrick M. Smith et al. "The Microbial Metabolites, Short-Chain Fatty Acids, Regulate Colonic Treg Cell Homeostasis". In: *Science (New York, N.Y.)* 341.6145 (Aug. 2, 2013), pp. 569–573. ISSN: 1095-9203. DOI: `10.1126/science.1241165`. pmid: 23828891.

[77] Naganari Ohkura et al. "T Cell Receptor Stimulation-Induced Epigenetic Changes and Foxp3 Expression Are Independent and Complementary Events Required for Treg Cell Development". In: *Immunity* 37.5 (Nov. 16, 2012), pp. 785–799. ISSN: 1097-4180. DOI: `10.1016/j.immuni.2012.09.010`. pmid: 23123060.

[78] Robert Hilbrands et al. "Induced Foxp3(+) T Cells Colonizing Tolerated Allografts Exhibit the Hypomethylation Pattern Typical of Mature Regulatory T Cells". In: *Frontiers in Immunology* 7 (2016), p. 124. ISSN: 1664-3224. DOI: `10.3389/fimmu.2016.00124`. pmid: 27148253.

[79] Xiaojing Yue et al. "Control of Foxp3 Stability through Modulation of TET Activity". In: *The Journal of Experimental Medicine* 213.3 (Mar. 7, 2016), pp. 377–397. ISSN: 1540-9538. DOI: `10.1084/jem.20151438`. pmid: 26903244.

[80] Manuela Battaglia et al. "Tr1 Cells: From Discovery to Their Clinical Application". In: *Seminars in Immunology* 18.2 (Apr. 2006), pp. 120–127. ISSN: 1044-5323. DOI: 10.1016/j.smim.2006.01.007. pmid: 16464609.

[81] Richard A. Peterson. "Regulatory T-Cells: Diverse Phenotypes Integral to Immune Homeostasis and Suppression". In: *Toxicologic Pathology* 40.2 (2012), pp. 186–204. ISSN: 1533-1601. DOI: 10.1177/0192623311430693. pmid: 22222887.

[82] Hye-Jung Kim and Harvey Cantor. "Regulation of Self-Tolerance by Qa-1-Restricted CD8(+) Regulatory T Cells". In: *Seminars in Immunology* 23.6 (Dec. 2011), pp. 446–452. ISSN: 1096-3618. DOI: 10.1016/j.smim.2011.06.001. pmid: 22136694.

[83] Ann J. Ligocki and Jerry Y. Niederkorn. "Advances on Non-CD4 + Foxp3+ T Regulatory Cells: CD8+, Type 1, and Double Negative T Regulatory Cells in Organ Transplantation". In: *Transplantation* 99.8 (Aug. 2015), pp. 1553–1559. ISSN: 1534-6080. DOI: 10.1097/TP.0000000000000813. pmid: 26193065.

[84] Z. X. Zhang et al. "Identification of a Previously Unknown Antigen-Specific Regulatory T Cell and Its Mechanism of Suppression". In: *Nature Medicine* 6.7 (July 2000), pp. 782–789. ISSN: 1078-8956. DOI: 10.1038/77513. pmid: 10888927.

[85] Adrian Hayday and Robert Tigelaar. "Immunoregulation in the Tissues by Gammadelta T Cells". In: *Nature Reviews. Immunology* 3.3 (Mar. 2003), pp. 233–242. ISSN: 1474-1733. DOI: 10.1038/nri1030. pmid: 12658271.

[86] Sally Huber, Cuixia Shi, and Ralph C. Budd. "Gammadelta T Cells Promote a Th1 Response during Coxsackievirus B3 Infection in Vivo: Role of Fas and Fas Ligand". In: *Journal of Virology* 76.13 (July 2002), pp. 6487–6494. ISSN: 0022-538X. DOI: 10.1128/jvi.76.13.6487-6494.2002. pmid: 12050361.

[87] M. S. Vincent et al. "Apoptosis of Fashigh CD4+ Synovial T Cells by Borrelia-Reactive Fas-Ligand(High) Gamma Delta T Cells in Lyme Arthritis". In: *The Journal of Experimental Medicine* 184.6 (Dec. 1, 1996), pp. 2109–2117. ISSN: 0022-1007. DOI: 10.1084/jem.184.6.2109. pmid: 8976167.

[88] C. M. Rudin, P. Engler, and U. Storb. "Differential Splicing of Thymosin Beta 4 mRNA". In: *Journal of Immunology (Baltimore, Md.: 1950)* 144.12 (June 15, 1990), pp. 4857–4862. ISSN: 0022-1767. pmid: 2351831.

[89] Michael Girardi et al. "Anti-Inflammatory Effects in the Skin of Thymosin-Beta4 Splice-Variants". In: *Immunology* 109.1 (May 2003), pp. 1–7. ISSN: 0019-2805. DOI: 10.1046/j.1365-2567.2003.01616.x. pmid: 12709011.

[90] M. Terabe et al. "NKT Cell-Mediated Repression of Tumor Immunosurveillance by IL-13 and the IL-4R-STAT6 Pathway". In: *Nature Immunology* 1.6 (Dec. 2000), pp. 515–520. ISSN: 1529-2908. DOI: 10.1038/82771. pmid: 11101874.

[91] S. Brian Wilson and Terry L. Delovitch. "Janus-like Role of Regulatory iNKT Cells in Autoimmune Disease and Tumour Immunity". In: *Nature Reviews. Immunology* 3.3 (Mar. 2003), pp. 211–222. ISSN: 1474-1733. DOI: 10.1038/nri1028. pmid: 12658269.

[92] Jamie Rossjohn et al. "Recognition of CD1d-Restricted Antigens by Natural Killer T Cells". In: *Nature Reviews. Immunology* 12.12 (Dec. 2012), pp. 845–857. ISSN: 1474-1741. DOI: 10.1038/nri3328. pmid: 23154222.

[93] Dale I. Godfrey and Mitchell Kronenberg. "Going Both Ways: Immune Regulation via CD1d-Dependent NKT Cells". In: *The Journal of Clinical Investigation* 114.10 (Nov. 2004), pp. 1379–1388. ISSN: 0021-9738. DOI: 10.1172/JCI23594. pmid: 15545985.

[94] Peter T. Lee et al. "Distinct Functional Lineages of Human V(Alpha)24 Natural Killer T Cells". In: *The Journal of Experimental Medicine* 195.5 (Mar. 4, 2002), pp. 637–641. ISSN: 0022-1007. DOI: 10.1084/jem.20011908. pmid: 11877486.

[95] David Masopust et al. "Activated Primary and Memory CD8 T Cells Migrate to Nonlymphoid Tissues Regardless of Site of Activation or Tissue of Origin". In: *The Journal of Immunology* 172.8 (Apr. 15, 2004), pp. 4875–4882. ISSN: 0022-1767, 1550-6606. DOI: 10.4049/jimmunol.172.8.4875. pmid: 15067066. URL: https://www.jimmunol.org/content/172/8/4875 (visited on 09/06/2019).

[96] Haoyu Sun et al. "Tissue-Resident Lymphocytes: From Adaptive to Innate Immunity". In: *Cellular & Molecular Immunology* 16.3 (Mar. 2019), pp. 205–215. ISSN: 2042-0226. DOI: 10.1038/s41423-018-0192-y. URL: https://www-nature-com.gate2.inist.fr/articles/s41423-018-0192-y (visited on 08/09/2019).

[97] C. R. Mackay et al. "Lymphocyte Subsets Show Marked Differences in Their Distribution between Blood and the Afferent and Efferent Lymph of Peripheral Lymph Nodes." In: *Journal of Experimental Medicine* 167.6 (June 1, 1988), pp. 1755–1765. ISSN: 0022-1007, 1540-9538. DOI: 10.1084/jem.167.6.1755. pmid: 3290379. URL: http://jem.rupress.org/content/167/6/1755 (visited on 09/20/2019).

[98] R. C. Fuhlbrigge et al. "Cutaneous Lymphocyte Antigen Is a Specialized Form of PSGL-1 Expressed on Skin-Homing T Cells". In: *Nature* 389.6654 (Oct. 30, 1997), pp. 978–981. ISSN: 0028-0836. DOI: 10.1038/40166. pmid: 9353122.

[99] C. Berlin et al. "Alpha 4 Beta 7 Integrin Mediates Lymphocyte Binding to the Mucosal Vascular Addressin MAdCAM-1". In: *Cell* 74.1 (July 16, 1993), pp. 185–195. ISSN: 0092-8674. DOI: 10.1016/0092-8674(93)90305-a. pmid: 7687523.

[100] W. Michael Gallatin, Irving L. Weissman, and Eugene C. Butcher. "A Cell-Surface Molecule Involved in Organ-Specific Homing of Lymphocytes". In: *Nature* 304.5921 (July 1983), pp. 30–34. ISSN: 1476-4687. DOI: 10.1038/304030a0. URL: https://www.nature.com/articles/304030a0 (visited on 09/20/2019).

[101] R. Förster et al. "CCR7 Coordinates the Primary Immune Response by Establishing Functional Microenvironments in Secondary Lymphoid Organs". In: *Cell* 99.1 (Oct. 1, 1999), pp. 23–33. ISSN: 0092-8674. DOI: 10.1016/s0092-8674(00)80059-8. pmid: 10520991.

[102] Haina Shin and Akiko Iwasaki. "Tissue-Resident Memory T Cells". In: *Immunological Reviews* 255.1 (2013), pp. 165–181. ISSN: 1600-065X. DOI: 10.1111/imr.12087. URL: http://onlinelibrary.wiley.com/doi/abs/10.1111/imr.12087 (visited on 09/21/2019).

[103] Kimberly D. Klonowski et al. "Dynamics of Blood-Borne CD8 Memory T Cell Migration in Vivo". In: *Immunity* 20.5 (May 2004), pp. 551–562. ISSN: 1074-7613. DOI: 10.1016/s1074-7613(04)00103-7. pmid: 15142524.

[104] Laura K. Mackay et al. "Long-Lived Epithelial Immunity by Tissue-Resident Memory T (TRM) Cells in the Absence of Persisting Local Antigen Presentation". In: *Proceedings of the National Academy of Sciences of the United States of America* 109.18 (May 1, 2012), pp. 7037–7042. ISSN: 1091-6490. DOI: 10.1073/pnas.1202288109. pmid: 22509047.

[105] Taheri Sathaliyawala et al. "Distribution and Compartmentalization of Human Circulating and Tissue-Resident Memory T Cell Subsets". In: *Immunity* 38.1 (Jan. 24, 2013), pp. 187–197. ISSN: 1097-4180. DOI: 10.1016/j.immuni.2012.09.020. pmid: 23260195.

[106] M. Zeitz et al. "Lymphocytes Isolated from the Intestinal Lamina Propria of Normal Non-human Primates Have Increased Expression of Genes Associated with T-Cell Activation". In: *Gastroenterology* 94.3 (Mar. 1988), pp. 647–655. ISSN: 0016-5085. DOI: 10.1016/0016-5085(88)90235-1. pmid: 3123303.

[107] J. C. Finerty. "Parabiosis in Physiological Studies". In: *Physiological Reviews* 32.3 (July 1952), pp. 277–302. ISSN: 0031-9333. DOI: 10.1152/physrev.1952.32.3.277. pmid: 12983225.

[108] Rachael A. Clark et al. "The Vast Majority of CLA+ T Cells Are Resident in Normal Skin". In: *Journal of Immunology (Baltimore, Md.: 1950)* 176.7 (Apr. 1, 2006), pp. 4431–4439. ISSN: 0022-1767. DOI: 10.4049/jimmunol.176.7.4431. pmid: 16547281.

[109] Kristin G. Anderson et al. "Intravascular Staining for Discrimination of Vascular and Tissue Leukocytes". In: *Nature Protocols* 9.1 (Jan. 2014), pp. 209–222. ISSN: 1750-2799. DOI: 10.1038/nprot.2014.005. pmid: 24385150.

[110] David Masopust and Andrew G. Soerens. "Tissue-Resident T Cells and Other Resident Leukocytes". In: *Annual Review of Immunology* 37 (Apr. 26, 2019), pp. 521–546. ISSN: 1545-3278. DOI: 10.1146/annurev-immunol-042617-053214. pmid: 30726153.

[111] Adrian Liston and Daniel H. D. Gray. "Homeostatic Control of Regulatory T Cell Diversity". In: *Nature Reviews. Immunology* 14.3 (Mar. 2014), pp. 154–165. ISSN: 1474-1741. DOI: 10.1038/nri3605. pmid: 24481337.

[112] Daniela Cipolletta. "Adipose Tissue-Resident Regulatory T Cells: Phenotypic Specialization, Functions and Therapeutic Potential". In: *Immunology* 142.4 (2014), pp. 517–525. ISSN: 1365-2567. DOI: 10.1111/imm.12262. URL: https://onlinelibrary.wiley.com/doi/abs/10.1111/imm.12262 (visited on 02/05/2019).

[113] Nicholas Arpaia et al. "A Distinct Function of Regulatory T Cells in Tissue Protection". In: *Cell* 162.5 (Aug. 27, 2015), pp. 1078–1089. ISSN: 0092-8674. DOI: 10.1016/j.cell.2015.08.021. URL: http://www.sciencedirect.com/science/article/pii/S009286741501034X (visited on 02/05/2019).

[114] Dalia Burzyn et al. "A Special Population of Regulatory T Cells Potentiates Muscle Repair". In: *Cell* 155.6 (Dec. 5, 2013), pp. 1282–1295. ISSN: 0092-8674. DOI: 10.1016/j.cell.2013.10.054. URL: http://www.sciencedirect.com/science/article/pii/S009286741301413X (visited on 09/23/2019).

[115] Chien-Chang Chen et al. "IL-33 Dysregulates Regulatory T (Treg) Cells and Impairs Established Immunological Tolerance in the Lungs". In: *The Journal of allergy and clinical immunology* 140.5 (Nov. 2017), 1351–1363.e7. ISSN: 0091-6749. DOI: 10.1016/j.jaci.2017.01.015. pmid: 28196763. URL: https://www.ncbi.nlm.nih.gov/pmc/articles/PMC5554091/ (visited on 09/25/2019).

[116] Nidhi Malhotra et al. "RORα-Expressing T Regulatory Cells Restrain Allergic Skin Inflammation". In: *Science Immunology* 3.21 (Feb. 3, 2018). ISSN: 2470-9468. DOI: 10.1126/sciimmunol.aao6923. pmid: 29500225.

[117] John T. Chang, E. John Wherry, and Ananda W. Goldrath. "Molecular Regulation of Effector and Memory T Cell Differentiation". In: *Nature Immunology* 15.12 (Dec. 2014), pp. 1104–1115. ISSN: 1529-2916. DOI: 10.1038/ni.3031. pmid: 25396352.

[118] Marisella Panduro, Christophe Benoist, and Diane Mathis. "Tissue Tregs". In: *Annual Review of Immunology* 34 (May 20, 2016), pp. 609–633. ISSN: 1545-3278. DOI: 10.1146/annurev-immunol-032712-095948. pmid: 27168246.

[119] Angelina M. Bilate et al. "Tissue-Specific Emergence of Regulatory and Intraepithelial T Cells from a Clonal T Cell Precursor". In: *Science Immunology* 1.2 (Aug. 26, 2016), eaaf7471. ISSN: 2470-9468. DOI: 10.1126/sciimmunol.aaf7471. pmid: 28783695.

[120] Joanna R DiSpirito et al. "Molecular Diversification of Regulatory T Cells in Nonlymphoid Tissues". In: *SCIENCE IMMUNOLOGY* (2018), p. 16.

[121] Michael Delacher et al. "Genome-Wide DNA-Methylation Landscape Defines Specialization of Regulatory T Cells in Tissues". In: *Nature Immunology* 18.10 (Oct. 2017), pp. 1160–1172. ISSN: 1529-2916. DOI: 10.1038/ni.3799. pmid: 28783152.

[122] Yonit Lavin et al. "Tissue-Resident Macrophage Enhancer Landscapes Are Shaped by the Local Microenvironment". In: *Cell* 159.6 (Dec. 4, 2014), pp. 1312–1326. ISSN: 1097-4172. DOI: 10.1016/j.cell.2014.11.018. pmid: 25480296.

[123] Dmitriy Kolodin et al. "Antigen- and Cytokine-Driven Accumulation of Regulatory T Cells in Visceral Adipose Tissue of Lean Mice". In: *Cell Metabolism* 21.4 (Apr. 7, 2015), pp. 543–557. ISSN: 1932-7420. DOI: 10.1016/j.cmet.2015.03.005. pmid: 25863247.

[124] Ajithkumar Vasanthakumar et al. "The Transcriptional Regulators IRF4, BATF and IL-33 Orchestrate Development and Maintenance of Adipose Tissue-Resident Regulatory T Cells". In: *Nature Immunology* 16.3 (Mar. 2015), pp. 276–285. ISSN: 1529-2916. DOI: 10.1038/ni.3085. pmid: 25599561.

[125] Daniela Cipolletta et al. "PPAR-γ Is a Major Driver of the Accumulation and Phenotype of Adipose Tissue Treg Cells". In: *Nature* 486.7404 (June 28, 2012), pp. 549–553. ISSN: 1476-4687. DOI: 10.1038/nature11132. pmid: 22722857.

[126] Daniela Cipolletta et al. "Appearance and Disappearance of the mRNA Signature Characteristic of Treg Cells in Visceral Adipose Tissue: Age, Diet, and PPARγ Effects". In: *Proceedings of the National Academy of Sciences of the United States of America* 112.2 (Jan. 13, 2015), pp. 482–487. ISSN: 1091-6490. DOI: 10.1073/pnas.1423486112. pmid: 25550516.

[127] Markus Feuerer et al. "Lean, but Not Obese, Fat Is Enriched for a Unique Population of Regulatory T Cells That Affect Metabolic Parameters". In: *Nature Medicine* 15.8 (Aug. 2009), pp. 930–939. ISSN: 1546-170X. DOI: 10.1038/nm.2002. pmid: 19633656.

[128] Saul J. Priceman et al. "Regulation of Adipose Tissue T Cell Subsets by Stat3 Is Crucial for Diet-Induced Obesity and Insulin Resistance". In: *Proceedings of the National Academy of Sciences of the United States of America* 110.32 (Aug. 6, 2013), pp. 13079–13084. ISSN: 1091-6490. DOI: 10.1073/pnas.1311557110. pmid: 23878227.

[129] Marta Fabrizi et al. "IL-21 Is a Major Negative Regulator of IRF4-Dependent Lipolysis Affecting Tregs in Adipose Tissue and Systemic Insulin Sensitivity". In: *Diabetes* 63.6 (June 2014), pp. 2086–2096. ISSN: 1939-327X. DOI: 10.2337/db13-0939. pmid: 24430438.

[130] Jeffrey Deiuliis et al. "Visceral Adipose Inflammation in Obesity Is Associated with Critical Alterations in Tregulatory Cell Numbers". In: *PloS One* 6.1 (Jan. 26, 2011), e16376. ISSN: 1932-6203. DOI: 10.1371/journal.pone.0016376. pmid: 21298111.

[131] Alexander S. Banks et al. "An ERK/Cdk5 Axis Controls the Diabetogenic Actions of PPARγ". In: *Nature* 517.7534 (Jan. 15, 2015), pp. 391–395. ISSN: 1476-4687. DOI: 10.1038/nature13887. pmid: 25409143.

[132] Jang Hyun Choi et al. "Antidiabetic Actions of a Non-Agonist PPARγ Ligand Blocking Cdk5-Mediated Phosphorylation". In: *Nature* 477.7365 (Sept. 4, 2011), pp. 477–481. ISSN: 1476-4687. DOI: 10.1038/nature10383. pmid: 21892191.

[133] Jang Hyun Choi et al. "Anti-Diabetic Drugs Inhibit Obesity-Linked Phosphorylation of PPARgamma by Cdk5". In: *Nature* 466.7305 (July 22, 2010), pp. 451–456. ISSN: 1476-4687. DOI: 10.1038/nature09291. pmid: 20651683.

[134] S. Armando Villalta et al. "Regulatory T Cells Suppress Muscle Inflammation and Injury in Muscular Dystrophy". In: *Science Translational Medicine* 6.258 (Oct. 15, 2014), 258ra142–258ra142. ISSN: 1946-6234, 1946-6242. DOI: 10.1126/scitranslmed.3009925. pmid: 25320234. URL: http://stm.sciencemag.org/content/6/258/258ra142 (visited on 09/23/2019).

[135] S. Armando Villalta et al. "Interleukin-10 Reduces the Pathology of Mdx Muscular Dystrophy by Deactivating M1 Macrophages and Modulating Macrophage Phenotype". In: *Human Molecular Genetics* 20.4 (Feb. 15, 2011), pp. 790–805. ISSN: 1460-2083. DOI: 10.1093/hmg/ddq523. pmid: 21118895.

[136] Y. C. Jang et al. "Skeletal Muscle Stem Cells: Effects of Aging and Metabolism on Muscle Regenerative Function". In: *Cold Spring Harbor Symposia on Quantitative Biology* 76 (2011), pp. 101–111. ISSN: 1943-4456. DOI: 10.1101/sqb.2011.76.010652. pmid: 21960527.

[137] M. A. Rudnicki et al. "The Molecular Regulation of Muscle Stem Cell Function". In: *Cold Spring Harbor Symposia on Quantitative Biology* 73 (2008), pp. 323–331. ISSN: 1943-4456. DOI: 10.1101/sqb.2008.73.064. pmid: 19329572.

[138] Mohammadsharif Tabebordbar, Eric T. Wang, and Amy J. Wagers. "Skeletal Muscle Degenerative Diseases and Strategies for Therapeutic Muscle Repair". In: *Annual Review of Pathology* 8 (Jan. 24, 2013), pp. 441–475. ISSN: 1553-4014. DOI: 10.1146/annurev-pathol-011811-132450. pmid: 23121053.

[139] Lidia Bosurgi, Angelo A. Manfredi, and Patrizia Rovere-Querini. "Macrophages in Injured Skeletal Muscle: A Perpetuum Mobile Causing and Limiting Fibrosis, Prompting or Restricting Resolution and Regeneration". In: *Frontiers in Immunology* 2 (2011), p. 62. ISSN: 1664-3224. DOI: 10.3389/fimmu.2011.00062. pmid: 22566851.

[140] Daniela Ruffell et al. "A CREB-C/EBPbeta Cascade Induces M2 Macrophage-Specific Gene Expression and Promotes Muscle Injury Repair". In: *Proceedings of the National Academy of Sciences of the United States of America* 106.41 (Oct. 13, 2009), pp. 17475–17480. ISSN: 1091-6490. DOI: 10.1073/pnas.0908641106. pmid: 19805133.

[141] Markus B. Geuking et al. "Intestinal Bacterial Colonization Induces Mutualistic Regulatory T Cell Responses". In: *Immunity* 34.5 (May 27, 2011), pp. 794–806. ISSN: 1097-4180. DOI: 10.1016/j.immuni.2011.03.021. pmid: 21596591.

[142] Koji Atarashi et al. "Induction of Colonic Regulatory T Cells by Indigenous Clostridium Species". In: *Science (New York, N.Y.)* 331.6015 (Jan. 21, 2011), pp. 337–341. ISSN: 1095-9203. DOI: 10.1126/science.1198469. pmid: 21205640.

[143] Allan M. Mowat and William W. Agace. "Regional Specialization within the Intestinal Immune System". In: *Nature Reviews. Immunology* 14.10 (Oct. 2014), pp. 667–685. ISSN: 1474-1741. DOI: 10.1038/nri3738. pmid: 25234148.

[144] Niwa Ali and Michael D. Rosenblum. "Regulatory T Cells in Skin". In: *Immunology* 152.3 (Nov. 2017), pp. 372–381. ISSN: 1365-2567. DOI: 10.1111/imm.12791. pmid: 28699278.

[145] Caspar Ohnmacht et al. "MUCOSAL IMMUNOLOGY. The Microbiota Regulates Type 2 Immunity through RORγt$^+$ T Cells". In: *Science (New York, N.Y.)* 349.6251 (Aug. 28, 2015), pp. 989–993. ISSN: 1095-9203. DOI: 10.1126/science.aac4263. pmid: 26160380.

[146]   Ahmed N. Hegazy and Fiona Powrie. "MICROBIOME. Microbiota RORgulates Intestinal
         Suppressor T Cells". In: *Science (New York, N.Y.)* 349.6251 (Aug. 28, 2015), pp. 929–930.
         ISSN: 1095-9203. DOI: 10.1126/science.aad0865. pmid: 26315421.

[147]   Esen Sefik et al. "MUCOSAL IMMUNOLOGY. Individual Intestinal Symbionts Induce a Distinct
         Population of RORγ$^+$ Regulatory T Cells". In: *Science (New York, N.Y.)* 349.6251 (Aug. 28,
         2015), pp. 993–997. ISSN: 1095-9203. DOI: 10.1126/science.aaa9420. pmid: 26272906.

[148]   Chris Schiering et al. "The Alarmin IL-33 Promotes Regulatory T-Cell Function in the Intes-
         tine". In: *Nature* 513.7519 (Sept. 25, 2014), pp. 564–568. ISSN: 1476-4687. DOI: 10.1038/
         nature13577. pmid: 25043027.

[149]   Steven Z. Josefowicz et al. "Extrathymically Generated Regulatory T Cells Control Mucosal
         TH2 Inflammation". In: *Nature* 482.7385 (Feb. 8, 2012), pp. 395–399. ISSN: 1476-4687. DOI:
         10.1038/nature10772. pmid: 22318520.

[150]   Tiffany C. Scharschmidt et al. "A Wave of Regulatory T Cells into Neonatal Skin Mediates
         Tolerance to Commensal Microbes". In: *Immunity* 43.5 (Nov. 17, 2015), pp. 1011–1021. ISSN:
         1097-4180. DOI: 10.1016/j.immuni.2015.10.016. pmid: 26588783.

[151]   Siyoung Yang et al. "Immune Tolerance. Regulatory T Cells Generated Early in Life Play a
         Distinct Role in Maintaining Self-Tolerance". In: *Science (New York, N.Y.)* 348.6234 (May 1,
         2015), pp. 589–594. ISSN: 1095-9203. DOI: 10.1126/science.aaa7017. pmid: 25791085.

[152]   Blythe D. Sather et al. "Altering the Distribution of Foxp3(+) Regulatory T Cells Results
         in Tissue-Specific Inflammatory Disease". In: *The Journal of Experimental Medicine* 204.6
         (June 11, 2007), pp. 1335–1347. ISSN: 0022-1007. DOI: 10.1084/jem.20070081. pmid:
         17548521.

[153]   J. J. Campbell et al. "The Chemokine Receptor CCR4 in Vascular Recognition by Cutaneous
         but Not Intestinal Memory T Cells". In: *Nature* 400.6746 (Aug. 19, 1999), pp. 776–780. ISSN:
         0028-0836. DOI: 10.1038/23495. pmid: 10466728.

[154]   Judith Alferink et al. "Compartmentalized Production of CCL17 in Vivo: Strong Inducibility in
         Peripheral Dendritic Cells Contrasts Selective Absence from the Spleen". In: *The Journal of
         Experimental Medicine* 197.5 (Mar. 3, 2003), pp. 585–599. ISSN: 0022-1007. DOI: 10.1084/
         jem.20021859. pmid: 12615900.

[155]   I. Lieberam and I. Förster. "The Murine Beta-Chemokine TARC Is Expressed by Subsets of
         Dendritic Cells and Attracts Primed CD4+ T Cells". In: *European Journal of Immunology* 29.9
         (Sept. 1999), pp. 2684–2694. ISSN: 0014-2980. DOI: 10.1002/(SICI)1521-4141(199909)29:
         09<2684::AID-IMMU2684>3.0.CO;2-Y. pmid: 10508243.

[156]   Sayuri Yamazaki et al. "Homeostasis of Thymus-Derived Foxp3+ Regulatory T Cells Is
         Controlled by Ultraviolet B Exposure in the Skin". In: *Journal of Immunology (Baltimore, Md.:
         1950)* 193.11 (Dec. 1, 2014), pp. 5488–5497. ISSN: 1550-6606. DOI: 10.4049/jimmunol.
         1400985. pmid: 25348622.

[157]   Elizabeth A. Wohlfert et al. "GATA3 Controls Foxp3$^+$ Regulatory T Cell Fate during Inflam-
         mation in Mice". In: *The Journal of Clinical Investigation* 121.11 (Nov. 2011), pp. 4503–4515.
         ISSN: 1558-8238. DOI: 10.1172/JCI57456. pmid: 21965331.

[158]   Oliver J. Harrison et al. "Commensal-Specific T Cell Plasticity Promotes Rapid Tissue Adapta-
         tion to Injury". In: *Science (New York, N.Y.)* 363.6422 (Apr. 1, 2019). ISSN: 1095-9203. DOI:
         10.1126/science.aat6280. pmid: 30523076.

[159]   Audrey Nosbaum et al. "Cutting Edge: Regulatory T Cells Facilitate Cutaneous Wound Healing".
         In: *Journal of Immunology (Baltimore, Md.: 1950)* 196.5 (Mar. 1, 2016), pp. 2010–2014. ISSN:
         1550-6606. DOI: 10.4049/jimmunol.1502139. pmid: 26826250.

[160] Niwa Ali et al. "Regulatory T Cells in Skin Facilitate Epithelial Stem Cell Differentiation". In: *Cell* 169.6 (June 1, 2017), 1119–1129.e11. ISSN: 1097-4172. DOI: 10.1016/j.cell.2017.05.002. pmid: 28552347.

[161] Natasha Whibley, Andrea Tucci, and Fiona Powrie. "Regulatory T Cell Adaptation in the Intestine and Skin". In: *Nature Immunology* 20.4 (Apr. 2019), pp. 386–396. ISSN: 1529-2916. DOI: 10.1038/s41590-019-0351-z. pmid: 30890797.

[162] W. Tietz et al. "CD4+ T Cells Migrate into Inflamed Skin Only If They Express Ligands for E- and P-Selectin". In: *Journal of Immunology (Baltimore, Md.: 1950)* 161.2 (July 15, 1998), pp. 963–970. ISSN: 0022-1767. pmid: 9670976.

[163] Bart N Lambrecht and Hamida Hammad. "The Immunology of Asthma". In: *Nature Immunology* 16.1 (Jan. 2015), pp. 45–56. ISSN: 1529-2908, 1529-2916. DOI: 10.1038/ni.3049. URL: http://www.nature.com/articles/ni.3049 (visited on 06/16/2019).

[164] Gary P. Anderson. "Endotyping Asthma: New Insights into Key Pathogenic Mechanisms in a Complex, Heterogeneous Disease". In: *Lancet (London, England)* 372.9643 (Sept. 20, 2008), pp. 1107–1119. ISSN: 1474-547X. DOI: 10.1016/S0140-6736(08)61452-X. pmid: 18805339.

[165] J. G. De Monchy et al. "Bronchoalveolar Eosinophilia during Allergen-Induced Late Asthmatic Reactions". In: *The American Review of Respiratory Disease* 131.3 (Mar. 1985), pp. 373–376. ISSN: 0003-0805. DOI: 10.1164/arrd.1985.131.3.373. pmid: 3977174.

[166] M. Humbert et al. "IL-4 and IL-5 mRNA and Protein in Bronchial Biopsies from Patients with Atopic and Nonatopic Asthma: Evidence against "Intrinsic" Asthma Being a Distinct Immunopathologic Entity". In: *American Journal of Respiratory and Critical Care Medicine* 154.5 (Nov. 1996), pp. 1497–1504. ISSN: 1073-449X. DOI: 10.1164/ajrccm.154.5.8912771. pmid: 8912771.

[167] A. M. Bentley et al. "Activated T-Lymphocytes and Eosinophils in the Bronchial Mucosa in Isocyanate-Induced Asthma". In: *The Journal of Allergy and Clinical Immunology* 89.4 (Apr. 1992), pp. 821–829. ISSN: 0091-6749. DOI: 10.1016/0091-6749(92)90437-7. pmid: 1532807.

[168] Patrick Flood-Page et al. "Anti-IL-5 Treatment Reduces Deposition of ECM Proteins in the Bronchial Subepithelial Basement Membrane of Mild Atopic Asthmatics". In: *The Journal of Clinical Investigation* 112.7 (Oct. 2003), pp. 1029–1036. ISSN: 0021-9738. DOI: 10.1172/JCI17974. pmid: 14523040.

[169] A. J. Coyle et al. "Cationic Protein-Induced Sensory Nerve Activation: Role of Substance P in Airway Hyperresponsiveness and Plasma Protein Extravasation". In: *The Journal of Clinical Investigation* 94.6 (Dec. 1994), pp. 2301–2306. ISSN: 0021-9738. DOI: 10.1172/JCI117594. pmid: 7527430.

[170] A. J. Coyle et al. "Human Eosinophil-Granule Major Basic Protein and Synthetic Polycations Induce Airway Hyperresponsiveness in Vivo Dependent on Bradykinin Generation". In: *The Journal of Clinical Investigation* 95.4 (Apr. 1995), pp. 1735–1740. ISSN: 0021-9738. DOI: 10.1172/JCI117850. pmid: 7706481.

[171] Derek K. Chu et al. "Indigenous Enteric Eosinophils Control DCs to Initiate a Primary Th2 Immune Response in Vivo". In: *Journal of Experimental Medicine* 211.8 (July 28, 2014), pp. 1657–1672. ISSN: 0022-1007, 1540-9538. DOI: 10.1084/jem.20131800. pmid: 25071163. URL: http://jem.rupress.org/content/211/8/1657 (visited on 10/03/2019).

[172]   Taylor A. Doherty et al. "CD4+ Cells Are Required for Chronic Eosinophilic Lung Inflammation
        but Not Airway Remodeling". In: *American Journal of Physiology. Lung Cellular and Molecular
        Physiology* 296.2 (Feb. 2009), pp. L229–235. ISSN: 1040-0605. DOI: 10.1152/ajplung.
        90543.2008. pmid: 19060225.

[173]   Dae Jin Song et al. "Anti-Siglec-F Antibody Reduces Allergen-Induced Eosinophilic Inflam-
        mation and Airway Remodeling". In: *Journal of Immunology (Baltimore, Md.: 1950)* 183.8
        (Oct. 15, 2009), pp. 5333–5341. ISSN: 1550-6606. DOI: 10.4049/jimmunol.0801421. pmid:
        19783675.

[174]   Ramzi Fattouh et al. "Eosinophils Are Dispensable for Allergic Remodeling and Immunity in a
        Model of House Dust Mite-Induced Airway Disease". In: *American Journal of Respiratory and
        Critical Care Medicine* 183.2 (Jan. 15, 2011), pp. 179–188. ISSN: 1535-4970. DOI: 10.1164/
        rccm.200905-0736OC. pmid: 20732990.

[175]   Marina Ostroukhova et al. "Tolerance Induced by Inhaled Antigen Involves CD4(+) T Cells
        Expressing Membrane-Bound TGF-Beta and FOXP3". In: *The Journal of Clinical Investigation*
        114.1 (July 2004), pp. 28–38. ISSN: 0021-9738. DOI: 10.1172/JCI20509. pmid: 15232609.

[176]   Dominik Hartl et al. "Quantitative and Functional Impairment of Pulmonary CD4+CD25hi
        Regulatory T Cells in Pediatric Asthma". In: *The Journal of Allergy and Clinical Immunology*
        119.5 (May 2007), pp. 1258–1266. ISSN: 0091-6749. DOI: 10.1016/j.jaci.2007.02.023.
        pmid: 17412402.

[177]   Raffi Tachdjian et al. "Pathogenicity of a Disease-Associated Human IL-4 Receptor Allele in
        Experimental Asthma". In: *The Journal of Experimental Medicine* 206.10 (Sept. 28, 2009),
        pp. 2191–2204. ISSN: 1540-9538. DOI: 10.1084/jem.20091480. pmid: 19770271.

[178]   Raffi Tachdjian et al. "In Vivo Regulation of the Allergic Response by the IL-4 Receptor Alpha
        Chain Immunoreceptor Tyrosine-Based Inhibitory Motif". In: *The Journal of Allergy and Clinical
        Immunology* 125.5 (May 2010), 1128–1136.e8. ISSN: 1097-6825. DOI: 10.1016/j.jaci.2010.
        01.054. pmid: 20392476.

[179]   David W. Haslam and W. Philip T. James. "Obesity". In: *The Lancet* 366.9492 (Oct. 1, 2005),
        pp. 1197–1209. ISSN: 0140-6736, 1474-547X. DOI: 10.1016/S0140-6736(05)67483-1. pmid:
        16198769. URL: https://www.thelancet.com/journals/lancet/article/PIIS0140-
        6736(05)67483-1/abstract (visited on 09/30/2019).

[180]   M. Yuan et al. "Reversal of Obesity- and Diet-Induced Insulin Resistance with Salicylates or
        Targeted Disruption of Ikkbeta". In: *Science (New York, N.Y.)* 293.5535 (Aug. 31, 2001),
        pp. 1673–1677. ISSN: 0036-8075. DOI: 10.1126/science.1061620. pmid: 11533494.

[181]   G. S. Hotamisligil, N. S. Shargill, and B. M. Spiegelman. "Adipose Expression of Tumor Necrosis
        Factor-Alpha: Direct Role in Obesity-Linked Insulin Resistance". In: *Science (New York, N.Y.)*
        259.5091 (Jan. 1, 1993), pp. 87–91. ISSN: 0036-8075. DOI: 10.1126/science.7678183.
        pmid: 7678183.

[182]   Jiro Hirosumi et al. "A Central Role for JNK in Obesity and Insulin Resistance". In: *Nature*
        420.6913 (Nov. 21, 2002), pp. 333–336. ISSN: 0028-0836. DOI: 10.1038/nature01137. pmid:
        12447443.

[183]   Stuart P. Weisberg et al. "Obesity Is Associated with Macrophage Accumulation in Adipose
        Tissue". In: *The Journal of Clinical Investigation* 112.12 (Dec. 2003), pp. 1796–1808. ISSN:
        0021-9738. DOI: 10.1172/JCI19246. pmid: 14679176.

[184]   Carey N. Lumeng et al. "Increased Inflammatory Properties of Adipose Tissue Macrophages
        Recruited during Diet-Induced Obesity". In: *Diabetes* 56.1 (Jan. 2007), pp. 16–23. ISSN:
        0012-1797. DOI: 10.2337/db06-1076. pmid: 17192460.

[185] A. D. Pradhan et al. "C-Reactive Protein, Interleukin 6, and Risk of Developing Type 2 Diabetes Mellitus". In: *JAMA* 286.3 (July 18, 2001), pp. 327–334. ISSN: 0098-7484. DOI: 10.1001/jama.286.3.327. pmid: 11466099.

[186] Haitao Wen et al. "Fatty Acid-Induced NLRP3-ASC Inflammasome Activation Interferes with Insulin Signaling". In: *Nature Immunology* 12.5 (May 2011), pp. 408–415. ISSN: 1529-2916. DOI: 10.1038/ni.2022. pmid: 21478880.

[187] Ajay Chawla, Khoa D. Nguyen, and Y. P. Sharon Goh. "Macrophage-Mediated Inflammation in Metabolic Disease". In: *Nature Reviews. Immunology* 11.11 (Oct. 10, 2011), pp. 738–749. ISSN: 1474-1741. DOI: 10.1038/nri3071. pmid: 21984069.

[188] Olivia Osborn and Jerrold M. Olefsky. "The Cellular and Signaling Networks Linking the Immune System and Metabolism in Disease". In: *Nature Medicine* 18.3 (Mar. 6, 2012), pp. 363–374. ISSN: 1546-170X. DOI: 10.1038/nm.2627. pmid: 22395709.

[189] Diane Mathis. "Immunological Goings-on in Visceral Adipose Tissue". In: *Cell Metabolism* 17.6 (June 4, 2013), pp. 851–859. ISSN: 1932-7420. DOI: 10.1016/j.cmet.2013.05.008. pmid: 23747244.

[190] Ting Liu et al. "NF-κB Signaling in Inflammation". In: *Signal Transduction and Targeted Therapy* 2 (July 14, 2017), p. 17023. ISSN: 2095-9907. DOI: 10.1038/sigtrans.2017.23. pmid: 29158945. URL: https://www.ncbi.nlm.nih.gov/pmc/articles/PMC5661633/ (visited on 10/15/2019).

[191] Vered Elgazar-Carmon et al. "Neutrophils Transiently Infiltrate Intra-Abdominal Fat Early in the Course of High-Fat Feeding". In: *Journal of Lipid Research* 49.9 (Sept. 2008), pp. 1894–1903. ISSN: 0022-2275. DOI: 10.1194/jlr.M800132-JLR200. pmid: 18503031.

[192] Saswata Talukdar et al. "Neutrophils Mediate Insulin Resistance in Mice Fed a High-Fat Diet through Secreted Elastase". In: *Nature Medicine* 18.9 (Sept. 2012), pp. 1407–1412. ISSN: 1546-170X. DOI: 10.1038/nm.2885. pmid: 22863787.

[193] Ari B. Molofsky et al. "Innate Lymphoid Type 2 Cells Sustain Visceral Adipose Tissue Eosinophils and Alternatively Activated Macrophages". In: *The Journal of Experimental Medicine* 210.3 (Mar. 11, 2013), pp. 535–549. ISSN: 1540-9538. DOI: 10.1084/jem.20121964. pmid: 23420878.

[194] Davina Wu et al. "Eosinophils Sustain Adipose Alternatively Activated Macrophages Associated with Glucose Homeostasis". In: *Science (New York, N.Y.)* 332.6026 (Apr. 8, 2011), pp. 243–247. ISSN: 1095-9203. DOI: 10.1126/science.1201475. pmid: 21436399.

[195] Roberto R. Ricardo-Gonzalez et al. "IL-4/STAT6 Immune Axis Regulates Peripheral Nutrient Metabolism and Insulin Sensitivity". In: *Proceedings of the National Academy of Sciences of the United States of America* 107.52 (Dec. 28, 2010), pp. 22617–22622. ISSN: 1091-6490. DOI: 10.1073/pnas.1009152108. pmid: 21149710.

[196] S. Caspar-Bauguil et al. "Adipose Tissues as an Ancestral Immune Organ: Site-Specific Change in Obesity". In: *FEBS letters* 579.17 (July 4, 2005), pp. 3487–3492. ISSN: 0014-5793. DOI: 10.1016/j.febslet.2005.05.031. pmid: 15953605.

[197] Satoshi Nishimura et al. "CD8 + Effector T Cells Contribute to Macrophage Recruitment and Adipose Tissue Inflammation in Obesity". In: *Nature Medicine* 15.8 (Aug. 2009), pp. 914–920. ISSN: 1546-170X. DOI: 10.1038/nm.1964. URL: https://www.nature.com/articles/nm.1964 (visited on 10/02/2019).

[198] Xuexian O. Yang et al. "T Helper 17 Lineage Differentiation Is Programmed by Orphan Nuclear Receptors ROR Alpha and ROR Gamma". In: *Immunity* 28.1 (Jan. 2008), pp. 29–39. ISSN: 1074-7613. DOI: 10.1016/j.immuni.2007.11.016. pmid: 18164222.

[199]    Luis A. Zúñiga et al. "IL-17 Regulates Adipogenesis, Glucose Homeostasis, and Obesity". In: *Journal of Immunology (Baltimore, Md.: 1950)* 185.11 (Dec. 1, 2010), pp. 6947–6959. ISSN: 1550-6606. DOI: 10.4049/jimmunol.1001269. pmid: 21037091.

[200]    Xiang Cheng et al. "A Guanidine-Rich Regulatory Oligodeoxynucleotide Improves Type-2 Diabetes in Obese Mice by Blocking T-Cell Differentiation". In: *EMBO molecular medicine* 4.10 (Oct. 2012), pp. 1112–1125. ISSN: 1757-4684. DOI: 10.1002/emmm.201201272. pmid: 23027613.

[201]    Ichiro Misumi et al. "Obesity Expands a Distinct Population of T Cells in Adipose Tissue and Increases Vulnerability to Infection". In: *Cell Reports* 27.2 (Apr. 2019), 514–524.e5. ISSN: 22111247. DOI: 10.1016/j.celrep.2019.03.030. URL: https://linkinghub.elsevier.com/retrieve/pii/S2211124719303468 (visited on 10/02/2019).

[202]    Albert Bendelac, Paul B. Savage, and Luc Teyton. "The Biology of NKT Cells". In: *Annual Review of Immunology* 25 (2007), pp. 297–336. ISSN: 0732-0582. DOI: 10.1146/annurev.immunol.25.022106.141711. pmid: 17150027.

[203]    Lan Wu et al. "Activation of Invariant Natural Killer T Cells by Lipid Excess Promotes Tissue Inflammation, Insulin Resistance, and Hepatic Steatosis in Obese Mice". In: *Proceedings of the National Academy of Sciences of the United States of America* 109.19 (May 8, 2012), E1143–1152. ISSN: 1091-6490. DOI: 10.1073/pnas.1200498109. pmid: 22493234.

[204]    Lan Wu and Luc Van Kaer. "Contribution of Lipid-Reactive Natural Killer T Cells to Obesity-Associated Inflammation and Insulin Resistance". In: *Adipocyte* 2.1 (Jan. 1, 2013), pp. 12–16. ISSN: 2162-3945. DOI: 10.4161/adip.22296. pmid: 23700548.

[205]    Daniel A. Winer et al. "B Cells Promote Insulin Resistance through Modulation of T Cells and Production of Pathogenic IgG Antibodies". In: *Nature Medicine* 17.5 (May 2011), pp. 610–617. ISSN: 1546-170X. DOI: 10.1038/nm.2353. pmid: 21499269.

[206]    A. D. van Dam et al. "IgG Is Elevated in Obese White Adipose Tissue but Does Not Induce Glucose Intolerance via Fcγ-Receptor or Complement". In: *International Journal of Obesity (2005)* 42.2 (Feb. 2018), pp. 260–269. ISSN: 1476-5497. DOI: 10.1038/ijo.2017.209. pmid: 28852207.

[207]    Satoshi Nishimura et al. "Adipose Natural Regulatory B Cells Negatively Control Adipose Tissue Inflammation". In: *Cell Metabolism* 18.5 (Nov. 5, 2013), pp. 759–766. ISSN: 1932-7420. DOI: 10.1016/j.cmet.2013.09.017. pmid: 24209772.

[208]    Xing Zhang et al. "Adipocyte mTORC1 Suppresses Treg Cell Development and Browning of White Adipose Tissue through CRTC2/COX-2/PGs Pathway". In: *Diabetes* 67 (Supplement 1 July 1, 2018), 34–OR. ISSN: 0012-1797, 1939-327X. DOI: 10.2337/db18-34-OR. URL: https://diabetes.diabetesjournals.org/content/67/Supplement_1/34-OR (visited on 10/02/2019).

[209]    Wenshan Wang and Patrick Seale. "Control of Brown and Beige Fat Development". In: *Nature reviews. Molecular cell biology* 17.11 (Nov. 2016), pp. 691–702. ISSN: 1471-0072. DOI: 10.1038/nrm.2016.96. pmid: 27552974. URL: https://www.ncbi.nlm.nih.gov/pmc/articles/PMC5627770/ (visited on 10/29/2019).

[210]    Dasa Medrikova et al. "Brown Adipose Tissue Harbors a Distinct Sub-Population of Regulatory T Cells". In: *PloS One* 10.2 (2015), e0118534. ISSN: 1932-6203. DOI: 10.1371/journal.pone.0118534. pmid: 25714366.

[211]    Ana Izcue, Janine L. Coombes, and Fiona Powrie. "Regulatory Lymphocytes and Intestinal Inflammation". In: *Annual Review of Immunology* 27 (2009), pp. 313–338. ISSN: 0732-0582. DOI: 10.1146/annurev.immunol.021908.132657. pmid: 19302043.

[212]   Judy H. Cho. "The Genetics and Immunopathogenesis of Inflammatory Bowel Disease". In: *Nature Reviews. Immunology* 8.6 (June 2008), pp. 458–466. ISSN: 1474-1741. DOI: 10.1038/nri2340. pmid: 18500230.

[213]   Frank Heller et al. "Oxazolone Colitis, a Th2 Colitis Model Resembling Ulcerative Colitis, Is Mediated by IL-13-Producing NK-T Cells". In: *Immunity* 17.5 (Nov. 2002), pp. 629–638. ISSN: 1074-7613. DOI: 10.1016/s1074-7613(02)00453-3. pmid: 12433369.

[214]   Efstathios Antoniou et al. "The TNBS-Induced Colitis Animal Model: An Overview". In: *Annals of Medicine and Surgery* 11 (Aug. 19, 2016), pp. 9–15. ISSN: 2049-0801. DOI: 10.1016/j.amsu.2016.07.019. pmid: 27656280. URL: https://www.ncbi.nlm.nih.gov/pmc/articles/PMC5021709/ (visited on 10/03/2019).

[215]   M. Neurath, I. Fuss, and W. Strober. "TNBS-Colitis". In: *International Reviews of Immunology* 19.1 (2000), pp. 51–62. ISSN: 0883-0185. pmid: 10723677.

[216]   Benoit Chassaing et al. "Dextran Sulfate Sodium (DSS)-Induced Colitis in Mice". In: *Current Protocols in Immunology* 104 (Feb. 4, 2014), Unit 15.25. ISSN: 1934-368X. DOI: 10.1002/0471142735.im1525s104. pmid: 24510619.

[217]   Lauren A. Zenewicz et al. "Innate and Adaptive Interleukin-22 Protects Mice from Inflammatory Bowel Disease". In: *Immunity* 29.6 (Dec. 19, 2008), pp. 947–957. ISSN: 1074-7613. DOI: 10.1016/j.immuni.2008.11.003. pmid: 19100701. URL: https://www.ncbi.nlm.nih.gov/pmc/articles/PMC3269819/ (visited on 10/03/2019).

[218]   Ignacio Juncadella et al. "A Pivotal Interplay between TNF Alpha and the IL-23-Axis Cytokines in Regulating Primary Human Intestinal Epithelial Cell Apoptosis (MUC5P.753)". In: *The Journal of Immunology* 194 (1 Supplement May 1, 2015), pp. 138.11–138.11. ISSN: 0022-1767, 1550-6606. URL: https://www.jimmunol.org/content/194/1_Supplement/138.11 (visited on 10/03/2019).

[219]   Christian Mottet, Holm H. Uhlig, and Fiona Powrie. "Cutting Edge: Cure of Colitis by CD4+CD25+ Regulatory T Cells". In: *The Journal of Immunology* 170.8 (Apr. 15, 2003), pp. 3939–3943. ISSN: 0022-1767, 1550-6606. DOI: 10.4049/jimmunol.170.8.3939. pmid: 12682220. URL: https://www.jimmunol.org/content/170/8/3939 (visited on 10/03/2019).

[220]   Ashutosh Chaudhry et al. "Interleukin-10 Signaling in Regulatory T Cells Is Required for Suppression of Th17 Cell-Mediated Inflammation". In: *Immunity* 34.4 (Apr. 22, 2011), pp. 566–578. ISSN: 1097-4180. DOI: 10.1016/j.immuni.2011.03.018. pmid: 21511185.

[221]   K. W. Moore et al. "Interleukin-10 and the Interleukin-10 Receptor". In: *Annual Review of Immunology* 19 (2001), pp. 683–765. ISSN: 0732-0582. DOI: 10.1146/annurev.immunol.19.1.683. pmid: 11244051.

[222]   Ming O. Li, Yisong Y. Wan, and Richard A. Flavell. "T Cell-Produced Transforming Growth Factor-Beta1 Controls T Cell Tolerance and Regulates Th1- and Th17-Cell Differentiation". In: *Immunity* 26.5 (May 2007), pp. 579–591. ISSN: 1074-7613. DOI: 10.1016/j.immuni.2007.03.014. pmid: 17481928.

[223]   Linda Fahlén et al. "T Cells That Cannot Respond to TGF-Beta Escape Control by CD4(+)CD25(+) Regulatory T Cells". In: *The Journal of Experimental Medicine* 201.5 (Mar. 7, 2005), pp. 737–746. ISSN: 0022-1007. DOI: 10.1084/jem.20040685. pmid: 15753207.

[224]   Marc Veldhoen et al. "TGFbeta in the Context of an Inflammatory Cytokine Milieu Supports de Novo Differentiation of IL-17-Producing T Cells". In: *Immunity* 24.2 (Feb. 2006), pp. 179–189. ISSN: 1074-7613. DOI: 10.1016/j.immuni.2006.01.001. pmid: 16473830.

[225]   Atsushi Mizoguchi et al. "Clinical Importance of IL-22 Cascade in IBD". In: *Journal of Gastroenterology* 53.4 (Apr. 2018), pp. 465–474. ISSN: 1435-5922. DOI: 10.1007/s00535-017-1401-7. pmid: 29075900.

[226]   B.-H. Yang et al. "Foxp3(+) T Cells Expressing RORγt Represent a Stable Regulatory T-Cell Effector Lineage with Enhanced Suppressive Capacity during Intestinal Inflammation". In: *Mucosal Immunology* 9.2 (Mar. 2016), pp. 444–457. ISSN: 1935-3456. DOI: 10.1038/mi.2015.74. pmid: 26307665.

[227]   Zaruhi Hovhannisyan et al. "Characterization of Interleukin-17-Producing Regulatory T Cells in Inflamed Intestinal Mucosa from Patients with Inflammatory Bowel Diseases". In: *Gastroenterology* 140.3 (Mar. 2011), pp. 957–965. ISSN: 1528-0012. DOI: 10.1053/j.gastro.2010.12.002. pmid: 21147109.

[228]   Ilona Kryczek et al. "IL-17+ Regulatory T Cells in the Microenvironments of Chronic Inflammation and Cancer". In: *Journal of Immunology (Baltimore, Md.: 1950)* 186.7 (Apr. 1, 2011), pp. 4388–4395. ISSN: 1550-6606. DOI: 10.4049/jimmunol.1003251. pmid: 21357259.

[229]   Gisela I. Mazaira et al. "The Nuclear Receptor Field: A Historical Overview and Future Challenges". In: *Nuclear receptor research* 5 (2018). ISSN: 2314-5706. DOI: 10.11131/2018/101320. pmid: 30148160. URL: https://www.ncbi.nlm.nih.gov/pmc/articles/PMC6108593/ (visited on 09/26/2019).

[230]   D. J. Mangelsdorf et al. "The Nuclear Receptor Superfamily: The Second Decade". In: *Cell* 83.6 (Dec. 15, 1995), pp. 835–839. ISSN: 0092-8674. DOI: 10.1016/0092-8674(95)90199-x. pmid: 8521507.

[231]   Ronald M. Evans and David J. Mangelsdorf. "Nuclear Receptors, RXR, and the Big Bang". In: *Cell* 157.1 (Mar. 27, 2014), pp. 255–266. ISSN: 0092-8674, 1097-4172. DOI: 10.1016/j.cell.2014.03.012. pmid: 24679540. URL: https://www.cell.com/cell/abstract/S0092-8674(14)00346-8 (visited on 09/26/2019).

[232]   R. F. Glascock and W. G. Hoekstra. "Selective Accumulation of Tritium-Labelled Hexoestrol by the Reproductive Organs of Immature Female Goats and Sheep". In: *The Biochemical Journal* 72 (Aug. 1959), pp. 673–682. ISSN: 0264-6021. DOI: 10.1042/bj0720673. pmid: 13828338.

[233]   M. Ashburner et al. "Temporal Control of Puffing Activity in Polytene Chromosomes". In: *Cold Spring Harbor Symposia on Quantitative Biology* 38 (1974), pp. 655–662. ISSN: 0091-7451. DOI: 10.1101/sqb.1974.038.01.070. pmid: 4208797.

[234]   S. Green et al. "Human Oestrogen Receptor cDNA: Sequence, Expression and Homology to v-Erb-A". In: *Nature* 320.6058 (Mar. 13, 1986–19), pp. 134–139. ISSN: 0028-0836. DOI: 10.1038/320134a0. pmid: 3754034.

[235]   S. M. Hollenberg et al. "Primary Structure and Expression of a Functional Human Glucocorticoid Receptor cDNA". In: *Nature* 318.6047 (Dec. 19, 1985), pp. 635–641. ISSN: 0028-0836. DOI: 10.1038/318635a0. pmid: 2867473.

[236]   Miguel Beato. "Gene Regulation by Steroid Hormones". In: *Cell* 56.3 (Feb. 10, 1989), pp. 335–344. ISSN: 0092-8674. DOI: 10.1016/0092-8674(89)90237-7. URL: http://www.sciencedirect.com/science/article/pii/0092867489902377 (visited on 09/29/2019).

[237]   R. J. Koenig et al. "Thyroid Hormone Receptor Binds to a Site in the Rat Growth Hormone Promoter Required for Induction by Thyroid Hormone". In: *Proceedings of the National Academy of Sciences of the United States of America* 84.16 (Aug. 1987), pp. 5670–5674. ISSN: 0027-8424. DOI: 10.1073/pnas.84.16.5670. pmid: 3475698.

[238] A. M. Näär et al. "The Orientation and Spacing of Core DNA-Binding Motifs Dictate Selective Transcriptional Responses to Three Nuclear Receptors". In: *Cell* 65.7 (June 28, 1991), pp. 1267–1279. ISSN: 0092-8674. DOI: 10.1016/0092-8674(91)90021-p. pmid: 1648451.

[239] K. Umesono and R. M. Evans. "Determinants of Target Gene Specificity for Steroid/Thyroid Hormone Receptors". In: *Cell* 57.7 (June 30, 1989), pp. 1139–1146. ISSN: 0092-8674. DOI: 10.1016/0092-8674(89)90051-2. pmid: 2500251.

[240] V. C. Yu et al. "RXR Beta: A Coregulator That Enhances Binding of Retinoic Acid, Thyroid Hormone, and Vitamin D Receptors to Their Cognate Response Elements". In: *Cell* 67.6 (Dec. 20, 1991), pp. 1251–1266. ISSN: 0092-8674. DOI: 10.1016/0092-8674(91)90301-e. pmid: 1662118.

[241] S. A. Kliewer et al. "Convergence of 9-Cis Retinoic Acid and Peroxisome Proliferator Signalling Pathways through Heterodimer Formation of Their Receptors". In: *Nature* 358.6389 (Aug. 27, 1992), pp. 771–774. ISSN: 0028-0836. DOI: 10.1038/358771a0. pmid: 1324435.

[242] T. H. Bugge et al. "RXR Alpha, a Promiscuous Partner of Retinoic Acid and Thyroid Hormone Receptors". In: *The EMBO journal* 11.4 (Apr. 1992), pp. 1409–1418. ISSN: 0261-4189. pmid: 1314167.

[243] D. J. Mangelsdorf et al. "Characterization of Three RXR Genes That Mediate the Action of 9-Cis Retinoic Acid". In: *Genes & Development* 6.3 (Mar. 1992), pp. 329–344. ISSN: 0890-9369. DOI: 10.1101/gad.6.3.329. pmid: 1312497.

[244] R. Kurokawa et al. "Differential Orientations of the DNA-Binding Domain and Carboxy-Terminal Dimerization Interface Regulate Binding Site Selection by Nuclear Receptor Heterodimers". In: *Genes & Development* 7 (7B July 1993), pp. 1423–1435. ISSN: 0890-9369. DOI: 10.1101/gad.7.7b.1423. pmid: 8392479.

[245] B. M. Forman et al. "Unique Response Pathways Are Established by Allosteric Interactions among Nuclear Hormone Receptors". In: *Cell* 81.4 (May 19, 1995), pp. 541–550. ISSN: 0092-8674. DOI: 10.1016/0092-8674(95)90075-6. pmid: 7758108.

[246] B. P. Leblanc and H. G. Stunnenberg. "9-Cis Retinoic Acid Signaling: Changing Partners Causes Some Excitement". In: *Genes & Development* 9.15 (Aug. 1, 1995), pp. 1811–1816. ISSN: 0890-9369. DOI: 10.1101/gad.9.15.1811. pmid: 7649469.

[247] Thomas Q. de Aguiar Vallim, Elizabeth J. Tarling, and Peter A. Edwards. "Pleiotropic Roles of Bile Acids in Metabolism". In: *Cell Metabolism* 17.5 (May 7, 2013), pp. 657–669. ISSN: 1932-7420. DOI: 10.1016/j.cmet.2013.03.013. pmid: 23602448.

[248] Matthew J. Potthoff, Steven A. Kliewer, and David J. Mangelsdorf. "Endocrine Fibroblast Growth Factors 15/19 and 21: From Feast to Famine". In: *Genes & Development* 26.4 (Feb. 15, 2012), pp. 312–324. ISSN: 1549-5477. DOI: 10.1101/gad.184788.111. pmid: 22302876.

[249] Anna C. Calkin and Peter Tontonoz. "Transcriptional Integration of Metabolism by the Nuclear Sterol-Activated Receptors LXR and FXR". In: *Nature Reviews. Molecular Cell Biology* 13.4 (Mar. 14, 2012), pp. 213–224. ISSN: 1471-0080. DOI: 10.1038/nrm3312. pmid: 22414897.

[250] Pieter de Lange et al. "Peroxisome Proliferator-Activated Receptor Delta: A Conserved Director of Lipid Homeostasis through Regulation of the Oxidative Capacity of Muscle". In: *PPAR research* 2008 (2008), p. 172676. ISSN: 1687-4757. DOI: 10.1155/2008/172676. pmid: 18815630.

[251] Jose A. Madrazo and Daniel P. Kelly. "The PPAR Trio: Regulators of Myocardial Energy Metabolism in Health and Disease". In: *Journal of Molecular and Cellular Cardiology* 44.6 (June 2008), pp. 968–975. ISSN: 1095-8584. DOI: 10.1016/j.yjmcc.2008.03.021. pmid: 18462747.

[252]   Vanessa Dubois et al. "Distinct but Complementary Contributions of PPAR Isotypes to Energy
         Homeostasis". In: *The Journal of Clinical Investigation* 127.4 (Apr. 3, 2017), pp. 1202–1214.
         ISSN: 0021-9738. DOI: 10.1172/JCI88894. URL: http://www.jci.org/articles/view/
         88894 (visited on 09/27/2019).

[253]   Fanny Lalloyer et al. "Peroxisome Proliferator-Activated Receptor Alpha Improves Pancreatic
         Adaptation to Insulin Resistance in Obese Mice and Reduces Lipotoxicity in Human Islets".
         In: *Diabetes* 55.6 (June 2006), pp. 1605–1613. ISSN: 0012-1797. DOI: 10.2337/db06-0016.
         pmid: 16731822.

[254]   Joseph G. Yu et al. "The Effect of Thiazolidinediones on Plasma Adiponectin Levels in Normal,
         Obese, and Type 2 Diabetic Subjects". In: *Diabetes* 51.10 (Oct. 2002), pp. 2968–2974. ISSN:
         0012-1797. DOI: 10.2337/diabetes.51.10.2968. pmid: 12351435.

[255]   M. Becker-André, E. André, and J. F. DeLamarter. "Identification of Nuclear Receptor mRNAs
         by RT-PCR Amplification of Conserved Zinc-Finger Motif Sequences". In: *Biochemical and
         Biophysical Research Communications* 194.3 (Aug. 16, 1993), pp. 1371–1379. ISSN: 0006-291X.
         DOI: 10.1006/bbrc.1993.1976. pmid: 7916608.

[256]   V. Giguère et al. "Isoform-Specific Amino-Terminal Domains Dictate DNA-Binding Properties of
         ROR Alpha, a Novel Family of Orphan Hormone Nuclear Receptors". In: *Genes & Development*
         8.5 (Mar. 1, 1994), pp. 538–553. ISSN: 0890-9369. DOI: 10.1101/gad.8.5.538. pmid:
         7926749.

[257]   C. Carlberg et al. "RZRs, a New Family of Retinoid-Related Orphan Receptors That Function
         as Both Monomers and Homodimers". In: *Molecular Endocrinology (Baltimore, Md.)* 8.6 (June
         1994), pp. 757–770. ISSN: 0888-8809. DOI: 10.1210/mend.8.6.7935491. pmid: 7935491.

[258]   G. B. Atkins et al. "Coactivators for the Orphan Nuclear Receptor RORalpha". In: *Molecular
         Endocrinology (Baltimore, Md.)* 13.9 (Sept. 1999), pp. 1550–1557. ISSN: 0888-8809. DOI:
         10.1210/mend.13.9.0343. pmid: 10478845.

[259]   E. F. Greiner et al. "Differential Ligand-Dependent Protein-Protein Interactions between
         Nuclear Receptors and a Neuronal-Specific Cofactor". In: *Proceedings of the National Academy
         of Sciences of the United States of America* 97.13 (June 20, 2000), pp. 7160–7165. ISSN:
         0027-8424. DOI: 10.1073/pnas.97.13.7160. pmid: 10860982.

[260]   David A. Gold et al. "RORalpha Coordinates Reciprocal Signaling in Cerebellar Development
         through Sonic Hedgehog and Calcium-Dependent Pathways". In: *Neuron* 40.6 (Dec. 18, 2003),
         pp. 1119–1131. ISSN: 0896-6273. DOI: 10.1016/s0896-6273(03)00769-4. pmid: 14687547.

[261]   H. P. Harding et al. "Transcriptional Activation and Repression by RORalpha, an Orphan Nuclear
         Receptor Required for Cerebellar Development". In: *Molecular Endocrinology (Baltimore, Md.)*
         11.11 (Oct. 1997), pp. 1737–1746. ISSN: 0888-8809. DOI: 10.1210/mend.11.11.0002. pmid:
         9328355.

[262]   B. A. Hamilton et al. "Disruption of the Nuclear Hormone Receptor RORalpha in Staggerer
         Mice". In: *Nature* 379.6567 (Feb. 22, 1996), pp. 736–739. ISSN: 0028-0836. DOI: 10.1038/
         379736a0. pmid: 8602221.

[263]   Markus Steinmayr et al. "Staggerer Phenotype in Retinoid-Related Orphan Receptor α-Deficient
         Mice". In: *Proceedings of the National Academy of Sciences* 95.7 (Mar. 31, 1998), pp. 3960–
         3965. ISSN: 0027-8424, 1091-6490. DOI: 10.1073/pnas.95.7.3960. pmid: 9520475. URL:
         http://www.pnas.org/content/95/7/3960 (visited on 09/27/2019).

[264] Caroline Chauvet, Brigitte Bois-Joyeux, and Jean-Louis Danan. "Retinoic Acid Receptor-Related Orphan Receptor (ROR) Alpha4 Is the Predominant Isoform of the Nuclear Receptor RORalpha in the Liver and Is up-Regulated by Hypoxia in HepG2 Human Hepatoma Cells". In: *The Biochemical Journal* 364 (Pt 2 June 1, 2002), pp. 449–456. ISSN: 0264-6021. DOI: 10.1042/BJ20011558. pmid: 12023888.

[265] Hong Soon Kang et al. "Gene Expression Profiling Reveals a Regulatory Role for ROR Alpha and ROR Gamma in Phase I and Phase II Metabolism". In: *Physiological Genomics* 31.2 (Oct. 22, 2007), pp. 281–294. ISSN: 1531-2267. DOI: 10.1152/physiolgenomics.00098.2007. pmid: 17666523.

[266] Thomas Meyer et al. "In Vitro and in Vivo Evidence for Orphan Nuclear Receptor RORα Function in Bone Metabolism". In: *Proceedings of the National Academy of Sciences* 97.16 (Aug. 1, 2000), pp. 9197–9202. ISSN: 0027-8424, 1091-6490. DOI: 10.1073/pnas.150246097. pmid: 10900268. URL: http://www.pnas.org/content/97/16/9197 (visited on 09/30/2019).

[267] David A. Gold, Peter M. Gent, and Bruce A. Hamilton. "ROR Alpha in Genetic Control of Cerebellum Development: 50 Staggering Years". In: *Brain Research* 1140 (Apr. 6, 2007), pp. 19–25. ISSN: 0006-8993. DOI: 10.1016/j.brainres.2005.11.080. pmid: 16427031.

[268] Makoto Akashi and Toru Takumi. "The Orphan Nuclear Receptor RORalpha Regulates Circadian Transcription of the Mammalian Core-Clock Bmal1". In: *Nature Structural & Molecular Biology* 12.5 (May 2005), pp. 441–448. ISSN: 1545-9993. DOI: 10.1038/nsmb925. pmid: 15821743.

[269] Hélène Duez and Bart Staels. "The Nuclear Receptors Rev-Erbs and RORs Integrate Circadian Rhythms and Metabolism". In: *Diabetes & Vascular Disease Research* 5.2 (June 2008), pp. 82–88. ISSN: 1479-1641. DOI: 10.3132/dvdr.2008.0014. pmid: 18537094.

[270] Se Kyu Oh et al. "RORα Is Crucial for Attenuated Inflammatory Response to Maintain Intestinal Homeostasis". In: *Proceedings of the National Academy of Sciences of the United States of America* (Sept. 30, 2019). ISSN: 1091-6490. DOI: 10.1073/pnas.1907595116. pmid: 31570593.

[271] B. Kopmels et al. "Evidence for a Hyperexcitability State of Staggerer Mutant Mice Macrophages". In: *Journal of Neurochemistry* 58.1 (Jan. 1992), pp. 192–199. ISSN: 0022-3042. DOI: 10.1111/j.1471-4159.1992.tb09295.x. pmid: 1727430.

[272] Neda Nejati Moharrami et al. "RORα Controls Inflammatory State of Human Macrophages". In: *PloS One* 13.11 (2018), e0207374. ISSN: 1932-6203. DOI: 10.1371/journal.pone.0207374. pmid: 30485323.

[273] Yong-Hyun Han et al. "RORα Induces KLF4-Mediated M2 Polarization in the Liver Macrophages That Protect against Nonalcoholic Steatohepatitis". In: *Cell Reports* 20.1 (July 2017), pp. 124–135. ISSN: 22111247. DOI: 10.1016/j.celrep.2017.06.017. URL: https://linkinghub.elsevier.com/retrieve/pii/S2211124717308148 (visited on 09/30/2019).

[274] Timotheus Y. F. Halim et al. "Retinoic-Acid-Receptor-Related Orphan Nuclear Receptor Alpha Is Required for Natural Helper Cell Development and Allergic Inflammation". In: *Immunity* 37.3 (Sept. 21, 2012), pp. 463–474. ISSN: 1074-7613. DOI: 10.1016/j.immuni.2012.06.012. URL: http://www.sciencedirect.com/science/article/pii/S1074761312003718 (visited on 09/30/2019).

[275] Bernard C. Lo et al. "The Orphan Nuclear Receptor ROR Alpha and Group 3 Innate Lymphoid Cells Drive Fibrosis in a Mouse Model of Crohn's Disease". In: *Science Immunology* 1.3 (Sept. 2, 2016). ISSN: 2470-9468. DOI: 10.1126/sciimmunol.aaf8864. pmid: 28670633.

[276]  Nathaniel S. Wang et al. "Divergent Transcriptional Programming of Class-Specific B Cell Memory by T-Bet and RORα". In: *Nature Immunology* 13.6 (May 6, 2012), pp. 604–611. ISSN: 1529-2916. DOI: 10.1038/ni.2294. pmid: 22561605.

[277]  Joris van der Veeken et al. "Memory of Inflammation in Regulatory T Cells". In: *Cell* 166.4 (Aug. 11, 2016), pp. 977–990. ISSN: 0092-8674. DOI: 10.1016/j.cell.2016.07.006. pmid: 27499023. URL: https://www.ncbi.nlm.nih.gov/pmc/articles/PMC4996371/ (visited on 10/22/2019).

[278]  Subhashini Sadasivam and James A. DeCaprio. "The DREAM Complex: Master Coordinator of Cell Cycle-Dependent Gene Expression". In: *Nature Reviews. Cancer* 13.8 (Aug. 2013), pp. 585–595. ISSN: 1474-1768. DOI: 10.1038/nrc3556. pmid: 23842645.

[279]  Jesse C. Patterson et al. "ROS and Oxidative Stress Are Elevated in Mitosis during Asynchronous Cell Cycle Progression and Are Exacerbated by Mitotic Arrest". In: *Cell Systems* 8.2 (Feb. 27, 2019), 163–167.e2. ISSN: 2405-4712. DOI: 10.1016/j.cels.2019.01.005. pmid: 30797774.

[280]  Haiyan Xu et al. "Chronic Inflammation in Fat Plays a Crucial Role in the Development of Obesity-Related Insulin Resistance". In: *The Journal of Clinical Investigation* 112.12 (Dec. 2003), pp. 1821–1830. ISSN: 0021-9738. DOI: 10.1172/JCI19451. pmid: 14679177.

[281]  William P. Cawthorn, Erica L. Scheller, and Ormond A. MacDougald. "Adipose Tissue Stem Cells Meet Preadipocyte Commitment: Going Back to the Future". In: *Journal of Lipid Research* 53.2 (Feb. 2012), pp. 227–246. ISSN: 0022-2275. DOI: 10.1194/jlr.R021089. pmid: 22140268. URL: https://www.ncbi.nlm.nih.gov/pmc/articles/PMC3269153/ (visited on 10/22/2019).

[282]  Mi-Ran Lee et al. "The Adipokine Retnla Modulates Cholesterol Homeostasis in Hyperlipidemic Mice". In: *Nature Communications* 5.1 (July 15, 2014), pp. 1–15. ISSN: 2041-1723. DOI: 10.1038/ncomms5410. URL: http://www.nature.com/articles/ncomms5410 (visited on 10/19/2019).

[283]  Harish Dharuri et al. "Downregulation of the Acetyl-CoA Metabolic Network in Adipose Tissue of Obese Diabetic Individuals and Recovery after Weight Loss". In: *Diabetologia* 57.11 (Nov. 2014), pp. 2384–2392. ISSN: 1432-0428. DOI: 10.1007/s00125-014-3347-0. pmid: 25099943.

[284]  Jake P. Mann and Quentin M. Anstee. "NAFLD: *PNPLA3* and Obesity: A Synergistic Relationship in NAFLD". In: *Nature Reviews Gastroenterology & Hepatology* 14.9 (Sept. 2017), pp. 506–507. ISSN: 1759-5053. DOI: 10.1038/nrgastro.2017.74. URL: http://www.nature.com/articles/nrgastro.2017.74 (visited on 10/19/2019).

[285]  Gouri Ranganathan et al. "The Lipogenic Enzymes DGAT1, FAS, and LPL in Adipose Tissue: Effects of Obesity, Insulin Resistance, and TZD Treatment". In: *Journal of Lipid Research* 47.11 (Nov. 2006), pp. 2444–2450. ISSN: 0022-2275. DOI: 10.1194/jlr.M600248-JLR200. pmid: 16894240.

[286]  Vanessa van Harmelen et al. "A Role of Lipin in Human Obesity and Insulin Resistance: Relation to Adipocyte Glucose Transport and GLUT4 Expression". In: *Journal of Lipid Research* 48.1 (Jan. 2007), pp. 201–206. ISSN: 0022-2275. DOI: 10.1194/jlr.M600272-JLR200. pmid: 17035674.

[287]  Yin Xiao et al. "Cathepsin K in Adipocyte Differentiation and Its Potential Role in the Pathogenesis of Obesity". In: *The Journal of Clinical Endocrinology and Metabolism* 91.11 (Nov. 2006), pp. 4520–4527. ISSN: 0021-972X. DOI: 10.1210/jc.2005-2486. pmid: 16912123.

[288] F. W. Kiefer et al. "Osteopontin Deficiency Protects against Obesity-Induced Hepatic Steatosis and Attenuates Glucose Production in Mice". In: *Diabetologia* 54.8 (Aug. 2011), pp. 2132–2142. ISSN: 1432-0428. DOI: 10.1007/s00125-011-2170-0. pmid: 21562757.

[289] Andrew G. Levine et al. "Stability and Function of Regulatory T Cells Expressing the Transcription Factor T-Bet". In: *Nature* 546.7658 (June 15, 2017), pp. 421–425. ISSN: 1476-4687. DOI: 10.1038/nature22360. pmid: 28607488.

[290] Ryan Newton, Bhavana Priyadharshini, and Laurence A Turka. "Immunometabolism of Regulatory T Cells". In: *Nature immunology* 17.6 (May 19, 2016), pp. 618–625. ISSN: 1529-2908. DOI: 10.1038/ni.3466. pmid: 27196520. URL: https://www.ncbi.nlm.nih.gov/pmc/articles/PMC5006394/ (visited on 10/15/2019).

[291] Makoto Kuwahara et al. "Bach2-Batf Interactions Control Th2-Type Immune Response by Regulating the IL-4 Amplification Loop". In: *Nature Communications* 7 (Jan. 9, 2016), p. 12596. ISSN: 2041-1723. DOI: 10.1038/ncomms12596. pmid: 27581382.

[292] Shin-ichi Tsukumo et al. "Bach2 Maintains T Cells in a Naive State by Suppressing Effector Memory-Related Genes". In: *Proceedings of the National Academy of Sciences of the United States of America* 110.26 (June 25, 2013), pp. 10735–10740. ISSN: 1091-6490. DOI: 10.1073/pnas.1306691110. pmid: 23754397.

[293] Christopher D. Green and Jing-Dong J. Han. "Epigenetic Regulation by Nuclear Receptors". In: *Epigenomics* 3.1 (Feb. 2011), pp. 59–72. ISSN: 1750-192X. DOI: 10.2217/epi.10.75. pmid: 22126153.

[294] Hiroshi Iwata et al. "PARP9 and PARP14 Cross-Regulate Macrophage Activation via STAT1 ADP-Ribosylation". In: *Nature Communications* 7 (Oct. 31, 2016), p. 12849. ISSN: 2041-1723. DOI: 10.1038/ncomms12849. pmid: 27796300.

[295] Djeneba Dabitao et al. "Cell-Specific Requirements for STAT Proteins and Type I IFN Receptor Signaling Discretely Regulate IL-24 and IL-10 Expression in NK Cells and Macrophages". In: *The Journal of Immunology* 200.6 (Mar. 15, 2018), pp. 2154–2164. ISSN: 0022-1767, 1550-6606. DOI: 10.4049/jimmunol.1701340. pmid: 29436412. URL: https://www.jimmunol.org/content/200/6/2154 (visited on 10/21/2019).

[296] Andrew N. Blackford and Stephen P. Jackson. "ATM, ATR, and DNA-PK: The Trinity at the Heart of the DNA Damage Response". In: *Molecular Cell* 66.6 (June 15, 2017), pp. 801–817. ISSN: 1097-2765. DOI: 10.1016/j.molcel.2017.05.015. URL: http://www.sciencedirect.com/science/article/pii/S1097276517303544 (visited on 10/21/2019).

[297] Xiaozeng Lin, Judy Yan, and Damu Tang. "ERK Kinases Modulate the Activation of PI3 Kinase Related Kinases (PIKKs) in DNA Damage Response". In: *Histology and Histopathology* 28.12 (Dec. 2013), pp. 1547–1554. ISSN: 1699-5848. DOI: 10.14670/HH-28.1547. pmid: 23832672.

[298] Helena Gylling et al. "Insulin Sensitivity Regulates Cholesterol Metabolism to a Greater Extent than Obesity: Lessons from the METSIM Study". In: *Journal of Lipid Research* 51.8 (Aug. 2010), pp. 2422–2427. ISSN: 0022-2275. DOI: 10.1194/jlr.P006619. pmid: 20436182. URL: https://www.ncbi.nlm.nih.gov/pmc/articles/PMC2903787/ (visited on 10/15/2019).

[299] Joel T. Haas et al. "Transcriptional Network Analysis Implicates Altered Hepatic Immune Function in NASH Development and Resolution". In: *Nature Metabolism* 1.6 (June 2019), pp. 604–614. ISSN: 2522-5812. DOI: 10.1038/s42255-019-0076-1. URL: http://www.nature.com/articles/s42255-019-0076-1 (visited on 10/24/2019).

[300] Ricardo J. Miragaia et al. "Single-Cell Transcriptomics of Regulatory T Cells Reveals Trajectories of Tissue Adaptation". In: *Immunity* 50.2 (Feb. 19, 2019), 493–504.e7. ISSN: 1097-4180. DOI: 10.1016/j.immuni.2019.01.001. pmid: 30737144.

[301] F. Chang et al. "Involvement of PI3K/Akt Pathway in Cell Cycle Progression, Apoptosis, and Neoplastic Transformation: A Target for Cancer Chemotherapy". In: *Leukemia* 17.3 (Mar. 2003), pp. 590–603. ISSN: 1476-5551. DOI: 10.1038/sj.leu.2402824. URL: http://www.nature.com/articles/2402824 (visited on 10/15/2019).

[302] Shih-Chin Cheng et al. "mTOR- and HIF-1α-Mediated Aerobic Glycolysis as Metabolic Basis for Trained Immunity". In: *Science (New York, N.Y.)* 345.6204 (Sept. 26, 2014), p. 1250684. ISSN: 1095-9203. DOI: 10.1126/science.1250684. pmid: 25258083.

[303] Xinbo Zhang et al. "Akt, FoxO and Regulation of Apoptosis". In: *Biochimica Et Biophysica Acta* 1813.11 (Nov. 2011), pp. 1978–1986. ISSN: 0006-3002. DOI: 10.1016/j.bbamcr.2011.03.010. pmid: 21440011.

[304] Rahul Roychoudhuri et al. "BACH2 Represses Effector Programs to Stabilize $T_{reg}$-Mediated Immune Homeostasis". In: *Nature* 498.7455 (June 2013), pp. 506–510. ISSN: 1476-4687. DOI: 10.1038/nature12199. URL: http://www.nature.com/articles/nature12199 (visited on 10/15/2019).

[305] Johanna Napetschnig and Hao Wu. "Molecular Basis of NF-κB Signaling". In: *Annual Review of Biophysics* 42.1 (2013), pp. 443–468. DOI: 10.1146/annurev-biophys-083012-130338. pmid: 23495970. URL: https://doi.org/10.1146/annurev-biophys-083012-130338 (visited on 10/15/2019).

[306] Markus Kleinewietfeld et al. "CCR6 Expression Defines Regulatory Effector/Memory-like Cells within the CD25+CD4+ T-Cell Subset". In: *Blood* 105.7 (Apr. 1, 2005), pp. 2877–2886. ISSN: 0006-4971. DOI: 10.1182/blood-2004-07-2505. URL: https://ashpublications.org/blood/article/105/7/2877/20218/CCR6-expression-defines-regulatory-effector-memory (visited on 10/15/2019).

[307] Bradley E. Bernstein et al. "Genomic Maps and Comparative Analysis of Histone Modifications in Human and Mouse". In: *Cell* 120.2 (Jan. 28, 2005), pp. 169–181. ISSN: 0092-8674. DOI: 10.1016/j.cell.2005.01.001. pmid: 15680324.

[308] Jason Buenrostro et al. "ATAC-Seq: A Method for Assaying Chromatin Accessibility Genome-Wide". In: *Current protocols in molecular biology / edited by Frederick M. Ausubel ... [et al.]* 109 (Jan. 5, 2015), pp. 21.29.1–21.29.9. ISSN: 1934-3639. DOI: 10.1002/0471142727.mb2129s109. pmid: 25559105. URL: https://www.ncbi.nlm.nih.gov/pmc/articles/PMC4374986/ (visited on 10/25/2019).

[309] Li Yu et al. "Global Assessment of Promoter Methylation in a Mouse Model of Cancer Identifies ID4 as a Putative Tumor-Suppressor Gene in Human Leukemia". In: *Nature Genetics* 37.3 (Mar. 2005), pp. 265–274. ISSN: 1061-4036. DOI: 10.1038/ng1521. pmid: 15723065.

[310] Anton M. Jetten. "Retinoid-Related Orphan Receptors (RORs): Critical Roles in Development, Immunity, Circadian Rhythm, and Cellular Metabolism". In: *Nuclear Receptor Signaling* 7 (2009), e003. ISSN: 1550-7629. DOI: 10.1621/nrs.07003. pmid: 19381306.

[311] Julio E. Ayala et al. "Standard Operating Procedures for Describing and Performing Metabolic Tests of Glucose Homeostasis in Mice". In: *Disease Models & Mechanisms* 3.9-10 (2010), pp. 525–534. ISSN: 1754-8403. DOI: 10.1242/dmm.006239. pmid: 20713647. URL: https://www.ncbi.nlm.nih.gov/pmc/articles/PMC2938392/ (visited on 10/26/2019).

[312] K. J. Livak and T. D. Schmittgen. "Analysis of Relative Gene Expression Data Using Real-Time Quantitative PCR and the 2(-Delta Delta C(T)) Method". In: *Methods (San Diego, Calif.)* 25.4 (Dec. 2001), pp. 402–408. ISSN: 1046-2023. DOI: 10.1006/meth.2001.1262. pmid: 11846609.

[313] Jill R. Johnson et al. "Continuous Exposure to House Dust Mite Elicits Chronic Airway Inflammation and Structural Remodeling". In: *American Journal of Respiratory and Critical Care Medicine* 169.3 (Feb. 1, 2004), pp. 378–385. ISSN: 1073-449X. DOI: 10.1164/rccm.200308-1094OC. URL: https://www.atsjournals.org/doi/full/10.1164/rccm.200308-1094OC (visited on 10/26/2019).

[314] Jeroen A. J. Vanoirbeek et al. "Noninvasive and Invasive Pulmonary Function in Mouse Models of Obstructive and Restrictive Respiratory Diseases". In: *American Journal of Respiratory Cell and Molecular Biology* 42.1 (Jan. 1, 2010), pp. 96–104. ISSN: 1044-1549. DOI: 10.1165/rcmb.2008-0487OC. URL: https://www.atsjournals.org/doi/full/10.1165/rcmb.2008-0487OC (visited on 10/26/2019).

[315] Bettina Harr and Christian Schlötterer. "Comparison of Algorithms for the Analysis of Affymetrix Microarray Data as Evaluated by Co-Expression of Genes in Known Operons". In: *Nucleic Acids Research* 34.2 (2006), e8. ISSN: 0305-1048. DOI: 10.1093/nar/gnj010. pmid: 16432259. URL: https://www.ncbi.nlm.nih.gov/pmc/articles/PMC1345700/ (visited on 10/30/2019).

[316] Yoav Benjamini and Yosef Hochberg. "Controlling the False Discovery Rate: A Practical and Powerful Approach to Multiple Testing". In: *Journal of the Royal Statistical Society. Series B (Methodological)* 57.1 (1995), pp. 289–300. ISSN: 0035-9246. URL: https://www.jstor.org/stable/2346101 (visited on 10/26/2019).

[317] Aravind Subramanian et al. "Gene Set Enrichment Analysis: A Knowledge-Based Approach for Interpreting Genome-Wide Expression Profiles". In: *Proceedings of the National Academy of Sciences of the United States of America* 102.43 (Oct. 25, 2005), pp. 15545–15550. ISSN: 0027-8424. DOI: 10.1073/pnas.0506580102. pmid: 16199517.

[318] Ben Langmead and Steven L Salzberg. "Fast Gapped-Read Alignment with Bowtie 2". In: *Nature methods* 9.4 (Mar. 4, 2012), pp. 357–359. ISSN: 1548-7091. DOI: 10.1038/nmeth.1923. pmid: 22388286. URL: https://www.ncbi.nlm.nih.gov/pmc/articles/PMC3322381/ (visited on 10/29/2019).

[319] *Model-Based Analysis of ChIP-Seq (MACS)*. URL: https://www-ncbi-nlm-nih-gov.proxy.insermbiblio.inist.fr/pmc/articles/PMC2592715/ (visited on 10/29/2019).

[320] *Spatial Clustering for Identification of ChIP-Enriched Regions (SICER) to Map Regions of Histone Methylation Patterns in Embryonic Stem Cells*. URL: https://www-ncbi-nlm-nih-gov.proxy.insermbiblio.inist.fr/pmc/articles/PMC4152844/ (visited on 10/29/2019).

[321] Aaron T. L. Lun and Gordon K. Smyth. "Csaw: A Bioconductor Package for Differential Binding Analysis of ChIP-Seq Data Using Sliding Windows". In: *Nucleic Acids Research* 44.5 (Mar. 18, 2016), e45. ISSN: 1362-4962. DOI: 10.1093/nar/gkv1191. pmid: 26578583.

[322] Enis Afgan et al. "The Galaxy Platform for Accessible, Reproducible and Collaborative Biomedical Analyses: 2018 Update". In: *Nucleic Acids Research* 46.W1 (Feb. 7, 2018), W537–W544. ISSN: 1362-4962. DOI: 10.1093/nar/gky379. pmid: 29790989.

[323] Denis A. Mogilenko et al. "Metabolic and Innate Immune Cues Merge into a Specific Inflammatory Response via the UPR". In: *Cell* 177.5 (May 16, 2019), 1201–1216.e19. ISSN: 1097-4172. DOI: 10.1016/j.cell.2019.03.018. pmid: 31031005.

# Appendix A

# Appendix

Here I summarize two projects I participated while working on my thesis. The articles published are enclosed.

## A.1 Metabolic and Innate Immune Cues Merge into a Specific Inflammatory Response via the UPR (Mogilenko et al. 2019 Cell 177(5),pp.1201-1216.e19)

This article unravels the general mechanism by which fatty acids exacerbate innate immune response [323]. Toll-like receptor (TLR) are one of the major family of pattern recognition receptors (PRR), the receptors used by several cell types to sense pathogen-associated mollecular patterns (PAMPs) and trigger innate responses. This response is modulated by both environmental signals and intracellular cues. Immune system and metabolism are reciprocally regulated, as seen in numerous examples such as obesity and type two diabetes (T2D). Metabolism of macrophages (MFs) and DCs plays an important role in inflammation. In particular, TLR stimulation induces glycolytic shift in intracellular metabolism. Immune cells may induce stress responses when exposed to certain environmental and metabolic signals. Among metabolic signals, fatty acids (FA) concentrations are dependend on nutrition and are involved in pathologies which had an inflammatory component. In this article, it was hypothesized that FA might induce metabolic adaptation in DCs during their activation. We shown that FA potentiate activation of DCs by directly inhibiting hexokinase (HK) activity without requiring their mitochondrial metabolization through fatty acid oxidation. This in turn compromises mitochondrial fitness and increases mitochondrial reactive oxygen species (mtROS) by complex I. It next exacerbates unfolded protein response (UPR) and is reflected by particular gene expression profile with strongly upregulated Il23a being a hallmark and increased interleukin-23 (IL-23) secretion. Experiments were performed using a granulocyte-macrophage colony-stimulating factor bone-marrow-derived dendritic cells (GM-DC) in vitro. Imiquimod (IMQ) was used for TLR7/8 activation and fatty acid-rich environment was modeled using treatment with palmitic acid (PA). However, the mechanisms identified was also at play forvarious TLR and FA. In vivo tests using a model of IMQ-induced psoriasis-like IL-23-dependent inflammation showed results in line with in vitro assays. High fat diet (HFD) feeding, which increases plasma levels of FA potentiated IL-23 synthesis and in turn exacerbated pathology. Furthermore, metabolic and mtROS alterations, associated to the increase in IL-23 in vitro were also reproduced in cDCs from inguinal lymph nodes of IMQ and HFD treated mice. mtROS effect was shown to be controlled through

PA-dependent reduction of glutamate and in turn glutathione levels. Transcriptionnal profiling showed that PA alone did not cause broad changes while IMQ led to substential differences. Importantly, co-treatment with PA and IMQ resulted in a strong shift in expression of genes even compared to treatment by IMQ alone. PA and IMQ together altered expression of genes associated with the UPR. Namely, they increase Hspa5, Ddit3, Xbp1s. Thus, activation of CHOP and XBP1 pathways by PA and IMQ co-treatment leads to exacerbated UPR response and increased expression of interleukin-6 (IL-6) and IL-23. My contribution to this work included assisting with GM-DC cell culture experiments, tests of gene expression and metabolic parameters as well as data analysis for these parameters and for metabolomics assays. I also helped to perform a mouse model of IMQ-induced skin inflammation and participated in several discussions.

# Metabolic and Innate Immune Cues Merge into a Specific Inflammatory Response via the UPR

## Graphical Abstract



## Highlights

- Extracellular FAs inhibit HK activity and rewire metabolism in late TLR activation

- FA-mediated adaptation of glycolysis leads to perturbed mitochondrial fitness

- Metabolic adaptation and mitochondrial ROS exacerbate TLR-induced UPR activation

- The UPR links metabolic alterations to a distinct inflammatory signature
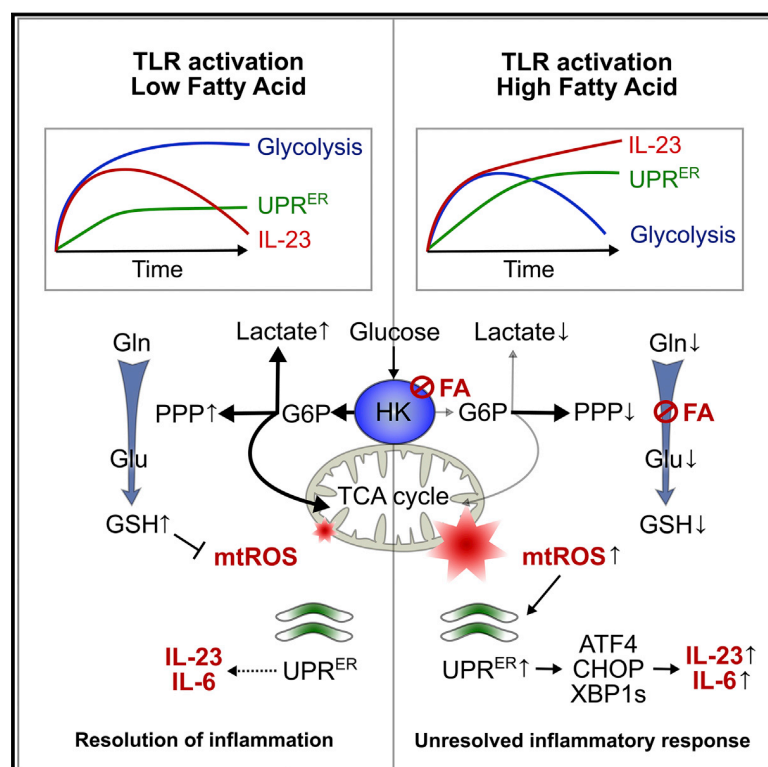
## Authors

Denis A. Mogilenko, Joel T. Haas, Laurent L'homme, ..., Ezra Aksoy, Bart Staels, David Dombrowicz

## Correspondence

david.dombrowicz@pasteur-lille.fr

## In Brief

A high-fat diet induces the metabolic rewiring of TLR-activated dendritic cells and exacerbates IL-23-mediated psoriatic skin inflammation.

# Article

# Metabolic and Innate Immune Cues Merge into a Specific Inflammatory Response via the UPR

Denis A. Mogilenko,[1] Joel T. Haas,[1] Laurent L'homme,[1] Sébastien Fleury,[1] Sandrine Quemener,[1] Matthieu Levavasseur,[1,2] Coralie Becquart,[1,2] Julien Wartelle,[1] Alexandra Bogomolova,[1] Laurent Pineau,[1] Olivier Molendi-Coste,[1] Steve Lancel,[1] Hélène Dehondt,[1] Celine Gheeraert,[1] Aurelie Melchior,[1] Cédric Dewas,[1] Artemii Nikitin,[1] Samuel Pic,[1] Nabil Rabhi,[3] Jean-Sébastien Annicotte,[3] Seiichi Oyadomari,[4] Talia Velasco-Hernandez,[5] Jörg Cammenga,[5] Marc Foretz,[6,7,8] Benoit Viollet,[6,7,8] Milica Vukovic,[9] Arnaud Villacreces,[9] Kamil Kranc,[9] Peter Carmeliet,[10,11] Guillemette Marot,[12] Alexis Boulter,[13] Simon Tavernier,[14] Luciana Berod,[15] Maria P. Longhi,[16] Christophe Paget,[17] Sophie Janssens,[18] Delphine Staumont-Sallé,[1,2,20] Ezra Aksoy,[19,20] Bart Staels,[1,20] and David Dombrowicz[1,21,*]

[1]University of Lille, EGID, INSERM, CHU Lille, Institut Pasteur de Lille, U1011, 59019 Lille, France
[2]Department of Dermatology, CHU Lille, 59045 Lille, France
[3]University of Lille, EGID, CNRS, CHU Lille, Institut Pasteur de Lille, UMR 8199, 59019 Lille, France
[4]Fujii Memorial Institute of Medical Sciences, Institute of Advanced Medical Sciences, Tokushima University, Tokushima 770-8503, Japan
[5]Department of Hematology, Institute for Clinical and Experimental Medicine, Linköping University, 58185 Linköping, Sweden
[6]Université Paris Descartes, Sorbonne Paris Cité, 75006 Paris, France
[7]INSERM U1016, Institut Cochin, 75014 Paris, France
[8]CNRS, UMR8104, 75014 Paris, France
[9]Centre for Haemato-Oncology, Barts, and the London School of Medicine and Dentistry, Queen Mary University of London, London EC1M 6BQ, UK
[10]Laboratory of Angiogenesis and Vascular Metabolism, Center for Cancer Biology, VIB, 3000 Leuven, Belgium
[11]Laboratory of Angiogenesis and Vascular Metabolism, Department of Oncology, University of Leuven, Leuven, 3000 Belgium
[12]Université Lille, MODAL Team, Inria Lille-Nord Europe, 59650 Villeneuve-d'Ascq, France
[13]University of Florida College of Medicine, Gainesville, FL 32610, USA
[14]Laboratory of Immunoregulation and Mucosal Immunology, VIB Center for Inflammation Research and Department of Internal Medicine and Pediatrics, Ghent University, 9052 Ghent, Belgium
[15]Institute of Infection Immunology, TWINCORE, Centre for Experimental and Clinical Infection Research, A Joint Venture between the Medical School Hannover (MHH) and the Helmholtz Centre for Infection Research (HZI), Hannover, Niedersachsen 30625, Germany
[16]William Harvey Research Institute, Barts, and the London School of Medicine and Dentistry, Queen Mary University of London, London EC1M 6BQ, UK
[17]Université de Tours, INSERM, Centre d'Etude des Pathologies Respiratoires (CEPR), UMR 1100, 37041 Tours, France
[18]ER Stress and Inflammation, VIB Center for Inflammation Research, and Department of Internal Medicine and Pediatrics, Ghent University, 9052 Ghent, Belgium
[19]Centre for Biochemical Pharmacology, William Harvey Research Institute, Queen Mary University of London, London EC1M 6BQ, UK
[20]These authors contributed equally
[21]Lead Contact
*Correspondence: david.dombrowicz@pasteur-lille.fr
https://doi.org/10.1016/j.cell.2019.03.018

## SUMMARY

Innate immune responses are intricately linked with intracellular metabolism of myeloid cells. Toll-like receptor (TLR) stimulation shifts intracellular metabolism toward glycolysis, while anti-inflammatory signals depend on enhanced mitochondrial respiration. How exogenous metabolic signals affect the immune response is unknown. We demonstrate that TLR-dependent responses of dendritic cells (DCs) are exacerbated by a high-fatty-acid (FA) metabolic environment. FAs suppress the TLR-induced hexokinase activity and perturb tricarboxylic acid cycle metabolism. These metabolic changes enhance mitochondrial reactive oxygen species (mtROS) production and, in turn, the unfolded protein response (UPR), leading to a distinct transcriptomic signature with IL-23 as hallmark. Interestingly, chemical or genetic suppression of glycolysis was sufficient to induce this specific immune response. Conversely, reducing mtROS production or DC-specific deficiency in XBP1 attenuated IL-23 expression and skin inflammation in an IL-23-dependent model of psoriasis. Thus, fine-tuning of innate immunity depends on optimization of metabolic demands and minimization of mtROS-induced UPR.

## INTRODUCTION

Metabolic adaptations play an important role in host response to pathogens (Wang et al., 2016; Weis et al., 2017). Inflammatory responses are triggered by pattern-recognition receptors (PRRs), such as Toll-like receptors (TLRs), which recognize pathogen-associated molecular patterns (PAMPs) (Medzhitov, 2001).
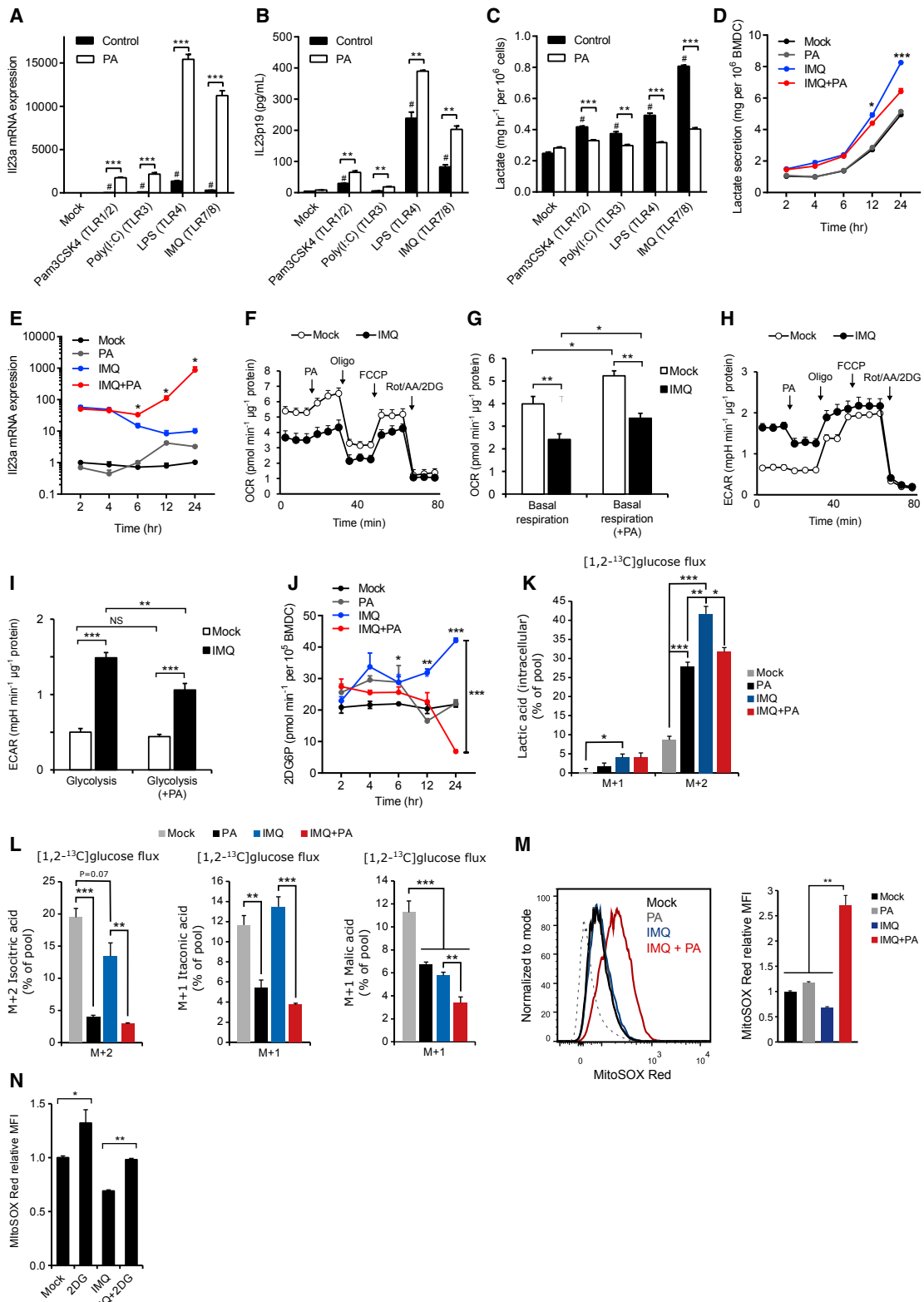
*(legend on next page)*

Inflammation is a tightly controlled process sensitive to dynamic changes in tissue environment and to the intrinsic state of immune cells, both contributing to initiation and resolution of inflammation (Netea et al., 2017). However, dysregulation of the transient inflammatory response can result in chronic inflammatory diseases (Fullerton and Gilroy, 2016).

Recent evidence shows that metabolism of macrophages and dendritic cells (DCs) plays a crucial role in inflammation (O'Neill and Pearce, 2016). Both DCs and macrophages undergo a robust increase of glycolysis after acute activation by TLR agonists, whereas mitochondrial activity is suppressed in such conditions (Krawczyk et al., 2010; Tannahil et al., 2013). This shift of metabolic activity, known as glycolytic reprogramming, results in altered mitochondrial function, increased reactive oxygen species (ROS) production, and elevated secretion of pro-inflammatory cytokines (Tannahil et al., 2013; Lampropoulou et al., 2016; Mills et al., 2016). Importantly, processes that drive glycolytic reprogramming in M1 macrophages, activated by the TLR4 agonist lipopolysaccharide (LPS), are downregulated in interleukin-4 (IL-4)-polarized M2 macrophages (Jha et al., 2015) or in response to IL-10 (Ip et al., 2017). In addition, a recent study demonstrated that the key hallmarks of M2 macrophages are fatty acid oxidation (FAO) independent and are not regulated by mitochondrial respiration (Divakaruni et al., 2018). Alterations of immune signaling have a profound impact on whole-body metabolism in metabolic diseases such as obesity and type 2 diabetes (Hotamisligil, 2017). Conversely, altered metabolic environment, for instance, due to obesity, affects myeloid cells during the innate inflammatory response (Duan et al., 2018). Immune cells sense environmental and metabolic cues that induce specialized stress responses in these cells (Chovatiya and Medzhitov, 2014). Flexibility of immune cells to adapt to different metabolic demands and diverse metabolic milieu via dynamic regulation of intracellular metabolism is an important component of inflammation and tissue homeostasis (Gaber et al., 2017). However, the underlying molecular mechanisms remain poorly understood. We hypothesized that metabolic adaptations during DC innate immune activation might be sensitive to extracellular metabolites such as FA, whose concentrations are altered by nutritional status and in several metabolic diseases (Karpe et al., 2011). Our results show that FAs enhance TLR-mediated innate activation by inhibiting hexokinase (HK) thereby impairing the glycolytic reprogramming, leading to disturbed mitochondrial fitness and increased mitochondrial reactive oxygen species (mtROS) generation. This results in an exacerbated unfolded protein response

(UPR) and, in turn, induces a distinct molecular signature and inflammatory response characterized by increased IL-23 production. Thus, adaptation of glycolysis to the metabolic environment links mtROS production to UPR activation and represents a specific mechanism regulating innate immunity.

## RESULTS

### FAs Alter TLR-Induced Innate Immune Response
To study whether the metabolic environment modulates the innate immune response, we analyzed the impact of FA on TLR-mediated activation of mouse granulocyte-macrophage colony-stimulating factor (GM-CSF) bone-marrow-derived DCs (GM-DCs). In GM-DCs, palmitic acid (PA), a common saturated FA in processed food diets, alone did not induce significant expression of pro-inflammatory cytokines, but it greatly modified *Il23a*, *Il6*, and *Il12a* expression in response to TLR activation (Figures 1A, 1B, and S1A–S1C). Moreover, PA potentiated IL-23 expression induced by activation of another PRR Dectin-2 (by furfurman), but not by Dectin-1 (by curdlan), as well as by tumor necrosis factor (TNF), but not by IL-1β (Figure S1D). Likewise, PA robustly increased IL-23 expression upon TLR4 and TLR7/8 activation in bone-marrow-derived macrophages (BMDMs) (Figure S1E). These data indicate that IL-23 expression is sensitive to the presence of a high-FA metabolic environment.

Next, we focused on activation of DCs with TLR7/8 ligand imiquimod (IMQ), which induced the strongest synergistic effects with PA. Interestingly, PA only modified expression of a subset of cytokines and chemokines among all induced by IMQ (Figure S1C), suggesting that FAs promote a distinct innate immune signature in TLR-activated DCs.

### PA Modulates Glycolysis in TLR-Activated DCs
TLR activation rapidly increases glycolysis in DCs (Everts et al., 2014; Krawczyk et al., 2010) Furthermore, PA affects early TLR4 signaling in macrophages (Lancaster et al., 2018). Consequently, we hypothesized that PA might modulate the DC inflammatory response either by acting as a signaling molecule or by altering intracellular metabolism. Stimulation of GM-DCs from wild-type and TLR4-deficient mice with IMQ and PA resulted in similar IL-23 induction (Figure S2A). Moreover, the upregulation of IL-23 by PA was not due to nuclear factor κB (NF-κB) signaling (Figure S2B) or c-Jun N-terminal kinase (JNK) signaling (Figures S2C and S2D). Furthermore, the monounsaturated oleic acid (OA) also increased IL-23 secretion upon IMQ activation,

---

**Figure 1. PA Rewires Inflammatory Response and Metabolism in TLR-Activated DCs**
GM-DCs were activated by TLR ligands during indicated time without (control) or with PA.
(A–C) *Il23a* expression (A), IL-23p19 secretion (B), and lactate secretion (C) at 24 h.
(D and E) Lactate secretion (D) and *Il23a* expression (E) at indicated time after activation.
(F–I) GM-DCs activated during 24 h, followed by extracellular flux analysis. Mitochondrial respiration calculated as OCR (F and G), glycolysis activity calculated as *ECAR* (H and I), before and after PA administration. Oligo, oligomycin; FCCP, carbonyl cyanide-4-(trifluoromethoxy)phenylhydrazone; AA, antimycin A; Rot, rotenone; 2DG, 2-deoxyglucose.
(J) HK activity in GM-DCs treated as in (D) and (E).
(K and L) Fluxes from 1,2-$^{13}$C-glucose into intracellular lactate (K), isocitric, itaconic, and malic acids (L).
(M and N) MitoSOX staining in GM-DCs activated by IMQ with or without PA (M) or with or without 2DG (N).
n = 3–5 per group. Data are shown as mean ± SEM. *p < 0.05, **p < 0.01, ***p < 0.001 (unpaired Student's t test or one-way ANOVA with Bonferroni test). #p < 0.05 as compared to mock or control-treated cells (one-way ANOVA with Bonferroni test).
See also Figures S1, S2, S3, S4, and S5 and Table S1.

independently of TLR4 (Figure S2E). Taken together, these results show that FAs increase IMQ-mediated IL-23 expression through a yet unknown mechanism. We thus investigated the impact of PA on intracellular metabolism in IMQ-stimulated DCs. The dose-dependent increase of IL-23 expression and secretion upon IMQ and PA late co-stimulation was associated with a decrease of lactate secretion (Figure S2F), indicating reduced glycolytic activity. Moreover, PA suppressed lactate production during the late PRR activation (Figures 1C and S2G). Notably, PA presence did not affect extracellular acidification rate (ECAR), a surrogate measurement of glycolytic activity, and oxygen consumption rate (OCR), a measurement of oxidative phosphorylation (OXPHOS), during the immediate response to IMQ activation (Figures S2H and S2I). These results indicate that PA suppresses late, but not early, steps of glycolytic reprogramming.

Next, we speculated that GM-DCs become sensitive to metabolic effects of PA once the cells acquire "Warburg-like" metabolism (O'Neill and Pearce, 2016). Indeed, GM-DCs demonstrated a highly glycolytic phenotype with inhibited mitochondrial respiration after IMQ activation (Figures 1F–1I). Interestingly, while PA rapidly increased mitochondrial respiration in resting and IMQ-activated GM-DCs (Figures 1F and 1G), only IMQ-activated "Warburg-like" cells displayed decreased glycolytic activity in response to PA (Figures 1H and 1I). Similarly, PA inhibited lactate secretion from TLR-activated "Warburg-like" BMDM (Figure S2J). Together, these data show that PA alters late stages of glycolytic reprogramming, resulting in a shift from aerobic glycolysis toward OXPHOS. This metabolic effect of PA was not due to alterations in glucose uptake (Figure S2K) or mitochondrial content (Figure S2L), nor was it explained by changes in activity of electron transport chain (ETC) complexes (Figure S2M). Although IMQ activation in GM-DCs increased ATP levels and decreased ATP/ADP ratio (indicating elevated energy utilization), PA presence did not alter these parameters in IMQ-stimulated cells (Figure S2N).

## PA Inhibits HK Activity and Increases IL-23 Expression Independently of FAO

Octanoic acid, a medium chain saturated FA, has been shown to inhibit key glycolytic enzymes in the liver (Weber et al., 1966). We hypothesized that PA might also inhibit glycolytic enzymes during the late-stage TLR activation in GM-DCs. Indeed, PA reversed the IMQ-induced increase of HK activity at 24 h (Figure 1J). Furthermore, various FAs were able to inhibit lactate secretion when added for 2 h to GM-DCs primed with IMQ for 24 h (Figure S2O). Interestingly, 2-methyl-PA failed to inhibit lactate secretion in this setting, suggesting that an intact carboxylic acid moiety is required for the PA-dependent regulation of HK activity. Finally, the PA-mediated inhibition of HK was not due to its dissociation from mitochondrial outer membrane into the cytosol (Figure S2P).

We next assessed whether PA activation to PA-CoA was required for the inhibition of glycolytic activity. As the effect of PA on glycolysis was not modulated by triacsin C, an inhibitor of long-chain-FA-CoA ligases 1, 3, and 4 (Figures S2O and S2Q), its conversion to PA-CoA by these enzymes appears dispensable. Mitochondrial FAO depends on the activity of FA importers CPT1A and CPT2 (Mehta et al., 2017). Cpt1a deficiency or silencing both Cpt1a and Cpt2 did not alter the PA-mediated increase in IL-23 expression (Figures S3A, S3B, and S3D–S3F). Moreover, Cpt1a deficiency did not affect the PA-mediated inhibition of HK activity in IMQ-activated GM-DCs (Figure S3C). In addition, using a FAO-specific concentration of CPT1 inhibitor etomoxir (Divakaruni et al., 2018) did not alter IL-23 expression (Figure S3F). Furthermore, activation with IMQ decreased Cpt1a expression and reduced complete PA oxidation to $CO_2$ in GM-DCs, despite a modest increase of acid-soluble metabolite (ASM) production, which was not rescued by pre-incubation with PA (Figures S3G and S3H), indicating greatly reduced PA catabolism. In line, IMQ activation led to elevated accumulation of free non-metabolized PA in GM-DCs (Figure S3I). These results indicate that elevated intracellular FA concentrations, rather than their metabolization via FAO, are critical for the inhibition of HK activity and ensuing increase in IL-23 production at the late stage of TLR activation.

## PA Inhibits Glycolytic Fluxes and Disturbs Mitochondrial Fitness

We next investigated whether the FAO-independent inhibition of glycolysis by PA was associated with alterations in the glycolytic pathway. IMQ-mediated DC activation induced the expression of genes encoding glycolytic enzymes and lactate transporters (Figures S4A and S4P, left). Interestingly, PA addition to IMQ repressed Ldha, Pfkl, and Pfkfb3 expression compared to IMQ alone (Figures S4A and S4P, right). In line with gene expression data, [1,2-$^{13}$C]glucose flux via glycolysis into lactate (M+2) was significantly reduced upon PA treatment in IMQ-activated GM-DCs, whereas the (M+1) flux via the oxidative pentose phosphate pathway (PPP) was not altered (Figure 1K). Analysis of glycolysis intermediates showed non-significant increases of total fructose-1,6-biphosphate, 3-phosphoglycerate and pyruvate upon IMQ stimulation (Figures S4C–S4F). However, GM-DCs co-stimulated with IMQ and PA displayed significantly decreased 3-phosphoglycerate compared to IMQ alone, in line with reduced glycolytic activity (Figures S4E and S4P).

IMQ activation generally downregulated genes in the tricarboxylic acid (TCA) cycle compared to resting cells (Figures S4G and S4P). These transcriptional changes led to accumulation of itaconate, fumarate, and malate levels, but no changes in citrate, isocitrate, and succinate were found in IMQ-activated GM-DCs (Figures S4G–S4M and S4P). By contrast, IMQ and PA stimulation increased expression of pyruvate dehydrogenase (Pdhb), malate dehydrogenase (Mdh1/2), and mitochondrial isocitrate dehydrogenase 2 (Idh2) but decreased lactate dehydrogenase (Ldha) expression compared to IMQ activation (Figures S4A, S4G, and S4P). Surprisingly, in this setting, [1,2-$^{13}$C] glucose fluxes into TCA metabolites, such as isocitrate, itaconate, and malate, were significantly inhibited by PA (Figure 1L), and intracellular citrate and itaconate levels were reduced (Figures S4H and S4J). Itaconate regulates the late inflammatory response in macrophages (Bambouskova et al., 2018). Because PA decreased itaconate levels, we treated Acod1$^{-/-}$ (also known as Irg1$^{-/-}$) GM-DCs, deficient in itaconate synthase, with IMQ and PA. While Irg1 deficiency affected IMQ+PA-induced IL-23 expression, the effect was relatively small

(Figure S4Q). Thus, the upregulation of IL-23 by PA is unlikely due to the modulation of intracellular itaconate.

Inhibited HK activity can lead to uncoupling of intra- from extramitochondrial metabolism (Robey and Hay, 2006), which might result in mitochondrial stress. Indicative of mitochondrial stress, mtROS generation was significantly increased by PA in IMQ-activated GM-DCs (Figure 1M). Moreover, inhibition of HK activity by 2-deoxyglucose (2DG) phenocopied the PA-induced increase of mtROS generation (Figure 1N). Taken together, these results indicate that the metabolic adaptation of glycolysis to a high-FA environment is associated with inhibition of glycolysis, reduced glycolytic flux into the TCA cycle, and elevated mitochondrial stress.

## PA Increases IL-23 Expression through Elevated Generation of mtROS by Complex I

As PA elevated mitochondrial stress and increased IL-23 expression, we investigated whether these events are functionally associated by inhibiting of mtROS generation. Both mitoTEMPO, an mtROS scavenger, and rotenone, an inhibitor of ETC complex I, diminished mtROS generation and blunted the PA-dependent increase in IL-23 expression (Figures 2A–2C). These results suggest that mtROS generation by complex I or III activity links FA to IL-23 expression. Notably, although it generally diminished mitochondrial respiration, mitoTEMPO neither prevented the PA-mediated inhibition of glycolytic and HK activities in IMQ-activated GM-DCs nor altered GAPDH activity (Figures S5A–S5E). Thus, the increased mtROS generation is rather the result of inhibited glycolytic activity, not the cause.

ROS generation has been shown to rapidly upregulate oxidative PPP activity in keratinocytes leading to increased NADPH production to insure stabilization of redox balance and ROS clearance (Kuehne et al., 2015). We investigated whether alterations in PPP might functionally link PA-mediated glycolysis inhibition with increased mtROS production. PA inhibited activity of G6PDH, a rate-limiting enzyme of the oxidative PPP, and treatment with mitoTEMPO diminished this effect (Figure S5F). In addition, the product of the oxidative PPP, ribose-5-phosphate (R5P), was decreased (Figure S5G), and [1,2-$^{13}$C]glucose fluxes into R5P via non-oxidative PPP (M+2), but not oxidative PPP (M+1), were decreased by PA in IMQ-activated GM-DCs (Figure S5H). Interestingly, PA treatment also affected the PPP metabolite sedoheptulose-7-phosphate (S7P) (Figures S5I and S5J). Altogether, these data show that extracellular FA establishes a new metabolic equilibrium involving a modulation of the PPP activity, redox balance, and mtROS generation in TLR-activated DCs.

## Increased Mitochondrial Activity Potentiates IL-23 Expression

To demonstrate the relevance of these results *in vivo*, we used a mouse model of IMQ-induced skin inflammation (van der Fits et al., 2009), which shares some features with human psoriasis, an IL-23-dependent disease (Teng et al., 2015). IMQ treatment and high-fat diet (HFD) feeding increased concentrations of non-esterified FA (NEFA) in plasma (Figures S6A and S6B) in agreement with published results (Stelzner et al., 2016). As reported (Kanemaru et al., 2015), HFD feeding increased epidermal thickening (Figures S6C and S6D). Moreover, in

IMQ-treated mice, HFD feeding increased the population of IL-23$^+$ conventional DCs (cDC) in skin draining inguinal lymph nodes (iLNs) (Figure 2D). Upon HFD feeding, IMQ-activated cDC exhibited increased expression of genes involved in OXPHOS (Figure S6E) and generated more mtROS (Figure S6F), similar to the *in vitro* findings (Figure 1M). Notably, HFD feeding enhanced the IL-23-induced expression of a subset of IMQ-responsive genes in skin (Suárez-Fariñas et al., 2013), while it did not exert such an effect in the absence of IMQ (Figure S6G), suggesting that increased IL-23 production links HFD feeding with exacerbated skin pathology. Indeed, IMQ-induced skin inflammation was abrogated upon treatment with an IL-23-blocking antibody (Figure S6H). Moreover, in HFD-fed mice treated with IMQ, Cpt1a deficiency in cDC did not alter IL-23 expression and skin pathology (Figures S6I–S6K), in agreement with *in vitro* data (Figure S3B). Taken together, these results indicate that IMQ-activated cDC respond to a high-FA environment *in vivo* via a FAO-independent mechanism by increasing mtROS generation and IL-23 expression. Next, we tested whether inhibition of ETC complex I activity could mitigate the effects of HFD feeding on increased IL-23 production *in vivo*. Metformin, a complex I inhibitor active in macrophages (Kelly et al., 2015), significantly reduced mitochondrial respiration in IMQ-activated GM-DCs in the presence of PA (Figure S6L) and decreased IL-23 expression induced by IMQ and PA (Figure 2E) through an AMPK-independent mechanism (Figure S6M). In HFD-fed mice, metformin significantly reduced IL-23$^+$ cDC numbers in iLNs and epidermal thickness induced by epicutaneous application of IMQ (Figure 2F) and mitigated psoriasis-associated gene expression in the skin (Figure S6N). Thus, *in vivo* IL-23 production by cDC is enhanced by HFD-derived NEFA through a mechanism dependent on complex I activity.

## PA-Mediated Increase of IL-23 Expression Is Associated with a Decrease in the Glutamate and Glutathione Axis

We noticed that the level of NADPH, a product of oxidative PPP, was decreased (Figure 2G) and NADP$^+$/NADPH ratio was increased by PA in IMQ-activated cells (Figure S5L). Decreased NADPH might thus explain the elevated mtROS generation in response to PA. Interestingly, mitoparaquat (mitoPQ), which increases mtROS generation, upregulated IL-23 expression in non-activated GM-DCs but failed to potentiate IL-23 expression in IMQ-activated cells (Figure 2H). Glutathione (GSH) is an important component of the cellular anti-oxidant system (Mailloux et al., 2013). IMQ treatment resulted in a robust increase of GSH levels during the late TLR7/8 response, but this effect was reversed in the presence of PA (Figure 2I). Metabolomic data analysis revealed a decrease of intracellular glutamine and glutamate levels in IMQ-activated GM-DCs treated with PA (Figure 2J), which was associated with inhibited flux into glutamate from glycolysis but not from glutaminolysis (Figure 2K). As glutamate is a key component for GSH synthesis, reduced glutamate may also account for the decreased levels of GSH, and thereby elevated mtROS generation, in GM-DCs treated with IMQ and PA.

To test whether glutamine plays a role in the regulation of IL-23, we deprived GM-DCs from glutamine before activation with IMQ and found significantly increased IL-23 expression (Figure 2L). Similarly, silencing of Gls and Gls2 (Figure 2M),
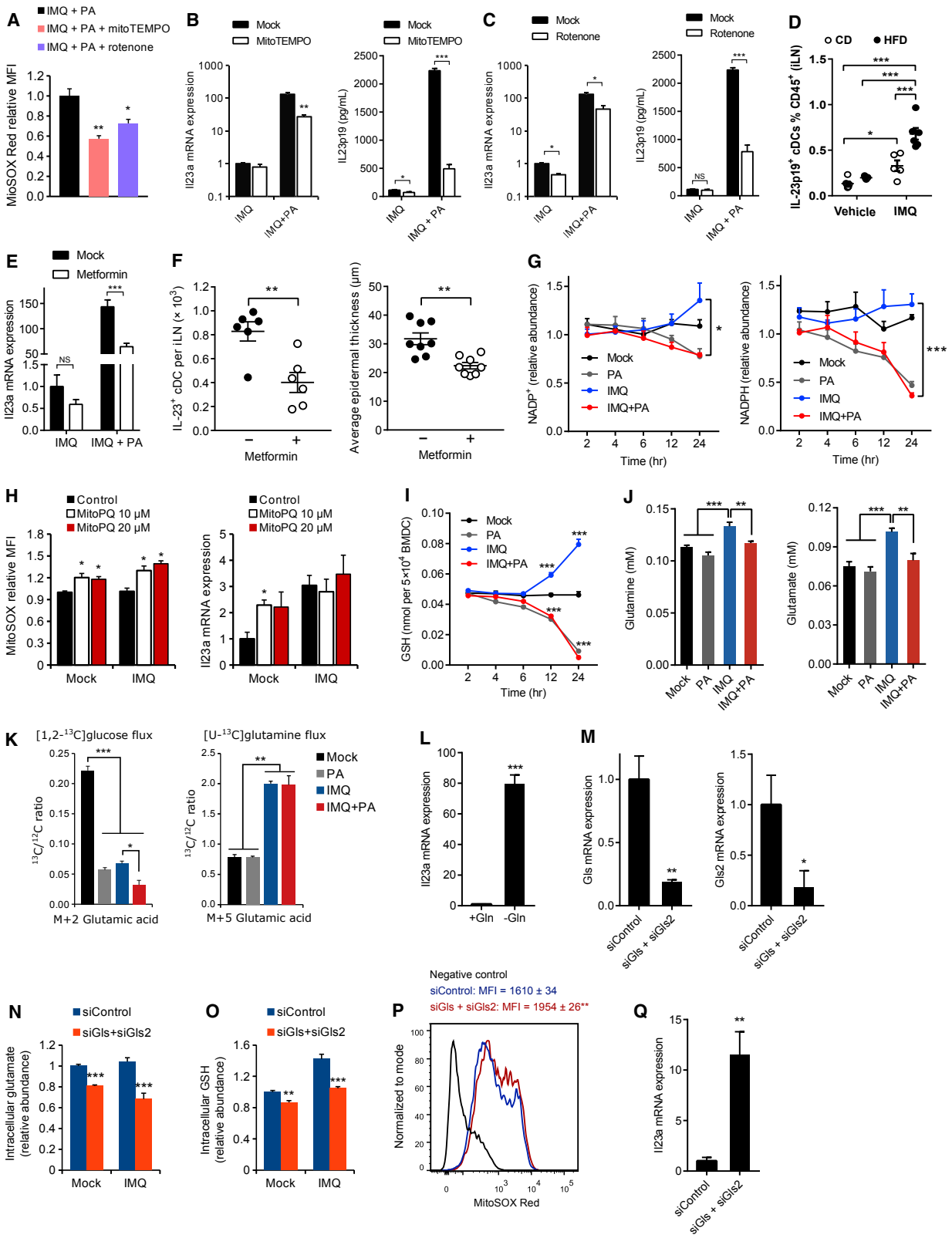
genes encoding enzymes mediating glutaminolysis, decreased glutamate and GSH levels (Figures 2N and 2O), and also increased mtROS generation and IL-23 expression in IMQ-activated GM-DCs (Figures 2P–2R). These results show that the pro-inflammatory effect of PA depends, at least in part, upon the reprogramming of the glutamine, glutamate, and GSH axis.

## Upper Glycolysis Inhibition Promotes IL-23 Expression

Because PA inhibited HK activity, we determined whether glycolytic inhibition was sufficient per se to enhance IL-23 expression. Treatment with 2DG led to elevated IL-23 expression in GM-DCs in synergy with IMQ activation (Figure 3A). In line, intraperitoneal injection of 2DG significantly increased the accumulation of IL-23$^+$ cDC in IMQ-treated mice (Figure 3B). Taken together, these results show that inhibition of HK activity promotes IL-23 expression in TLR7/8-activated DCs in vitro and in vivo. PA inhibited aerobic glycolysis in part through transcriptional regulation with a pronounced effect on Pfkfb3 gene (Figure S4A). PFKFB3 increases glycolysis in macrophages (Jiang et al., 2016). Upon activation by IMQ and PA, IL-23 expression was significantly increased in Pfkfb3-knocked-down GM-DCs (Figure 3C). We next evaluated whether lower glycolysis was critical for IL-23 expression. Combined inactivation of Pfkl (liver-type phosphofructokinase 1) and Pfkp (6-phosphofructo-1-kinase) decreased lactate secretion in IMQ-activated DCs (Figure S7). However, this inactivation failed to upregulate IL-23 expression (Figure S6O), indicating that the activity of upper, but not lower, glycolysis is essential for the regulation of IL-23 expression.

We further confirmed the role of upper glycolysis on IL-23 regulation using a model of genetic inactivation of HIF1α, which controls glycolytic activity in myeloid cells (Corcoran and O'Neill, 2016). Accordingly, lactate secretion and HK activity were significantly decreased in IMQ-activated HIF1α-deficient GM-DCs (Figures 3D–3F), while mtROS generation was significantly elevated (Figure 3G). In line, IMQ-activated, but not resting, HIF1α-deficient GM-DCs displayed increased IL-23 expression and secretion (Figure 3H). Similar results were observed in HIF1α-deficient GM-DCs from Hif1a$^{Vav/Vav}$ mice and tamoxifen-treated Hif1a$^{fl/fl}$Rosa26CreER mice (data not shown). Finally, the increase of IL-23 expression in IMQ-activated HIF1α-deficient GM-DCs was abrogated by inhibiting mtROS

generation, but not pyruvate dehydrogenase kinase (PDK) activity (Figure 3I). Taken together, these results show that chemical or genetic inhibitions of upper glycolysis lead to increased mtROS generation and IL-23 expression.

## Metabolic Adaptation to a High-FA Environment Is Associated with a Distinct Transcriptional Program

To get further insight into the mechanisms of metabolic adaptation of DCs to a high-FA environment, we performed microarray analysis of GM-DCs activated by IMQ and PA. IMQ alone induced pronounced changes in the DC transcriptional program, whereas PA alone only modestly affected gene expression (Figure 4A). By contrast, combined PA and IMQ treatment resulted in robust alteration of the DC transcriptional program, significantly modulating the expression of 874 genes (594 upregulated and 280 downregulated) compared to GM-DCs treated with IMQ alone (Figures 4A and 4B). Analysis of the 594 upregulated genes revealed an enrichment in the UPR, IRE1α and XBP1 pathway, and N-linked glycosylation (Figure 4C), including upregulated expression of multiple genes from the UPR and the integrated stress response pathways (Figure 4D). Similarly, transcriptomic analysis of cDC isolated from IMQ-treated mice showed that, compared to CD, HFD feeding led to an increase in the UPR gene signature (Figure 4E). Taken together, these results suggest that metabolic adaptation of IMQ-activated DCs to a high-FA environment induces a distinct transcriptional program associated with exacerbated UPR.

## PA Potentiates the UPR in TLR-Activated DCs

The UPR regulates immune homeostasis and responses in DCs (Martinon et al., 2010; Osorio et al., 2014; Tavernier et al., 2017). Thus, we further analyzed the impact of UPR alterations on IL-23 expression. While PA alone acted on a very restricted gene subset, compared to IMQ alone, PA and IMQ differentially altered the expression of genes involved in the UPR (Figure S7A). In particular, combined action of IMQ and PA resulted in an additional increase of protein and/or gene expression of Hspa5 (encoding binding immunoglobulin protein [BIP]), Ddit3 (encoding CCAAT-enhancer-binding protein homologous protein [CHOP]), and the spliced form of Xbp1 (XBP1s), but not the cleaved form of ATF6 p50 (Figures 5A, 5B, and S7B). Likewise,

---

**Figure 2. PA Increases IL-23 through Mitochondrial Respiration and mtROS Generation**

GM-DCs were activated by IMQ without (control) or with PA in the presence of indicated inhibitors for 24 h.

(A–C) MitoSOX staining (A), Il23a expression (B), and IL-23p19 secretion (C) in the presence of mitoTEMPO or rotenone.

(D) Male mice were fed CD or HFD, and abdominal skin was treated with IMQ or vehicle during 6 days. Proportion of IL-23$^+$ cDC in iLNs. n = 4–6 mice per group.

(E) Il23a expression in response to metformin.

(F) Male mice were fed HFD with or without metformin supplementation of drinking water during 3 days followed by IMQ application to belly skin. Number of IL-23$^+$ cDC in iLNs 18 h after IMQ treatment and average epidermal thickness after 5 days of IMQ treatment. n = 6–8 mice per group.

(G) NADP$^+$ and NADPH levels in GM-DCs activated by IMQ with or without PA for 2–24 h.

(H) MitoSOX staining in GM-DCs activated by IMQ with or without mitoParaquat (mitoPQ).

(I) Intracellular GSH in GM-DCs treated as in Figure 1D.

(J) Intracellular glutamine and glutamate.

(K) Carbon fluxes from 1,2-$^{13}$C-glucose and U-$^{13}$C-glutamine into intracellular glutamate.

(L) Il23a expression in GM-DCs pre-incubated with or without 2 mM glutamine for 4 h and treated with IMQ for 24 h.

(M–Q) Gls and Gls2 expression (M), intracellular glutamate (N) and GSH (O), mtROS levels (P), and Il23a expression (Q) in GM-DCs transfected with small interfering RNA (siRNA) against Gls and Gls2 or control siRNA and 48 h later treated with IMQ in media containing glutamine for 24 h.

n = 3–6 per group. Data are shown as mean ± SEM. *p < 0.05, **p < 0.01, ***p < 0.001 by unpaired Student's t test.

See also Figures S4 , S5, and S6 and Table S1.
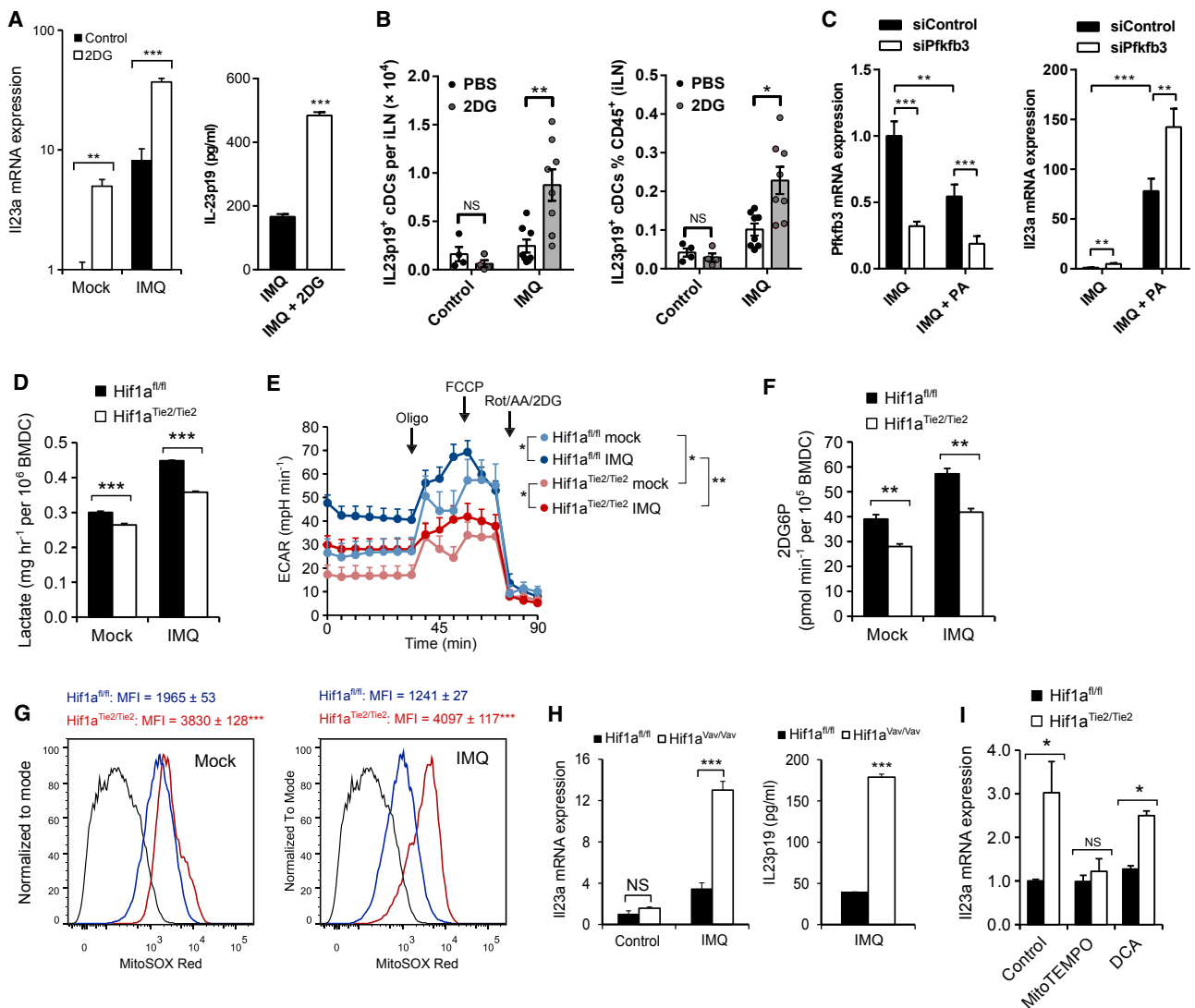
**Figure 3. Upper Glycolysis Decreases IL-23 Expression**

(A) *Il23a* expression and IL-23 protein secretion in GM-DCs activated by IMQ and treated with 2DG.

(B) Number and proportion of IL-23+ cDC in iLNs in mice 18 h after IMQ application to abdominal skin and intraperitoneal injection with PBS or 2DG. n = 4–8 mice per group.

(C) *Pfkfb3* and *Il23a* expression in GM-DCs transfected with siRNA against *Pfkfb3* or control siRNA and 48 h later treated with IMQ.

(D–J) *Hif1a*fl/fl and *Hif1a*Tie2/Tie2 GM-DCs treated with IMQ.

(D–G) Lactate secretion (D), ECAR (E), hexokinase activity (F), MitoSOX+ staining (G).

(H and I) *Il23a* expression and IL-23 secretion in *Hif1a*fl/fl and *Hif1a*Vav/Vav (H), and *I23a* expression in *Hif1a*fl/fl and *Hif1a*Tie2/Tie2 (I) GM-DCs treated with IMQ in the presence of mitoTEMPO and DCA.

n = 3–5 per group. Data are shown as mean ± SEM. *p < 0.05, **p < 0.01, ***p < 0.001 (unpaired Student's t test or two-way ANOVA with Sidak post hoc test). See also Figures S3, S4, and S6 and Table S1.

in sorted cDC, key UPR genes were differentially expressed in response to HFD feeding (Figure S7C). Notably, this was not associated with elevated expression of the UPR receptors PERK or IRE1α (Figures 5A and S7B). In line with these data, the accumulation of XBP1s protein was maximal after 24 h of combined treatment with IMQ and PA (Figures S7D and S7E). Furthermore, PA potentiated UPR activation by TLR2, 3, and 4 in GM-DCs (Figure 5B), indicating that this effect is not limited

to TLR7/8 pathway. These results thus show that the late metabolic adaptation of TLR-activated DCs to a high-FA environment results in a synergistic induction of the UPR.

**PA-Induced Metabolic Adaptations Hyperactivate the UPR**

Next, we determined whether metabolic adaptations to PA directly potentiate TLR-mediated UPR activation. In GM-DCs
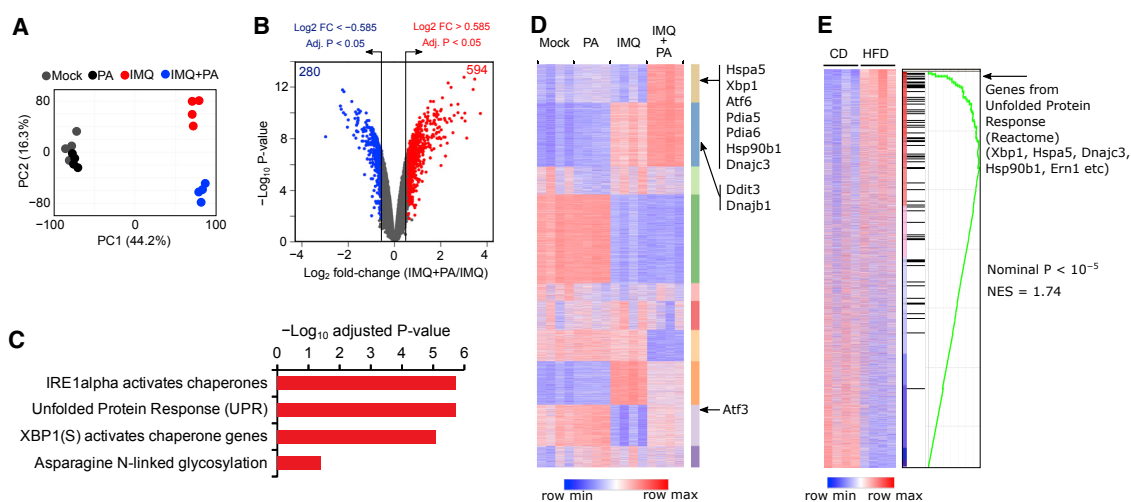
**Figure 4. PA and HFD Feeding Alter Transcription Program and Induce the UPR in IMQ-Activated DCs**

(A) Principal-component (PC) analysis of 15,000 genes with maximal average expression in GM-DCs.

(B) Volcano plot of differential gene expression in GM-DCs treated with IMQ versus treated with IMQ plus PA; number of genes with fold change >1.5 and <0.67 and adjusted p < 0.05 are shown.

(C) Gene set enrichment analysis (GSEA) of the 594 genes from (B) using the Reactome database.

(D) K-mean clustering of the 15,000 genes.

(E) GSEA using the "Unfolded Protein Response (UPR)" pathway in cDC sorted from iLNs from IMQ-treated mice fed CD or HFD (15,000 genes with maximal average expression).

n = 4 in each group.

treated with IMQ and PA, complex I and mtROS inhibition decreased CHOP and XBP1s expression (Figures 5C–5H). Furthermore, inhibition of glycolysis in IMQ-activated GM-DCs resulted in an increase of Ddit3 and Xbp1s expression (Figures 5I and 5J). Accordingly, Ddit3 and Xbp1s expression were significantly increased in HIF1α-deficient GM-DCs that failed to increase glycolytic activity upon TLR activation (Figures 5K and 5L). Importantly, Xbp1 deficiency neither affected glycolytic activity, nor altered mitochondrial respiration in IMQ-activated GM-DCs (Figure S7F), indicating that the increased UPR is a consequence rather than a cause of the inhibited glycolytic activity driven by PA. Taken together, these results indicate that metabolic adaptations to PA control the UPR in TLR-activated DCs.

**UPR Increases IL-23 Expression through the PERK and CHOP and IRE1α and XBP1 Pathways**

Tunicamycin, a direct activator of the UPR, significantly increased IL-23 expression in resting GM-DCs (Figure 6A). Interestingly, it synergistically enhanced IL-23 expression in IMQ-activated GM-DCs (Figures 6A and 6B). Specific inhibitors of IRE1α-dependent splicing activity and PERK signaling resulted in a significant and additive decrease of IL-23 expression in GM-DCs treated with IMQ and PA (Figures 6C and 6D). Because these inhibitors also significantly decreased Xbp1s, Atf4, and Ddit3 expression (data not shown), downstream IRE1α and PERK targets, we evaluated the impact of these transcription factors on IL-23 expression. Atf4 silencing decreased IL-23 expression in GM-DCs activated with IMQ and PA, but

not IMQ alone (Figure S7G). Likewise, CHOP-deficient Ddit3$^{-/-}$ GM-DCs (Oyadomari et al., 2001) displayed lower IL-23 expression compared to Ddit3$^{+/+}$ cells (Figures 6E and 6F). IL-23 expression was also decreased in XBP1-deficient Xbp1$^{CD11c/CD11c}$ GM-DCs (Osorio et al., 2014; Cubillos-Ruiz et al., 2015; Tavernier et al., 2017) upon IMQ and PA activation (Figures 6G and 6H). Moreover, Ddit3$^{-/-}$Xbp1$^{CD11c/CD11c}$ GM-DCs (Tavernier et al., 2017), deficient for both XBP1 and CHOP (Figure S7H), showed a further decrease in IL-23 expression (Figures 6G and 6H). Of note, in IMQ-activated GM-DCs, IL-6 induction by PA was dependent on mtROS generation, and XBP1- and CHOP deficiency significantly attenuated IL-6 expression (Figures S7I and S7J). Furthermore, in IMQ-activated GM-DCs, single or combined XBP1 and CHOP deficiency diminished IL-23 expression potentiated upon glycolysis inhibition by 2DG (Figures 6I–6J). GM-DC activation by IMQ and PA lead to increased mitochondrial UPR (UPR$^{mt}$) (Wu et al., 2014), and diminished mitochondrial localization of ATF5, a master regulator of the UPR$^{mt}$ in mammals (Shpilka and Haynes, 2018) (Figures S7K and S7L). However, Atf5 knockdown did not alter IL-23 expression in GM-DCs (Figure S7M). Moreover, silencing Atf3, a transcription factor that controls the integrated stress response (Jiang et al., 2004), increased IL-23 expression in GM-DCs activated with IMQ and PA (Figure S7N).

Finally, chromatin immunoprecipitation (ChIP)-qPCR analysis revealed that CHOP and XBP1 interact with the mouse Il23a gene promoter in GM-DCs and their binding increased by treatment with IMQ and/or PA (Figure 6K). Together, these results indicate that the endoplasmic reticulum UPR (UPR$^{ER}$), rather
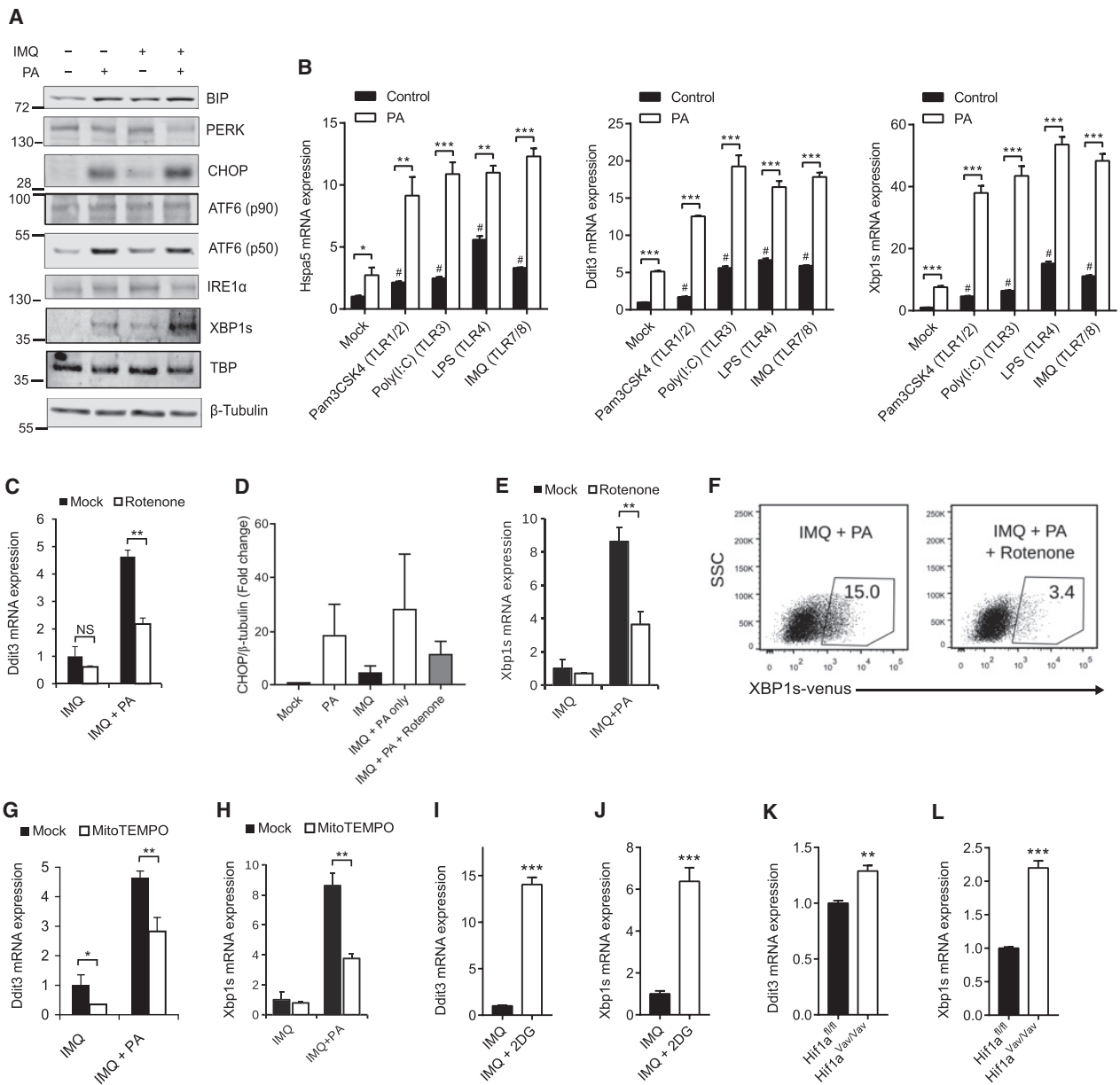
**Figure 5. PA Enhances the UPR through mtROS Generation and Inhibition of Glycolysis**

(A) Representative western blot analysis of the UPR proteins in GM-DCs treated with IMQ and PA. TBP (TATA-binding protein) and β-tubulin were used as loading controls.

(B) *Hspa5*, *Ddit3*, and *Xbp1s* expression in GM-DCs treated with various TLR ligands without PA (Control) or with PA.

(C and D) *Ddit3* expression (C) and CHOP analysis by western blot (D) in GM-DCs treated as in (A) in the presence of rotenone.

(E) *Xbp1s* expression in GM-DCs treated as in (C).

(F) Representative flow cytometric analysis of XBP1s-venus[+] GM-DCs from ER stress activated indicator (ERAI) mice treated as in (C).

(G–J) *Ddit3* (G and I) and *Xbp1s* (H and J) expression in GM-DCs treated as in (A) (G and H) or with IMQ and 2DG (I and J) in the presence of mitoTEMPO (G and H).

(K and L) *Ddit3* (K) and *Xbp1s* (L) expression in Hif1a^{fl/fl} and Hif1a[Vav/Vav] GM-DCs treated with IMQ.

n = 2–5 per group. Data are shown as mean ± SEM. *p < 0.05, **p < 0.01, ***p < 0.001 (unpaired Student's t test or one-way ANOVA with Bonferroni test). #p < 0.05 as compared to mock or control-treated cells (one-way ANOVA with Bonferroni test).

See also Figure S7 and Table S1.
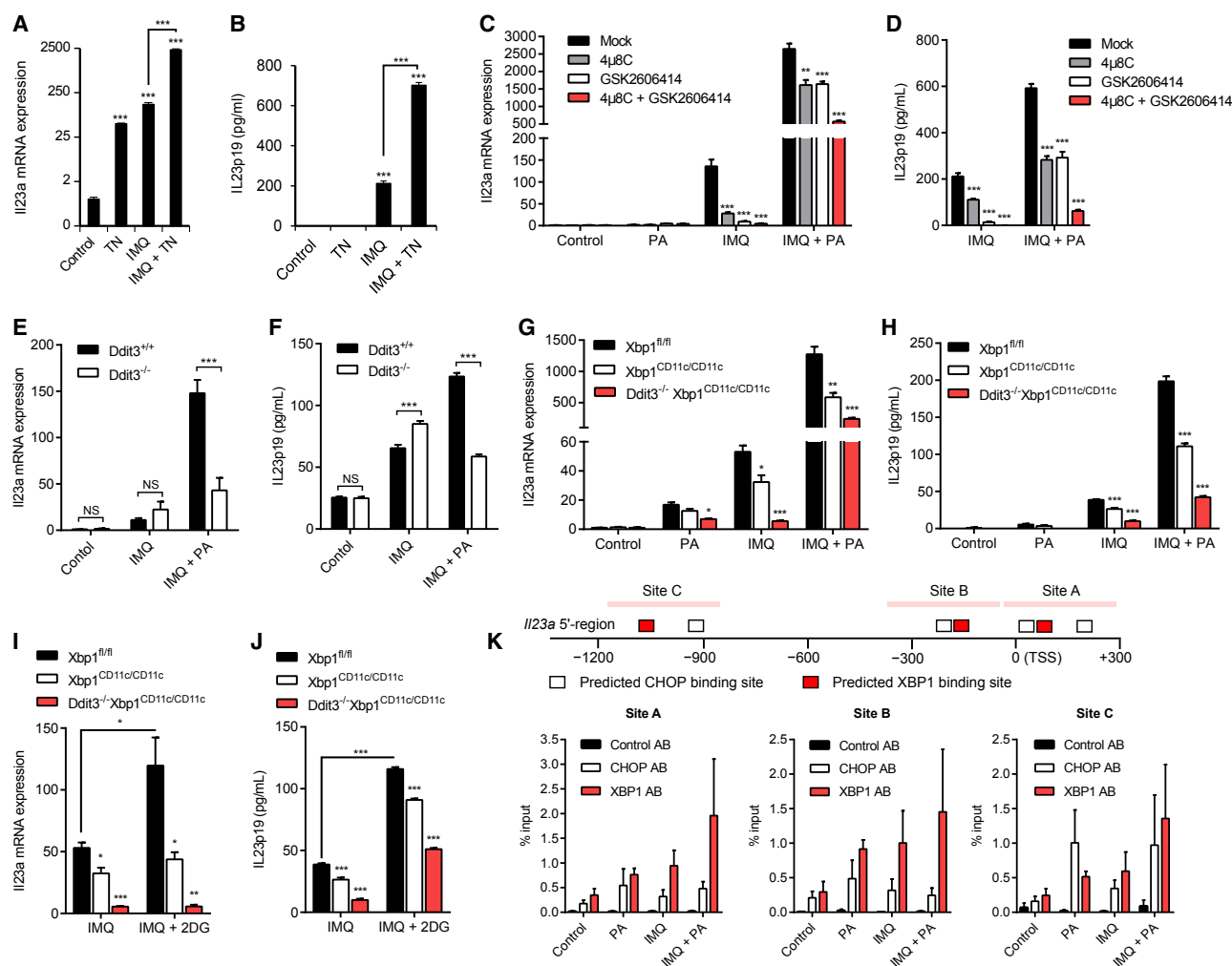
**Figure 6. PA and 2DG Increase IL-23 Expression through CHOP and XBP1s**

(A and B) *Il23a* expression (A) and IL-23p19 secretion (B) by GM-DCs activated by IMQ and treated with tunicamycin (TN).

(C and D) *Il23a* expression (C) and IL-23p19 secretion (D) by GM-DCs activated by IMQ and PA and treated with 4μ8C (IRE1α inhibitor) and/or GSK2606414 (PERK inhibitor).

(E and F) *Il23a* expression (E) and IL-23p19 secretion (F) by Ddit3$^{+/+}$ and Ddit3$^{-/-}$ GM-DCs activated by IMQ and PA.

(G–J) *Il23a* expression (G and I) and IL-23p19 secretion (H and J) by Xbp1$^{fl/fl}$, Xbp1$^{CD11c/CD11c}$, and Ddit3$^{-/-}$Xbp1$^{CD11c/CD11c}$ GM-DCs activated by IMQ and PA or 2DG.

(K) Schematic map of potential CHOP and XBP1 binding sites within the 5′ region of *Il23a* mouse gene and ChIP-qPCR analysis of XBP1 and CHOP binding to these sites in GM-DCs treated as in (C) and (D). Data are shown as percentage of DNA input enrichment for each site. TSS, transcription start site.

n = 3–5 per group. Data are shown as mean ± SEM. *p < 0.05, **p < 0.01, ***p < 0.001 (unpaired Student's t test or one-way ANOVA with Bonferroni test).

See also Figure S7 and Tables S1 and S2.

than UPR$^{mt}$ or the ATF3-dependent pathway, links metabolic adaptation to elevated extracellular FA concentrations to IL-23 expression in DCs.

### HFD Feeding Exacerbates IMQ-Mediated Inflammation through DC-Specific XBP1-Dependent Regulation of IL-23

To assess the contribution of the UPR to exacerbation of inflammatory response by HFD feeding, we evaluated IMQ-induced skin inflammation in mice harboring DC-specific XBP1 deficiency (Osorio et al., 2014). Whereas the number and

proportion of IL-23$^+$ and IL-6$^+$ cDC were not significantly lower in CD-fed Xbp1$^{CD11c/CD11c}$ mice compared to their Xbp1$^{fl/fl}$ littermates, XBP1 deficiency in cDC strongly prevented the increase in IL-23$^+$ and IL-6$^+$ cDC in response to HFD feeding in IMQ-treated mice (Figures 7A–7D). Importantly, Xbp1$^{CD11c/CD11c}$ mice displayed ameliorated IMQ-induced psoriasis-like skin inflammation but showed no obvious difference in skin morphology without IMQ treatment (Figures 7E and 7F). These results show that UPR activation in DCs contributes to TLR-mediated IL-23-driven inflammation enhanced by a high-FA environment.
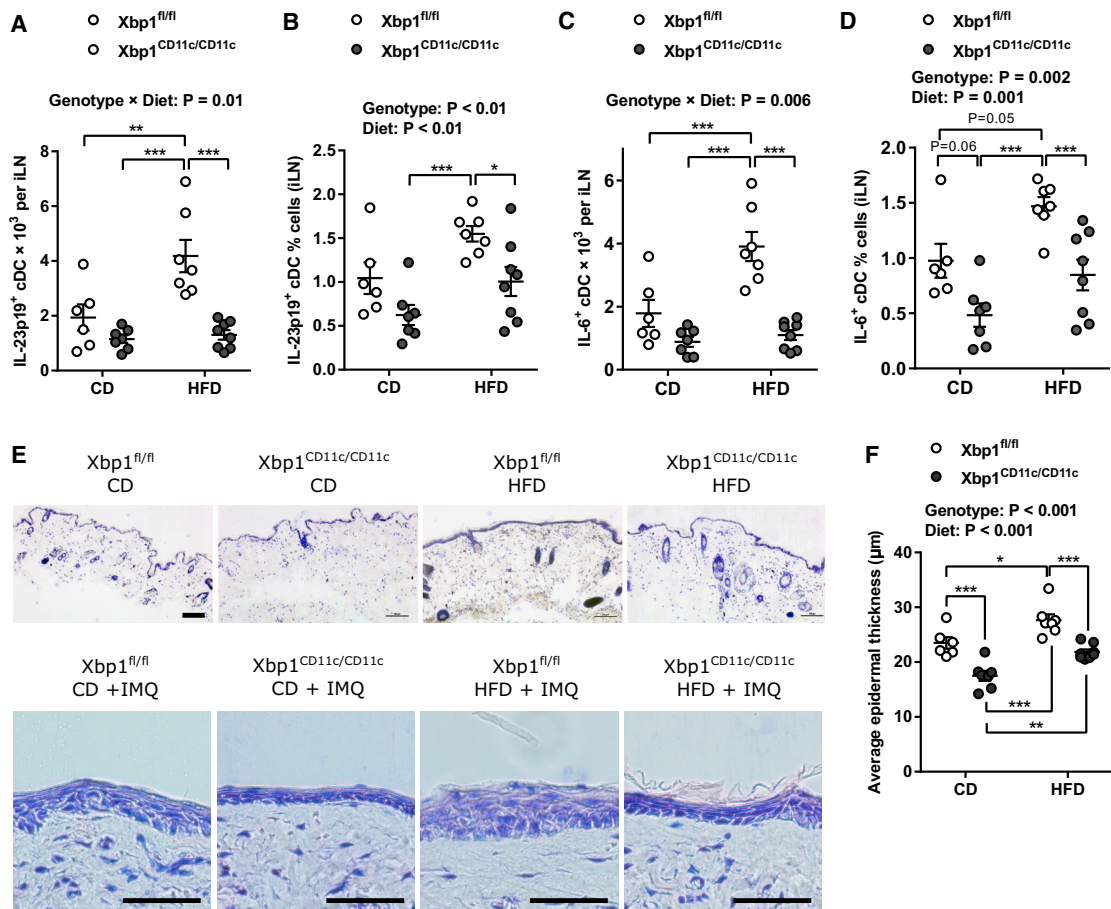
**Figure 7. HFD Feeding Exacerbates Psoriasis-like Inflammation through the Xbp1-Dependent Increase of IL-23 Expression in cDCs**

Xbp1^fl/fl and Xbp1^CD11c/CD11c littermate male mice were untreated or daily treated by application of IMQ to shaved abdominal skin during 5 days and fed CD or HFD.

(A–D) Number and proportion of IL-23$^+$ (A and B) and IL-6$^+$ (C and D) cDCs in iLNs.

(E) Representative May Grünwald Giemsa (MGG) staining of sections from abdominal skin. Scale bar 50 $\mu$m.

(F) Average epidermal thickness of abdominal skin.

n = 6–8 mice per group (IMQ treated) and n = 2 mice per group (untreated). Data are shown as mean ± SEM. *p < 0.05, **p < 0.01, ***p < 0.001 (two-way ANOVA with Tukey's post hoc test; significance of genotype and diet effects or their interaction is shown).

## DISCUSSION

Here, we demonstrate that the UPR integrates the signal driven by metabolic adaptation of activated DCs to a high-FA environment into a specific inflammatory program, characterized by elevated expression of IL-23. Upon pathogen-mediated activation via PRRs, innate immune cells must meet the high energetic demand required for anti-infectious defenses while ensuring moderate ROS levels to preserve the host from cell damage. Hence, a trade-off exists between highly effective ATP synthesis by OXPHOS and excessive mtROS production. Here, we demonstrate that, in DCs, glycolysis is sensitive to a high-FA environment at the late stage of PRR activation. Mechanistically, this metabolic adaptation to excessive FA exposure is due to the inhibition of HK activity, resulting in metabolic stress, in a decrease of carbon fluxes from glycolysis into the TCA cycle

and, ultimately, in decreased mitochondrial fitness. In turn, it increases mtROS generation and drives a distinct immune response associated with hyperactivation of the UPR. Increased IL-23 and IL-6 are hallmarks of this metabolically driven inflammatory response, and their expression is controlled by XBP1 and CHOP. IL-23 and IL-6 are known targets of NF-κB signaling upon TLR activation (Matsusaka et al., 1993; Sheikh et al., 2010). However, in our model, regulation of IL-23 by PA was not due to elevated NF-κB signaling. We also excluded the involvement of the UPR^mt and ATF3-dependent pathway in regulation of IL-23 by PA. Similarly, a recently described JNK-dependent modulation of the early TLR response by PA (Lancaster et al., 2018) did not explain the PA-dependent upregulation of IL-23 expression. On the other hand, we found that the glutamine, glutamate, and GSH axis contributes, in addition to decreased NADPH levels, to elevated mtROS levels upon PA treatment and, in

turn, to increased IL-23 expression. By contrast, our data show that itaconate is unlikely to be involved in the PA-mediated upregulation of IL-23 expression. Further studies are, however, needed to better understand such integrated reprogramming mechanisms.

Different types of TLR ligands, myeloid cell origins, and the microenvironment, as well as duration of activation, can lead to differential metabolic responses (Stienstra et al., 2017). LPS treatment rewires glycolysis and TCA cycle metabolism in macrophages (Jha et al., 2015). We found similar transcriptional and metabolic alterations in DCs activated by IMQ alone, where accumulation of non-metabolized PA and inhibited FAO suggest that FAs are likely diverted from OXPHOS to avoid activation of the ETC and generation of mtROS. It is also possible that triglyceride synthesis acts as a transient buffer for extracellular FA. However, excessive extracellular FAs likely overwhelm this protective mechanism (Chitraju et al., 2017), inhibiting HK activity and resulting in a metabolic disequilibrium and upregulation of IL-23 and IL-6.

FAO contributes to polarization of M2 macrophages (Huang et al., 2014) or tolerogenic DCs (Malinarich et al., 2015; Zhao et al., 2018), at least in the absence of an acute inflammatory stimulus. Importantly, a recent study challenged the role of FAO in M2 macrophage polarization as widely used etomoxir concentrations show multiple FAO-independent metabolic effects that are absent in genetic models of FAO deficiency (Divakaruni et al., 2018). In line, we found that the PA-mediated increase of IL-23 expression is FAO independent and rather due to direct FA-mediated inhibition of upper glycolysis in DCs. HK has been shown to be an innate immune receptor for bacterial peptidoglycan detection, and its activity controls a dialog between mitochondria and inflammasome (Wolf et al., 2016). PFKFB3 has been recently described as an important glycolytic activator controlling antiviral immune responses in macrophages (Jiang et al., 2016). Our results suggest that HK and PFKFB3 link the metabolic adaptation of glycolysis to high extracellular PA with inflammatory responses, including increased IL-23 expression. Given that glycolysis controls a specific inflammatory signature, manipulating its activity is a potential therapeutic approach to control innate inflammation.

Various TLR ligands and ROS are known UPR inducers (Grootjans et al., 2016; Martinon et al., 2010) and our data confirm these findings. Importantly, our results demonstrate a finely regulated cross-talk between the adaptation of glycolytic activity to the metabolic environment and the UPR in TLR-activated DCs. Elevated glycolytic activity and reduced mtROS generation in TLR-activated DCs are protective mechanisms that cells use to prevent excessive UPR activation upon inflammation. This hypothesis is in line with the observation that glucose utilization prevents UPR-induced neuronal damage during TLR3-induced and viral inflammation (Wang et al., 2016). The UPR has been shown to induce certain pro-inflammatory cytokines, such as IL-6, via NOD1/2—another class of PRRs (Keestra-Gounder et al., 2016). Whether a similar cross-talk also plays a role in the integration of environmental metabolic signals with PRRs, other than TLRs and Dectin-2, remains to be investigated.

Different branches of the UPR are involved in the homeostasis and the control of immune responses in DCs (Janssens et al.,

2014; Osorio et al., 2014; Tavernier et al., 2017). XBP1 regulates transcription of IL-6 and TNF in mouse macrophages (Martinon et al., 2010) and IL-23 production in human DCs in response to zymosan (Márquez et al., 2017), while CHOP increases IL-23 expression in human DCs in response to LPS and tunicamycin (Goodall et al., 2010). However, whether these effects require metabolic adaptations has not been investigated.

Our results show that XBP1 and the UPR are potential therapeutic targets for IL-23-dependent inflammatory diseases. Interestingly, a recent study identified that activation of XBP1s by lipid peroxidation results in abnormal lipid accumulation in tumor-associated DCs and inhibits their capacity to support anti-tumor T lymphocytes (Cubillos-Ruiz et al., 2015), suggesting that XBP1 provides a strong link between metabolic and immune functions in DCs.

IL-23 is a cytokine associated to protective immunity against some pathogens (Aychek et al., 2015). Moreover, IL-23 plays a role in autoimmune diseases including psoriasis, psoriatic arthritis, and ankylosing spondylitis (Pfeifle et al., 2017; Teng et al., 2015). It is likely that the mechanism of metabolic adaptation reported here is relevant to psoriasis and other IL-23-dependent pathologies. During acute inflammation, elevated FAs, produced by lipolysis in adipose tissue (Rittig et al., 2016), may potentiate IL-23 and IL-6 production by DCs, thereby promoting inflammatory effects against pathogens. The innate immune system may have evolved to utilize the UPR as a sensor of elevated FA that tunes acute inflammatory responses of DCs to the metabolic milieu. However, excessive FA in obesity and upon feeding with a HFD may result in hyperactivation of the UPR in DCs and chronically increased production of IL-23 and IL-6.

In conclusion, our results demonstrate that adaptation of the glycolysis and mtROS axis to a metabolic environment rich in FAs and ensuing hyperactivation of the UPR represents a new regulatory mechanism of the innate immune response.

## STAR★METHODS

Detailed methods are provided in the online version of this paper and include the following:

- KEY RESOURCES TABLE
- CONTACT FOR REAGENT AND RESOURCE SHARING
- EXPERIMENTAL MODEL AND SUBJECT DETAILS
    - Mice
    - Cell culture
- METHOD DETAILS
    - IMQ-induced psoriasis-like skin inflammation
    - Isolation of cells from iLN
    - Flow cytometry
    - Sorting of cDCs from iLN
    - Activation of GM-DC
    - siRNA transfection
    - 2-NBDG uptake
    - Analysis of mitochondrial content
    - Mitochondrial ROS production
    - Mitochondrial respiration assay
    - Chromatin Immunoprecipitation
    - RNA isolation

- ○ Reverse transcription and real-time PCR
- ○ Microarray analysis
- ○ Protein Analysis
- ○ Seahorse assays
- ○ Measurement of fatty acid oxidation
- ○ Metabolomics
- ○ Histology
- ● QUANTIFICATION AND STATISTICAL ANALYSES
  - ○ Statistical analyses of biological data
- ● DATA AND SOFTWARE AVAILABILITY

## SUPPLEMENTAL INFORMATION

Supplemental Information can be found online at https://doi.org/10.1016/j.cell.2019.03.018.

## AUTHOR CONTRIBUTIONS

## DECLARATION OF INTERESTS

The authors declare no competing interests.

## REFERENCES

Aychek, T., Mildner, A., Yona, S., Kim, K.-W., Lampl, N., Reich-Zeliger, S., Boon, L., Yogev, N., Waisman, A., Cua, D.J., and Jung, S. (2015). IL-23-mediated mononuclear phagocyte crosstalk protects mice from *Citrobacter rodentium*-induced colon immunopathology. Nat. Commun. *6*, 6525.

Bambouskova, M., Gorvel, L., Lampropoulou, V., Sergushichev, A., Loginicheva, E., Johnson, K., Korenfeld, D., Mathyer, M.E., Kim, H., Huang, L.-H., et al. (2018). Electrophilic properties of itaconate and derivatives regulate the IκBζ-ATF3 inflammatory axis. Nature *556*, 501–504.

Chitraju, C., Mejhert, N., Haas, J.T., Diaz-Ramirez, L.G., Grueter, C.A., Imbriglio, J.E., Pinto, S., Koliwad, S.K., Walther, T.C., and Farese, R.V., Jr. (2017). Triglyceride Synthesis by DGAT1 Protects Adipocytes from Lipid-Induced ER Stress during Lipolysis. Cell Metab. *26*, 407–418.

Chovatiya, R., and Medzhitov, R. (2014). Stress, inflammation, and defense of homeostasis. Mol. Cell *54*, 281–288.

Corcoran, S.E., and O'Neill, L.A.J. (2016). HIF1α and metabolic reprogramming in inflammation. J. Clin. Invest. *126*, 3699–3707.

Cubillos-Ruiz, J.R., Silberman, P.C., Rutkowski, M.R., Chopra, S., Perales-Puchalt, A., Song, M., Zhang, S., Bettigole, S.E., Gupta, D., Holcomb, K., et al. (2015). ER Stress Sensor XBP1 Controls Anti-tumor Immunity by Disrupting Dendritic Cell Homeostasis. Cell *161*, 1527–1538.

Divakaruni, A.S., Hsieh, W.Y., Minarrieta, L., Duong, T.N., Kim, K.K.O., Desousa, B.R., Andreyev, A.Y., Bowman, C.E., Caradonna, K., Dranka, B.P., et al. (2018). Etomoxir Inhibits Macrophage Polarization by Disrupting CoA Homeostasis. Cell Metab. *28*, 490–503.

Duan, Y., Zeng, L., Zheng, C., Song, B., Li, F., Kong, X., and Xu, K. (2018). Inflammatory Links Between High Fat Diets and Diseases. Front. Immunol. *9*, 2649.

Everts, B., Amiel, E., Huang, S.C.-C., Smith, A.M., Chang, C.-H., Lam, W.Y., Redmann, V., Freitas, T.C., Blagih, J., van der Windt, G.J.W., et al. (2014). TLR-driven early glycolytic reprogramming via the kinases TBK1-IKKε supports the anabolic demands of dendritic cell activation. Nat. Immunol. *15*, 323–332.

Fullerton, J.N., and Gilroy, D.W. (2016). Resolution of inflammation: a new therapeutic frontier. Nat. Rev. Drug Discov. *15*, 551–567.

Gaber, T., Strehl, C., and Buttgereit, F. (2017). Metabolic regulation of inflammation. Nat. Rev. Rheumatol. *13*, 267–279.

Gautier, L., Cope, L., Bolstad, B.M., and Irizarry, R.A. (2004). affy–analysis of Affymetrix GeneChip data at the probe level. Bioinformatics *20*, 307–315.

Goodall, J.C., Wu, C., Zhang, Y., McNeill, L., Ellis, L., Saudek, V., and Gaston, J.S.H. (2010). Endoplasmic reticulum stress-induced transcription factor, CHOP, is crucial for dendritic cell IL-23 expression. Proc. Natl. Acad. Sci. USA *107*, 17698–17703.

Grootjans, J., Kaser, A., Kaufman, R.J., and Blumberg, R.S. (2016). The unfolded protein response in immunity and inflammation. Nat. Rev. Immunol. *16*, 469–484.

Haas, J.T., Miao, J., Chanda, D., Wang, Y., Zhao, E., Haas, M.E., Hirschey, M., Vaitheesvaran, B., Farese, R.V., Jr., Kurland, I.J., et al. (2012). Hepatic insulin signaling is required for obesity-dependent expression of SREBP-1c mRNA but not for feeding-dependent expression. Cell Metab. *15*, 873–884.

Hotamisligil, G.S. (2017). Inflammation, metaflammation and immunometabolic disorders. Nature *542*, 177–185.

Huang, S.C.-C., Everts, B., Ivanova, Y., O'Sullivan, D., Nascimento, M., Smith, A.M., Beatty, W., Love-Gregory, L., Lam, W.Y., O'Neill, C.M., et al. (2014). Cell-intrinsic lysosomal lipolysis is essential for alternative activation of macrophages. Nat. Immunol. *15*, 846–855.

Ip, W.K.E., Hoshi, N., Shouval, D.S., Snapper, S., and Medzhitov, R. (2017). Anti-inflammatory effect of IL-10 mediated by metabolic reprogramming of macrophages. Science *356*, 513–519.

Irizarry, R.A., Hobbs, B., Collin, F., Beazer-Barclay, Y.D., Antonellis, K.J., Scherf, U., and Speed, T.P. (2003). Exploration, normalization, and summaries of high density oligonucleotide array probe level data. Biostatistics *4*, 249–264.

Iwawaki, T., Akai, R., Kohno, K., and Miura, M. (2004). A transgenic mouse model for monitoring endoplasmic reticulum stress. Nat. Med. *10*, 98–102.

Janssens, S., Pulendran, B., and Lambrecht, B.N. (2014). Emerging functions of the unfolded protein response in immunity. Nat. Immunol. *15*, 910–919.

Jha, A.K., Huang, S.C.-C., Sergushichev, A., Lampropoulou, V., Ivanova, Y., Loginicheva, E., Chmielewski, K., Stewart, K.M., Ashall, J., Everts, B., et al. (2015). Network integration of parallel metabolic and transcriptional data reveals metabolic modules that regulate macrophage polarization. Immunity *42*, 419–430.

Jiang, H.-Y., Wek, S.A., McGrath, B.C., Lu, D., Hai, T., Harding, H.P., Wang, X., Ron, D., Cavener, D.R., and Wek, R.C. (2004). Activating transcription factor 3 is integral to the eukaryotic initiation factor 2 kinase stress response. Mol. Cell. Biol. *24*, 1365–1377.

Jiang, H., Shi, H., Sun, M., Wang, Y., Meng, Q., Guo, P., Cao, Y., Chen, J., Gao, X., Li, E., and Liu, J. (2016). PFKFB3-Driven Macrophage Glycolytic Metabolism Is a Crucial Component of Innate Antiviral Defense. J. Immunol. *197*, 2880–2890.

Johnsen, L.G., Skou, P.B., Khakimov, B., and Bro, R. (2017). Gas chromatography - mass spectrometry data processing made easy. J. Chromatogr. A *1503*, 57–64.

Jørgensen, S.B., Viollet, B., Andreelli, F., Frøsig, C., Birk, J.B., Schjerling, P., Vaulont, S., Richter, E.A., and Wojtaszewski, J.F.P. (2004). Knockout of the alpha2 but not alpha1 5′-AMP-activated protein kinase isoform abolishes 5-aminoimidazole-4-carboxamide-1-beta-4-ribofuranosidebut not contraction-induced glucose uptake in skeletal muscle. J. Biol. Chem. *279*, 1070–1079.

Kanemaru, K., Matsuyuki, A., Nakamura, Y., and Fukami, K. (2015). Obesity exacerbates imiquimod-induced psoriasis-like epidermal hyperplasia and interleukin-17 and interleukin-22 production in mice. Exp. Dermatol. *24*, 436–442.

Karpe, F., Dickmann, J.R., and Frayn, K.N. (2011). Fatty acids, obesity, and insulin resistance: time for a reevaluation. Diabetes *60*, 2441–2449.

Keestra-Gounder, A.M., Byndloss, M.X., Seyffert, N., Young, B.M., Chávez-Arroyo, A., Tsai, A.Y., Cevallos, S.A., Winter, M.G., Pham, O.H., Tiffany, C.R., et al. (2016). NOD1 and NOD2 signalling links ER stress with inflammation. Nature *532*, 394–397.

Kelly, B., Tannahill, G.M., Murphy, M.P., and O'Neill, L.A.J. (2015). Metformin Inhibits the Production of Reactive Oxygen Species from NADH:ubiquinone Oxidoreductase to Limit Induction of IL-1β, and Boosts IL-10 in LPS-activated Macrophages. J. Biol. Chem. *290*, 20348–20359.

Krawczyk, C.M., Holowka, T., Sun, J., Blagih, J., Amiel, E., DeBerardinis, R.J., Cross, J.R., Jung, E., Thompson, C.B., Jones, R.G., and Pearce, E.J. (2010). Toll-like receptor-induced changes in glycolytic metabolism regulate dendritic cell activation. Blood *115*, 4742–4749.

Kuehne, A., Emmert, H., Soehle, J., Winnefeld, M., Fischer, F., Wenck, H., Gallinat, S., Terstegen, L., Lucius, R., Hildebrand, J., and Zamboni, N. (2015). Acute Activation of Oxidative Pentose Phosphate Pathway as First-Line Response to Oxidative Stress in Human Skin Cells. Mol. Cell *59*, 359–371.

Lampropoulou, V., Sergushichev, A., Bambouskova, M., Nair, S., Vincent, E.E., Loginicheva, E., Cervantes-Barragan, L., Ma, X., Huang, S.C.-C., Griss, T., et al. (2016). Itaconate Links Inhibition of Succinate Dehydrogenase with Macrophage Metabolic Remodeling and Regulation of Inflammation. Cell Metab. *24*, 158–166.

Lancaster, G.I., Langley, K.G., Berglund, N.A., Kammoun, H.L., Reibe, S., Estevez, E., Weir, J., Mellett, N.A., Pernes, G., Conway, J.R.W., et al. (2018). Evidence that TLR4 Is Not a Receptor for Saturated Fatty Acids but Mediates Lipid-Induced Inflammation by Reprogramming Macrophage Metabolism. Cell Metab. *27*, 1096–1110.

Lien, F., Berthier, A., Bouchaert, E., Gheeraert, C., Alexandre, J., Porez, G., Prawitt, J., Dehondt, H., Ploton, M., Colin, S., et al. (2014). Metformin interferes with bile acid homeostasis through AMPK-FXR crosstalk. J. Clin. Invest. *124*, 1037–1051.

Mailloux, R.J., McBride, S.L., and Harper, M.-E. (2013). Unearthing the secrets of mitochondrial ROS and glutathione in bioenergetics. Trends Biochem. Sci. *38*, 592–602.

Malinarich, F., Duan, K., Hamid, R.A., Bijin, A., Lin, W.X., Poidinger, M., Fairhurst, A.-M., and Connolly, J.E. (2015). High mitochondrial respiration and glycolytic capacity represent a metabolic phenotype of human tolerogenic dendritic cells. J. Immunol. *194*, 5174–5186.

Márquez, S., Fernández, J.J., Terán-Cabanillas, E., Herrero, C., Alonso, S., Azogil, A., Montero, O., Iwawaki, T., Cubillos-Ruiz, J.R., Fernández, N., and Crespo, M.S. (2017). Endoplasmic Reticulum Stress Sensor IRE1α Enhances IL-23 Expression by Human Dendritic Cells. Front. Immunol. *8*, 639.

Martinon, F., Chen, X., Lee, A.-H., and Glimcher, L.H. (2010). TLR activation of the transcription factor XBP1 regulates innate immune responses in macrophages. Nat. Immunol. *11*, 411–418.

Matsusaka, T., Fujikawa, K., Nishio, Y., Mukaida, N., Matsushima, K., Kishimoto, T., and Akira, S. (1993). Transcription factors NF-IL6 and NF-kappa B synergistically activate transcription of the inflammatory cytokines, interleukin 6 and interleukin 8. Proc. Natl. Acad. Sci. USA *90*, 10193–10197.

Medzhitov, R. (2001). Toll-like receptors and innate immunity. Nat. Rev. Immunol. *1*, 135–145.

Mehta, M.M., Weinberg, S.E., and Chandel, N.S. (2017). Mitochondrial control of immunity: beyond ATP. Nat. Rev. Immunol. *17*, 608–620.

Mills, E.L., Kelly, B., Logan, A., Costa, A.S.H., Varma, M., Bryant, C.E., Tourlomousis, P., Däbritz, J.H.M., Gottlieb, E., Latorre, I., et al. (2016). Succinate Dehydrogenase Supports Metabolic Repurposing of Mitochondria to Drive Inflammatory Macrophages. Cell *167*, 457–470.

Netea, M.G., Balkwill, F., Chonchol, M., Cominelli, F., Donath, M.Y., Giamarellos-Bourboulis, E.J., Golenbock, D., Gresnigt, M.S., Heneka, M.T., Hoffman, H.M., et al. (2017). A guiding map for inflammation. Nat. Immunol. *18*, 826–831.

O'Neill, L.A.J., and Pearce, E.J. (2016). Immunometabolism governs dendritic cell and macrophage function. J. Exp. Med. *213*, 15–23.

Osorio, F., Tavernier, S.J., Hoffmann, E., Saeys, Y., Martens, L., Vetters, J., Delrue, I., De Rycke, R., Parthoens, E., Pouliot, P., et al. (2014). The unfolded-protein-response sensor IRE-1α regulates the function of CD8α+ dendritic cells. Nat. Immunol. *15*, 248–257.

Oyadomari, S., Takeda, K., Takiguchi, M., Gotoh, T., Matsumoto, M., Wada, I., Akira, S., Araki, E., and Mori, M. (2001). Nitric oxide-induced apoptosis in pancreatic beta cells is mediated by the endoplasmic reticulum stress pathway. Proc. Natl. Acad. Sci. USA *98*, 10845–10850.

Paglia, G., Hrafnsdóttir, S., Magnúsdóttir, M., Fleming, R.M.T., Thorlacius, S., Palsson, B.Ø., and Thiele, I. (2012). Monitoring metabolites consumption and secretion in cultured cells using ultra-performance liquid chromatography quadrupole-time of flight mass spectrometry (UPLC-Q-ToF-MS). Anal. Bioanal. Chem. *402*, 1183–1198.

Pfeifle, R., Rothe, T., Ipseiz, N., Scherer, H.U., Culemann, S., Harre, U., Ackermann, J.A., Seefried, M., Kleyer, A., Uderhardt, S., et al. (2017). Regulation of autoantibody activity by the IL-23-T$_H$17 axis determines the onset of autoimmune disease. Nat. Immunol. *18*, 104–113.

Rittig, N., Bach, E., Thomsen, H.H., Pedersen, S.B., Nielsen, T.S., Jørgensen, J.O., Jessen, N., and Møller, N. (2016). Regulation of Lipolysis and Adipose Tissue Signaling during Acute Endotoxin-Induced Inflammation: A Human Randomized Crossover Trial. PLoS ONE *11*, e0162167.

Robey, R.B., and Hay, N. (2006). Mitochondrial hexokinases, novel mediators of the antiapoptotic effects of growth factors and Akt. Oncogene *25*, 4683–4696.

Sheikh, S.Z., Matsuoka, K., Kobayashi, T., Li, F., Rubinas, T., and Plevy, S.E. (2010). Cutting edge: IFN-gamma is a negative regulator of IL-23 in murine macrophages and experimental colitis. J. Immunol. *184*, 4069–4073.

Shpilka, T., and Haynes, C.M. (2018). The mitochondrial UPR: mechanisms, physiological functions and implications in ageing. Nat. Rev. Mol. Cell Biol. *19*, 109–120.

Smart, K.F., Aggio, R.B.M., Van Houtte, J.R., and Villas-Bôas, S.G. (2010). Analytical platform for metabolome analysis of microbial cells using methyl chloroformate derivatization followed by gas chromatography-mass spectrometry. Nat. Protoc. *5*, 1709–1729.

Smyth, G.K. (2005). limma: Linear Models for Microarray Data. In Bioinformatics and Computational Biology Solutions Using R and Bioconductor. Statistics for Biology and Health, R. Gentleman, V.J. Carey, W. Huber, R.A. Irizarry, and S. Dudoit, eds. (Springer), pp. 397–420.

Stelzner, K., Herbert, D., Popkova, Y., Lorz, A., Schiller, J., Gericke, M., Klöting, N., Blüher, M., Franz, S., Simon, J.C., and Saalbach, A. (2016). Free fatty acids sensitize dendritic cells to amplify TH1/TH17-immune responses. Eur. J. Immunol. *46*, 2043–2053.

Stienstra, R., Netea-Maier, R.T., Riksen, N.P., Joosten, L.A.B., and Netea, M.G. (2017). Specific and Complex Reprogramming of Cellular Metabolism

in Myeloid Cells during Innate Immune Responses. Cell Metab. *26*, 142–156.

Suárez-Fariñas, M., Arbeit, R., Jiang, W., Ortenzio, F.S., Sullivan, T., and Krueger, J.G. (2013). Suppression of molecular inflammatory pathways by Toll-like receptor 7, 8, and 9 antagonists in a model of IL-23-induced skin inflammation. PLoS ONE *8*, e84634.

Tannahil, G.M., Curtis, A.M., Adamik, J., Palsson-McDermott, E.M., McGettrick, A.F., Goel, G., Frezza, C., Bernard, N.J., Kelly, B., Foley, N.H., et al. (2013). Succinate is an inflammatory signal that induces IL-1β through HIF-1α. Nature *496*, 238–242.

Tavernier, S.J., Osorio, F., Vandersarren, L., Vetters, J., Vanlangenakker, N., Van Isterdael, G., Vergote, K., De Rycke, R., Parthoens, E., van de Laar, L., et al. (2017). Regulated IRE1-dependent mRNA decay sets the threshold for dendritic cell survival. Nat. Cell Biol. *19*, 698–710.

Teng, M.W.L., Bowman, E.P., McElwee, J.J., Smyth, M.J., Casanova, J.-L., Cooper, A.M., and Cua, D.J. (2015). IL-12 and IL-23 cytokines: from discovery to targeted therapies for immune-mediated inflammatory diseases. Nat. Med. *21*, 719–729.

van der Fits, L., Mourits, S., Voerman, J.S.A., Kant, M., Boon, L., Laman, J.D., Cornelissen, F., Mus, A.-M., Florencia, E., Prens, E.P., and Lubberts, E. (2009). Imiquimod-induced psoriasis-like skin inflammation in mice is mediated via the IL-23/IL-17 axis. J. Immunol. *182*, 5836–5845.

Vukovic, M., Sepulveda, C., Subramani, C., Guitart, A.V., Mohr, J., Allen, L., Panagopoulou, T.I., Paris, J., Lawson, H., Villacreces, A., et al. (2016). Adult hematopoietic stem cells lacking Hif-1α self-renew normally. Blood *127*, 2841–2846.

Wang, A., Huen, S.C., Luan, H.H., Yu, S., Zhang, C., Gallezot, J.-D., Booth, C.J., and Medzhitov, R. (2016). Opposing Effects of Fasting Metabolism on Tissue Tolerance in Bacterial and Viral Inflammation. Cell *166*, 1512–1525.

Weber, G., Convery, H.J., Lea, M.A., and Stamm, N.B. (1966). Feedback inhibition of key glycolytic enzymes in liver: action of free fatty acids. Science *154*, 1357–1360.

Weis, S., Carlos, A.R., Moita, M.R., Singh, S., Blankenhaus, B., Cardoso, S., Larsen, R., Rebelo, S., Schäuble, S., Del Barrio, L., et al. (2017). Metabolic Adaptation Establishes Disease Tolerance to Sepsis. Cell *169*, 1263–1275.

Wolf, A.J., Reyes, C.N., Liang, W., Becker, C., Shimada, K., Wheeler, M.L., Cho, H.C., Popescu, N.I., Coggeshall, K.M., Arditi, M., and Underhill, D.M. (2016). Hexokinase Is an Innate Immune Receptor for the Detection of Bacterial Peptidoglycan. Cell *166*, 624–636.

Wu, Y., Williams, E.G., Dubuis, S., Mottis, A., Jovaisaite, V., Houten, S.M., Argmann, C.A., Faridi, P., Wolski, W., Kutalik, Z., et al. (2014). Multilayered genetic and omics dissection of mitochondrial activity in a mouse reference population. Cell *158*, 1415–1430.

Zhao, F., Xiao, C., Evans, K.S., Theivanthiran, T., DeVito, N., Holtzhausen, A., Liu, J., Liu, X., Boczkowski, D., Nair, S., et al. (2018). Paracrine Wnt5a-β-Catenin Signaling Triggers a Metabolic Program that Drives Dendritic Cell Tolerization. Immunity *48*, 147–160.

# STAR★METHODS

## KEY RESOURCES TABLE

| REAGENT or RESOURCE | SOURCE | IDENTIFIER |
|---|---|---|
| **Antibodies** | | |
| GRP78 (BiP), rabbit polyclonal Ab | Abcam | Cat# ab21685; RRID:AB_2119834 |
| PERK, clone C33E10, rabbit monoclonal Ab | Cell Signaling | Cat 3192; RRID:AB_2095847 |
| IRE1$\alpha$, clone 14C10, rabbit monoclonal Ab | Cell Signaling | Cat 3294; RRID:AB_823545 |
| GADD 153 (CHOP), rabbit polyclonal Ab | Santa Cruz | Cat# sc-575; RRID:AB_631365 |
| GADD 153 (CHOP), clone B-3, mouse monoclonal Ab | Santa Cruz | Cat# sc-7351; RRID:AB_627411 |
| TBP, clone mAbcam 51841, mouse monoclonal Ab | Abcam | Cat# ab51841; RRID:AB_945758 |
| $\beta$-Tubulin, clone TUB 2.1, mouse monoclonal Ab | Sigma | Cat# T5201; RRID:AB_609915 |
| XBP-1, rabbit polyclonal Ab | Santa Cruz | Cat# sc-7160; RRID:AB_794171 |
| ATF6, clone 70B1413, mouse monoclonal Ab | Abcam | Cat# ab11909; RRID:AB_298691 |
| Hexokinase I, clone C35C4, mouse monoclonal Ab | Cell Signaling | Cat 2024; RRID:AB_2116996 |
| ATF5, clone EPR18286, rabbit monoclonal Ab | Abcam | Cat# ab184923 |
| VDAC1, clone B-6, mouse monoclonal Ab | Santa Cruz | Cat# sc-390996; RRID:AB_2750920 |
| JNK, rabbit polyclonal Ab | Cell Signaling | Cat 9252; RRID:AB_2250373 |
| Phospho-JNK, clone G9, mouse monoclonal Ab | Cell Signaling | Cat 9255; RRID:AB_2307321 |
| Normal rabbit IgG | Cell Signaling | Cat# 2729; RRID:AB_1031062 |
| CD19 PE-CF594, clone 1D3, mouse monoclonal Ab | BD Biosciences | Cat 562291; RRID:AB_11154223 |
| CD3 FITC, clone 145-2C11, hamster monoclonal Ab | BD Biosciences | Cat# 562286; RRID:AB_11153307 |
| CD64 BV711, clone X54-5/7.1, mouse monoclonal Ab | Biolegend | Cat# 139311; RRID:AB_2563846 |
| Ly6G PE-Cy7, clone 1A8, rat monoclonal Ab | Biolegend | Cat# 127618; RRID:AB_1877261 |
| MHCII IA/IE Alexa Fluor 700 | Biolegend | Cat# 107622; RRID:AB_493727 |
| CD11c APC-Cy7, clone M5/114.15.2, rat monoclonal Ab | Biolegend | Cat# 117324; RRID:AB_830649 |
| IL-6 PE, clone MP5-20F3, rat monoclonal Ab | Biolegend | Cat# 504504; RRID:AB_315338 |
| IL23p19 eFlour660, clone fc23cpg, rat monoclonal Ab | eBioscience | Cat# 50-7023-80; RRID:AB_10598203 |
| **Chemicals, Peptides, and Recombinant Proteins** | | |
| Recombinant mouse GM-CSF | PeproTech | Cat# 315-03 |
| 2-NBDG | Thermo Fisher | Cat# N13195 |
| MitoTracker Green FM | Thermo Fisher | Cat# M7514 |
| MitoSOX Red | Thermo Fisher | Cat# M36008 |
| LPS from *E. coli* | Sigma | Cat# L3024 |
| Pam3CSK4 | InvivoGen | Cat# tlrl-pms |
| Poly(I:C) | InvivoGen | Cat# tlrl-pic |
| Imiquimod | Calbiochem | Cat CAS 99001-02-6 |
| Curdlan | InvivoGen | Cat# tlrl-curd |
| Furfurman | InvivoGen | Cat# tlrl-ffm |
| SN50 | Enzo | Cat# BML-P600-0005 |
| Sodium dichloroacetate (DCA) | Tocris | Cat# 2755 |
| Triacsin C | Cayman chemical | Cat# 76896-80-5 |
| Recombinant murine TNF-$\alpha$ | PeproTech | Cat# 315-01A |
| Recombinant murine IL-1$\beta$ | PeproTech | Cat# 211-11B |
| *MitoPQ* | Abcam | Cat# ab146819 |
| Palmitic acid | Sigma | Cat# P0500 |
| Oleic acid | Sigma | Cat# O1008 |

*Continued*

| REAGENT or RESOURCE | SOURCE | IDENTIFIER |
|---|---|---|
| 2-methylhexadecanoic acid | Sigma | Cat# PH010298 |
| Linoleic acid | Sigma | Cat# L1376 |
| Octanoic acid | Sigma | O3907 |
| Bovine serum Albumin, essentially fatty acid free | Sigma | Cat# A6003 |
| Etomoxir | Sigma | Cat# E1905 |
| *2-deoxy-D-glucose* | Sigma | Cat# D6134 |
| *Rotenone* | Sigma | Cat# R8875 |
| Metformin | Sigma | Cat# D150959 |
| *MitoTEMPO* | Sigma | Cat# SML0737 |
| *4μ8C* | Tocris | Cat# 4479 |
| *GSK2606414* | Calbiochem | Cat# CAS 1337531-89-1 |
| *Tunicamycin* | Sigma | Cat# SMB00071 |
| Glucose | Sigma | Cat# G8769 |
| RIPA buffer | Cell Signaling | Cat# 9806 |
| Complete Protease inhibitor cocktail | Sigma | Cat# 000000011697498001 |
| PhosSTOP | Sigma | Cat# 00000004906845001 |
| Aldara 5% IMQ cream | Meda AB | N/A |
| Control "Lanette" cream | Fagron | Cat# 1289-511 |
| DMEM media | Thermo Fisher | Cat# 11960044 |
| HyClone Fetal calf serum (FCS) | GE Healthcare | Cat# SH30071 |
| Critical Commercial Assays | | |
| Zombie UV Fixable Viability Kit | Biolegend | Cat# 423107 |
| Ovation Pico WTA System V2 | NuGen | Cat# 3302 |
| GeneChip WT PLUS Reagent Kit | Affymetrix | Cat# 902118 |
| GeneChip WT Terminal Labeling Kit | Affymetrix | Cat# 900720 |
| GeneChip Mouse Gene 2.0 ST Array | Affymetrix | Cat# 902500 |
| Pierce Protein A/G magnetic beads | Thermo Fisher | Cat# 88802 |
| Agencourt AMPure | Beckman Coulter | Cat# A63880 |
| Mouse IL-23 DuoSet ELISA | R&D Systems | Cat# DY1887 |
| RNAaeasy Micro Kit | QIAGEN | Cat# 74004 |
| Dnase I, Rnase-free | Thermo Fisher | Cat# EN0521 |
| High-capacity cDNA reverse transcription kit | Thermo Fisher | Cat# 4319983 |
| NuPAGE LDS Sample buffer | Thermo Fisher | Cat# NP0007 |
| NuPAGE 4-12% Bis-Tris Protein Gel | Thermo Fisher | Cat# NP0321BOX |
| iBlot 2 nitrocellulose Transfer stacks | Thermo Fisher | Cat# IB23001 |
| Lactate Assay Kit | Trinity Biotech | Cat# 735-10 |
| GSH-Glo Glutathione Assay | Promega | Cat# V6911 |
| Glucose Uptake-Glo Assay | Promega | Cat# J1341 |
| Glucose-6-Phosphate Dehydrogenase Activity Assay | Cayman | Cat# 700300 |
| KDalert GAPDH Assay | Thermo Fischer | Cat# AM1639 |
| ADP/ATP Ratio Assay Kit | Abcam | Cat# ab65313 |
| Trizol reagent | Thermo Fisher | Cat# A33251 |
| Mouse Dendritic Cell Nucleofector Kit / Nucleofector II/2b | Lonza | Cat# VPA-1011 |
| Seahorse XF Cell Mito Stress Test Kit | Agilent Technologies | Cat# 103015-100 |
| Mitochondrial Respirometry Solution (MiR05) | Oroboros Instruments | # 60101-01 http://www.bioblast.at/index.php/MiR05-Kit |
| ImmunoHistoFix | Gentaur | # amp-202 |

**Continued**

| REAGENT or RESOURCE | SOURCE | IDENTIFIER |
|---|---|---|
| ImmunoHistoWax | Gentaur | # amp-201 |
| SYBR Green Master Mix | Diagenode | Cat# DMMLD2D600 |
| Deposited Data | | |
| Mouse skin microarray data | This paper | GEO: GSE68750 |
| GM-DC microarray data | This paper | GEO: GSE110962 |
| cDC microarray data | This paper | GEO: GSE110963 |
| Experimental Models: Cell Lines | | |
| Bone marrow-derived dendritic cells differentiated in the presence of GM-CSF (GM-DC) | This paper | N/A |
| Experimental Models: Organisms/Strains | | |
| Mouse: Tlr4$^{-/-}$: B6.B10ScN-Tlr4lps-del/JthJ | Institut Pasteur de Lille, France | 007227 |
| Mouse: Acod1$^{-/-}$: C57BL/6NJ-Acod1em1(IMPC)J/J | Institut Pasteur de Lille, France | MGI:5749792 |
| Mouse: Prkaa1$^{+/-}$: 129S2/SvPas-Prkaa1$^{tm1Sbj}$ | Institut Cochin, Rene Descartes University, Paris, France | MGI:3029359 |
| Mouse: Prkaa1$^{-/-}$: 129S2/SvPas-Prkaa1$^{tm1Sbj}$ | Institut Cochin, Rene Descartes University, Paris, France | MGI:3029359 |
| Mouse: Hif1a$^{Vav/Vav}$: B6.129-Hif1atm3Rsjo/J; (CBA/Ca x C57BL/10)F2-Tg(Vav1-icre)A2Kio | MRC Centre for Regenerative Medicine, University of Edinburgh, UK | N/A |
| Mouse: Hif1a$^{fl/fl}$Rosa26CreE: B6.129-Hif1atm3Rsjo/J; B6-129-Gt(ROSA)26Sortm1(cre/ERT)Nat/J; | Department of Molecular Medicine and Gene Therapy, Lund Stem Cell Center, Sweden | N/A |
| Mouse: Ddit3$^{-/-}$: B6.129S(Cg)-Ddit3tm2.1Dron/J | Division of Molecular Biology. Institute for Genome Research, Tokushima University, Japan | 005530 |
| Mouse: Xbp1$^{CD11c/CD11c}$: 129S6/SvEvTac-Xbp1tm2Glm; B6.Cg-Tg(Itgax-cre)1-1Reiz/J | VIB Center for Inflammation, Gent University, Belgium; or Department of Medicine, Weill Cornell Medical College, New York, USA | N/A |
| Mouse: Ddit3$^{-/-}$Xbp1$^{CD11c/CD11c}$: B6.129S(Cg)-Ddit3tm2.1Dron/J; 129S6/SvEvTac-Xbp1tm2Glm; B6.Cg-Tg(Itgax-cre)1-1Reiz/J | VIB Center for Inflammation, Gent University, Belgium | N/A |
| Mouse: ERAi: Tg(CAG-XBP1*/Venus)#Miur | VIB Center for Inflammation, Gent University, Belgium | MGI:4939273 |
| Mouse: Hif1a$^{Tie2/Tie2}$: B6.129-Hif1atm3Rsjo/J; (B6.Cg-Tg(Tek-cre)1Ywa/J | William Harvery Research Institutes, Queen Mary University London, UK | N/A |
| Mouse: Cpt1a$^{Itgax/Itgax}$: Cpt1atm1.1Pec; B6.Cg-Tg(Itgax-cre)1-1Reiz/J | Institute of Infection Immunology, Hannover, Germany | N/A |
| Mouse: Cpt1a$^{Zbtb46/Zbtb46}$: Cpt1atm1.1Pec; Zbtb46tm1Kmm/J | William Harvery Research Institutes, Queen Mary University London, UK | N/A |
| Mouse: WT: C57BL/6J | Charles River | 027 |
| Oligonucleotides | | |
| Mouse Cpt1a siRNA | Dharmacon | Cat# M-042456 |
| Mouse Cpt2 siRNA | Dharmacon | Cat# M-043177 |
| Mouse Pfkl siRNA | Dharmacon | Cat# M-060388 |
| Mouse Pfkp siRNA | Dharmacon | Cat# M-059341 |
| Mouse Atf3 siRNA | Dharmacon | Cat# M-058604 |
| Mouse Atf4 siRNA | Dharmacon | Cat# M-042737 |
| Mouse Atf5 siRNA | Dharmacon | Cat# M-045123 |
| Mouse Mapk8 siRNA | Dharmacon | Cat# M-040128 |
| Mouse Mapk9 siRNA | Dharmacon | Cat# M-040134 |

**Continued**

| REAGENT or RESOURCE | SOURCE | IDENTIFIER |
|---|---|---|
| Mouse Gls siRNA | Dharmacon | Cat# M-043336 |
| Mouse Gls2 siRNA | Dharmacon | Cat# M-063540 |
| SiGENOME non-targeting siRNA pool #1 | Dharmacon | Cat# D-001206 |
| Mouse Pfkfb3 siRNA | OriGene | Cat# SR416726 |
| Universal scrambled negative control siRNA | OriGene | Cat# SR30004 |
| Mouse qPCR Primers, see Table S1 | N/A | N/A |
| ChIP-qPCR Primers, see Table S2 | N/A | N/A |
| Software and Algorithms | | |
| Prism version 6 | GraphPad | N/A |
| GSEA Desktop v3.0 | Broad Institute | http://software.broadinstitute.org/gsea/index.jsp |
| Affy version 1.60.0 | Bioconductor | http://bioconductor.org/packages/release/bioc/html/affy.html |
| Limma version 3.38.3 | Bioconductor | http://bioconductor.org/packages/release/bioc/html/limma.html |
| FlowJo version 8 | Tree Star | https://www.flowjo.com/ |
| Phantasus | Artyomov Lab, Washington University in St. Louis | https://artyomovlab.wustl.edu/phantasus/ |
| Diva version 7.0 | Becton Dickinson | http://www.bdbiosciences.com/us/instruments/research/software/flow-cytometry-acquisition/bd-facsdiva-software/m/111112/overview |
| Other | | |
| High Fat Diet (HFD; 60% kcal fat) | Research diets | Cat# D12492 |

## CONTACT FOR REAGENT AND RESOURCE SHARING

Further information and requests for resources and reagents should be directed to and will be fulfilled by the Lead Contact, David Dombrowicz (david.dombrowicz@pasteur-lille.fr).

## EXPERIMENTAL MODEL AND SUBJECT DETAILS

### Mice

Wild-type male C57BL/6 mice (8 weeks of age) were purchased from Charles River Laboratories (France). Tlr4$^{-/-}$ mice were a gift from Jean-Claude Sirard (Inserm U1019, Institut Pasteur de Lille, France). Acod1$^{-/-}$ mice were a gift from Eik Hoffmann (CIIL, Institut Pasteur de Lille, France). Prkaa1$^{+/-}$ and Prkaa1$^{-/-}$ mice (Jørgensen et al., 2004) were from Institut Cochin, Université Paris Descartes, Paris, France. Hif1a$^{Vav/Vav}$ mice (Vukovic et al., 2016) and Hif1a$^{Tie2/Tie2}$ mice were from MRC Centre for Regenerative Medicine, University of Edinburgh, UK. Hif1a$^{fl/fl}$Rosa26CreER mice were from Department of Molecular Medicine and Gene Therapy, Lund Stem Cell Center, Sweden. Ddit3$^{-/-}$ mice (Oyadomari et al., 2001) were from Division of Molecular Biology, Institute for Genome Research, Tokushima University, Japan. Xbp1$^{CD11c/CD11c}$ mice (Cubillos-Ruiz et al., 2015; Osorio et al., 2014) were from VIB Center for Inflammation, Gent University, Belgium or Department of Medicine, and Weill Cornell Medical College, New York, USA. Ddit3$^{-/-}$Xbp1$^{CD11c/CD11c}$ mice (Tavernier et al., 2017) and ERAI Xbp1-venus reporter mice (Iwawaki et al., 2004) were from VIB Center for Inflammation, Gent University, Belgium. Cpt1a$^{CD11c/CD11c}$ mice (Divakaruni et al., 2018) were from Institute of Infection Immunology, Hannover, Germany. Cpt1a$^{Zbtb46/Zbtb46}$ mice were from William Harvey Research Institute, London, UK. Mice were maintained in pathogen-free environment (12:12 hr light/dark cycle, 21°C-24°C) at the Institut Pasteur de Lille. 8-12-week-old male mice were used for all experiments with ad libitum access to water and food. During the experiments, food and bedding was changed daily to prevent any accumulation of food in the cages. Mice were randomized into the different treatment and diet groups equilibrated for body weight and age. Mice were fed a control diet (CD, standard rodent chow, 5% kcal fat) or high fat diet (HFD, 60% kcal fat) for the indicated period of time. Mice with fight wounds at the skin were excluded from analyses. All experiments were performed following approval by the Ethics Committee for Animal Experimentation from Nord-Pas de Calais Region (CEEA75-n°01-2002R and APAFIS#7160-2017040313471173).

## Cell culture

Bone marrow-derived dendritic cells differentiated in the presence of GM-CSF (GM-DC) were obtained from femurs of WT, Tlr4$^{-/-}$, Prkaa1$^{+/-}$, Prkaa1$^{-/-}$, Hif1a$^{Tie2/Tie2}$, Hif1a$^{Vav/Vav}$, Ddit3$^{-/-}$, Xbp1$^{CD11c/CD11c}$, Ddit3$^{-/-}$Xbp1$^{CD11c/CD11c}$, Cpt1a$^{CD11c/CD11c}$, and ERAI Xbp1-venus reporter mice (C57BL/6 background, 8-12 weeks of age), cultured in DMEM media containing 10% fetal calf serum (FCS), 10 $\mu$M 2-mercaptoethanol, 25 mM HEPES, 10 $\mu$g/ml gentamycin and 20 ng/ml GM-CSF. Medium was refreshed every 3 days. GM-DC were used for experiments on day 14$^{th}$ of culture (mature GM-DC expressed CD11c$^+$MHCII$^+$ in > 80%–90% cells). Bone marrow-derived macrophages differentiated in the presence of M-CSF (BMDM) were obtained from femurs of WT mice (C57BL/6 background, 8 weeks of age), cultured in RPMI media containing 10% FCS, 10 $\mu$M 2-mercaptoethanol, 10 $\mu$g/ml genta-mycin and 20 ng/ml M-CSF and used at day 6. Cell viability was tested by 7AAD or trypan blue assays and was between 70%–90% of live cells depending on type of treatment.

## METHOD DETAILS

### IMQ-induced psoriasis-like skin inflammation

IMQ-induced psoriasis-like inflammation was induced as previously described (van der Fits et al., 2009). Mice were treated with a daily topical dose (62.5mg) of IMQ cream (Aldara 5%) or control "Lanette" cream, *unless stated otherwise*, on the shaved abdominal skin for 5 days and sacrificed 24 hr later. Mice were fed HFD or control chow diet for the treatment duration. In some experiments, mice were treated by metformin in drinking water (0.5g/l) (Lien et al., 2014), starting at 3 days before and during treatment with IMQ. At the time of sacrifice, skin samples were directly frozen in liquid N$_2$ for RNA isolation or fixed in Immunohistofix for histological analysis.

For bone marrow chimeras, 8 – 10 week old C57BL/6 male mice were gamma-irradiated twice with 5 Gy 3 hr apart. Mice were reconstituted 3 hr later by intravenous (i.v.) injection with marrow cells (3 10$^6$ cells) harvested from the femurs and tibias of Cpt1$^{aZbtb46/Zbtb46}$ mice and control Cpt1$^{+/+}$ WT littermates. Mice were maintained on acidified water containing Baytril (Enrofloxacin) during the critical 3-week reconstitution period. Six weeks after reconstitution, animals were fed a HFD or CD and psoriasis-like inflammation was induced by IMQ application as described.

### Isolation of cells from iLN

Mouse iLN were mechanically homogenized, passed through 70 $\mu$m filter and centrifugated at 400 g for 10 min. Cell pellets were washed two times with cold PBS and used for cell sorting or flow cytometry. For IL-23p19 staining, cells were incubated in DMEM containing brefeldin A (1$\mu$g/ml) at +37$^\circ$C, 5% CO$_2$ for 4 hr.

### Flow cytometry

Cells were stained with Zombie UV viability reagent during 15 min *at +20$^\circ$C*, washed two times with cold PBS + 0.5% BSA, incubated with Fc block and antibodies mentioned in the figure legends and the Key Resources Table in PBS + 0.5% BSA during 30 min *at +4$^\circ$C*, washed two times with cold PBS + 0.5% BSA, fixed with 1% PFA and used for flow cytometry. Flow cytometry analyses were performed on BD LSRFortessa X-20 flow cytometer. Results were acquired with the Diva software and analyzed using FlowJo software. cDC were defined as CD3$^-$CD19$^-$CD64$^-$Ly6G$^-$CD11c$^+$MHCII$^+$ cells.

### Sorting of cDCs from iLN

CD3$^-$CD19$^-$CD64$^-$Ly6G$^-$CD11c$^+$MHCII$^+$ DCs were sorted from mouse iLN using BD Influx Cell Sorter (BD Biosciences). 5-8 × 10$^5$ sorted cDC were used for RNA isolation with Arcturus Picopure RNA isolation Kit.

### Activation of GM-DC

GM-DC (5 × 10$^5$ per ml) were incubated in DMEM containing 10% FCS, 2 mM L-glutamine, 4.5 g/L glucose, and 10 $\mu$g/ml gentamycin and treated with 100 ng/ml Pam3CSK4, 10 $\mu$g/ml Poly(I:C), 100 ng/ml LPS, and 3$\mu$g/ml Imiquimod,100 $\mu$g/ml curdlan, 1 $\mu$g/ml furfur-man, 50 ng/ml TNF, 50 ng/ml IL-1$\beta$ with or without PA or other FA conjugated with BSA (0.065-0.5mM, molar ratio PA:BSA 6:1, OA:BSA 6:1) in the presence of 3 $\mu$M etomoxir, 5 mM 2-deoxyglucose, 1 $\mu$M rotenone, 5 mM metformin, 0.5 mM MitoTEMPO, 10 $\mu$M 4$\mu$8C, 2 $\mu$M GSK2606414, 1 $\mu$M tunicamycin, 100 $\mu$g/ml SN50, 5 mM dichloroacetate (DCA), 10 $\mu$M triacsin C, 10 $\mu$M or 20 $\mu$M MitoPQ as indicated in figure legends. Reagents were added to cells simultaneously with IMQ or LPS, unless stated otherwise. SN50, MitoTEMPO, GSK2606414, 4$\mu$8C, etomoxir, triacsin C and DCA were added 1 hr before other reagents. GM-DC were activated during 24 hr unless otherwise indicated.

### siRNA transfection

5 × 10$^5$ GM-DC per biological replicate were transfected with siRNA using Mouse Dendritic Cell Nucleofector Kit and Nucleofector II/2b device according to manufacturer's instructions. Cells were incubated during 48 hr in DMEM + 10% FCS and treated with IMQ and PA as described in TLR activation of GM-DC. Used siRNAs are mentioned in the figure legends and the Key Resources Table.

### 2-NBDG uptake

$5 \times 10^5$ GM-DC per biological replicate were incubated in DMEM without glucose during 1 hr following by incubation in the presence of 0.1 mM 2-NBDG during 10 min, washed two times with PBS and analyzed by flow cytometry.

### Analysis of mitochondrial content

$5 \times 10^5$ GM-DC per biological replicate were incubated in DMEM in the presence of 1 $\mu$M MitoTracker Green FM during 15 min, washed two times with PBS and analyzed by flow cytometry.

### Mitochondrial ROS production

To detect mitochondrial ROS, $5 \times 10^5$ GM-DC or cells isolated from iLN per biological replicate were incubated with 5 $\mu$M MitoSOX Red mitochondrial superoxide indicator at 37°C for 20 min in DMEM, washed two times with PBS, stained with surface antibody if indicated, and then analyzed with flow cytometry.

### Mitochondrial respiration assay

$4 \times 10^6$ GM-DC per biological replicate were placed into the O2K chambers (Oroboros Instruments) and filled with MiR05 as described on the Oroboros website (http://www.bioblast.at/index.php/MiR05). After digitonin permeabilization for 10 min, mitochondrial respiration was studied at 25°C by adding sequentially the following compounds: glutamate (10 mM) and malate (2 mM), ADP (2.5 mM), succinate (10 mM), rotenone (0.5 $\mu$M), antimycin A (2.5 $\mu$M), TMPD / Ascorbate (0.5 mM / 2 mM), cytochrome $c$ (10 $\mu$M) and sodium azide (100 mM).

### Chromatin Immunoprecipitation

$5 \times 10^6$ GM-DC per biological replicate were cross-linked with 1% PFA at room temperature for 10 min, lysed, nuclei were isolated and resuspended in 0.4 mL nuclear lysis buffer containing 0.5% SDS. Nuclei were sonicated using a Bioruptor (Diagenode) according to the manufacturer's protocol, and chromatin was immunoprecipitated with antibodies against CHOP, XBP-1, and control IgG overnight at 4°C, followed by 4 hr incubation in the presence of Protein A/G beads. After washing, bead-bound chromatin was subject to decrosslinking for 4 hr at 65°C. DNA was purified using Agencourt AMPure beads. Relative DNA enrichment was quantified and normalized to input DNA by qPCR using SYBR Green Master Mix. Primers used for ChIP are listed in Table S2.

### RNA isolation

Total RNA was isolated from GM-DC using Trizol reagent. Total RNA from sorted cDC was isolated using RNeasy Micro Kit.

### Reverse transcription and real-time PCR

500 ng of total RNA isolated from GM-DC was treated with DNase I and used to generate cDNA with High-capacity cDNA reverse transcription kit. Gene expression was measured by SybrGreen based qPCR. Results were normalized to the housekeeping genes *Hprt1* and *Rpl4*, and the $\Delta\Delta C$t method was employed for all real-time PCR analyses. Primers used for real-time PCR are listed in Table S1.

### Microarray analysis

200 ng RNA from GM-DC was amplified with GeneChip WT PLUS Reagent Kit, labeled with GeneChip WT Terminal Labeling Kit. 5 ng RNA from sorted cDC was amplified with Ovation Pico WTA Systems V2, labeled with GeneChip WT Terminal Labeling Kit. The resulting complementary RNAs were hybridized on the GeneChip Mouse Gene 2.0 ST Array (Affymetrix) according to the manufacturer's protocol. Microarray data were normalized by the Robust Multi-Average method (Irizarry et al., 2003) by using affy R package (Gautier et al., 2004). Transcripts associated with annotated genes were selected for analysis. The expression dataset was collapsed to gene levels using a max-median approach following selection of top 15000 genes with maximal average expression levels among all experimental groups using Phantasus. Differentially expressed genes were identified by using limma R package (Smyth, 2005), which uses an empirical Bayesian approach to estimate variances in moderated t tests. Raw P values were adjusted for multiple testing using the Benjamini–Hochberg procedure.

### Protein Analysis

Whole cell lysate from $1 \times 10^6$ GM-DC was extracted using RIPA lysis buffer supplemented with complete protease inhibitor cocktail and PhosSTOP phosphotase inhibitors. Proteins were diluted in Nupage LDS sample buffer, heated at 65°C for 5 min, and loaded on 4–12% NuPAGE Bis-Tris Gel. Proteins were transferred to nitrocellulose membrane using iBlot 2 Transfer stacks and blotted with commercial antibodies mentioned in the figure legends and the Key Resources Table.

### Seahorse assays

$2.5 \times 10^5$ GM-DC per well were seeded in a XF24 plate and analyzed in a Seahorse XFe24 Analyzer. Oxygen consumption rate (OCR) and extracellular acidification rate (ECAR) were measured in DMEM with 25 mM glucose and 2 mM glutamine with or without of 0.5 mM PA, before and after the sequential injection of 0.75 $\mu$M oligomycin, 1.5 $\mu$M FCCP, 1$\mu$M of rotenone/antimycin A, and

50 mM 2-deoxyglucose. Mixing, waiting, and measurement times were 4, 2, and 2 min (3, 1, and 1 min in some experiments), respectively. Measures were normalized by total protein. Basal and maximal respiration values were calculated by subtraction of OCR value after treatment of cells with rotenone and antimycin A (which corresponds to non-mitochondrial respiration) from OCR values in cells treated with glucose or with oligomycin and FCCP, respectively. Glycolysis and glycolytic capacity values were calculated by subtraction of ECAR value after treatment of cells with 2-deoxyglucose (which corresponds to non-glycolytic acidification) from ECAR values in cells treated with glucose or with oligomycin, respectively.

### Measurement of fatty acid oxidation

Fatty acid oxidation was measured as described previously (Haas et al., 2012). Briefly, $5 \times 10^5$ GM-DC per biological replicate were pre-treated for 21 hr with IMQ or IMQ + 500μM PA. Cells were then switched to oxidation media containing 1mM carnitine, 500 μM PA, and 1μCi/mL $^{14}$C-PA for 3 hr. Media was acidified with 70% perchloric acid and $CO_2$ was captured with 1N NaOH. Complete oxidation (captured $CO_2$) and incomplete oxidation (acid soluble metabolites, ASMs) were calculated by counting the NaOH and cleared, acidified media.

### Metabolomics

Metabolite extraction of GM-DC was performed on 2.5 million per well using 70°C aqueous 70% ethanol as described previously (Jha et al., 2015). Prior to collection, cells were treated with BSA (control), 500μM PA, IMQ or IMQ + 500μM PA for 24 hours. At collection, cells were placed immediately on ice, the media was removed and cells were washed three times with ice-cold PBS to remove residual media. Intracellular metabolites were extracted twice with hot ethanol using 10μM norvaline as an internal control. For LCMS, samples where dried under nitrogen flow and reconstituted in a milliQ water/acetonitrile (1:1) mixture for injection using a UPLC Acquity (Waters) separation system coupled with a Xevo G2 ToF (Waters) as described (Paglia et al., 2012) with slight modification. Compounds were ionized using an electrospray ionization source in negative mode. Data processing was performed in MATLAB (Mathworks, Inc.) using a custom made in-house protocol. Compound identification was performed using both retention time of authentic standards and accurate mass with an accepted deviation of 0.005 Da. For GCMS, samples were derivatized with methyl chloroformate as described (Smart et al., 2010) with slight modifications. Analysis was performed using GC (7890B, Agilent) coupled to a quadropole detector (59977B, Agilent) and controlled by ChemStation software (Agilent). Raw data was converted to netCDF format using Chemstation (Agilent), before processing in MATLAB R2014b (Mathworks, Inc.) using PARADISe software as described (Johnsen et al., 2017). In both cases, samples were randomized prior to injection. All MS sample processing and analysis were performed by MS-Omics, Inc. (Copenhagen, Denmark).

### Histology

Mouse skin samples were fixed in ImmunoHistoFix and embedded in ImmunoHistoWax at 37°C. 5μm sections were stained with May-Grünwald Giemsa for measurement of epidermal thickness by using a Nikon Eclipse Ti-E microscope with NIS-Elements imaging software. Average epidermal thickness was determined as a mean of 10 measures calculated for each skin sample. We did blind investigators during epidermal thickness measurement.

## QUANTIFICATION AND STATISTICAL ANALYSES

### Statistical analyses of biological data

Data are presented as mean ± SEM. We tested whether data were normally distributed by Shapiro-Wilk test and examined quantile-quantile plots. Levene's test was used to analyze homogeneity of variances. For a two-group comparison two-sided Student's t test was used. For more than two groups data were analyzed by ANOVA, or two-way ANOVA, followed by Tukey's (when we compared each group with every other group) or Sidak (when we compared groups within separate time points in repeated-measures ANOVA) post hoc tests for multiple comparisons. In case of data showing differences compared to normal distribution we applied two-sided Mann-Whitney U-test. Statistical analyses were performed with Prism 6 or R software. $p < 0.05$ was considered to be statistically significant and is presented as * $p < 0.05$, ** $p < 0.01$, *** $p < 0.001$, or **** $p < 0.0001$.

## DATA AND SOFTWARE AVAILABILITY

The accession numbers for microarray datasets reported in this paper are publicly available at the NCBI Gene Expression Omnibus under accession numbers GEO: GSE68750, GSE110962, and GSE110963.
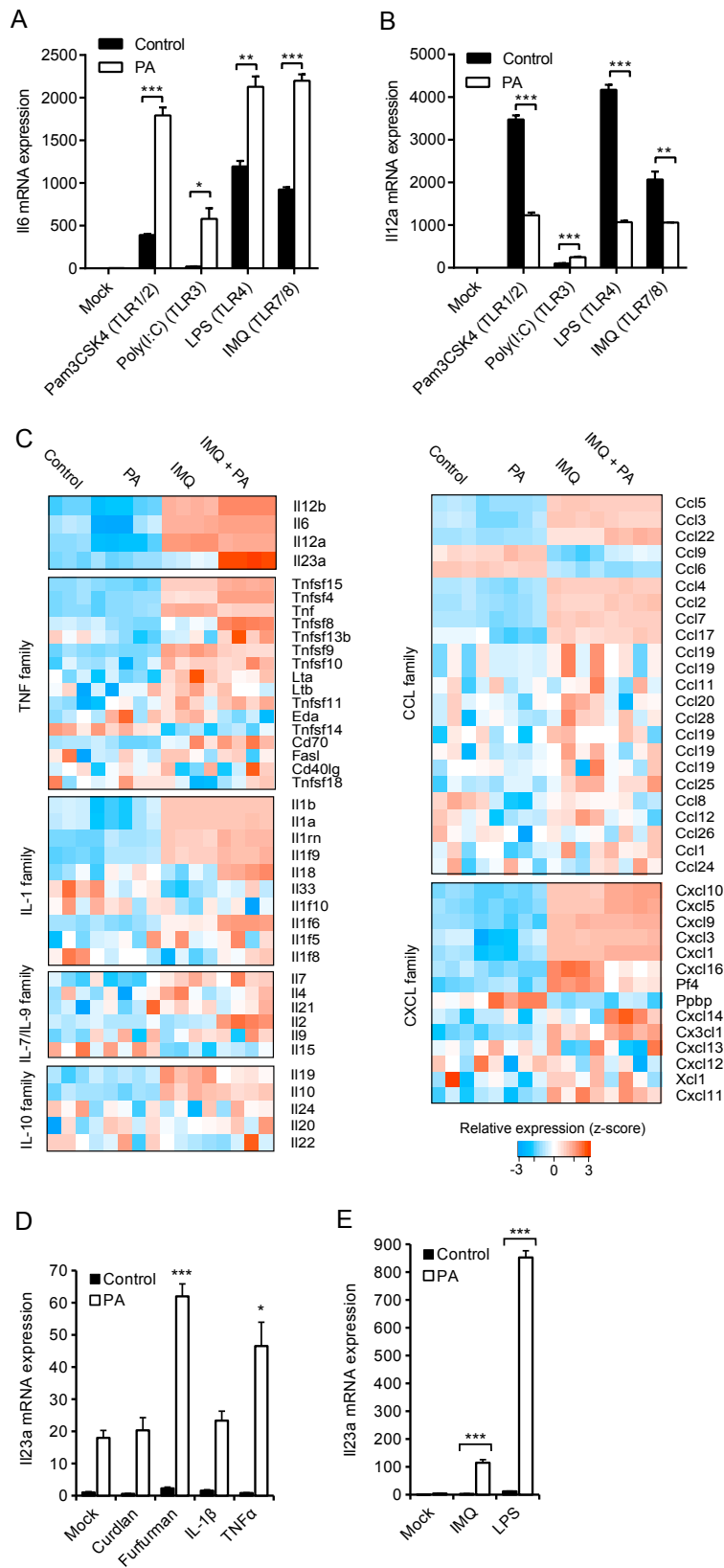
**Figure S1. PA Alters Expression of Cytokines and Chemokines in PRR-Activated DCs and Macrophages, Related to Figure 1**

(A-B) Expression of Il6 and Il12a mRNAs in GM-DC activated by indicated TLR ligands during 24 hr in fatty acid-free medium (Control) or in the presence of PA. n = 3 per group. (C) Expression of cytokine and chemokine genes in GM-DC treated as in (A-B), analyzed by microarray. Data are shown as heatmap with relative expression values (z-score). (D) Expression of Il23a mRNA in GM-DC treated with curdlan, furfurman, TNF or IL-1$\beta$ in fatty acid-free medium (Control) or in the presence of PA for 24 hr. n = 4 per group. (E) Expression of Il23a mRNA in BMDM treated with IMQ or LPS in fatty acid-free medium (Control) or in the presence of PA for 24 hr. n = 4 per group. Data are shown as mean ± SEM. *p < 0.05, **p < 0.01, ***p < 0.001 (unpaired Student's t test).
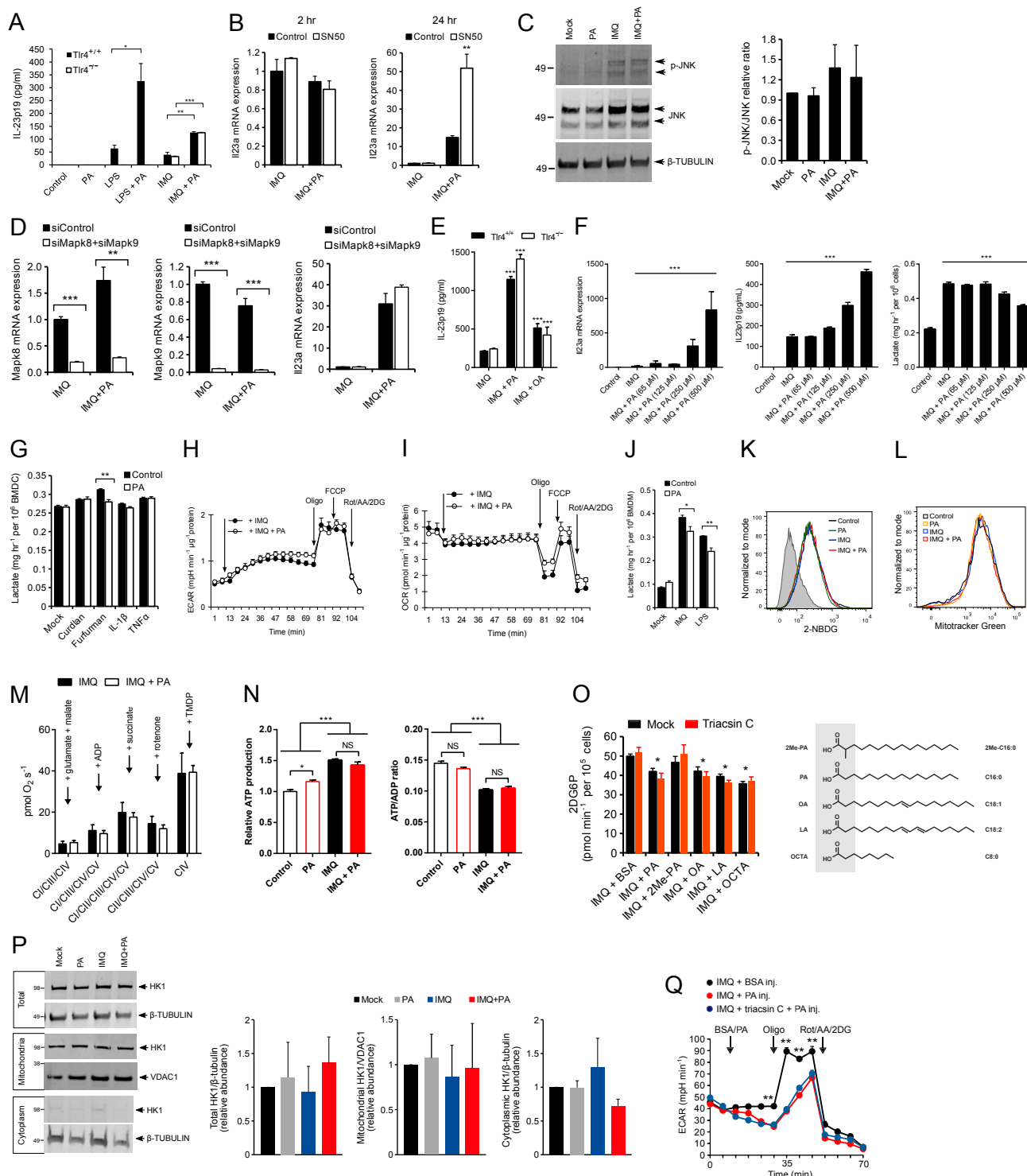
**Figure S2. PA-Mediated Regulation of IL-23 Expression in DCs and Macrophages, Related to Figure 1**

(A) IL-23p19 secretion by Tlr4$^{+/+}$ and Tlr4$^{-/-}$ GM-DC activated by IMQ or LPS during 24 hr in the presence of 0.5 mM PA. n = 3–4 per group. (B) Il23a mRNA expression in GM-DC activated with IMQ and PA for 2 or 24 hr with/without NF-κB inhibitory peptide SN50. n = 3 per group. (C) WB analysis of JNK and p-JNK in GM-DC treated with IMQ and PA for 24 hr. n = 3 per group. (D) Mapk8, Mapk9, and Il23a mRNA expression in GM-DC transfected with siRNA against Mapk8 and Mapk9 and 48 hr later activated with IMQ and PA for 24 hr. n = 4 per group. (E) Il-23p19 secretion by GM-DC activated with IMQ in the presence of PA or OA for 24 hr. n = 4 per group. (F) Il23a mRNA expression, IL-23p19 secretion, and lactate secretion by GM-DC activated by IMQ during 24 hr in fatty acid-free medium

*(legend continued on next page)*

(Control) or in the presence of indicated concentrations of PA. n = 3 per group. (G) Lactate secretion from GM-DC treated as in Figure S1D. (H-I) Real time changes of ECAR (H) and OCR (I) measured by the extracellular flux analyzer in GM-DC incubated in fatty acid-free medium in the presence on glucose after administration of IMQ alone or IMQ plus PA. Time of injection of compounds during the test is indicated by arrow. n = 4 per group. (J) Lactate secretion from BMDM treated as in Figure S1E. (K-L) GM-DC activated by IMQ in fatty acid-free medium or in the presence of PA during 24 hr. Representative flow cytometric analysis of 2-NBDG uptake (K), mitochondrial content measured by staining with Mitotracker Green (L). Data from one of three reproducible independent experiments are shown. (M) Activity of electron transport chain complexes in permeabilized cells after addition of indicated substrates and inhibitors measured as oxygen consumptions by Oxygraph-2 k high-resolution respirometry in GM-DC activated by IMQ in fatty acid-free medium or in the presence of PA and/or etomoxir during 24 hr. n = 4 per group. (N) Relative ATP production and ATP/ADP ratio in GM-DC activated by IMQ in fatty acid-free medium or in the presence of PA during 24 hr. n = 4 per group. (O) Hexokinase activity in GM-DC treated with IMQ for 24 hr and after that incubated with 0.5 mM of indicated FA for 2 hr. PA, palmitic acid (C16:0); 2Me-PA, 2-methylpalmitic acid (2Me-C16:0); OA, oleic acid (C18:1); LA, linoleic acid (C18:2); OCTA, octanoic acid (C8:0). n = 4 per group. (P) WB analysis of hexokinase 1 (HK1) protein in total cell lysates and isolated mitochondria and the cytosol from GM-DC activated with IMQ and PA fro 24 hr. n = 3 per group. (Q) ECAR in GM-DC activated with IMQ with/without triacsin C for 24 hr and injected with BSA or PA during the "Seahorse" assay. n = 4 per group. Data are shown as mean ± SEM. *p < 0.05, **p < 0.01, ***p < 0.001 (unpaired Student's t test or one-way ANOVA). NS – not significant.
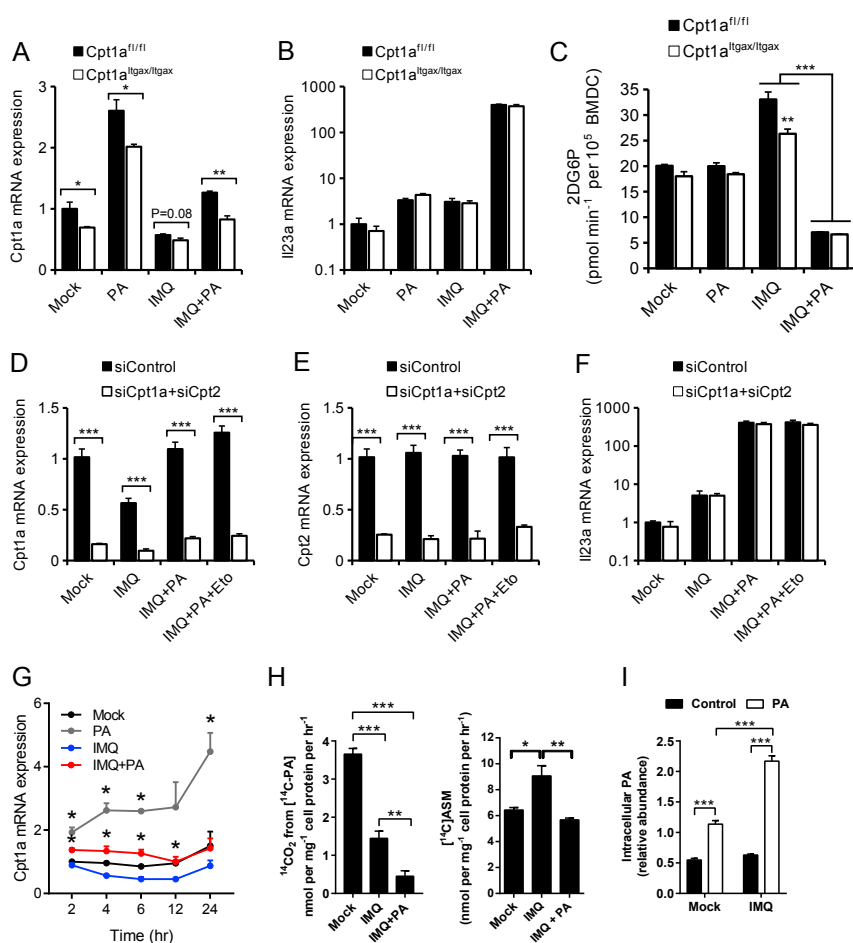
**Figure S3. FAO-Independent IL-23 Expression in DCs, Related to Figure 1**

(A-C) Cpt1a (A), Il-23a (B) mRNAs expression, and HK activity (C) in Cpt1a$^{fl/fl}$ and Cpt1a$^{Itgax/Itgax}$ GM-DC activated with IMQ and PA for 24 hr. (D-F) Cpt1a (D), Cpt2 (E), and Il23a (F) mRNA expression GM-DC transfected with control siRNA or siRNAs against Cpt1a and Cpt2, treated with or without 3 μM etomoxir (Eto) and activated with IMQ and PA for 24 hr. (G) Cpt1a mRNA expression in BMDC activated with IMQ and PA for indicated time. (H) $^{14}CO_2$ production and accumulation of 14C in the acid-soluble metabolite fraction from GM-DC treated with IMQ and PA for 20 hr and incubated with $^{14}C$-PA for consecutive 4 hr. (I) Relative abundance of intracellular PA measured by GC-MS in GM-DC treated treated with or without IMQ for 20 hr and incubated with PA for consecutive 4 hr. n = 3-6 per group. Data are shown as mean ± SEM. *p < 0.05, **p < 0.01, ***p < 0.001 by t test.
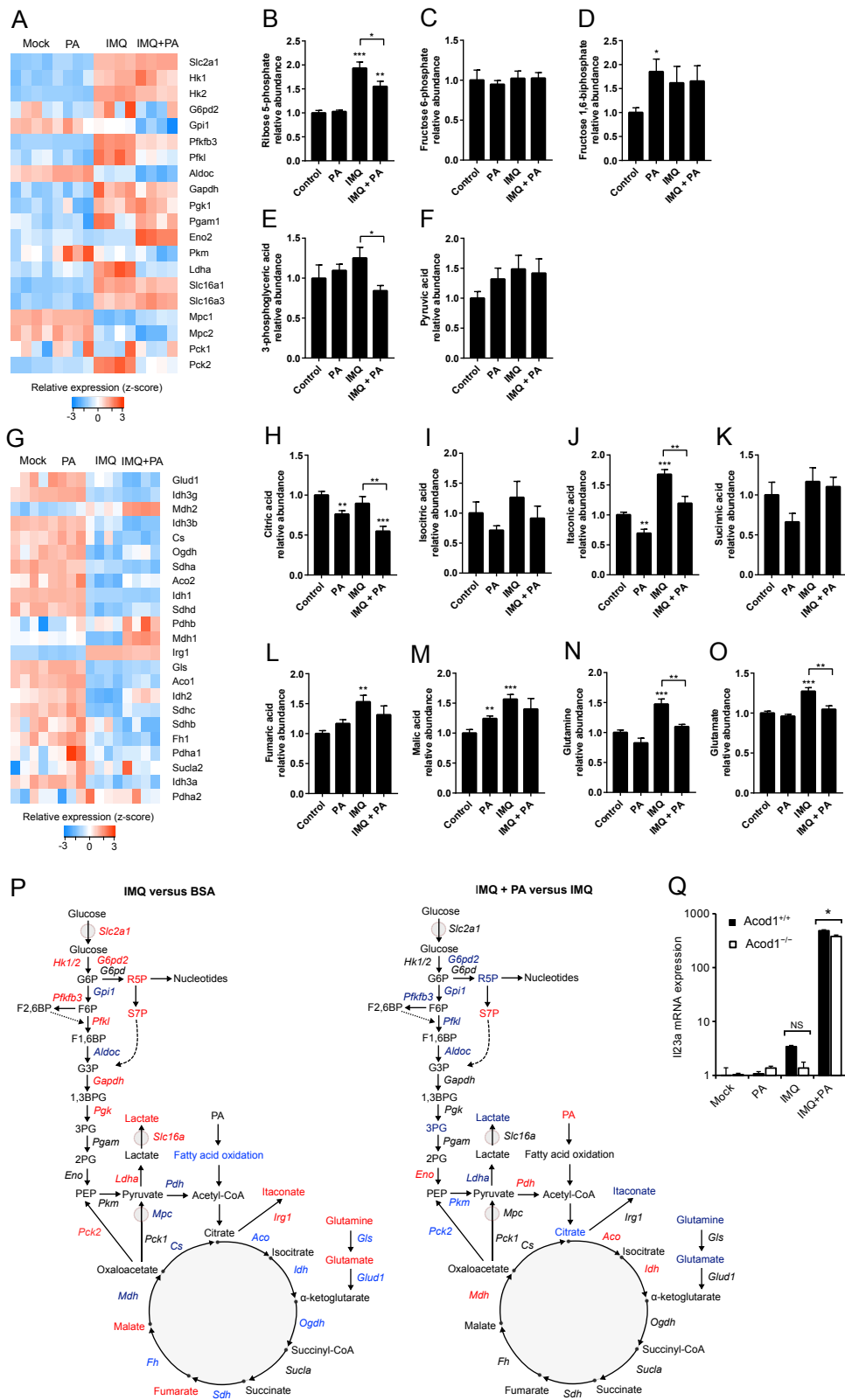
(legend on next page)

**Figure S4. Interaction between IMQ and PA Results in Rewiring of Glycolysis and TCA Cycle Metabolism in DCs, Related to Figures 1, 2, and 3**

(A-O) GM-DC activated by IMQ in fatty acid-free medium or in the presence of PA during 24 hr. Relative expression of genes controlling glycolysis (A) and TCA cycle metabolism (G) analyzed by microarray. Relative abundance of metabolites implicated in glycolysis (B-F) and TCA cycle (H-O) measured by LC-MS and GC-MS. (P) Schematic diagrams of gene and metabolite alterations in GM-DC activated by IMQ with/without PA. Upregulated genes/metabolites are shown as red, downregulated – blue. G6P, glucose 6-phosphate; F6P, fructose 6-phosphate; R5P, ribose 5-phosphate; S7P, sedoheptulose 7-phosphate; F1,6BP, fructose 1,6-bisphosphate; G3P, glyceraldehyde 3-phosphate; 1,3BPG, 1,3-bisphosphoglyceric acid; 3PG, 3-phosphoglyceric acid; 2PG, 2-phosphoglyceric acid; PEP, phosphoenolpyruvic acid. Results from n = 4-6 per group. (Q) Il23a mRNA expression in Acod1+/+ and Acod1$-/-$ GM-DC treated with IMQ and PA for 24 hr. n = 4 per group. Data are shown as mean ± SEM. *$p < 0.05$, **$p < 0.01$, ***$p < 0.001$ (unpaired Student's t test).
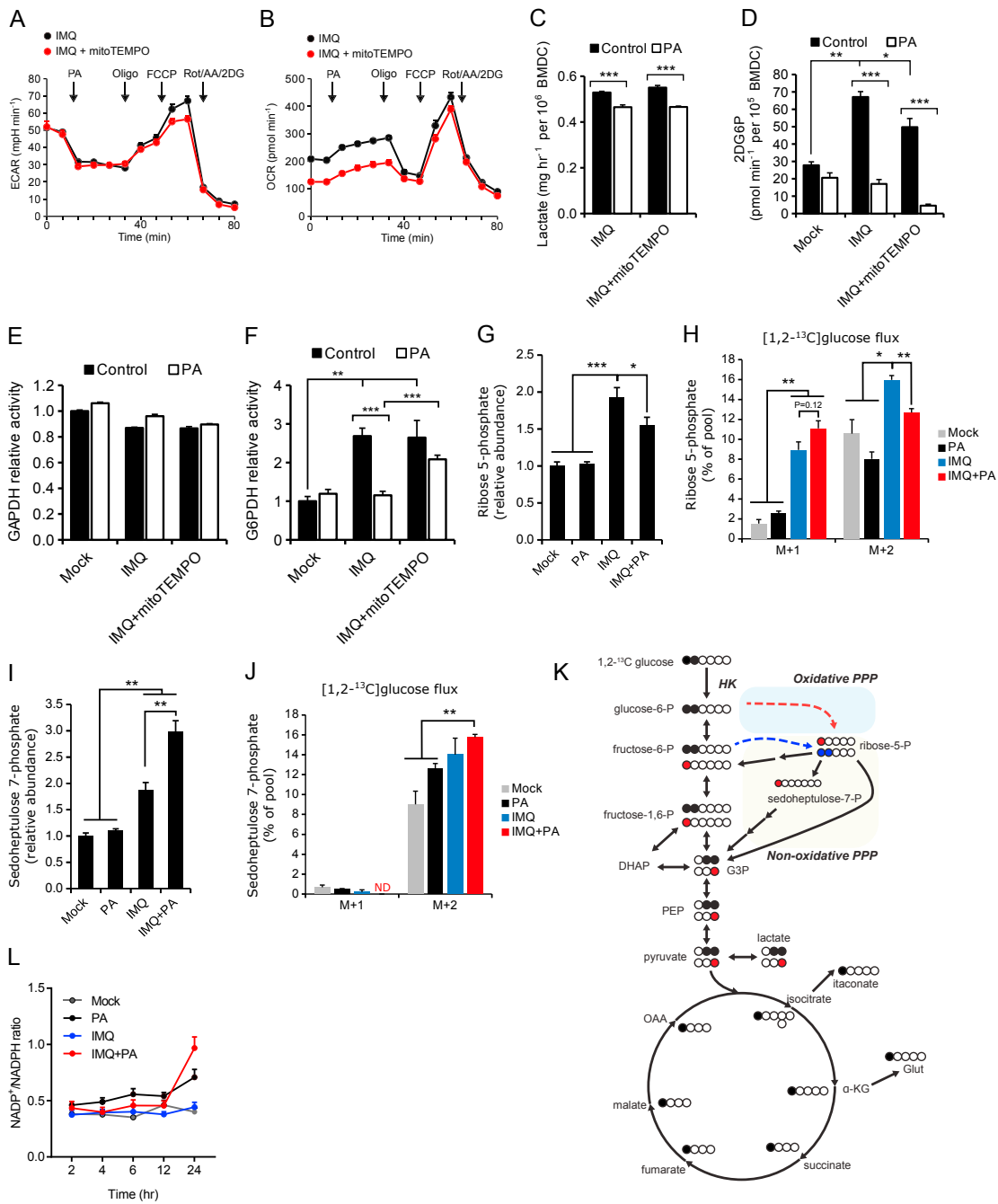
**Figure S5. Effects of PA to Glycolysis and the PPP in DCs, Related to Figure 2**

(A-B) ECAR (A) and OCR (B) in GM-DC activated by IMQ with/without mitoTEMPO for 24 hr and injected with PA during the "Seahorse" assay. n = 4 per group. (C-F) Lactate secretion (C), HK activity (D), GAPDH activity (E), G6PDH activity (F) in GM-DC activate by IMQ and PA with/without mitoTEMPO for 24 hr. n = 3-4 per group. (G-K) Relative level of ribose-5-phosphate (G), carbon flux from 1,2-$^{13}$C-glucose into ribose-5-phosphate (H), relative level of sedoheptulose-7-phosphate (I), carbon flux from 1,2-$^{13}$C-glucose into sedoheptulose-7-phosphate (J) and schematic representation of the flux (I) in GM-DC treated with IMQ and PA for 24 hr. n = 3-6 per group. (L) NADP$^+$/NADPH ratios in GM-DC treated with IMQ and PA for indicated time. n = 4 per group. Data are shown as mean ± SEM. *p < 0.05, **p < 0.01, ***p < 0.001 (unpaired Student's t test or one-way ANOVA).
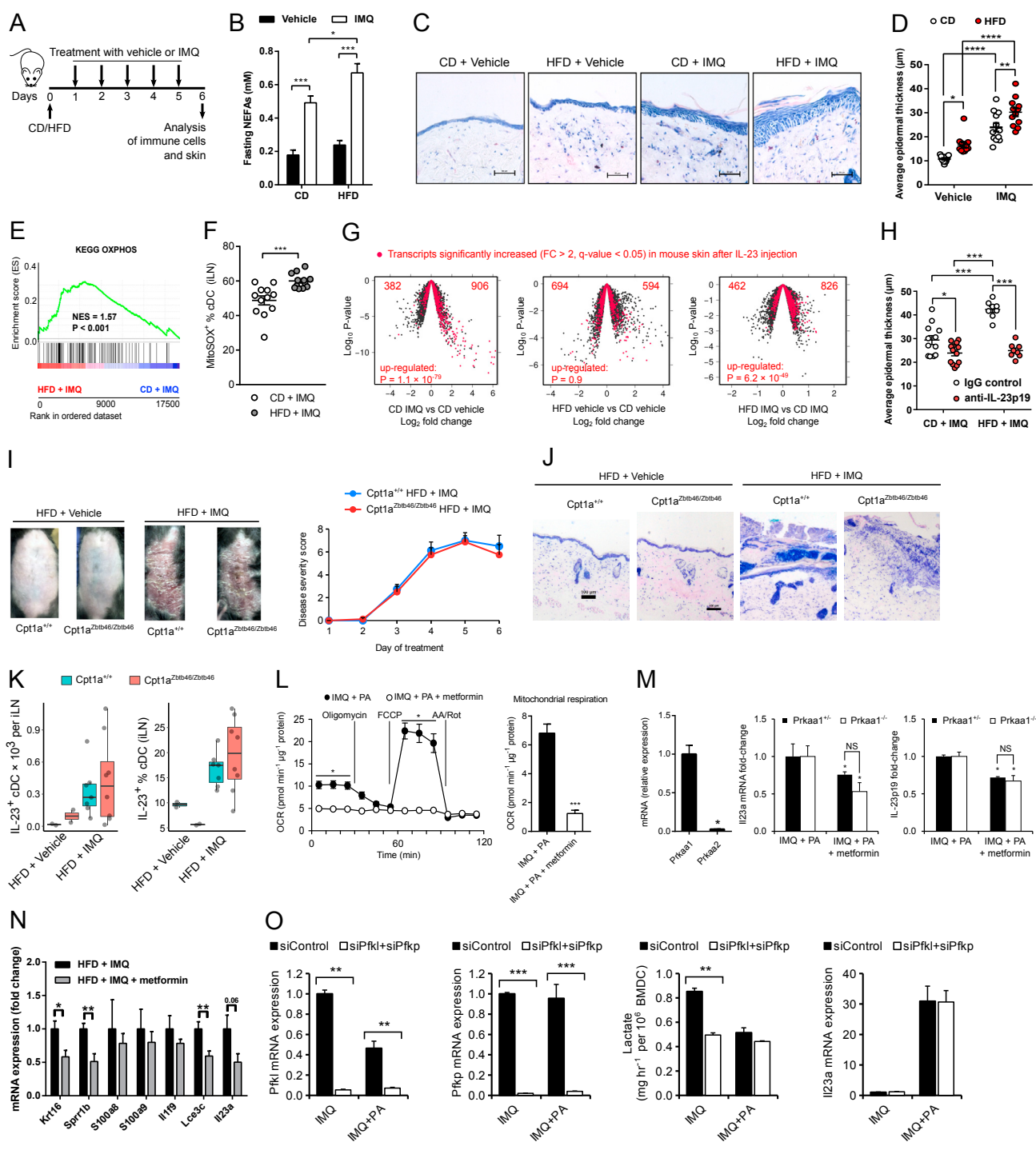
**Figure S6. HFD Feeding Exacerbates Psoriasis-like Inflammation through Accumulation of IL-23⁺ cDC in iLNs and Increased IL-23 Signaling in the Skin, Related to Figure 2**

(A-G) Male mice were treated daily by application of vehicle or IMQ to shaved abdominal skin during 5 days and fed CD or HFD. Schematic design of this experiment (A). Concentration of non-esterified fatty acids (NEFAs) in plasma after day 5 of treatment (B). Representative MGG staining of abdominal skin sections (scale bar 50 μm) (C). Average epidermal thickness of abdominal skin (D). GSEA of genes from KEGG OXPHOS pathway in cDC sorted from iLN and analyzed by microarray (E). Proportion of mitoSOX⁺ cDC in iLN (F). Volcano plots with log₂ fold change versus log₁₀ P value of all transcripts (GSE69750, gray dots), including 1288 significantly upregulated transcripts after intradermal injection IL-23 (GSE50400, fold change (FC) > 2, q-value < 0.05) (red dots). Numbers of up- and downregulated among the 1288 transcripts, and statistical significance levels of upregulation of this entire IL-23-dependent set of transcripts are

*(legend continued on next page)*

shown (G). (H) Mice were treated daily by application of IMQ to shaved abdominal skin during 5 days, injected IP with 3 mg anti-IL-23p19 neutralizing antibody or control IgG at 1st and 4th days, and fed CD or HFD. Average epidermal thickness in abdominal skin. Data are pooled from two independent experiments and shown as mean ± SEM n = 4-12 mice per group. (I-K) Irradiated C57BL/6 mice reconstituted with bone marrow from Cpt1a$^{+/+}$ or Cpt1a$^{Zbtb46/Zbtb46}$ mice and fed 6 weeks post-irradiation with CD or HFD and epicutaneously treated with vehicle- or IMQ-containing cream for 5 days. Macroscopic aspect of lesions and disease activity score (I). MGG staining of lesions (J). Numbers and per cent IL-23$^{+}$ cDC (K) in iLN. n = 2-8 mice per group. Data are shown as mean ± SEM or boxplots with median ± first-third quartiles. (L-M) GM-DC treated with IMQ and PA in the presence or absence of metformin during 24 hr. Oxygen consumption rate (OCR) and mitochondrial respiration (L), Prkaa1, Prkaa2, and Il23a mRNA expression and IL-23p19 protein secretion (M). (N) mRNA expression of indicated genes in the skin from mice treated as in Figure 2D. n = 2-4 mice per group. (O) Pfkl, Pfkp, Il23a mRNA expression and lactate secretion in GM-DC transfected with siRNA against Pfkl and Pfkp or control siRNA and 48 hr later treated with IMQ and PA for 24 hr. n = 4 per group. Data are shown as mean ± SEM. *p < 0.05, **p < 0.01, ***p < 0.001 (unpaired Student's t test or two-way ANOVA with Tukey's post hoc test). NS – not significant.
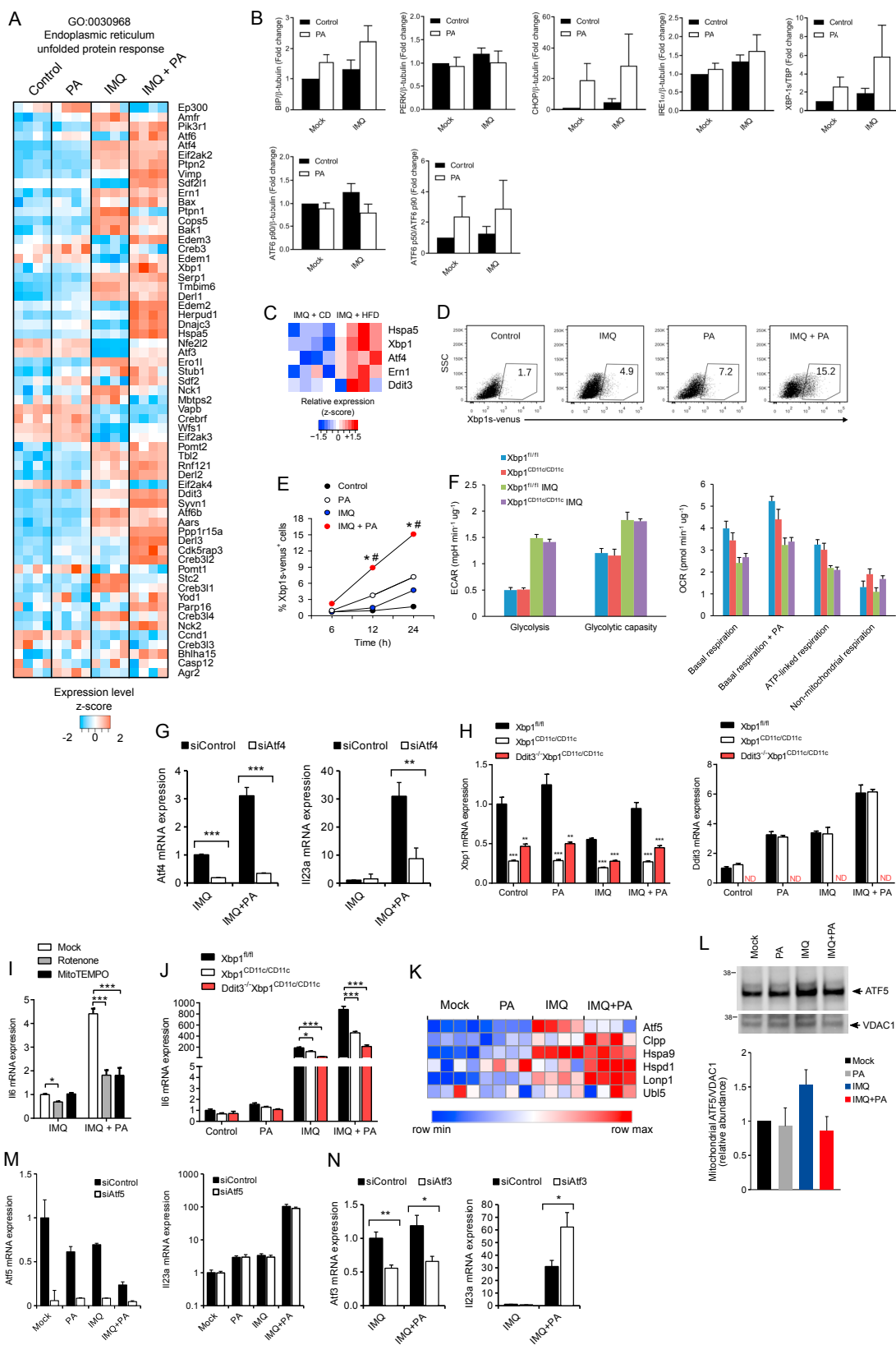
**Figure S7. PA Increases the UPR in IMQ-Activated DCs, Related to Figures 5 and 6**

(A) Heat-map with relative expression of genes from GO:0030968 "Endoplasmic reticulum unfolded protein response" analyzed by microarray analysis in GM-DC activated by IMQ in fatty acid-free medium or in the presence of PA during 24 hr. n = 4 per group. (B) Quantification of WB from Figure 5A. n = 5 per group. (C) Heat-map with relative expression of genes implicated in the UPR analyzed by microarray analysis in cDC isolated from iLN from mice treated with IMQ and fed CD or HFD. n = 4 mice per group. (D-E) GM-DC differentiated from the ER stress activated indicator (ERAI) mice. Representative flow cytometric analysis (D) and proportion (E) of Xbp1s-venus$^+$ GM-DC treated with IMQ and PA during 24 hr. n = 2 per group. #p < 0.05 versus control groups and *p < 0.05 versus IMQ groups. (F) Glycolytic and mitochondrial activities in Xbp1$^{fl/fl}$ and Xbp1$^{CD11c/CD11c}$ GM-DC activated with IMQ for 24 hr. n = 5 per group. (G) Atf4 and Il23a mRNA expression in GM-DC transfected with siRNA against Atf4 or control siRNA and 48 hr later activated by IMQ and PA for 24 hr. n = 4 per group. (H) Xbp1$^{fl/fl}$, Xbp1$^{CD11c/CD11c}$, and Ddit3$^{-/-}$Xbp1$^{CD11c/CD11c}$ GM-DC activated by IMQ in fatty acid-free medium or in the presence of PA during 24 hr. Deletion-specific qPCR forXbp1 and Ddit3 mRNA expression. n = 4 per group. (I) Il6 mRNA expression in GM-DC activated by IMQ with or without PA during 24 hr in the presence of rotenone or mitoTEMPO. n = 5 per group. (J) Il6 mRNA expression in Xbp1$^{fl/fl}$, Xbp1$^{CD11c/CD11c}$ and Ddit3$^{-/-}$Xbp1$^{CD11c/CD11c}$ GM-DC activated by IMQ with or without PA during 24 hr. n = 4 per group. (K) Expression of genes from the mitochondrial UPR transcriptional signature in GM-DC. (L) WB analysis and quantification of ATF5 in isolated mitochondria from GM-DC. n = 2 per group. (M-N) Il23a, Atf5, and Atf3 mRNA expression in GM-DC transfected with control siRNA or siRNAs against Atf5 or Atf3 and 48 hr later activated by IMQ and PA for 24 hr. n = 4 per group. Data are shown as mean ± SEM. ND – not detected.*p < 0.05, **p < 0.01, ***p < 0.001 (unpaired Student's t test), #p < 0.05 versus PA groups (unpaired Student's t test).

## A.2 Transcriptional network analysis implicates altered hepatic immune function in NASH development and resolution (Haas et al. 2019. Nat. Met. 1:604-614)

This study utilizes unbiased approach to investigate mechanisms associated to the reversible progression from nonalcoholic fattty liver (NAFL) to nonalcoholic steatohepatitis (NASH) and highlights the importance of cDC1, cDC2 and CD8+ T cells in this process [299]. Nonalcoholic fattty liver disease (NAFLD) are the most common chronic liver diseases, which are induced by lifestyle. Obesity, insulin resistance (IR), T2D are risk factors of NAFLD. NAFLD encompasse a continuum of states/stages from benign steatosis at early stages progressing to NASH, characterized by lobular inflammation, hepatocyte ballooning, and further evolving into fibrosis and cirrhosis, a major risk factor for developing hepatocellular carcinoma. Lipid accumulation in the liver affects metabolic and stress pathways in hepatocytes and, together with inflammatory processes, triggered by different immune cells, leads to NASH development. Lifestyle intervention (LSI) and bariatric surgery (BS) are the main common strategies for NASH improvement. In a large cohort of patients with histologically proven NASH, 30% of most variably expressed genes were used for weighted gene co-expression network analysis (WGCNA) along with clinical parameters. Of nine gene modules identified, four were associated with BS (Roux-en-Y gastric bypass (RYGB)), among which one displayed downregulation in LSI responders, but not in LSI non-responders. This module was picked for further analysis as containing co-expressed genes associated with reduction of NASH activity independent of body weight change. Numerous pathways enriched in this module were inflammation-related, including tumor necrosis factor alpha (TNFα) and IL-6 signaling, KRAS-signaling, coagulation, apoptosis. Fasting plasma insulin and C-reactive protein (CRP) levels were also associated with this module. A major part of the genes identified was downregulated after 1 year follow-up. These genes included those of pro-inflammatory chemokines and cytokines, cytotoxic cells, infiltration of immune cells into tissues, major histocompatibility complex (MHC)I and II. Flow cytometry analysis of blood immune populations in NASH vs non-NASH patients and unsupervised hierarchical classification of these populations revealed several clusters. Cluster 1 was associated with NASH, but not with T2D. Cluster 1 included natural killer cells, inflammatory monocytes and cells alike cDC2. Cluster 2, which was positively associated with both NASH and T2D, contained activated and cytotoxic CD8+ lymphocytes. Cluster 3 was negatively associated with NASH and included T-helper (TH)2 cells, regulatory T cell (TREG) cells, cDC1 and pDC. Populations of cells, associated with NASH correlated well with respective NASH activity hepatic gene signatures. These findings were confirmed by liver flow cytometry of diet-induced mouse model of NASH. CD8+ cells were increased upon NASH, as well as cDC2, whereas cDC1 were decreased. Presence of CD8+ T cells in histological sections of patients' livers also significantly correlated with several NASH parameters like lobular inflammation, ballooning and activity index. CD8 T lymphocytes were located mainly within inflammatory foci. In line, these cells also displayed upregulation of genes from the module associated with NASH by WGCNA, including cytotoxic genes and genes associated with antigen presentation. My contribution to this work included performing mouse diet-induced NASH model, sample collection and processing, flow cytometry and data analysis for this assay.

# Transcriptional network analysis implicates altered hepatic immune function in NASH development and resolution

Joel T. Haas [1,6], Luisa Vonghia [2,3,6*], Denis A. Mogilenko [1,6], An Verrijken[3,4],
Olivier Molendi-Coste[1], Sébastien Fleury[1], Audrey Deprince[1], Artemii Nikitin[1], Eloïse Woitrain[1],
Lucie Ducrocq-Geoffroy[1], Samuel Pic[1], Bruno Derudas[1], Hélène Dehondt[1], Céline Gheeraert[1],
Luc Van Gaal[3,4], Ann Driessen[5], Philippe Lefebvre [1], Bart Staels[1,7], Sven Francque [2,3,7] and
David Dombrowicz [1,7*]

**Progression of fatty liver to non-alcoholic steatohepatitis (NASH) is a rapidly growing health problem. The presence of inflammatory infiltrates in the liver and hepatocyte damage distinguish NASH from simple steatosis. However, the underlying molecular mechanisms involved in the development of NASH remain to be fully understood. Here we perform transcriptional and immune profiling of patients with NASH before and after lifestyle intervention (LSI). Analysis of liver microarray data from a cohort of patients with histologically assessed non-alcoholic fatty liver disease (NAFLD) reveals a hepatic gene signature, which is associated with NASH and is sensitive to regression of NASH activity on LSI independently of body weight loss. Enrichment analysis reveals the presence of immune-associated genes linked to inflammatory responses, antigen presentation and cytotoxic cells in the NASH-linked gene signature. In an independent cohort, NASH is also associated with alterations in blood immune cell populations, including conventional dendritic cells (cDC) type 1 and 2, and cytotoxic CD8 T cells. Lobular inflammation and ballooning are associated with the accumulation of CD8 T cells in the liver. Progression from simple steatosis to NASH in a mouse model of diet-driven NASH results in a comparable immune-related hepatic expression signature and the accumulation of intrahepatic cDC and CD8 T cells. These results show that NASH, compared to normal liver or simple steatosis, is associated with a distinct hepatic immune-related gene signature, elevated hepatic CD8 T cells, and altered antigen-presenting and cytotoxic cells in blood. These findings expand our understanding of NASH and may identify potential targets for NASH therapy.**

NAFLD is the most common chronic liver disease. Its increasing prevalence is driven by high-calorie diets and sedentary lifestyles. Central obesity, insulin resistance and type 2 diabetes (T2D) are strong independent risk factors of NAFLD[1,2]. NAFLD exists on a histological continuum encompassing stages ranging from isolated steatosis (NAFLD) to NASH, characterized by lobular inflammatory infiltrates, hepatocyte ballooning and cell death, to fibrosis and ultimately cirrhosis[3]. NASH development results from complex interactions of metabolic and stress pathways in hepatocytes, initiated by chronic excessive lipid accumulation, with inflammatory processes driven by various immune cell populations, collectively inducing the histological picture of an active steatohepatitis[1]. Several lesions can be present, but lobular inflammation and ballooning are the most relevant histological markers of NASH and their combination is referred to as NASH activity, clearly distinguishing the activity of the steatohepatitis from the features of steatosis[4,5].

Ballooned hepatocytes are thought to be stressed and damaged cells that lose their rectangular shape and swell due to cytoskeleton degeneration, possibly responding inadequately to pro-apoptotic and danger signals[6].

Inflammatory infiltrates within the liver lobules are a hallmark of active steatohepatitis, and specialized immune populations, both resident and infiltrating, are linked with NASH[7]. Although certain circulating and hepatic immune populations have been associated with NASH[8–10], a systematic and in-depth analysis of the cellular immune system in NASH is missing. Despite current strategies to treat NASH targeting to reduce both lobular inflammation and ballooning[11,12], the molecular mechanisms underlying these components of NASH are poorly understood. Previous studies mainly aimed to identify molecular pathways correlated with NASH versus no NASH[12,13], without distinguishing steatosis from disease activity. Functional signatures associated with NASH and the activity that distinguishes NASH from steatosis as such remain unexplored. Transcriptional signatures of NASH and its activity can be identified by comparing liver transcriptomics from patients with histologically proven lobular inflammation and ballooning versus patients with simple steatosis, as well as by longitudinally assessing regression

[1]University of Lille, Inserm, CHU Lille, Institut Pasteur de Lille, U1011-EGID, Lille, France. [2]Department of Gastroenterology and Hepatology, Antwerp University Hospital, Antwerp, Belgium. [3]Laboratory of Experimental Medicine and Paediatrics, Faculty of Medicine and Health Sciences, University of Antwerp, Antwerp, Belgium. [4]Department of Endocrinology, Diabetology and Metabolism, Antwerp University Hospital, University of Antwerp, Antwerp, Belgium. [5]Department of Pathology, Antwerp University Hospital, University of Antwerp, Antwerp, Belgium. [6]These authors contributed equally: Joel T. Haas, Luisa Vonghia, Denis A. Mogilenko. [7]These authors jointly supervised this work: Bart Staels, Sven Francque, David Dombrowicz. *e-mail: luisa.vonghia@uza.be; david.dombrowicz@pasteur-lille.fr

of NASH on LSI or bariatric surgery (BS), which can lead to NASH resolution[14,15].

Using systems biology and experimental approaches, we set out to identify gene sets associated with NASH presence and activity at baseline and whose expression is normalized in patients displaying reduced ballooning and lobular inflammation on LSI. We identify a NASH transcriptomic signature strongly enriched in genes controlling immune inflammatory processes, antigen presentation and cytotoxic cells. We further show that NASH activity is associated with altered blood immune cell populations, including cDC subsets and cytotoxic CD8 T cells. Moreover, in an obesity-driven mouse model of NASH exhibiting profound liver inflammation and hepatic damage, we also find increased hepatic expression of genes from the NASH transcriptomic signature, and altered hepatic populations of cDC and CD8 T cells. These results show that distinct immune cell populations play an important role in NASH activity and therefore constitute targets for NASH therapy.

## Results

**NASH associates with a hepatic immune-related gene module.**
Using transcriptome data[16], we first searched for groups of genes with hepatic expression patterns linked with NASH in a large cohort of obese patients with or without histologically proven NASH (Supplementary Table 1). To this end, weighted gene co-expression network analysis (WGCNA), a method allowing identification of clusters (modules) of co-expressed genes with similar expression patterns in different experimental conditions, was used[17]. WGCNA of the approximately 30% most variable hepatic transcripts across patients identified nine co-expressed gene modules (Fig. 1a,b and Supplementary Table 2). To assess whether these gene modules linked with NASH, we first analysed alterations in the modules' expression in response to improvement in NASH activity in patients with NASH at baseline and in whom a liver biopsy was available 1 year after Roux-en-Y gastric bypass (RYGB) ($n=21$, Supplementary Table 3). In agreement with the reported effects of RYGB on NAFLD[15], steatosis, lobular inflammation and ballooning were significantly reduced in these patients at 1 year after RYGB (Supplementary Table 3). Interestingly, RYGB resulted in a significant alteration in transcriptional activity of four gene modules at follow-up compared to baseline (Fig. 1c). To decipher which gene modules were associated with common mechanisms of NASH regression, rather than with transcriptional alterations in the liver due to body weight loss, we tested these modules in LSI responders (patients with NASH at baseline with decreased lobular inflammation and/or ballooning at 1 year follow-up, for details see Methods) and LSI non-responders in terms of NASH activity reduction, but who showed similar body weight loss at 1 year follow-up (Supplementary Table 4). Among the four gene modules affected by RYGB, only module 'blue' displayed significant downregulation at follow-up versus baseline in LSI responders, whereas its expression pattern hardly changed in non-responders (Fig. 1c,d).

As overall gene expression levels in module 'blue' were similarly decreased in patients with RYGB and LSI responders, but not in LSI non-responders (Fig. 1c,d), this module is associated with reduction of NASH activity, independent of body weight changes. Indeed, the change in module 'blue' expression was not correlated with percentage body weight change in either the LSI or BS groups (Supplementary Fig. 1b).

Module 'blue' included 786 transcripts (Supplementary Table 2) and was significantly enriched for inflammation-related pathways, such as complement, tumour-necrosis factor-α (TNF-α) and interleukin (IL)-6 signalling, as well as Kristen rat sarcoma virus (KRAS) signalling, coagulation and apoptosis (Fig. 1e). Moreover, fasting plasma insulin and C-reactive protein (CRP) levels were also associated with module 'blue' expression, highlighting the close link between insulin resistance, systemic inflammation and NASH (Supplementary Fig. 1c). Among the 786 transcripts in module 'blue', 507 were significantly downregulated at 1 year follow-up, including 195 transcripts significantly downregulated in both patients with RYGB and LSI responders, but not in LSI non-responders, with other transcripts being preferentially decreased in patients with RYGB (93 genes) or LSI responders (187 genes) (Fig. 1f). Most of these genes were related to immune system functions, including pro-inflammatory cytokines and chemokines, cytotoxic cells, infiltration of immune cells into tissues, and major histocompatibility complex (MHC) I and II antigen presentation (Fig. 1f). Interestingly, among key interferon-α (IFN-α)-responsive genes (*IFIT1*, *OAS1*, *MIX1* and *ISG15*), only *MX1* showed a modest, nonsignificant association with NAFLD severity at baseline and *IFIT1* was significantly increased and ISG15 decreased only after RYGB (Supplementary Fig. 1d,e).

To determine whether module 'blue' is associated with NASH and its severity in terms of activity at baseline, we correlated the expression levels of its transcripts with the NASH activity index (sum of lobular inflammation and ballooning score) in the 155 patients. Importantly, many genes from module 'blue', including immune-related genes, associated positively with activity index (Fig. 1g), suggesting links with NASH disease activity. Moreover, some of these genes were also decreased in patients with RYGB or LSI responders at 1 year follow-up (Fig. 1f). In addition, hepatic expression levels of some of these immune-related genes, for instance chemokine (C-X-C motif) ligand (*CXCL*) 9 and 10 and lysozyme (*LYZ*), were significantly higher in patients with NASH versus those with NAFL at baseline (Fig. 1h). Taken together, these results indicate that NASH regression associates with the response of a specific gene module, containing multiple co-regulated genes involved in inflammation, antigen presentation, cytotoxic response and activation of T cells.

**Blood immune cell signatures of NASH.** As the gene module 'blue' identified the immune system as a key player in NASH regression on LSI, we next assessed whether blood immune cells correlate with

**Fig. 1 | Identification of hepatic transcriptomic signature of NASH. a**, WGCNA performed with 11,784 transcripts in the liver in patients with or without histologically proven NASH ($n=155$ patients, see Supplementary Table 1). Clustering of co-expressed genes in nine gene modules. **b**, Number of transcripts in each gene module. **c**, Overall transcriptional regulation of gene modules on RYGB ($n=21$ patients), LSI in responders ($n=10$ patients) and LSI in non-responders ($n=10$ patients) at 1 year follow-up compared to baseline (see Supplementary Tables 3 and 4). $P$ values are calculated by meanrank gene set test using the geneSetTest function as described in detail in Methods. **d**, Volcano plots of average $\log_2$(fold changes) versus $P$ values (paired moderated $t$-test using limma package) of all transcripts (grey dots) and transcripts from gene module 'blue' (red dots) in patients with RYGB ($n=21$ patients), LSI responders ($n=10$ patients) and LSI non-responders at 1 year follow-up compared to baseline. **e**, Top hallmark pathways enriched in gene module 'blue' ($n=786$ transcripts), calculated using GSEA software as described in detail in Methods. **f**, Venn diagrams with transcripts in gene module 'blue' downregulated ($P<0.05$ by moderated paired $t$-test using limma package) in three groups of patients at follow-up versus baseline; immune-related genes are shown. **g**, Spearman correlations between NASH activity index and hepatic expression levels of genes in gene module 'blue' in the 155 patients at baseline; top genes with maximal positive correlation coefficients are shown. **h**, *CXCL9*, *CXCL10* and *LYZ* expression (by microarray) in patients with NAFL ($n=22$ patients) and NASH ($n=106$ patients) at baseline. Data are presented as median with first and third quartiles as the box edges. *$P<0.05$, **$P<0.01$ by unpaired two-sided Mann–Whitney $U$-test.

the presence of NASH and with its activity by performing a deep immunophenotyping analysis in patients without ($n = 17$) or with NASH ($n = 21$), stratified for T2D, a major risk factor for NASH (Supplementary Table 5). All patients were obese, with the highest

body mass index (BMI) in the no-NASH T2D group. Patients with T2D were also older than patients without T2D. Although lobular inflammation was absent, the level of steatosis was already higher in the no-NASH T2D group compared to no-NASH no-T2D
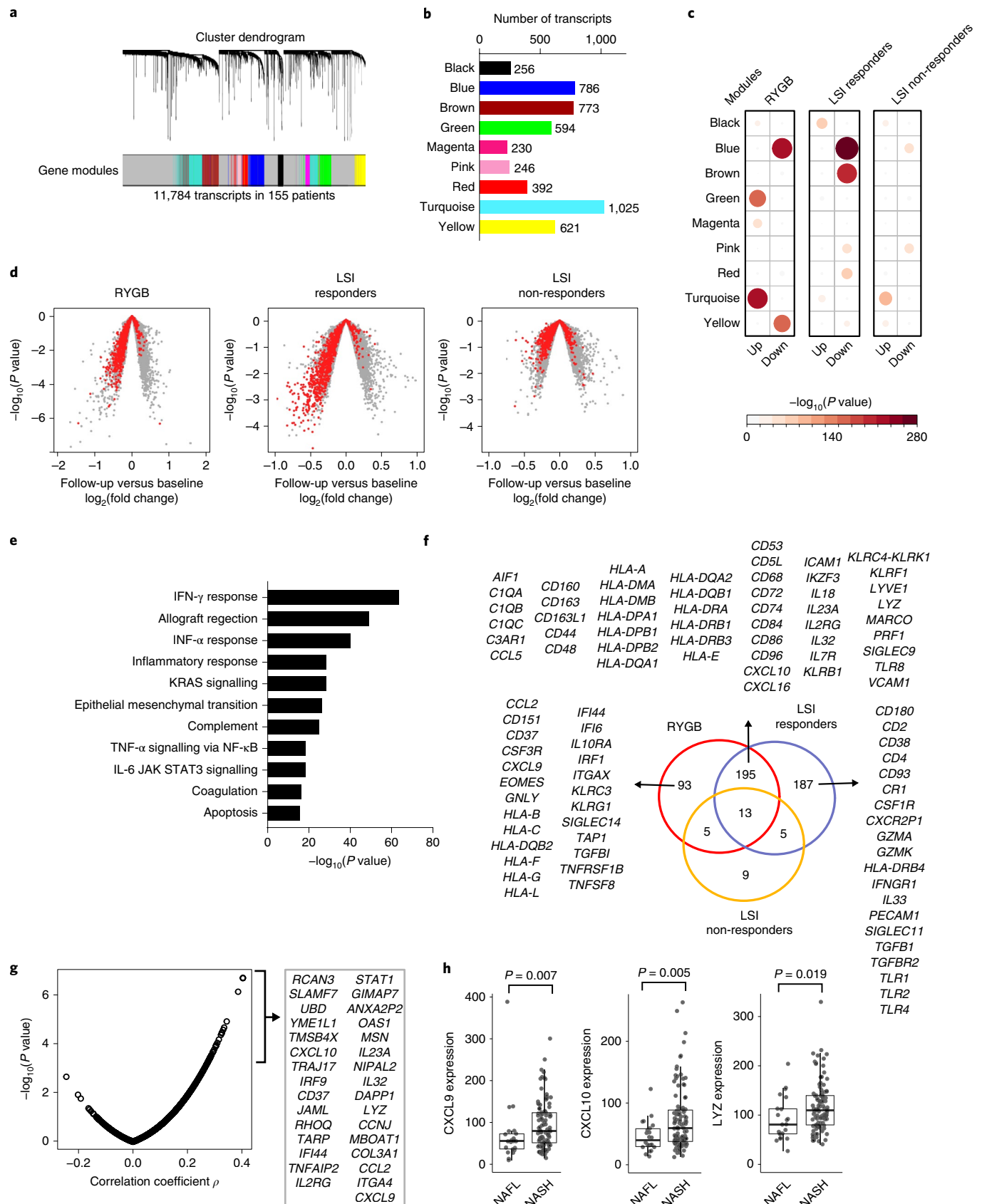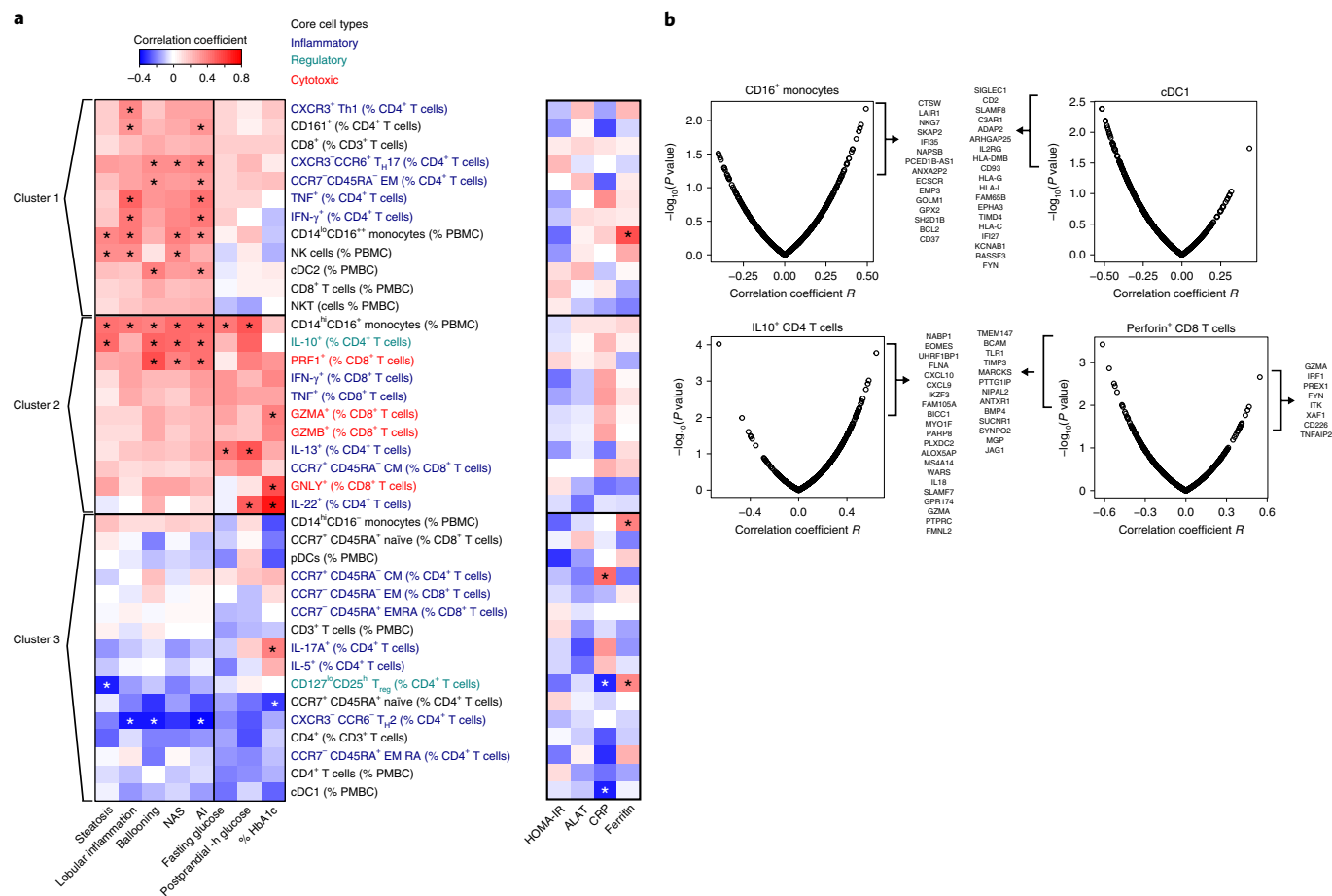
**Fig. 2 | Correlations between blood immune cell populations, disease activity in NASH and genes in module 'blue'. a**, Hierarchical clustering of correlation coefficients in 38 patients (see Supplementary Table 5) between proportions of blood immune cell populations and histological liver parameters (Spearman's correlation), T2D-associated parameters (Pearson correlation) and systemic inflammation markers (Pearson correlation). Asterisks indicate $P < 0.05$ for the given correlation. **b**, Pearson correlations between selected immune cell populations in blood from a subset of 29 patients (see Supplementary Table 5) and hepatic expression levels of genes from module 'blue'. NAS, NAFLD activity score; AI, activity index; EM, effector memory; CM, central memory; EMRA, effector memory CD45RA^{+}.

group and a few patients featured some ballooning (Supplementary Table 5), indicating that early stages of hepatocyte damage are already present in these patients.

Flow cytometry analysis of blood immune populations was performed in these 38 patients and correlations assessed between the 39 measured immune cell populations and clinical parameters (Fig. 2a and Supplementary Fig. 2). Unsupervised hierarchical clustering grouped immune cell populations based on the similarity of their correlation patterns with clinical parameters for NASH and glucose metabolism, and yielded three main clusters: Cluster 1 associated with NASH but showed weak or absent correlations with T2D; Cluster 2 positively associated with NASH and T2D; and Cluster 3 negatively correlated with most parameters specific for NASH and T2D (Fig. 2a). Within Cluster 1, NASH activity positively correlated with natural killer (NK) cells, atypical CD16^{++} monocytes and HLA-DR^{+}CD123^{-}CD11c^{+}CD141^{-} cells, similar to classical dendritic cells type 2 (cDC2). Likewise, $T_H1$ lymphocytes and NKT cells were positively associated with lobular inflammation, ballooning and NASH activity index. Immune cell populations within Cluster 2 were positively associated with lobular inflammation, ballooning, and glucose or HbA1c levels, thus linking NASH activity and T2D (Fig. 2a). Cluster 2 included pro-inflammatory CD16^{+} monocytes and IL-10^{+} CD4 T lymphocytes, the latter probably reflecting a compensatory anti-inflammatory response to increased disease activity, as previously described in mice[18]. Interestingly, within Cluster 2 we

also found activated and cytotoxic CD8 T lymphocytes correlating with NASH activity (Fig. 2a). CD8 T cells appear to be functionally linked to hepatic damage and inflammation in mouse models of NASH[10,19,20], but have not been well studied in human NASH. Cluster 3 immune cell populations were mostly negatively associated with NASH and glucose parameters. Among them are $T_H2$ lymphocytes, including IL-5^{+} cells, as well as regulatory T cells ($T_{reg}$). While cDC2 were positively associated with NASH (Cluster 1), both HLA-DR^{+}CD123^{-}CD11c^{+}CD141^{+} cDC1 and HLA-DR^{+}CD123^{+} plasmacytoid DC (pDC) were inversely correlated with NASH and glucose levels (Cluster 3). This indicates that pDC, cDC1 and cDC2 may play opposing roles in NASH. These results show that both NASH and T2D are associated with pronounced changes in blood immune cell populations, which may contribute to the high incidence of NASH in T2D.

**Blood immune cell populations correlate with liver gene signature.** Analysis of hepatic transcriptome and blood immune cell populations suggest that interplay between antigen-presenting cells (probably cDC), CD4 T cells and cytotoxic lymphocytes is linked with the presence and activity of NASH. We thus probed for correlations between blood immune cell populations and expression levels of genes from the NASH transcriptomic signature (module 'blue') in the 28 patients with both liver microarray and blood flow cytometry data. CD16^{+} monocytes correlated with elevated expression

of immune and stress genes from module 'blue' (Fig. 2b). cDC1 and cDC2 oppositely linked with NASH activity (Fig. 2a), and cDC1, but not cDC2, displayed negative associations with hepatic expression of genes involved in immune regulation and antigen presentation (Fig. 2b and data not shown). Interestingly, elevated IL-10^{+} CD4 T cells were linked with increased hepatic expression of genes related to inflammation, chemotaxis and cytotoxic responses (Fig. 2b), again indicative of a possible compensatory increase of immunoregulatory IL-10 expression in CD4 T cells in NASH. Finally, we tested correlations between genes from module 'blue' and cytotoxic CD8 T cells expressing perforin (strongly associated with NASH activity and T2D) (Fig. 2a,b). This immune cell population showed associations with hepatic genes related to cytotoxic and IFN-γ responses (*GZMA*, *CD226*, *IRF1*), T helper differentiation (*ITK*) and TNF-α signalling (*TNFAIP2*) (Fig. 2b). Taken together, these results show a remarkable similarity and associations between hepatic immune pathways predicted by gene module 'blue' and the repertoire of NASH-associated immune populations in the blood. These data suggest a cross-talk between immune cells and hepatocytes, probably via cytokines, and direct infiltration of immune cells into the liver.

**Diet-induced NASH drives increased liver cDC2 and CD8 T cells.** Next, we assessed whether lifestyle-induced NASH leads to hepatic accumulation of the immune cell populations identified in the clinical study, such as cDC and cytotoxic cells. Since disease-inducing protocols are unethical and flow cytometric analysis of hepatic immune populations in humans is challenging due to the limited tissue access, we studied liver immune cells in a diet-induced model of murine NASH. Most published NASH models used to analyse hepatic immune cells do not develop obesity[2] and hepatic immune populations have not yet been characterized in two published mouse models of obesity-associated NASH[21,22]. The diet-induced NASH model recapitulated the main known dietary drivers of this disease in humans[23,24] and displayed hallmarks of well-established NASH, such as steatosis, hepatocyte damage and lobular inflammatory infiltrates (Supplementary Fig. 3 and Supplementary Information). Flow cytometric analysis of mouse liver showed unaltered neutrophil population and decreased proportions of B lymphocytes and CLEC4F^{+} Kupffer cells, whereas inflammatory macrophages and monocytes were increased in livers of mice with NASH (Supplementary Fig. 4a–f). Hepatic NK, NKT and CD4 T cells were not affected on NASH induction, whereas hepatic FOXP3^{+} T_reg cells tended to be elevated (Supplementary Fig. 4g–j).

Systems biology analysis in humans predicted an important role of hepatic antigen-presenting cDC and cytotoxic cells in NASH regression on LSI (Fig. 1f). Interestingly, mouse CD172a^{+} cDC, phenotypically similar to human cDC2, were significantly increased in mouse livers on NASH induction (Fig. 3a,b). In contrast, NASH induction in mice led to a decrease of hepatic XCR1^{+} cDC (analogous to human cDC1) (Fig. 3a,c), driving a marked decrease in the cDC1/cDC2 ratio (Fig. 3d). This shift in cDC populations was specific to the liver, as no changes were found in these cDC subsets in the spleen (data not shown). Moreover, the proportion of CD8 T cells was significantly increased in livers of mice with NASH (Fig. 3e,f), suggesting that hepatic accumulation of CD8 T cells may be linked with antigen presentation by CD172a^{+} cDC2. These results in a lifestyle-induced NASH model corroborate the hepatic NASH gene expression and blood immune signatures in humans and indicate that hepatic accumulation of CD8 T cells and disturbance in hepatic cDC populations are the main immune hallmarks of NASH activity and progression.

Finally, we studied hepatic expression of inflammatory cytokines and chemokines in the diet-induced NASH model. NASH induction increased expression of *Tnf*, macrophage colony-stimulating factor (*Csf*)1, *Il23a*, *Il33*, C-C motif chemokine ligand (*Ccl*)2 and *Cxcl10* (Fig. 3g), with the latter four genes present in the gene expression

signature of NASH responsive to intervention (Fig. 1f). IFN-α-responsive genes *Ifit1* and *Oas1a* were also induced in NASH-diet-compared to conventional-diet-fed mice (Supplementary Fig. 3g). These data indicate that this diet-induced NASH model in mice affects the same hepatic immune populations and inflammatory pathways that are modified on regression of NASH activity induced by LSI in humans.

**Activated CD8 T cells are elevated in NASH and T2D in humans.** Given that both gene expression analysis in human livers and flow cytometric analysis in mouse livers revealed an association of cytotoxic CD8 T cells with obesity-related NASH, we next focused on these cells to better understand their potential role in NASH in humans. Indeed, both NASH and T2D enhanced the proportions of IFN-γ[+] and TNF-α[+] circulating CD8 T cells (Fig. 4a). Cytotoxic functions of CD8 T cells were also increased both in NASH and T2D as evidenced by increased expression of granzyme A and B, and perforin (Fig. 4b,c). Because T2D is a major risk factor for NASH, its effects towards CD8 T cells may link these diseases. Indeed, in the absence of NASH (no-NASH T2D group), T2D was associated with elevated expression of IFN-γ, TNF-α and cytotoxic molecules in CD8 T cells and some of these patients already displayed steatosis and ballooning. These results show that both patients with NASH and T2D have a blood signature of increased populations of activated and cytotoxic CD8 T cells, which may link these diseases.

**Hepatic CD8 T cells correlate with NASH in humans.** Finally, we investigated whether the increase of circulating cytotoxic CD8 T lymphocytes in obese patients with NASH is accompanied by an accumulation of these cells in the liver. CD8^{+} cells with lymphoid morphology were detected on sections from all groups of patients (Fig. 5a). While both NASH and T2D were associated with significantly increased levels of CD8 T lymphocytes in the liver, no further increase was observed in patients with NASH and T2D (Fig. 5b). CD8 T lymphocytes localized within inflammatory foci in the parenchymal compartment in close proximity to steatotic and ballooned hepatocytes (Fig. 5c). Liver CD8 T lymphocyte numbers showed relatively little association with steatosis, but significantly correlated with lobular inflammation, ballooning and activity index (Fig. 5d). No significant correlation was found between liver CD8 T lymphocytes and glucose levels or HbA1c (data not shown), suggesting that the T2D-associated accumulation of CD8 T lymphocytes is not driven by dysfunctional glucose metabolism. Notably, liver CD8 T lymphocytes significantly correlated with blood CD8 T lymphocytes and with the subset of perforin-expressing CD8 T cells (Supplementary Fig. 5a). Hepatic CD8 T cells also significantly correlated with expression of perforin (*PRF1*) and granzyme A (*GZMA*) in the liver, two cytotoxic genes from the module 'blue', but not granzyme B (*GZMB*) and granulysin (*GNLY*) (Supplementary Fig. 5b). Finally, we found that hepatic CD8 T cells positively correlated with expression levels of multiple genes from module 'blue', including genes related to T cells (*CD2*, *CD226*), cytotoxic responses (*KLRC4-KLRK1*) and MHCII-mediated antigen presentation (*HLA-DQB1*) (Fig. 5e). Interestingly, the strongest correlation with hepatic CD8 T cells was observed for *PTPN22* (protein tyrosine phosphatase, non-receptor type 22), which controls T-cell receptor (TCR) responsiveness and is associated with inflammatory and autoimmune diseases in humans[25]. Taken together, these results indicate that disease activity (lobular inflammation and ballooning) in NASH is associated with the accumulation of CD8 T lymphocytes in the liver. Moreover, hepatic CD8 T cells are linked to an increased expression of genes from the signature of active NASH. Thus, hepatic gene expression and immune signatures of NASH activity regression reveals CD8 T cells as a potential target to control hepatic inflammation, cytotoxic responses in the liver and NASH activity.
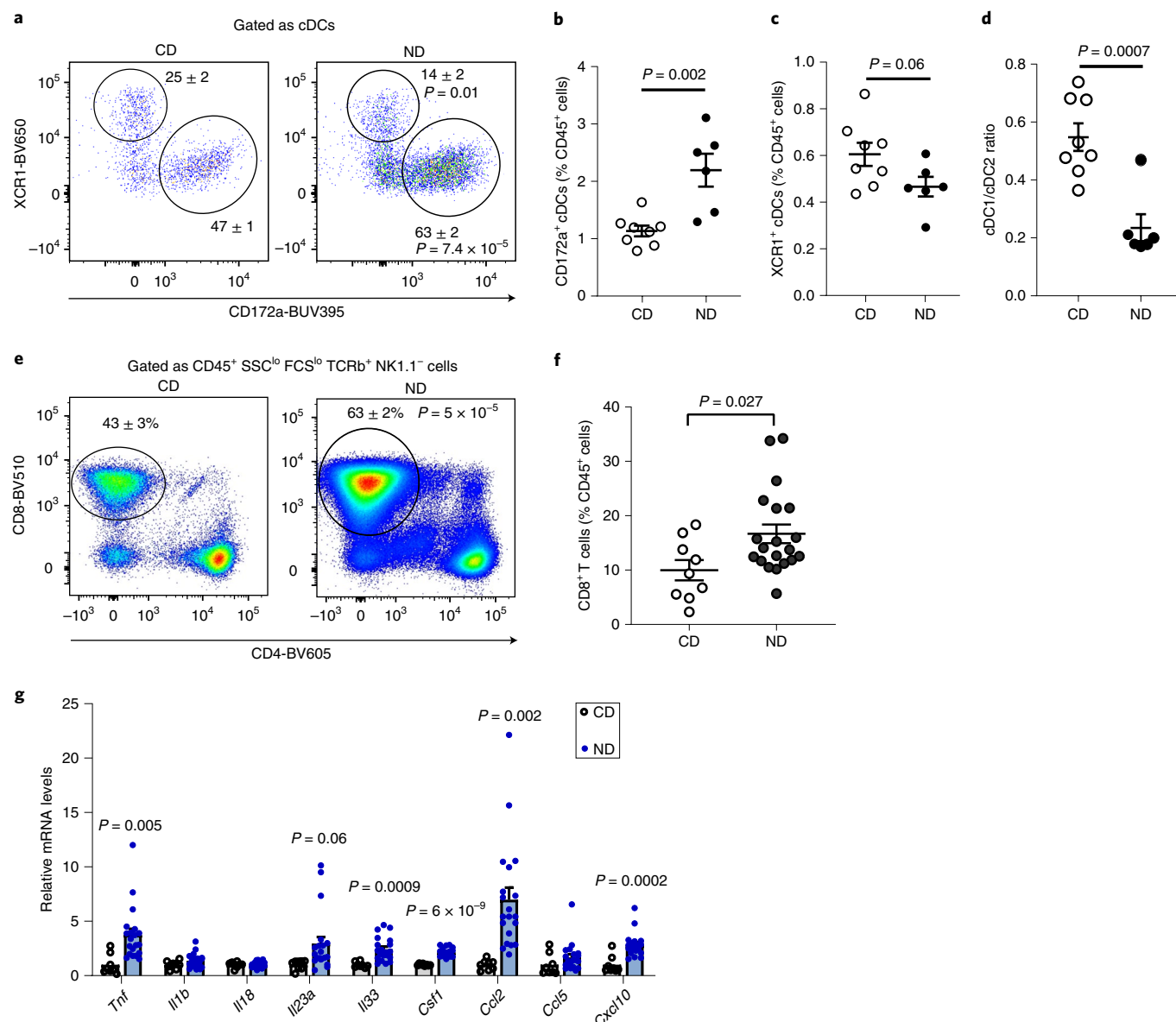
**Fig. 3 | A diet-induced NASH model alters cDC and CD8 T cells and inflammation in the liver.** Male C57BL/6J mice were fed conventional diet (CD) or NASH-diet (ND) for 24 weeks (see Supplementary Information). **a**, Representative flow cytometry plots of cDC in the liver: proportions of XCR1+ and CD172a+ of total cDC are shown (n = 8 mice CD; n = 6 mice ND). **b**, CD172a+ cDC2 cells as a proportion of CD45+ cells (n = 8 mice CD; n = 6 mice ND). **c**, XCR1+ cDC1 cells as a proportion of CD45+ cells (n = 8 mice CD; n = 6 mice ND). **d**, Ratio of cDC1/cDC2 cells (n = 8 mice CD; n = 6 mice ND). **e**, Representative flow cytometry plots of TCR-β+ T cells in the liver: proportions of CD4+ and CD8+ of total TCR-β+ T cells are shown. **f**, The proportion of CD8+ T cells of CD45+ immune cells in the liver (n = 9 mice CD; n = 20 mice ND). **g**, Quantitative PCR analysis of inflammatory gene expression in mouse livers (n = 9 mice CD; n = 20 mice ND). Data are shown as mean ± s.e.m. Statistical significance of differences between groups was analysed by unpaired two-sided t-test. mRNA, messenger RNA.

## Discussion

The global epidemic of NASH is an important health problem, as effective pharmacological approaches to treat NASH are not yet available. LSI and BS are the best available strategies to reduce NASH activity in some patients[14,15,26]. Here, we identify a hepatic transcriptomic signature of NASH in humans that is distinct from NAFL and responsive to RYGB and LSI, suggesting a shared mechanism of NASH regression by these different weight-loss methods. Interestingly, weight loss alone was apparently not sufficient to improve NASH in all patients as weight loss was similar in LSI responders and non-responders. The reversible transcriptomic signature of NASH is highly enriched by immune genes such as cytokines and chemokines and their receptors, genes involved in

activation of lymphocytes by antigen-presenting cells and genes linked to cytotoxic cells. Some of these genes have already been described as associated with NASH. For example, CD44, a molecule mediating leucocyte recruitment into the liver, plays a role in methionine-choline deficient diet (MCD)-induced NASH in preclinical models[27]. Although the MCD model has obvious limitations in representing human NASH within the framework of the metabolic syndrome, it reproduces NASH in its hepatic phenotype and is therefore an interesting model to study intrahepatic changes in NASH. Furthermore, the same study also found elevated CD44 in human NASH biopsies. The pro-inflammatory cytokine CXCL10 also drives NASH in the MCD NASH model and is increased in blood from patients with NASH[28]. Here we show that downregulation
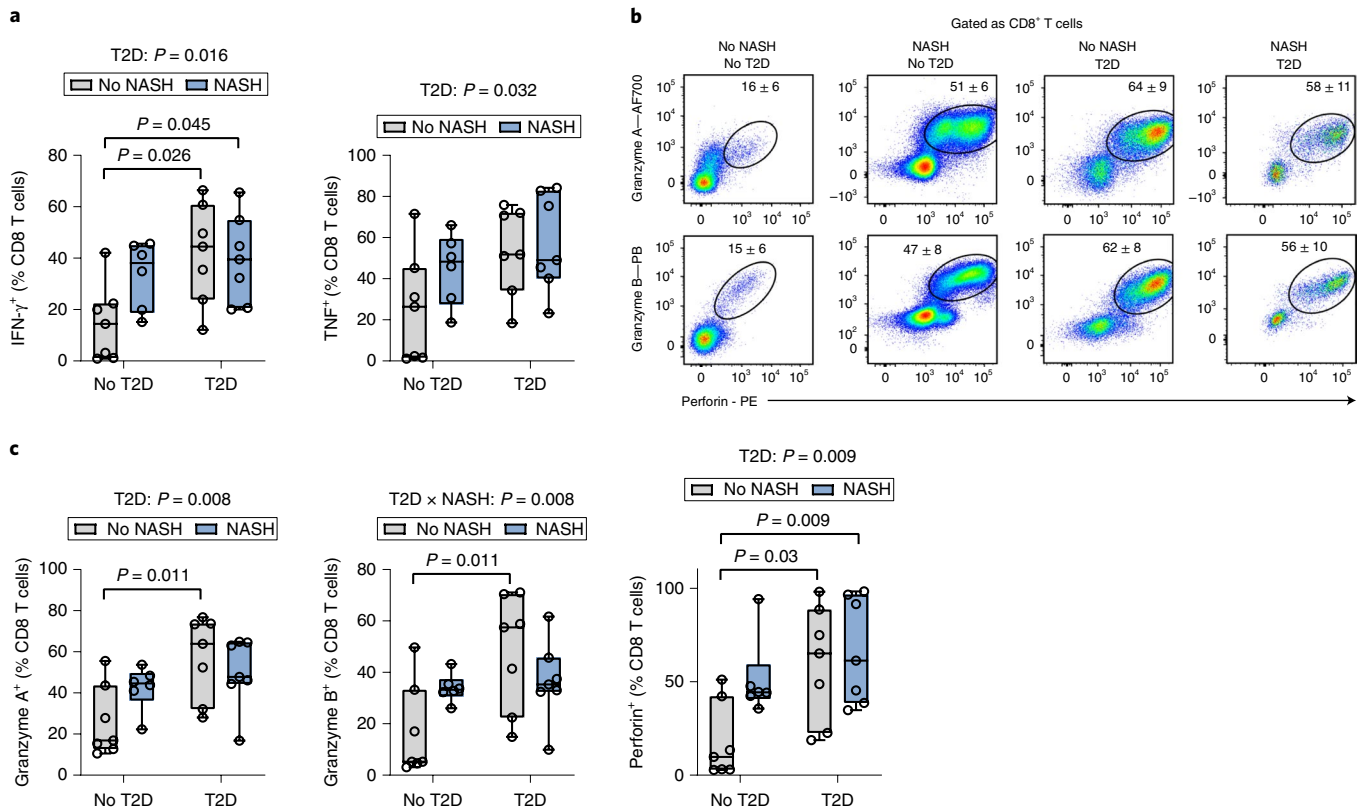
**Fig. 4 | NASH and T2D alter activity of cytotoxic CD8 T cells. a**, Proportion of IFN-γ⁺ and TNF-α⁺ CD8 T lymphocytes in blood from patients with/without NASH and/or T2D (see Supplementary Table 5). Groups: $n = 7$ patients with no NASH and no T2D; $n = 6$ with NASH and no T2D; $n = 7$ patients with no NASH and T2D; $n = 7$ patients with NASH and T2D. Data are shown as median with first and third quartiles. Statistical significance of differences between groups was analysed by unpaired two-way ANOVA for effects of NASH and T2D followed by Tukey's post-hoc test. **b,c**, Representative flow cytometric plots (**b**) and proportions of perforin, granzyme A and B expression in blood CD8 T lymphocytes from patients (**c**). Groups: $n = 7$ patients with no NASH and no T2D; $n = 6$ patients with NASH and no T2D; $n = 7$ patients with no NASH and T2D; $n = 7$ patients with NASH and T2D. Data are shown as median with first and third quartiles. Statistical significance of differences between groups was analysed by moderated paired $t$-test or two-way ANOVA (for effects of NASH and T2D) followed by Tukey's post-hoc test.

of hepatic pro-inflammatory pathways accompanies regression of NASH activity on intervention in patients. Moreover, these pathways increase on lifestyle induction of NASH in a mouse model. Thus, the reversible transcriptomic signature of NASH reveals new biological targets for specific therapy of NASH focusing on its activity. While the present study focuses on NASH improvement driven by weight loss or lifestyle modification, effective pharmacological treatments could target this immune signature and act in synergy with other metabolism-focused pathways. Because the transcriptomic analysis here was performed on total RNA from liver biopsies, it is conceivable that single-cell RNA analysis may reveal more subtle differences in hepatocyte versus non-parenchymal cell responses in NASH.

Increasing evidence demonstrates a close interaction between the immune system and metabolism in the development of NASH[29]. Our data are in line with recent publications on associations of different immune cells with NAFLD in humans[8,9,30,31]. However, our study includes a global analysis of circulating immune cell populations in relation to the presence of NASH and its severity. Integrative analysis revealed a species-conserved phenotype of NASH implicating antigen-presenting cDC subtypes and cytotoxic CD8 T cells. Whereas cDC1 are thought to present antigens to CD8⁺ T cells and cDC2 present antigens to CD4⁺ T cells[32,33], we surprisingly found that blood cDC1 correlate inversely with NASH activity, whereas blood cDC2 and CD8⁺ T cells both positively correlate with NASH. Similarly, CD172a⁺ cDC2 replace XCR1⁺ cDC1 in mouse livers on

NASH induction. Moreover, elevated hepatic expression of multiple genes involved in antigen presentation in NASH is reversible on intervention. In the MCD model, total cDC have been shown to protect against NASH[34]. However, whether these effects are mediated by cDC1 and/or cDC2 subpopulations is unclear. As cDC subtypes control pro-inflammatory and tolerogenic immune responses depending on the tissue environment[35], a shift between cDC1 and cDC2 in mice and humans might be associated with elevated hepatic inflammation and hepatocyte damage in NASH. Interestingly, depletion of CD141⁺ cDC1 has been shown to occur in human liver on inflammation[36], suggesting an inflammation-mediated mechanism of suppression of cDC1 in relation to NASH activity. Among the hepatic myeloid populations identified in mice (such as, Kupffer cells, monocyte-derived macrophages and DC), the present gating strategy was unable to exhaustively phenotype these clearly important immune populations. Further studies are thus necessary to better understand the evolution of the hepatic immune milieu and confirm our findings in human NASH biopsies.

Previous studies demonstrated associations of CD8 T cells with liver damage in mouse models of NASH[10,19,20]. We show that, in patients, circulating and hepatic cytotoxic CD8 T lymphocytes are significantly linked to histological hallmarks of NASH, such as lobular inflammation and ballooning. Moreover, CD8 T lymphocytes correlate with hepatic markers of inflammation and antigen presentation in NASH. Polymorphisms in one of these genes, *HLA-DQB1*, a MHCII haplotype, is associated with NAFLD[37,38]. Another gene,
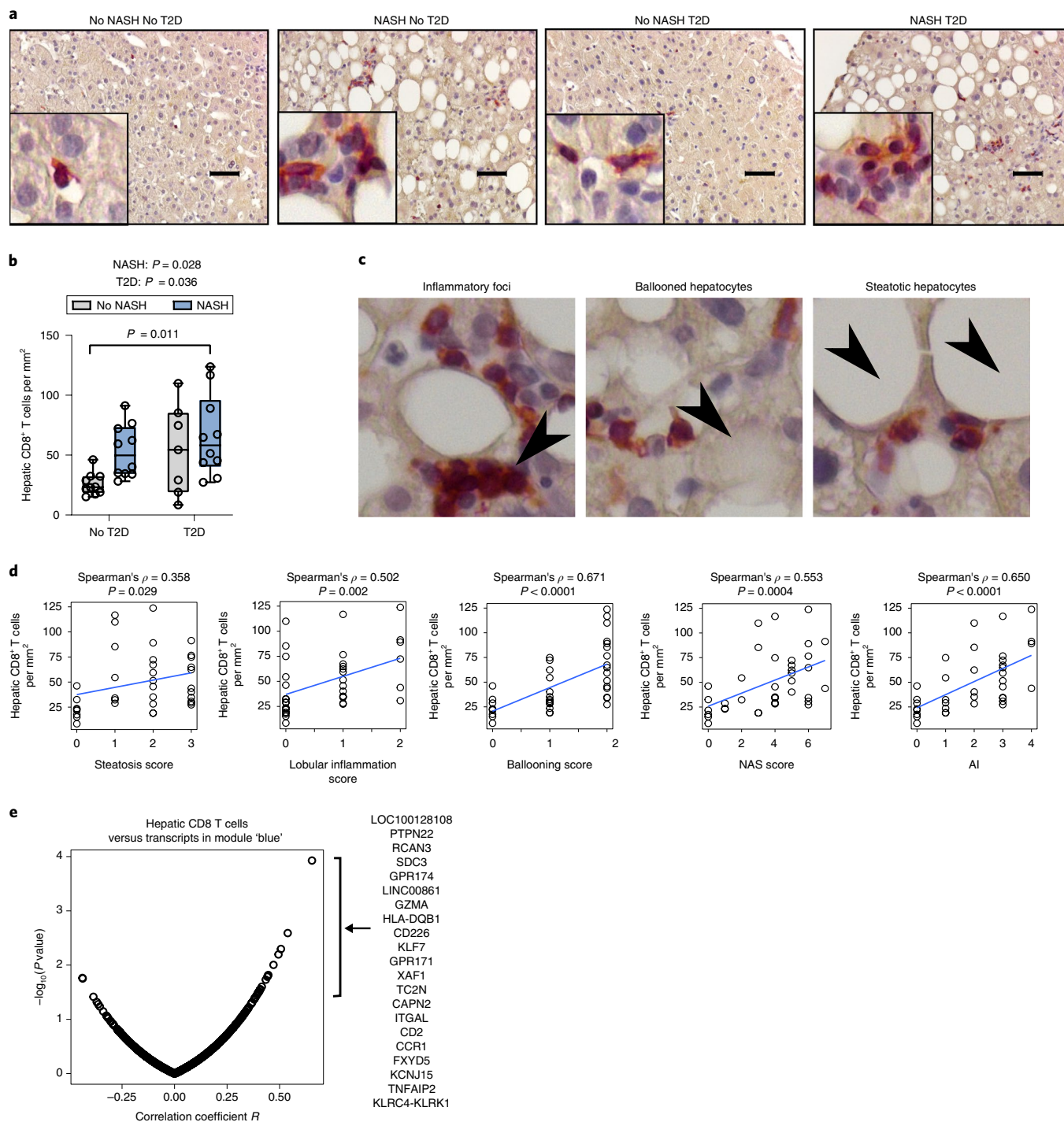
**Fig. 5 | Hepatic CD8 T lymphocytes correlate with lobular inflammation, ballooning and transcriptomic signature of NASH. a**, Representative immunostaining for CD8 (red) with haematoxylin counterstaining on liver biopsies from patients with/without NASH and/or T2D. **b**, Quantification of CD8+ cells per mm². No NASH, no T2D $n=10$; NASH, no T2D, $n=10$; no NASH, T2D, $n=7$; NASH, T2D, $n=9$. Data are shown as median with first and third quartiles. **c**, Localization of CD8 T lymphocytes (red) near immune infiltrates, steatosis and ballooned hepatocytes (indicated by arrows) in the liver from a patient with NASH. Scale bar, 50 μm. **d**, Correlations between hepatic CD8 T lymphocyte number and histological features in the liver ($n=36$). **e**, Pearson correlations and $-\log_{10}(P$ values) between hepatic CD8 T lymphocyte and expression levels of genes from module 'blue' ($n=29$, Supplementary Table 5). Statistical significance of differences between groups was analysed by unpaired two-way ANOVA (for effects of NASH and T2D) followed by Tukey's post-hoc test.

*PTPN22*, is an important regulator of TCR signalling and linked with several autoimmune diseases[25]. Furthermore, in the lifestyle-induced NASH model, elevated hepatic CD8 T cells associated with CD172a+ cDC2, suggesting a possible role of antigen presentation and TCR activation of CD8 T cells in NASH. CD8 T lymphocytes

appear to contribute to insulin resistance in a mouse model of diet-induced obesity[38]. Similarly, hepatic CD8 T lymphocytes and type I IFN signalling promote glucose intolerance and insulin resistance in mice[39,40]. Interestingly, the reversible transcriptomic signature of NASH that we identified to be enriched by cytokines and cytotoxic

molecules in circulating CD8 T cells is linked to NASH activity and T2D in humans. Curiously, dysregulated glucose metabolism in patients with T2D does not explain the increased numbers of CD8 T cells in the liver, suggesting that other factors contribute to the T2D-mediated accumulation of hepatic CD8 T cells. Moreover, in addition to elevated hepatic CD8 T cells, some patients with T2D, without an unequivocal NASH diagnosis, already display ballooning. Together, these results suggest a role of CD8 T cells in the interplay between T2D and NASH. We found that the reversible transcriptomic signature of NASH is enriched by apoptosis pathway and NF-κB target genes (data not shown). These hepatic NF-κB target genes are downregulated on NASH activity reduction accompanied by decreased ballooning. Ballooning is a poorly understood but essential hallmark of NASH, representing a specific form of 'undead cells' with features of initiated but not resolved apoptosis[6]. Because the apoptotic machinery is controlled by the NF-κB signalling pathway[41], downregulation of the pathway on LSI or BS might resolve apoptosis and thereby eliminate ballooned cells from the liver. Moreover, associations of the blood immune signature of NASH, particularly cytotoxic CD8 T cells, with ballooning suggest a cross-talk between the immune system and stressed hepatocytes in NASH. Although our results identify a pathway contributing to NASH resolution in a manner independent of body weight, it is clear that metabolic control through direct action on the liver or via extra-hepatic organs also contributes to NAFLD. Indeed, adipose tissue may directly contribute to NAFLD progression through systemic cytokine and immune signalling and drive hepatic injury in the context of obesity[39,42,43].

Our study provides insights into the molecular mechanisms implicated in NASH and its regression on intervention. In patients and a mouse model, we comprehensively and consistently show surprisingly pronounced associations of immune pathways and cell populations with NASH activity. These pathways, as well as the exact molecular targets revealed by this study, underline an important role of innate and acquired immunity in the development and severity of NASH, which may be targeted for treatment.

## Methods

**Patients.** All patients were consecutively recruited at the Liver Clinic and Obesity Clinic of the Antwerp University Hospital and underwent hepatologic and metabolic work-ups. Blood analysis included blood cell count and white blood cell formula. Exclusion criteria were alcohol consumption >2 units per day for women and >3 units per day for men, liver diseases other than NAFLD, age <18 years and liver cirrhosis. For the baseline gene expression analysis in the liver, patients (*n* = 155, including no liver disease *n* = 27, simple steatosis *n* = 22, NASH *n* = 106) were selected from a cohort recruited since 2006 (ref. [16]). Selected obese patients with NASH with paired biopsies at 1 year follow-up (LSI *n* = 20, RYGB *n* = 21) were included for gene expression analysis (Supplementary Fig. 1). For immunophenotyping analysis, patients (*n* = 38) were consecutively recruited between 2014 and 2016. Gene expression analysis was performed on a subset of these patients (*n* = 29) who were included in the baseline gene expression analysis (Supplementary Fig. 1). The study protocol is part of the Hepadip protocol (Belgian registration number B30020071389) and was approved by the Ethical Committee of the Antwerp University Hospital (file 6/25/125). Written informed consent was obtained from all patients.

**Selection of patients.** From patients visiting the Obesity Clinic at the Antwerp University Hospital, who were recruited from 2006 to 2016, 155 patients with hepatic RNA microarray and clinical data available at baseline were enrolled[16,44]. Among the 155 patients, 41 obese non-diabetic patients with NASH at baseline were selected for comparative baseline and 1 year follow-up hepatic RNA microarray and clinical data analysis. Of these 41 patients with NASH at baseline, 31 patients displayed an improvement in disease activity, with decreases of lobular inflammation and/or ballooning, 1 year after RYGB (*n* = 21) or LSI (*n* = 10), whereas 10 patients did not improve 1 year after LSI. We defined the LSI patients with NASH at baseline who improved ballooning and/or lobular inflammation at 1 year follow-up as responders to intervention and those who did not as non-responders to intervention. In a second independent cohort, immune cell populations were analysed in consecutive patients with four clearly distinct phenotypes enrolled based on their metabolic (T2D) and histological (NASH) phenotype (total *n* = 38): 17 patients without NASH in which some degree of simple steatosis was allowed (without (*n* = 7) and with (*n* = 10) T2D) and

21 patients with unequivocal NASH based on histological parameters (without (*n* = 11) and with (*n* = 10) T2D). The group without T2D and NASH consisted of a slightly lower number of patients, as liver biopsies were only performed on clinical indication of the potential presence of NASH. High-quality RNA appropriate for microarray analysis was obtained from liver biopsies in 29 out of 38 patients (13 patients without NASH and 16 patients with NASH).

**Clinical assessment and biological measurements.** Fasting blood glycaemia was analysed in the morning. A 2-h oral glucose tolerance test (75 g of glucose), including insulin quantification, was performed. Homeostatic Model Assessment for Insulin Resistance (HOMA-IR) was calculated[45]. BMI, glucose and percentage of HbA1c were measured[46]. Liver biopsies were performed for suspected NAFLD as indicated by elevated serum transaminase levels or a steatotic liver on ultrasound as described previously[44].

**Histological assessment of the liver biopsies.** All liver biopsies were stained (haematoxylin-eosin, Sirius red, reticulin and Perls' iron stain) and scored by two expert pathologists blinded to all clinical information. Histological features of NAFLD (steatosis, ballooning, lobular inflammation and fibrosis) were assessed using the NASH Clinical Research Network Scoring System criteria[47]. The NAFLD activity score was calculated as the sum of steatosis, lobular inflammation and ballooning scores. An activity index was also calculated as the sum of ballooning (range 0–2) and lobular inflammation (range 0–3) in line with recent observations of the distinct roles of steatosis versus activity of disease[5]. NASH was defined by the simultaneous presence of steatosis ≥1 AND ballooning ≥1 AND lobular inflammation ≥1[47]. As outlined, the sum of ballooning and lobular inflammation was calculated and indicated as the activity score.

**Mouse model of diet-induced NASH.** Wild-type male C57BL/6J mice (8 weeks of age) were purchased from Charles River Laboratories (France). Mice were maintained in a pathogen-free environment (12:12 h light/dark cycle, 21 °C–24 °C) and were given ad libitum access to water and food. Alternatively, Foxp3-YFP reporter mice[48] maintained on a C57BL/6J background were used to monitor hepatic T$_{reg}$ populations. Littermate animals were randomized by body weight before the start of the diet. No power calculations were performed to determine sample size. Mice were fed either a control diet (standard rodent chow, 5% kcal fat) or a 'NASH' diet (45% kcal fat, 40% kcal carbohydrate, 15% kcal protein with 1% (by weight) cholesterol; SAFE diets, France) for 24 weeks. All experiments were performed following approval by the Ethics Committee for Animal Experimentation from Nord-Pas de Calais Region (APAFIS#5746-2016040109244171 and APAFIS#7160-2017040313471173).

**Histology and immunohistochemistry.** Human liver biopsy sections were incubated for 1 h at 22 °C with rabbit monoclonal anti-CD8a (SP16) (Thermo Fisher Scientific), followed by staining with a mouse anti-rabbit HRP-conjugated antibody, and revealed with Vector ImmPRESS HRP Reagent Kit and Vector NovaRED Substrate Kit. Sections were counterstained by haematoxylin. Mouse liver samples were fixed with 4% paraformaldehyde, embedded in paraffin and stained with haematoxylin-eosin. Images were obtained by conventional microscopy using a Nikon Ti-U microscope.

**Flow cytometry.** EDTA blood samples from patients were collected and peripheral blood mononuclear cells (PBMC) isolated using Percoll. For cytokine staining, cells were incubated with 20 ng ml$^{-1}$ phorbol 12-myristate 13-acetate (PMA), 1 μg ml$^{-1}$ ionomycin and 1 μg ml$^{-1}$ brefeldin A in Roswell Park Memorial Institute (RPMI) 1640 medium for 4 h at 37 °C, 5% CO$_2$. Then 1 × 10$^6$ PBMC were pre-incubated with Fc Block to minimize non-specific binding and they were labelled with conjugated antibodies CD3 (UCHT1, PE-CF594), CD4 (OKT4, APC-CY7), CD45RA (HI100, V500), CD56 (HCD56, BV605), CD8 (HIT8a, PE-CY7), CCR10 (6588-5, PE), CD11b (ICRF44, AF700), CD11c (3.9, PB), CD123 (6H6, PE-CY7), CD127 (A7R34, BV605), CD14 (HCD14, PerCP-CY5.5), CD141 (B-A35, FITC), CD16 (3G8, V500), CD161 (HP-3G10, PB), CD172a (15-414, APC), CXCR3 (G025H7, APC), CD19 (HIB19, PE-CF594), CCR6 (R6H1, PE), CD197/CCR7 (3D12, FITC), HLA-DR (G46-6, AF700 or APC-CY7), Perforin (dG9, PE), Granulysin (DH2, AF647), Granzyme A (CB9, AF700), Granzyme B (GB11, PB), TNF (MAb11, AF700), IFN-γ (4S.B3, BV421), IL-10 (JES3-9D7, eFluor660), IL-17A (BL168, AF700), IL-22 (22URTI, eFluor660), IL-5 (TRFK5, APC). Intracellular staining was performed using the Cytofix/Cytoperm kit (BD Biosciences) according to the manufacturer's instructions.

Immune cells were isolated from mouse liver, digested 45 min with collagenase D, using centrifugation at 1,000g with 30% Percoll. Cells were treated with Zombie UV to discriminate live and dead cells, and then incubated with Fc Block and labelled with conjugated antibodies: CD45 (BUV737, clone 104), CD11b (BUV395, clone M1/70), CCR2 (BV421, clone SA203G11), Ly6C (BV785, clone HK1.4), F4/80 (BV711, clone BM8), NK1.1 (AF700, clone PK136), CD4 (BV605, clone RM4-5), CD8a (BV510, clone 53-6.7), Ly6G (PE-Cy7, clone 1A8), IA/IE (BV650, clone M5/114.15.2), CD11c (APC-Cy7, clone N418), CD19 (PE-CF594, clone 1D3), TCRb (APC, clone H57-597). For myeloid cell staining, an additional panel was used with the following antibodies: CD45 (PE-CF594, clone 30-F11), CD172a

(BUV395, clone P84), CCR2 (BV421, clone SA203G11), B220 (BV510, RA3-6B2), CD26 (BV605, clone H194-112), XCR1 (BV650, clone ZET), F4/80 (BV711, clone BM8), Ly6C (BV786, clone HK1.4), MHCII (FITC, clone M5/114.15.2), CD64 (PE, clone x54-5/7.1), CLEC4F (PE-Cy7, clone 370901), CD19 (APC, clone eBio1D3), CD3 (AF700, clone 500A2), NK1.1 (AF700, clone PK136), CD11c (APC-Cy7, clone N418). The CLEC4F antibody was coupled to PE-Cy7 using the Abcam Antibody Coupling Kit (reference ab102903) and used at a final dilution of 1:100.

Flow cytometry analysis was performed on a BD LSRFortessa X-20 (Becton Dickinson). Results were acquired with the Diva software (Becton Dickinson) and analysed using FlowJo software (Tree Star). Additional details are provided in the Reporting Summary.

**RNA extraction.** For human samples, the entire biopsy was homogenized for RNA extraction, purification and processing as described previously[44]. Total RNA was isolated from mouse liver using Trizol reagent and used for PCR with reverse transcription and real-time PCR. RNA from human liver biopsies was isolated using RNeasy Mini Kit (Qiagen) and used for microarray analysis. Quantification and RNA integrity number (RIN) was tested using the Agilent 2100 Bioanalyzer System. Only RNA samples with $RIN \geq 6$ were used for microarray analysis.

**PCR with reverse transcription and real-time PCR.** Total RNA (500 ng) isolated from mouse liver was treated with DNase I and used to generate complementary DNA with a high-capacity cDNA reverse transcription kit. Gene expression was measured by SybrGreen-based real-time PCR. Results were normalized to the normalization factor calculated as average expression of housekeeping genes *Ppia* and *Tbp*, and the $\Delta\Delta Ct$ method was used for all real-time PCR analyses. Primers sequences are provided in Supplementary Table 6.

**Microarray analysis.** Transcriptome analysis was performed with the Affymetrix GeneChip HuGene 2.0 ST arrays[16,49]. All liquid handling procedures were performed on a GeneChip Fluidic Station 450. GeneChips were scanned with a GeneChip Scanner 3000-7G (Affymetrix) using Command Console v.4.1.2. Quality controls were performed using the Affymetrix expression console.

**Microarray data processing and WGCNA.** Microarray data were normalized by the robust multi-average method[50] using oligo/Bioconductor and corrected for batch effects using SVA/Bioconductor R packages[51]. In total, 38,598 annotated transcripts were selected for analysis, and 11,784 transcripts with maximal variability across all patients at baseline ($n = 155$) based on median absolute deviation were selected for WGCNA and tested using the WGCNA R package[17]. Biweight midcorrelations and weighted adjacency matrix were calculated using the power threshold of 11, which was selected based on the scale-free topology fit model. Gene modules were identified using the 'hybrid' method and parameters deepSplit = 4 and mergeCutHeight = 0.15. For creation of volcano plots, $\log_{10}(P$ values) and $\log_2$(fold changes) were calculated using the limma R package[52]. Selected sets of transcripts of gene modules were tested for differential expression with geneSetTest from the limma R package[53]. The Gene Expression Omnibus repository accession number for the microarray data is GSE106737. Gene set enrichment analysis of gene modules was performed using GSEA software (http://software.broadinstitute.org/gsea/).

**Statistical analysis.** No statistical method was used to predetermine the sample size. For animal studies, mice were randomized by body weight before dietary challenge and no blinding was performed for subsequent analysis. For comparison in patients at baseline and 1 year after BS or LSI, the paired moderated *t*-test or the paired Mann–Whitney *U*-test was used. For comparison of the four groups of patients, data were analysed by two-way analysis of variance (ANOVA), using NASH and T2D as factors, followed by Tukey's post-hoc test for multiple comparisons. For histological quantification of hepatic CD8+ cells, the observer was blinded from the clinical parameters of each patient. Parametric Pearson correlation (continuous data) or non-parametric Spearman's rank-order correlation (categorical data) and hierarchical clustering were performed using R. Gene networks were visualized using Cytoscape. Values of $P < 0.05$ were considered significant. $P$ values were adjusted using the Benjamini–Hochberg procedure. Statistical analyses were performed with Prism 6 (GraphPad Software, Inc.) or R v.3.4.4.

**Reporting Summary.** Further information on research design is available in the Nature Research Reporting Summary linked to this article.

## Data availability
Microarray data used in this study were from the Gene Expression Omnibus repository under accession number GSE106737 and GSE83452. Requests for other data should be made to the corresponding author.

## References
1. Haas, J. T., Francque, S. & Staels, B. Pathophysiology and mechanisms of nonalcoholic fatty liver disease. *Annu. Rev. Physiol.* **78**, 181–205 (2016).
2. Luyckx, F. H., Lefebvre, P. J. & Scheen, A. J. Non-alcoholic steatohepatitis: association with obesity and insulin resistance, and influence of weight loss. *Diabetes Metab.* **26**, 98–106 (2000).
3. Brunt, E. M. Pathology of nonalcoholic fatty liver disease. *Nat. Rev. Gastroenterol. Hepatol.* **7**, 195–203 (2010).
4. Brunt, E. M. et al. Nonalcoholic fatty liver disease (NAFLD) activity score and the histopathologic diagnosis in NAFLD: distinct clinicopathologic meanings. *Hepatology* **53**, 810–820 (2011).
5. Bedossa, P. et al. Histopathological algorithm and scoring system for evaluation of liver lesions in morbidly obese patients. *Hepatology* **56**, 1751–1759 (2012).
6. Hirsova, P. & Gores, G. J. Ballooned hepatocytes, undead cells, sonic hedgehog, and vitamin E: therapeutic implications for nonalcoholic steatohepatitis. *Hepatology* **61**, 15–17 (2015).
7. Vonghia, L., Michielsen, P. & Francque, S. Immunological mechanisms in the pathophysiology of non-alcoholic steatohepatitis. *Int. J. Mol. Sci.* **14**, 19867–19890 (2013).
8. Liaskou, E. et al. Monocyte subsets in human liver disease show distinct phenotypic and functional characteristics. *Hepatology* **57**, 385–398 (2013).
9. Rau, M. et al. Progression from nonalcoholic fatty liver to nonalcoholic steatohepatitis is marked by a higher frequency of Th17 cells in the liver and an increased Th17/resting regulatory T cell ratio in peripheral blood and in the liver. *J. Immunol.* **196**, 97–105 (2016).
10. Wolf, M. J. et al. Metabolic activation of intrahepatic CD8+ T cells and NKT cells causes nonalcoholic steatohepatitis and liver cancer via cross-talk with hepatocytes. *Cancer Cell* **26**, 549–564 (2014).
11. Kleiner, D. E. & Bedossa, P. Liver histology and clinical trials for nonalcoholic steatohepatitis-perspectives from 2 pathologists. *Gastroenterology* **149**, 1305–1308 (2015).
12. Ryaboshapkina, M. & Hammar, M. Human hepatic gene expression signature of non-alcoholic fatty liver disease progression, a meta-analysis. *Sci. Rep.* **7**, 12361 (2017).
13. Moylan, C. A. et al. Hepatic gene expression profiles differentiate presymptomatic patients with mild versus severe nonalcoholic fatty liver disease. *Hepatology* **59**, 471–482 (2014).
14. Vilar-Gomez, E. et al. Weight loss through lifestyle modification significantly reduces features of nonalcoholic steatohepatitis. *Gastroenterology* **149**, 367–378 e365 (2015).
15. Lassailly, G. et al. Bariatric surgery reduces features of nonalcoholic steatohepatitis in morbidly obese patients. *Gastroenterology* **149**, 379–388 (2015).
16. Lefebvre, P. et al. Interspecies NASH disease activity whole-genome profiling identifies a fibrogenic role of PPARalpha-regulated dermatopontin. *JCI Insight* **2**, e92264 (2017).
17. Langfelder, P. & Horvath, S. WGCNA: an R package for weighted correlation network analysis. *BMC Bioinformatics* **9**, 559 (2008).
18. Vonghia, L. et al. CD4+ROR gamma t++ and tregs in a mouse model of diet-induced nonalcoholic steatohepatitis. *Mediators Inflamm.* **2015**, 239623 (2015).
19. Bhattacharjee, J. et al. Hepatic natural killer T-cell and CD8+ T-cell signatures in mice with nonalcoholic steatohepatitis. *Hepatol. Commun.* **1**, 299–310 (2017).
20. Sutti, S. et al. Adaptive immune responses triggered by oxidative stress contribute to hepatic inflammation in NASH. *Hepatology* **59**, 886–897 (2014).
21. Clapper, J. R. et al. Diet-induced mouse model of fatty liver disease and nonalcoholic steatohepatitis reflecting clinical disease progression and methods of assessment. *Am. J. Physiol. Gastrointest. Liver Physiol.* **305**, G483–G495 (2013).
22. Asgharpour, A. et al. A diet-induced animal model of non-alcoholic fatty liver disease and hepatocellular cancer. *J. Hepatol.* **65**, 579–588 (2016).
23. Jensen, T. et al. Fructose and sugar: a major mediator of non-alcoholic fatty liver disease. *J. Hepatol.* **68**, 1063–1075 (2018).
24. Ioannou, G. N. The role of cholesterol in the pathogenesis of NASH. *Trends Endocrinol. Metab.* **27**, 84–95 (2016).
25. Bottini, N. & Peterson, E. J. Tyrosine phosphatase PTPN22: multifunctional regulator of immune signaling, development, and disease. *Annu. Rev. Immunol.* **32**, 83–119 (2014).
26. Froylich, D. et al. Effect of Roux-en-Y gastric bypass and sleeve gastrectomy on nonalcoholic fatty liver disease: a comparative study. *Surg. Obes. Relat. Dis.* **12**, 127–131 (2016).
27. Patouraux, S. et al. CD44 is a key player in non-alcoholic steatohepatitis. *J. Hepatol.* **67**, 328–338 (2017).
28. Zhang, X. et al. CXCL10 plays a key role as an inflammatory mediator and a non-invasive biomarker of non-alcoholic steatohepatitis. *J. Hepatol.* **61**, 1365–1375 (2014).

29. Tilg, H., Moschen, A. R. & Roden, M. NAFLD and diabetes mellitus. *Nat. Rev. Gastroenterol. Hepatol.* **14**, 32–42 (2017).

30. Syn, W. K. et al. Accumulation of natural killer T cells in progressive nonalcoholic fatty liver disease. *Hepatology* **51**, 1998–2007 (2010).

31. Miura, K., Yang, L., van Rooijen, N., Ohnishi, H. & Seki, E. Hepatic recruitment of macrophages promotes nonalcoholic steatohepatitis through CCR2. *Am. J. Physiol. Gastrointest. Liver Physiol.* **302**, G1310–G1321 (2012).

32. Durai, V. & Murphy, K. M. Functions of murine dendritic cells. *Immunity* **45**, 719–736 (2016).

33. Vu Manh, T. P., Bertho, N., Hosmalin, A., Schwartz-Cornil, I. & Dalod, M. Investigating evolutionary conservation of dendritic cell subset identity and functions. *Front. Immunol.* **6**, 260 (2015).

34. Henning, J. R. et al. Dendritic cells limit fibroinflammatory injury in nonalcoholic steatohepatitis in mice. *Hepatology* **58**, 589–602 (2013).

35. Worbs, T., Hammerschmidt, S. I. & Forster, R. Dendritic cell migration in health and disease. *Nat. Rev. Immunol.* **17**, 30–48 (2017).

36. Kelly, A. et al. CD141(+) myeloid dendritic cells are enriched in healthy human liver. *J. Hepatol.* **60**, 135–142 (2014).

37. Doganay, L. et al. HLA DQB1 alleles are related with nonalcoholic fatty liver disease. *Mol. Biol. Rep.* **41**, 7937–7943 (2014).

38. Nishimura, S. et al. CD8+ effector T cells contribute to macrophage recruitment and adipose tissue inflammation in obesity. *Nat. Med.* **15**, 914–920 (2009).

39. Wieser, V. et al. Adipose type I interferon signalling protects against metabolic dysfunction. *Gut* **67**, 157–165 (2018).

40. Ghazarian, M. et al. Type I interferon responses drive intrahepatic T cells to promote metabolic syndrome. *Sci. Immunol.* **2**, eaai7616 (2017).

41. Luo, J. L., Kamata, H. & Karin, M. IKK/NF-kappaB signaling: balancing life and death—a new approach to cancer therapy. *J. Clin. Invest.* **115**, 2625–2632 (2005).

42. du Plessis, J. et al. Association of adipose tissue inflammation with histologic severity of nonalcoholic fatty liver disease. *Gastroenterology* **149**, 635–648 e614 (2015).

43. Bijnen, M. et al. Adipose tissue macrophages induce hepatic neutrophil recruitment and macrophage accumulation in mice. *Gut* **67**, 1317–1327 (2018).

44. Francque, S. et al. PPARalpha gene expression correlates with severity and histological treatment response in patients with non-alcoholic steatohepatitis. *J. Hepatol.* **63**, 164–173 (2015).

45. Matthews, D. R. et al. Homeostasis model assessment: insulin resistance and beta-cell function from fasting plasma glucose and insulin concentrations in man. *Diabetologia* **28**, 412–419 (1985).

46. Verrijken, A. et al. A gene variant of PNPLA3, but not of APOC3, is associated with histological parameters of NAFLD in an obese population. *Obesity (Silver Spring)* **21**, 2138–2145 (2013).

47. Kleiner, D. E. et al. Design and validation of a histological scoring system for nonalcoholic fatty liver disease. *Hepatology* **41**, 1313–1321 (2005).

48. Rubtsov, Y. P. et al. Regulatory T cell-derived interleukin-10 limits inflammation at environmental interfaces. *Immunity* **28**, 546–558 (2008).

49. Pawlak, M. et al. The transrepressive activity of peroxisome proliferator-activated receptor alpha is necessary and sufficient to prevent liver fibrosis. *Hepatology* **60**, 1593–1606 (2014).

50. Irizarry, R. A. et al. Exploration, normalization, and summaries of high density oligonucleotide array probe level data. *Biostatistics* **4**, 249–264 (2003).

51. Leek, J. T. & Storey, J. D. Capturing heterogeneity in gene expression studies by surrogate variable analysis. *PLoS Genet.* **3**, 1724–1735 (2007).

52. Smyth, G. K., Michaud, J. & Scott, H. S. Use of within-array replicate spots for assessing differential expression in microarray experiments. *Bioinformatics* **21**, 2067–2075 (2005).

53. Goeman, J. J. & Buhlmann, P. Analyzing gene expression data in terms of gene sets: methodological issues. *Bioinformatics* **23**, 980–987 (2007).

## Author contributions

L.V. and S. Francque collected human biopsies, histological and biochemical data. L.V., S. Francque, L.V.G. and A.V. supervised the human biopsies collection and analysis. A. Driessen performed the histology of the liver biopsies. J.T.H. and D.A.M. performed mouse experiments, flow cytometry, immunological and transcriptomic analysis, and WGCNA. S. Fleury performed immunohistochemistry. B.D., H.D., C.G. and P.L. performed microarray analysis. O.M.-C., A. Deprince, A.N., E.W., L.D.G. and S.P. performed mouse experiments and flow cytometry. D.A.M., L.V., J.T.H., S. Francque, B.S. and D.D. conceived the study, interpreted data and wrote the manuscript.

## Competing interests

B.S. and S. Francque are consultants for Genfit S.A. S. Francque and LV are consultants for Inventiva. All other authors have nothing to declare.

## Additional information

**Supplementary information** is available for this paper at https://doi.org/10.1038/s42255-019-0076-1.

**Reprints and permissions information** is available at www.nature.com/reprints.

**Correspondence and requests for materials** should be addressed to L.V. or D.D.

**Peer review information:** Primary Handling Editors: Elena Bellafante, Christoph Schmitt.

**Publisher's note:** Springer Nature remains neutral with regard to jurisdictional claims in published maps and institutional affiliations.

# nature research

| Corresponding author(s): | David Dombrowicz, Luisa Vonghia |
|---|---|
| Last updated by author(s): | Apr 30, 2019 |

# Reporting Summary

Nature Research wishes to improve the reproducibility of the work that we publish. This form provides structure for consistency and transparency in reporting. For further information on Nature Research policies, see Authors & Referees and the Editorial Policy Checklist.

## Statistics

For all statistical analyses, confirm that the following items are present in the figure legend, table legend, main text, or Methods section.

| n/a | Confirmed | |
|---|---|---|
| ☐ | ☒ | The exact sample size (*n*) for each experimental group/condition, given as a discrete number and unit of measurement |
| ☐ | ☒ | A statement on whether measurements were taken from distinct samples or whether the same sample was measured repeatedly |
| ☐ | ☒ | The statistical test(s) used AND whether they are one- or two-sided<br>*Only common tests should be described solely by name; describe more complex techniques in the Methods section.* |
| ☐ | ☒ | A description of all covariates tested |
| ☐ | ☒ | A description of any assumptions or corrections, such as tests of normality and adjustment for multiple comparisons |
| ☐ | ☒ | A full description of the statistical parameters including central tendency (e.g. means) or other basic estimates (e.g. regression coefficient) AND variation (e.g. standard deviation) or associated estimates of uncertainty (e.g. confidence intervals) |
| ☐ | ☒ | For null hypothesis testing, the test statistic (e.g. *F*, *t*, *r*) with confidence intervals, effect sizes, degrees of freedom and *P* value noted<br>*Give P values as exact values whenever suitable.* |
| ☒ | ☐ | For Bayesian analysis, information on the choice of priors and Markov chain Monte Carlo settings |
| ☐ | ☒ | For hierarchical and complex designs, identification of the appropriate level for tests and full reporting of outcomes |
| ☒ | ☐ | Estimates of effect sizes (e.g. Cohen's *d*, Pearson's *r*), indicating how they were calculated |

*Our web collection on statistics for biologists contains articles on many of the points above.*

## Software and code

Policy information about availability of computer code

| Data collection | Stratagene MXPro v4.1 was used to collect real-time PCR data<br>Nikon Elements v4.20.08 was used to acquire histological image<br>Affymetrix Command Console v4.1.2 was used to collect microarray data.<br>BD FACS Diva v8.0 was used to acquire flow cytometry data |
|---|---|
| Data analysis | The R packages (WGCNA v1.66, limma v3.36.5, sva v3.28.0) were used to analyze microarray data and perform statistical analysis and Cytoscape (v.3.7.0) visualization. These are all open source and the specific settings used for each are described in the methods section in detail. GraphPad Prism v6 and R v3.4.4 were used to perform statistical analysis and plot results. FlowJo v10.0.7 was used to analyze FACS data. |

For manuscripts utilizing custom algorithms or software that are central to the research but not yet described in published literature, software must be made available to editors/reviewers. We strongly encourage code deposition in a community repository (e.g. GitHub). See the Nature Research guidelines for submitting code & software for further information.

## Data

Policy information about availability of data

All manuscripts must include a data availability statement. This statement should provide the following information, where applicable:
- Accession codes, unique identifiers, or web links for publicly available datasets
- A list of figures that have associated raw data
- A description of any restrictions on data availability

Microarray data has been deposited under the accession number GSE106737 are available starting June 1, 2019

# Field-specific reporting

Please select the one below that is the best fit for your research. If you are not sure, read the appropriate sections before making your selection.

☒ Life sciences ☐ Behavioural & social sciences ☐ Ecological, evolutionary & environmental sciences

For a reference copy of the document with all sections, see nature.com/documents/nr-reporting-summary-flat.pdf

# Life sciences study design

All studies must disclose on these points even when the disclosure is negative.

| Sample size | 6-20 mice per group were used for animal studies. Human subjects were recruited as available, we included all patients in the given recruitment period that met the study inclusion criteria and could be appropriately classified in the study design. No prior sample size calculation was performed. Group sizes for animal studied were established by considering previous experience with effect sizes of various physiological parameters and ethical concerns regarding limits on group sizes. |
|---|---|
| Data exclusions | In flow cytometry analysis some samples were excluded due to insufficient cell recovery yielding unreliable quantification of low-abundance populations. No other data exclusions were made. Samples with less than 50 000 events were considered unreliable. |
| Replication | Results of animal experiments are based on representative results of 3 independent cohorts of mice following the same protocol. All findings were replicated successfully. |
| Randomization | Animals were randomized by bodyweight prior to dietary challenge. No randomization was performed for the human study as groups were based on actual disease response rather than other clinical characteristics of the patients. |
| Blinding | For histological scoring of CD8+ cells, the observer was blinded to the sample data. No other blinding was performed. |

# Reporting for specific materials, systems and methods

We require information from authors about some types of materials, experimental systems and methods used in many studies. Here, indicate whether each material, system or method listed is relevant to your study. If you are not sure if a list item applies to your research, read the appropriate section before selecting a response.

## Materials & experimental systems

| n/a | Involved in the study |
|---|---|
| ☐ | ☒ Antibodies |
| ☒ | ☐ Eukaryotic cell lines |
| ☒ | ☐ Palaeontology |
| ☐ | ☒ Animals and other organisms |
| ☐ | ☒ Human research participants |
| ☐ | ☒ Clinical data |

## Methods

| n/a | Involved in the study |
|---|---|
| ☒ | ☐ ChIP-seq |
| ☐ | ☒ Flow cytometry |
| ☒ | ☐ MRI-based neuroimaging |

# Antibodies

| Antibodies used | Histology Antibody:<br>rabbit monoclonal anti-CD8a (SP16) Thermo Fisher Scientific<br>Human Antibodies for FACS:<br>CD3 (1:200, UCHT1, PE-CF594), CD4 (1:250, OKT4, APC-CY7), CD45RA (1:1000, HI100, V500), CD56 (1:200, HCD56, BV605), CD8 (1:250, HIT8a, PE-CY7), CCR10 (1:100, 6588-5, PE), CD11b (1:1000, ICRF44, AF700), CD11c (1:200, 3.9, PB), CD123 (1:250, 6H6, PE-CY7), CD127 (1:100, A7R34, BV605), CD14 (1:250, HCD14, PerCP-CY5.5), CD141 (1:100, B-A35, FITC), CD16 (1:400, 3G8, V500), CD161 (1:80, HP-3G10, PB), CD172a (1:200, 15-414, APC), CXCR3 (1:100, G025H7, APC), CD19 (1:200, HIB19, PE-CF594), CCR6 (1:100, R6H1, PE), CD197/CCR7 (1:80, 3D12, FITC), HLA-DR (1:250, G46-6, AF700 or APC-CY7), Perforin (1:100, dG9, PE), Granulysin (1:100, DH2, AF647), Granzyme A (1:100, CB9, AF700), Granzyme B (1:100, GB11, PB), TNF (1:100, MAb11, AF700), IFNg (1:80, 4S.B3, BV421), IL-10 (1:100, JES3-9D7, eFluor660), IL-17A (1:100, BL168, AF700), IL-22 (1:100, 22URTI, eFluor660), IL-5 (1:100, TRFK5, PE).<br>Mouse Antibodies for FACS:<br>CD45 (1:200, BUV737, clone 104), CD11b (1:100, BUV395, clone M1/70), CCR2 (1:50, BV421, clone SA203G11), Ly6C (1:400, BV785, clone HK1.4), F4/80 (1:200, BV711, clone BM8), NK1.1 (1:200, AF700, clone PK136), CD4 (1:100, BV605, clone RM4-5), CD8a (1:100, BV510, clone 53-6.7), Ly6G (1:200, PE-Cy7, clone 1A8), IA/IE (1:200, BV650, clone M5/114.15.2), CD11c (1:200, APC-Cy7, clone N418), CD19 (1:200, PE-CF594, clone 1D3), TCRb (1:100, APC, clone H57-597). For myeloid cell staining, an additional panel was used with the following antibodies: CD45 (1:100, PE-CF594, clone 30-F11), CD172a (1:100, BUV395, clone P84), CCR2 (1:50, BV421, clone SA203G11), B220 (1:100, BV510, RA3-6B2), CD26 (1:100, BV605, clone H194-112), XCR1 (1:100, BV650, clone ZET), F4/80 (1:100, BV711, clone BM8), Ly6C (1:500, BV786, clone HK1.4), MHCII (1:100, FITC, clone M5/114.15.2), |
|---|---|

CD64 (1:100, PE, clone x54-5/7.1), Clec4F (1:100, PE-Cy7, clone #370901), CD19 (1:100, APC, clone eBio1D3), CD3 (1:100, AF700, clone 500A2), NK1.1 (1:100, AF700, clone PK136), CD11c (1:100, APC-Cy7, clone N418).

Validation | The antibody was validated by the manufacturer for use in immunohistochemistry https://www.thermofisher.com/antibody/product/CD8-Antibody-clone-SP16-Monoclonal/MA5-14548

## Animals and other organisms

Policy information about studies involving animals; ARRIVE guidelines recommended for reporting animal research

Laboratory animals | C57BL/6J male mice were purchased from Charles River France, aged 8-10 weeks at start of diet.

Wild animals | Wild animals were not used in this study

Field-collected samples | Field collected animals were not used in this study

Ethics oversight | Animal Protocols were approved by the regional and national ethics committees. Approval numbers: APAFIS#5746-2016040109244171 and APAFIS#7160-2017040313471173

Note that full information on the approval of the study protocol must also be provided in the manuscript.

## Human research participants

Policy information about studies involving human research participants

Population characteristics | Patients were obese, non-diabetic with little or no prior medical treatment for metabolic abnormalities. Average age: 43.2 ± 12.9 years Range: 18-74 years, BMI average 39.9 ± 5.6 (kg/m^2) range: 27-69.1 (kg/m^2).

Recruitment | Subjects were recruited through the Antwerp University Hospital Obesity Clinic

Ethics oversight | The study protocol is part of the Hepadip protocol (Belgian registration number B30020071389) and was approved by the Ethical Committee of the Antwerp University Hospital (file 6/25/125). Written informed consent was obtained from all patients.

Note that full information on the approval of the study protocol must also be provided in the manuscript.

## Clinical data

Policy information about clinical studies

All manuscripts should comply with the ICMJE guidelines for publication of clinical research and a completed CONSORT checklist must be included with all submissions.

Clinical trial registration | This study is not part of a clinical trial.

Study protocol | Hepadip protocol (Belgian registration number B30020071389)

Data collection | All Data collection was performed at Antwerp University Hospital

Outcomes | NASH diagnosis before or after intervention was determined by histological assessment according to the NASH Clinical Research Network Criteria

## Flow Cytometry

### Plots

Confirm that:

☒ The axis labels state the marker and fluorochrome used (e.g. CD4-FITC).

☒ The axis scales are clearly visible. Include numbers along axes only for bottom left plot of group (a 'group' is an analysis of identical markers).

☒ All plots are contour plots with outliers or pseudocolor plots.

☒ A numerical value for number of cells or percentage (with statistics) is provided.

### Methodology

Sample preparation | Immune cells were isolated from mouse liver, digested 45 min with collagenase D, using centrifugation with 30% Percoll. Cells were treated with Zombie UV to discriminate live and dead cells, incubated with Fc-block and labelled with conjugated antibodies

Instrument | BD LSRFortessa X-20 (Becton Dickinson).

Software | BD FACS Diva was used to used to acquire data and FlowJo (Tree Star) was used for analysis

Cell population abundance | In most cases, cell populations are calculated as %CD45+ Live cells. For DC and T-Cell subsets (e.g. cDC1 and cDC2 or CD4+ and CD8+) the % of parent gate is also provided.

Gating strategy | The precise gating strategy is provided in Supplementary Figures 3 and 4.

☒ Tick this box to confirm that a figure exemplifying the gating strategy is provided in the Supplementary Information.

In the format provided by the authors and unedited.

# Transcriptional network analysis implicates altered hepatic immune function in NASH development and resolution

Joel T. Haas [1,6], Luisa Vonghia [2,3,6]*, Denis A. Mogilenko [1,6], An Verrijken[3,4],
Olivier Molendi-Coste[1], Sébastien Fleury[1], Audrey Deprince[1], Artemii Nikitin[1], Eloïse Woitrain[1],
Lucie Ducrocq-Geoffroy[1], Samuel Pic[1], Bruno Derudas[1], Hélène Dehondt[1], Céline Gheeraert[1],
Luc Van Gaal[3,4], Ann Driessen[5], Philippe Lefebvre [1], Bart Staels[1,7], Sven Francque [2,3,7] and
David Dombrowicz [1,7]*

[1]University of Lille, Inserm, CHU Lille, Institut Pasteur de Lille, U1011-EGID, Lille, France. [2]Department of Gastroenterology and Hepatology, Antwerp University Hospital, Antwerp, Belgium. [3]Laboratory of Experimental Medicine and Paediatrics, Faculty of Medicine and Health Sciences, University of Antwerp, Antwerp, Belgium. [4]Department of Endocrinology, Diabetology and Metabolism, Antwerp University Hospital, University of Antwerp, Antwerp, Belgium. [5]Department of Pathology, Antwerp University Hospital, University of Antwerp, Antwerp, Belgium. [6]These authors contributed equally: Joel T. Haas, Luisa Vonghia, Denis A. Mogilenko. [7]These authors jointly supervised this work: Bart Staels, Sven Francque, David Dombrowicz.
*e-mail: luisa.vonghia@uza.be; david.dombrowicz@pasteur-lille.fr

**Supplementary Figure 1. a**. Study design and cohort of patients. **b**. A dot plot of change in blue module expression versus % body weight change at 1 year follow-up in LSI and BarS patients (n=42 patients). **c**. A heatmap of Pearson correlation coefficients for clinical parameters of the baseline cohort (n=155) with expression of the different gene modules identified by WGCNA. **d.** Type-I interferon responsive gene expression measured in the baseline cohort (n=155) Data are shown as median and 1$^{st}$ and 3$^{rd}$ quartiles (box). **e.** Type-I interferon responsive gene expression in the LSI (n=10 patients responders, n=10 patients non-responders) and BS (n=21 patients) groups before and 1 year after intervention. Data are shown as mean ± 95% CI in **e.** Statistical significance of differences between groups are analyzed by paired two-sided Wilcoxon test (*P < 0.05).

**Supplementary Figure 2.** Gating strategy for flow cytometry analysis of immune cells in human blood. Mononuclear cells were isolated from blood, stained with antibodies and analyzed as described in Material and Methods.

**Supplementary Figure 3.** A diet-induced mouse model of NASH. Male 57BL/6J mice were fed conventional diet (CD) or NASH-diet (ND) during 24 weeks. **a**. Body weight change (n=9 mice CD and n=20 mice ND). Data are expressed as mean ± SEM. Statistical significance of differences was assessed by repeated measures ANOVA. **b**. Representative liver morphology and **c**. liver weight after 24 weeks of feeding with CD or ND (n=9 mice CD and n=20 mice ND). Data are expressed as mean ± SEM. Statistical significance of differences was assessed by unpaired two-sided t-test. **d**. Representative liver histology, H&E staining, scale bar 100$\mu$m. 1 mouse per diet from the same lot of mice is shown from three independent lots of mice with similar histological findings. **e**. TG levels in the liver. (n=9 mice CD and n=12 mice ND). Data are expressed as mean ± SEM. Statistical significance of differences was assessed by unpaired two-sided t-test. **f**. Alanine aminotransferase (ALT) activity in plasma after 24 weeks of feeding with CD or ND (n=9 mice CD and n=12 mice ND). Data are expressed as mean ± SEM. Statistical significance of

differences was assessed by unpaired two-sided t-test. **g.** qPCR analysis of IFN$\alpha$-responsive genes in mouse livers after 24 weeks of feeding with CD or ND. (n=10 mice CD and n=11 mice ND). Data are shown as mean ± SEM. Statistical significance of differences between groups are analyzed by unpaired two-sided t-test..

**Supplementary Figure 4.** Hepatic immune cells in a diet-induced mouse model of NASH. **a.** Gating strategy of flow cytometry analysis in the liver. **b-j**. Proportions and representative flow cytometric plots of **b**. neutrophils (n=9 mice CD, n=20 mice ND), **c**. B cells (n=9 mice CD, n=20 mice ND), **d**. Clec4F$^+$ Kupffer cells (n=8 mice CD, n=6 mice ND) **e**. CD11b$^+$Ly6C$^{hi}$ inflammatory monocytes (n=9 mice CD, n=20 mice ND), **f**. CD11b$^+$CCR2$^{hi}$ infiltrating macrophages, **g**. NK cells (n=9 mice CD, n=20 mice ND), **h**. NKT cells, **i**. CD4 T cells (n=9 mice CD, n=20 mice ND), **j**. and FOXP3$^+$ regulatory T cells in the liver (n=9 mice CD, n=20 mice ND),. Data are shown as mean ± SEM. Statistical significance of differences between groups are analyzed by unpaired two-sided t-test (*P < 0.05, **P < 0.01, ***P < 0.001, ****P < 0.0001).

**Supplementary Figure 5.** CD8 T lymphocytes are associated with active NASH in humans. **a**. Correlations between hepatic CD8 T cells and populations of circulation CD8 T cells (n=36 patients). **b**. Correlations between hepatic CD8 T cells and hepatic expression of PRF1, GZMA, GZMB, and GNLY (n=28 patients). **c.** Correlations between hepatic CD8 T cells and plasma markers of insulin resistance and systemic inflammation n=32 patients).

**Table legends**

**Supplementary Table S1.** Characteristics of 155 patients at baseline used for WGCNA analysis in the liver. Data are presented as mean ± SD, min and max values and number of patients in each category are shown.

**Table S2**. Transcripts from hepatic gene modules from WGCNA of the 155 patients at baseline.

**Supplementary Table S3.** Characteristics of 21 NASH patients treated by RYGB used for gene expression analysis in the liver at baseline and one year follow-up. Data are presented as mean ± SD. Statistical significance between baseline and one year follow-up is analyzed by paired two-sided Mann-Whitney test.

**Supplementary Table S4.** Characteristics of 20 NASH patients treated by LSI used for gene expression analysis in the liver at baseline and one year follow-up. 10 patients decreased NASH lobular inflammation and/or ballooning (responders), and 10 patient did not decrease these parameters (non-responders) at one year follow-up. Data are presented as mean ± SD. Statistical significance between baseline and one year follow-up is analyzed by paired two-sided Mann-Whitney test.

**Supplementary Table S5.** Clinical and biochemical characteristics and information about treatment across subgroups of patients selected based on the diagnosis of NASH and/or T2D. Data are presented as mean ± SD. Statistical significance between groups were analyzed by non-paired two-sided Mann-Whitney test; a, b, c, d indicate P < 0.05 as compared to No-NASH No-T2D (a), NASH No-T2D (b), or No-NASH T2D (c) subgroup. An indicated part of patients was treated with insulin in case of diagnosed T2D.

**Supplementary Table S6.** Real Time Quantitative PCR primer sequences used in this study.

**Supplementary information**

**A diet-induced mouse model of NASH**

We fed C57BL/6J male mice with a high fat diet supplemented with sucrose and cholesterol (herein referred as "NASH diet", ND) for 24 weeks. ND feeding led to a significant increase of body weight compared to chow diet (CD)-fed mice (Supplementary Fig. 3a). Notably, it also resulted in significant enlargement of the liver (hepatomegaly) (Supplementary Fig. 3c,d). Histological analysis of the liver showed that ND-fed mice displayed the main features of NASH: micro- and macro-steatosis, immune infiltrates in parenchymal tissue (inflammatory foci), and amorphic hepatocytes lacking normal hexagonal structure, similar to ballooned hepatocytes (Supplementary Fig. 3d). In line with histologically analysis, ND-fed mice had significantly increased liver triglyceride (TG) levels (Supplementary Fig. 3e). Moreover, histological features of stressed hepatocytes were accompanied by a significant increase of serum alanine aminotransferase (ALT), indicative of hepatocyte damage, in ND- compared to CD-fed mice (Supplementary Fig. 3f).

# Supplementary Figure 1

**a**

**Study Cohorts and Design**

Liver transcriptomics

Baseline WGCNA cohort
(n=155)

Baseline RYGB
NASH patients (n=21)

Baseline
LSI NASH patients (n=20)

1 year follow-up
(n=21)

1 year follow-up
LSI responders
(n=10)

1 year follow-up
LSI non-responders
(n=10)
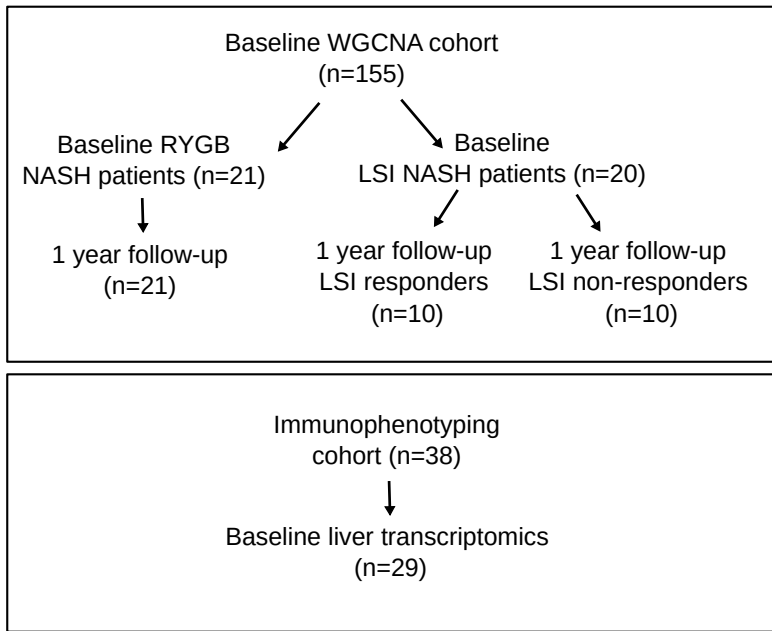
Liver transcriptomics
Blood immunophenotyping
Liver immunostaining

Immunophenotyping
cohort (n=38)

Baseline liver transcriptomics
(n=29)
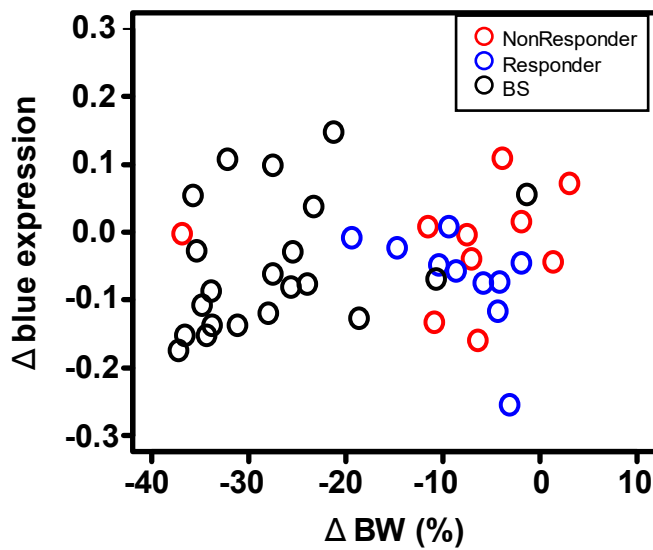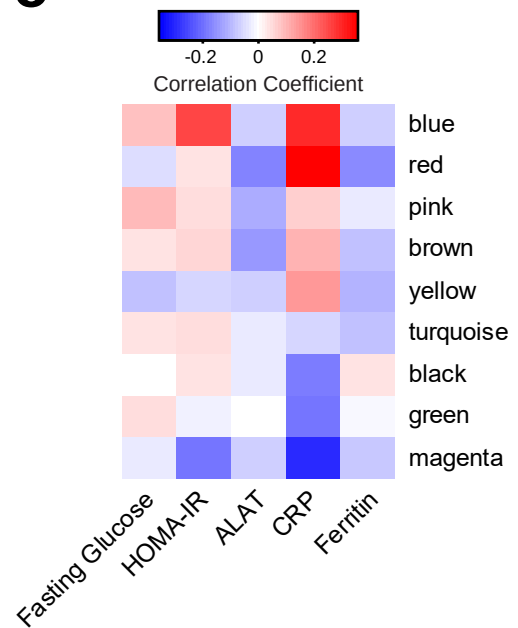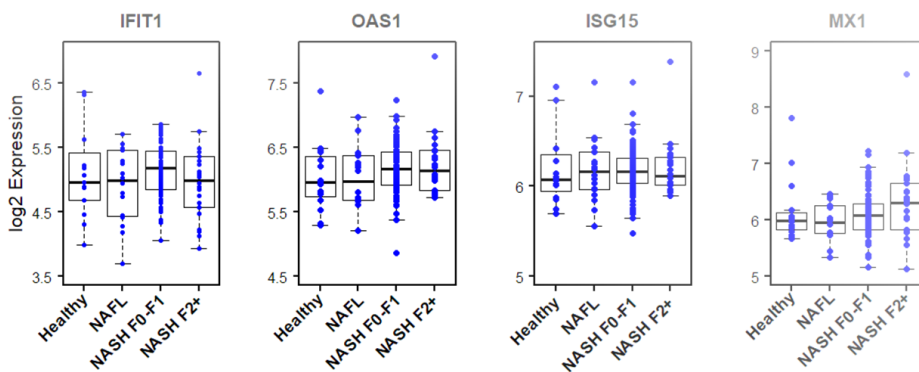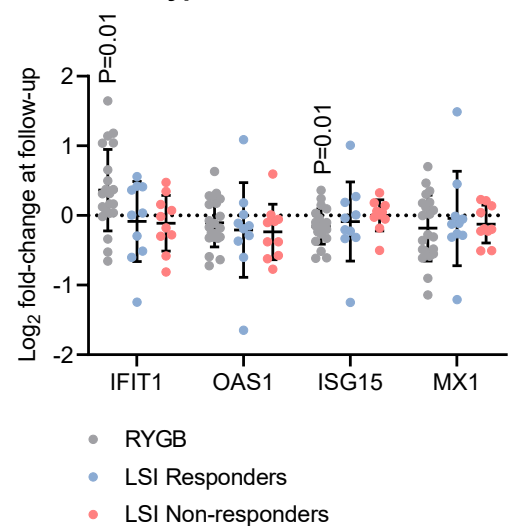
# Supplementary Figure 2
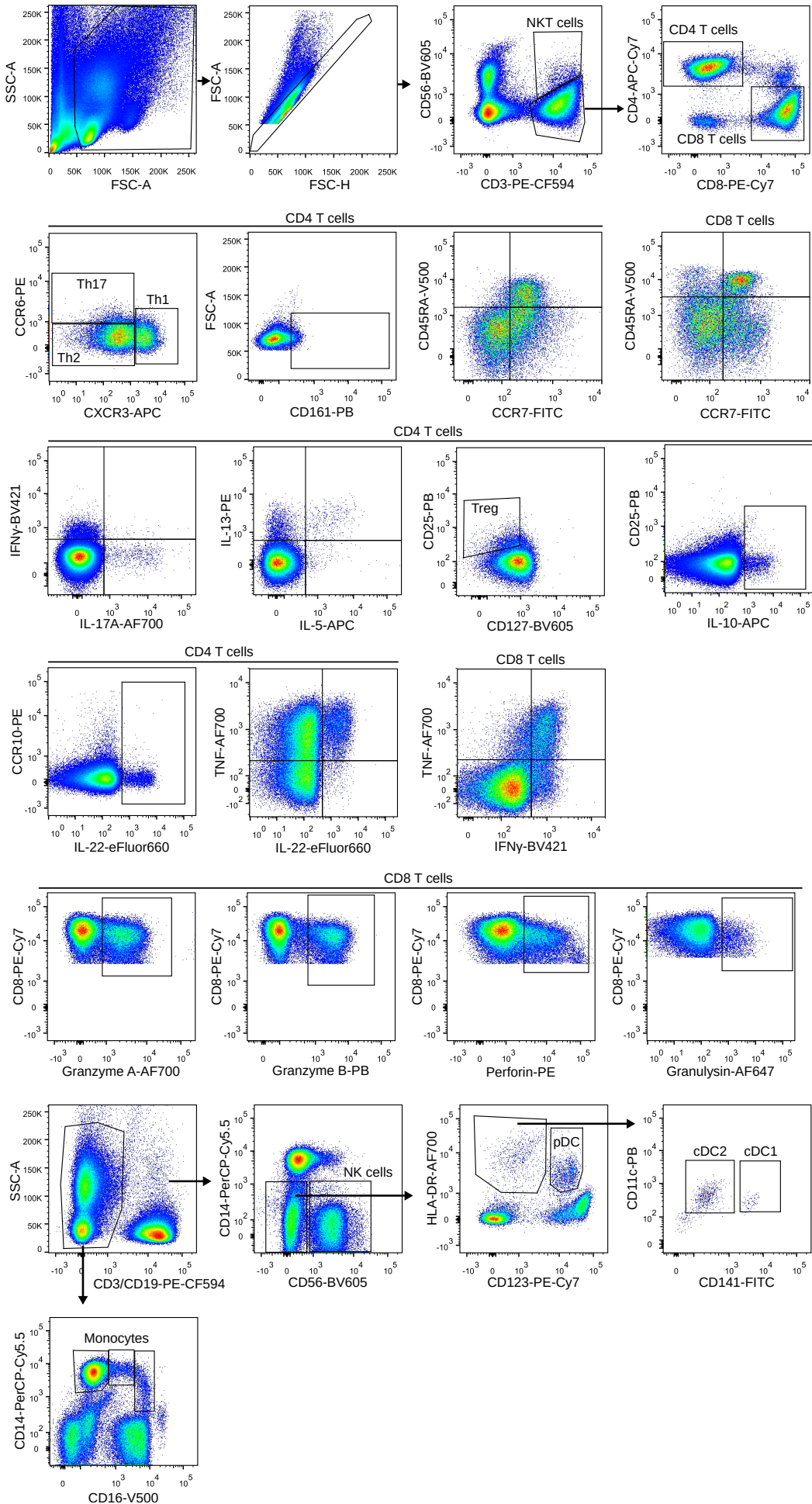
# Supplementary Figure 3
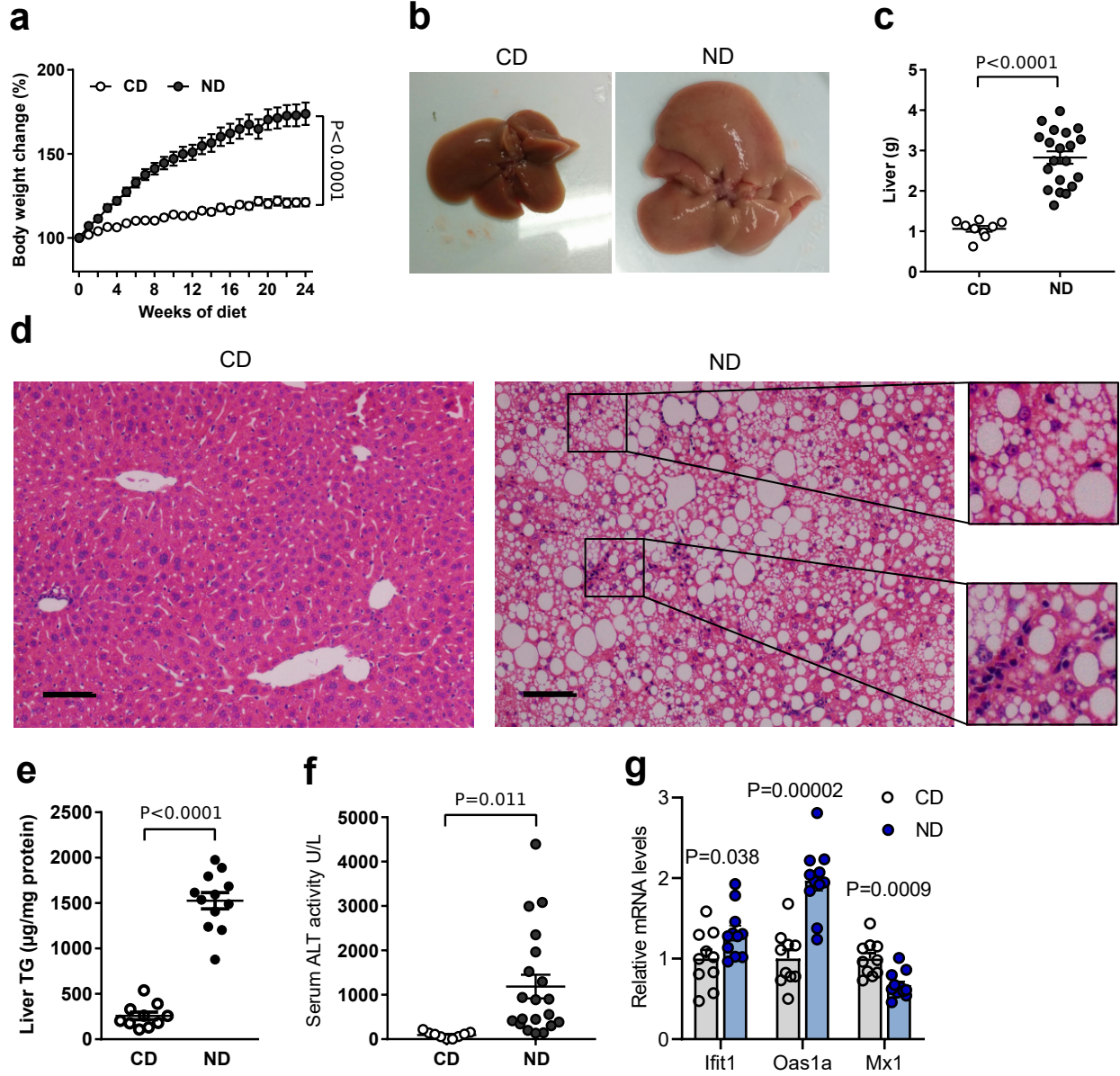
# Supplementary Figure 4
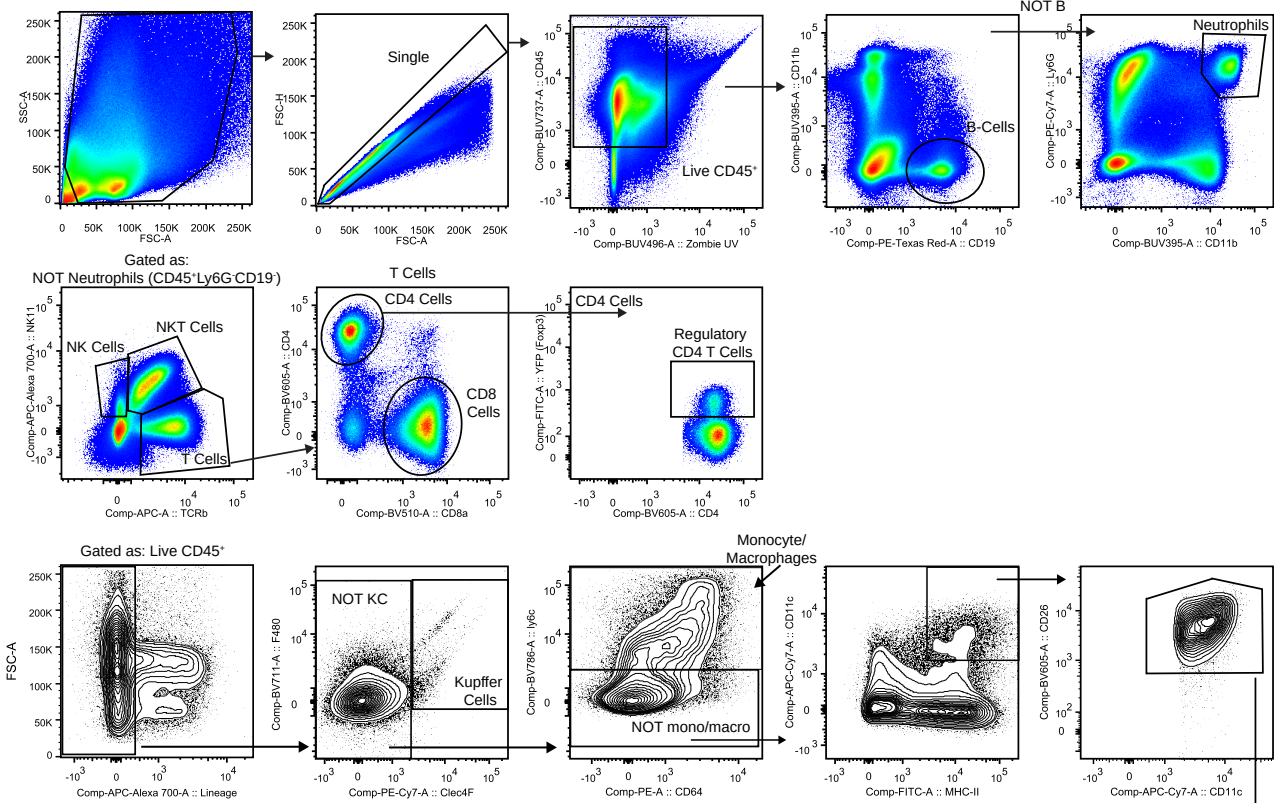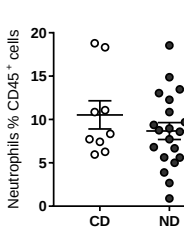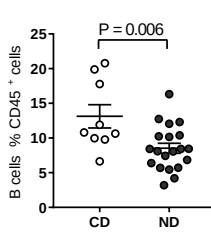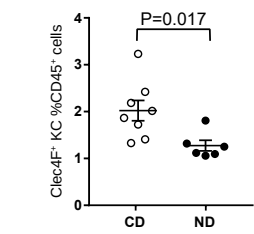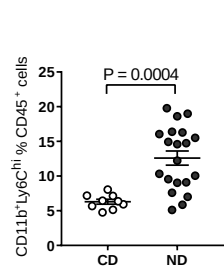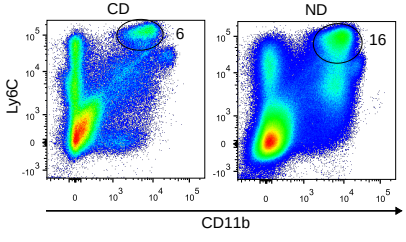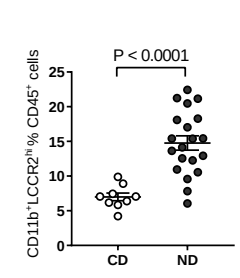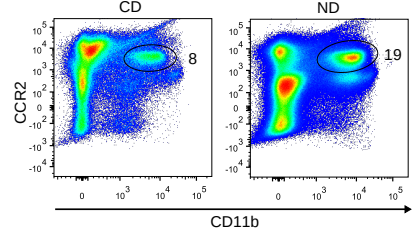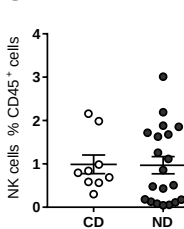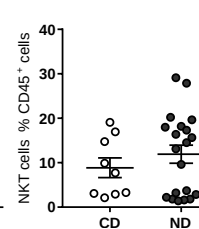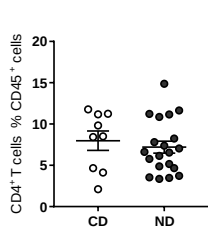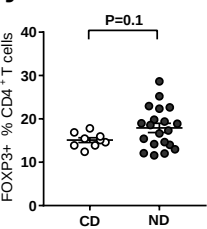
# Supplementary Figure 5
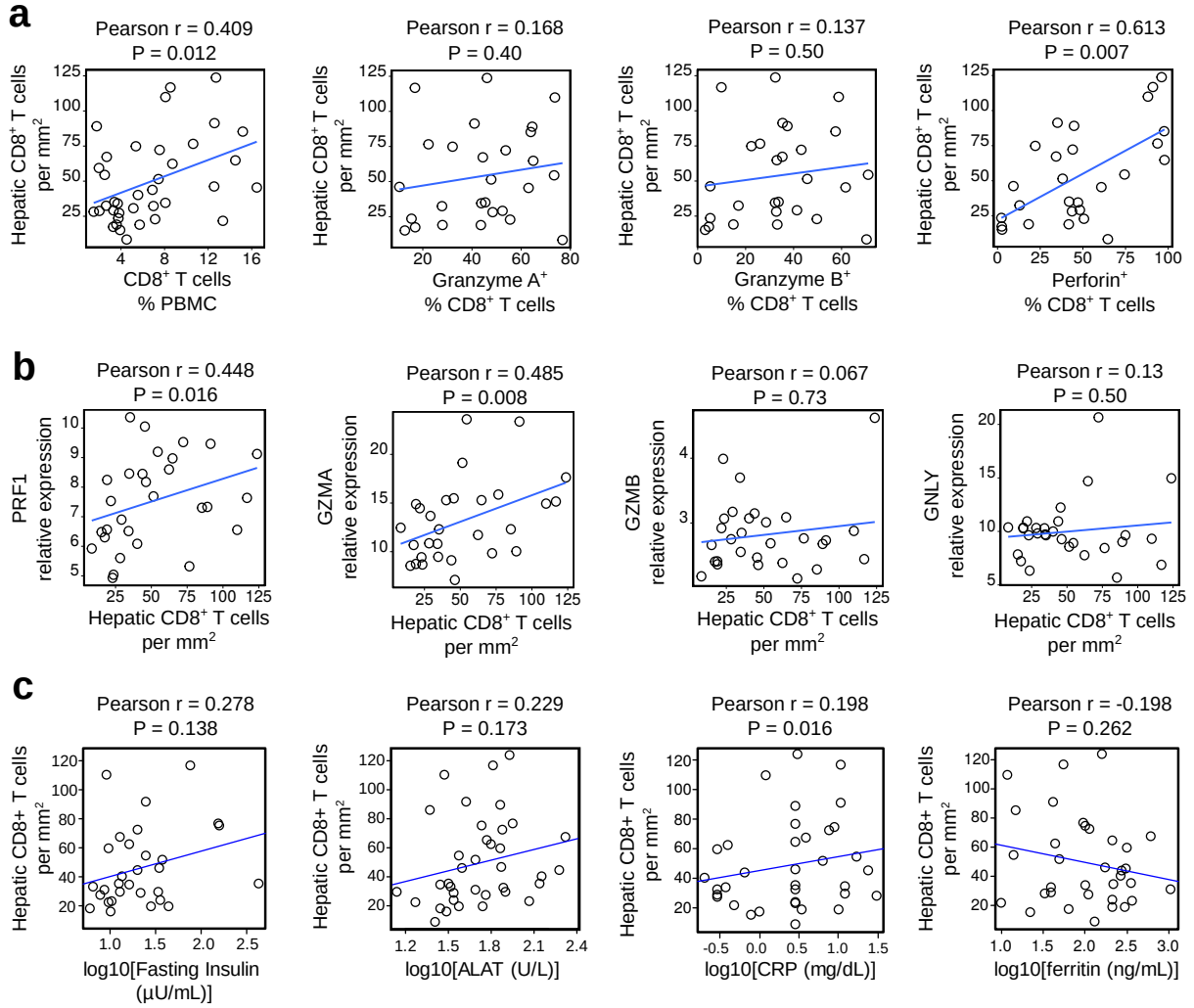
Supplementary Table 1

|  |  | Min/Max | Distribution |
|---|---|---|---|
| N (men/women) | 155 (55/100) |  |  |
| NO NASH/NASH | 49/106 |  |  |
| Age (years) | 43.2 ± 12.9 | 18/74 |  |
| BMI (kg m$^{-2}$) | 39.9 ± 5.6 | 27/69.1 |  |
| Lobular inflammation (score) | 1.1± 0.8 | 0/3 | 0(34); 1(80); 2(31); 3(10) |
| Ballooning (score) | 1.0 ± 0.7 | 0/2 | 0(40); 1(72); 2(43) |
| Steatosis (score) | 1.5 ± 1.1 | 0/3 | 0(27); 1(54); 2(37); 3(37) |
| NAS score | 3.7 ± 2.1 | 0/8 |  |
| Fasting glucose (mg dl$^{-1}$) | 86.1 ± 13.8 | 61/192 |  |
| 2 hr postprandial glucose (mg dl$^{-1}$) | 146.2 ± 37.9 | 55/274 |  |

## Supplementary Table 3

|  | Baseline | 1 year follow up | P-value |
|---|---|---|---|
| N (men/women) | 21 (8/13) | | |
| Age (years) | 46.7 ± 15.2 | | |
| BMI (kg m$^{-2}$) | 40.6 ± 4.9 | 29.3 ± 3.9 | < 0.001 |
| Body Weight (kg) | 114.8 ± 21.1 | 82.3 ± 13.8 | < 0.001 |
| Lobular inflammation (score) | 1.4 ± 0.6 | 0.2 ± 0.4 | < 0.001 |
| Ballooning (score) | 1.4 ± 0.5 | 0.4 ± 0.6 | < 0.001 |
| Steatosis (score) | 2.0 ± 0.9 | 0.2 ± 0.5 | < 0.001 |
| NAS score | 4.9 ± 1.2 | 0.9 ± 1.3 | < 0.001 |
| Fasting glucose (mg dl$^{-1}$) | 88.7 ± 13.5 | 80.2 ± 8.7 | 0.01 |
| 2 hr postprandial glucose (mg dl$^{-1}$) | 143.4 ± 47.8 | 80.3 ± 24.6 | < 0.001 |

Supplementary Table 4

| | LSI responders | | | LSI non-responders | | |
|---|---|---|---|---|---|---|
| | Baseline | Follow up | P-value | Baseline | Follow up | P-value |
| N (men/women) | 10 (3/7) | | | 10 (5/5) | | |
| Age (years) | 45.0 ± 13.9 | | | 45.7 ± 14.2 | | |
| BMI (kg m$^{-2}$) | 40.3 ± 11.2 | 37.0 ± 10.5 | 0.002 | 38.0 ± 5.5 | 34.7 ± 5.5 | 0.01 |
| Body Weight (kg) | 113.9 ± 26.2 | 104.6 ± 24.6 | 0.001 | 112.2 ± 21.2 | 102.2 ± 18.4 | 0.04 |
| Lobular inflammation (score) | 1.6 ± 0.8 | 0.5 ± 0.7 | 0.01 | 1.6 ± 0.8 | 1.7 ± 0.5 | NS |
| Ballooning (score) | 1.7 ± 0.5 | 0.5 ± 0.5 | 0.003 | 1.4 ± 0.5 | 1.6 ± 0.5 | NS |
| Steatosis (score) | 1.6 ± 0.8 | 0.7 ± 0.8 | 0.058 | 2.5 ± 0.7 | 1.9 ± 0.6 | NS |
| NAS score | 4.9 ± 1.4 | 1.7 ± 1.9 | 0.006 | 5.5 ± 1.2 | 5.2 ± 1.1 | NS |
| Fasting glucose (mg dl$^{-1}$) | 83.2 ± 17.9 | 84.2 ± 13.7 | NS | 80.1 ± 11.3 | 85.7 ± 6.6 | NS |
| 2 hr postprandial glucose (mg dl$^{-1}$) | 153.5 ± 45.5 | 120.3 ± 41.4 | 0.002 | 130.2 ± 19.1 | 131.0 ± 30.0 | NS |

## Supplementary Table 5

| | No NASH No T2D (a) | NASH No T2D (b) | No NASH T2D (c) | NASH T2D (d) |
|---|---|---|---|---|
| N (men/women) | 10 (7/3) | 11 (3/8) | 7 (4/3) | 10 (6/4) |
| Age (years) | 49.8 ± 10.9 | 46.1 ± 10.9 | 61.8 ± 9.6[a b] | 57.9 ± 8.5[b] |
| BMI (kg m$^{-2}$) | 30.1 ± 8.2 | 33.6 ± 7.2 | 40.4 ± 8.6[a] | 34.1 ± 7.5 |
| Lobular inflammation (score) | 0.0 ± 0.0 | 1.2 ± 0.4[a] | 0.0 ± 0.0[b] | 1.4 ± 0.5[a c] |
| Ballooning (score) | 0.3 ± 0.5 | 1.5 ± 0.5[a] | 1.1 ± 0.7[a] | 1.9 ± 0.3[a b c] |
| Steatosis (score) | 0.4 ± 0.7 | 2.5 ± 0.7[a] | 1.6 ± 1.1[a] | 2.3 ± 0.7[a] |
| NAS score | 0.8 ± 1.0 | 5.1 ± 0.9[a] | 2.7 ± 1.4[a b] | 5.5 ± 1.0[a c] |
| Fasting glucose (mg dl$^{-1}$) | 87.7 ± 6.0 | 92.0 ± 10.1 | 105.3 ± 13.4[a b] | 138.6 ± 50.8[a b] |
| 2 hr postprandial glucose (mg dl$^{-1}$) | 113.7 ± 24.9 | 140.8 ± 19.4 | 237.7 ± 90.3[a b] | 250.8 ± 95.7[a b] |
| Metformin treatment | 0/10 | 1/11 | 3/7 | 6/10 |
| Insulin treatment | 0/10 | 0/11 | 1/7 | 0/10 |
| Liver microarray | 7/10 | 9/11 | 6/7 | 7/10 |

**Supplementary Table 6.** Primer Sequences Used in This Study

| Gene | Forward | Reverse |
|------|---------|---------|
| *Ppia* | GCATACGGGTCCTGGCATCTTGTCC | ATGGTGATCTTCTTGCTGGTCTTGC |
| *Tbp* | TAGTCCAATGATGCCTTACGGC | TTGCTACTGCCTGCTGTTGTTG |
| *Il23a* | CCAGCAGCTCTCTCGGAATC | AAGCAGAACTGGCTGTTGTC |
| *Tnf* | GTCTACTGAACTTCGGGGTGA | CTCCTCCACTTGGTGGTTTG |
| *Ifit1* | GCTCTGCTGAAAACCCAGAGA | AAGGAACTGGACCTGCTCTGA |
| *Il1b* | AGGTGCTCATGTCCTCATCC | CAGGCAGGCAGTATCACTCA |
| *Il18* | GGCTTTCTTTGTCCTGATGC | GGTTCTCTGTGGTTCCATGC |
| *Il33* | TCCTTGCTTGGCAGTATCCA | TGCTCAATGTGTCAACAGACG |
| *Csf1* | AGCATGGACAGGCAGGGAC | CTGCGTGCCTTTATGCCTTT |
| *Ccl2* | GCCAACTCTCACTGAAGCC | GCTGGTGAATGAGTAGCAGC |
| *Ccl5* | CCTGCTGCTTTGCCTACCTCT | ACTTGGCGGTTCCTTCGAGT |
| *Cxcl10* | GGTCTGAGTGGGACTCAAGG | GTGGCAATGATCTCAACACG |
| *Mx1* | CTCTGGGTGTGGAGCAGGA | CAATACCACTGCCTCTGGGG |
| *Oas1a* | CAGCTGACCCAACAGGGAAT | TCGTGTCAGGAGCCTGCATT |
| *Cxcl10* | GGTCTGAGTGGGACTCAAGG | GTGGCAATGATCTCAACACG |
| *Mx1* | CTCTGGGTGTGGAGCAGGA | CAATACCACTGCCTCTGGGG |
| *Oas1a* | CAGCTGACCCAACAGGGAAT | TCGTGTCAGGAGCCTGCATT |

# Contents

## Bibliography                                                                                       65

## Contents                                                                                           163

## Abstract

Transcription factors of the nuclear receptor superfamily have a vast influence on development and function of $T_{REG}$ cells. $T_{REG}$ cells are suppressive immune cells of adaptive immune system. Their main functions are control of inflammatory response mounted by other immune cells and maintenance of local tissue homeostasis. As $T_{REG}$ act at various sites of the body and both in homeostatic and inflammatory state, they need to adequately respond to local tissue-specific cues as well as adapt to aggressive immune environments while preserving their long-lasting tolerogenic properties. This is achieved by weaving complex transcriptional networks, converging at transcription factors with various coordination functions, the main being FOXP3. During last few years, many studies focused on $T_{REG}$ cells found in NLT. These populations of $T_{REG}$ are examined in the contexts of homeostasis and many inflammatory diseases, and tissue- or function-specific TF were assigned to some of them as regulators of development, activation, proliferation, stability, migration and suppressive functions. ROR$\alpha$ is a nuclear receptor, which controls cerebellum development, liver and whole-body metabolism and differentiation of $T_H17$, ILC2 and ILC3. ROR$\alpha$ is highly expressed in NLT $T_{REG}$, including populations in VAT, intestine and skin, and gets more and more mentions in the articles dedicated to $T_{REG}$ in NLT. These ROR$\alpha$-expressing populations of $T_{REG}$ were all shown to be involved in various pathologies. However, ROR$\alpha$ role in $T_{REG}$ was directly addressed only once in a recent study. It's active involvement in various processes, high expression in NLT $T_{REG}$ and lack of knowledge make ROR$\alpha$ an attractive target for investigation, to deepen current view of homeostasis control by $T_{REG}$ and thus better understand mechanisms of development of associated diseases. To attain these objectives, a mouse strain with $T_{REG}$-specific ROR$\alpha$ deficiency was generated. Our central hypothesis is that ROR$\alpha$ controls development or function of $T_{REG}$ cells in homeostasis of NLT and potentially in inflammatory diseases. For studying a role of ROR$\alpha$ in NLT $T_{REG}$ during control of tissue homeostasis, in particular, VAT $T_{REG}$, we have charachterized phenotype of untreated ROR$\alpha^{Foxp3/Foxp3}$ mice and challenged mice with a model of DIO. In both cases we have found an important role of $T_{REG}$-expressed ROR$\alpha$. To further investigate a role of ROR$\alpha$ in $T_{REG}$ during pathologies and it's contribution to various types of immune response we have tested an involvement of ROR$\alpha$ in $T_{REG}$ in the model of allergic pathology, namely HDM-induced AAI model.

To elucidate molecular mechanisms of ROR$\alpha$ action in $T_{REG}$ cells, we have performed gene expression profiling of $T_{REG}$ cells from examined tissues and conditions *in vivo*, as well as *in vitro*. We also have studied a role of ROR$\alpha$ in epigenetic landscape of $T_{REG}$ cells *in vitro* by probing histone acetylation marks genome wide. As a result of this study, we have gained a broader understanding of $T_{REG}$ control by nuclear receptors and TF in general in homeostatic conditions and during inflammation. Nuclear receptors proved to be useful targets for therapeutic agents thanks to their versatile functions inside the cell and to ligand-dependency. Given the crucial importance of $T_{REG}$ cells in organismal homeostasis and their involvement in numerous pathologies, targeting particular cues inside these cells may be a powerful tool in new treatment strategies. Results of our study might serve as a basis for development of novel pharmaceutical agents targeting ROR$\alpha$.

**Resumé**

Les facteurs de transcription de la superfamille des récepteurs nucléaires jouent de multiples rôles dans le développement et la fonction des lymphocytes T régulateurs ($T_{REG}$). Les $T_{REG}$ sont des cellules régulatrices/suppressives qui contrôlent les réponses d'autres types cellulaires et l'homéostasie locale des tissus. Comme les $T_{REG}$ sont actives au sein de divers organes, tant à l'homéostasie qu'en conditions inflammatoires, ils doivent répondre à la fois aux contexte local au sein du tissus et à un environnement immunologiquement agressif tout en préservant leurs propriétés tolérogéniques au cours du temps. Ces caractéristiques apparemment antinomiques sont contrôlées par un réseau transcriptionnel complexe au sein duquel le facteur de transcription FOXP3 joue un rôle prédominant. Au cours des dernières années, de nombreuses études se sont intéressées aux $T_{REG}$ présent dans les tissus non lymphoïdes (NLT). Ces populations ont été étudiées aussi bien à l'homéostasie qu'en conditions inflammatoires dans diverses pathologies. Des facteurs de transcriptions spécifiques d'un tissus ou d'une fonction déterminées ont été mis en évidence et leur rôle régulateur dans le développement, l'activation, la migration et l'immunosuppression a été caractérisé. ROR$\alpha$ est un récepteur nucléaire qui contrôle le développement cérebellaire et hépatique, le métabolisme systémique, la différenciation des lymphocytes auxiliaires $T_H17$, des cellules lymphoïdes innées (ILC) de type 2 et 3. ROR$\alpha$ est fortement exprimé dans les $T_{REG}$ des NLT, y compris dans le tissu adipeux viscéral (VAT), l'intestin et la peau. . . .Ces populations de $T_{REG}$ exprimant ROR$\alpha$ ont été associées à diverses pathologies. Cependant seule une étude récente a été consacrée à leur rôle précis. L'implication de ROR$\alpha$ dans de nombreuses fonction, sa forte expression au sein des $T_{REG}$ des NLT nous a poussé a étudier le rôle de ces $T_{REG}$ exprimant ROR$\alpha$ dans diverses pathologies. Dans ce butit, nous avons généré des souris spécifiquement déficientes pour ROR$\alpha$ au sein des $T_{REG}$ (ROR$\alpha^{Foxp3/Foxp3}$). Nous avons émis l'hypothèse que ROR$\alpha$ contrôle le développement ou la fonction des $T_{REG}$ en conditions homéostatiques et dans des pathologies inflammatoires des NLT. Aussi nous avons caractérisé le phénotype des animaux ROR$\alpha^{Foxp3/Foxp3}$ et en particulier les $T_{REG}$ du VAT à l'homéostasie, où la réponse de type 2 est protectrice. et dans un modèle d'obésité (et d'insulino-résistance) induit par l'obésité (DIO) dans laquelle les . Nous avons mis en évidence un rôle protecteur important des $T_{REG}$ exprimant ROR$\alpha$ dans ces deux conditions expérimentales. Nous également étudié la contribution de ces cellules dans un modèle d'inflammation allergique (AAI) induite par un acarien (HDM) caractérisé par une forte réponse de type 2 et montré une aggravation de la pathologie. Pour étudier le mécanisme moléculaire de l'action de ROR$\alpha$ au sein des $T_{REG}$, nous avons procédé à une analyse transcriptomique des cellules isolées dans diverses conditions expérimentales *in vivo* et *in vitro* et avons étudié le rôle de ROR$\alpha$ dans les modifications épigénétiques au sein des $T_{REG}$ en caractérisation l'acétylation des histones dans le génome entier. Cette étude nous a permis de mieux appréhender comment les $T_{REG}$ étaient régulées par un facteur nucléaire à l'homéostasie et en conditions inflammatoires. Les récepteurs nucléaires représentent des cibles thérapeutiques intéressantes compte tenu de leur action pléiotropique et de leurs ligands de petite taille. Compte tenu de l'importance des $T_{REG}$ dans l'homéostasie tissulaire et dans de nombreuses pathologies, cibler de tels facteurs au sein de populations cellulaires spécifiques représente une stratégie prometteuse dans le case de ROR$\alpha$ et des $T_{REG}$.